

THE UNIVERSITY OF MANITOBA

Magnetic and Electrical Properties of
Dilute
PdNi, PdFe, and (PdFe)Mn Alloys

BY

ZHONGQUAN WANG

A THESIS SUBMITTED TO THE FACULTY OF GRADUATE STUDIES OF
THE UNIVERSITY OF MANITOBA IN PARTIAL FULFILLMENT OF THE
REQUIREMENTS OF THE DEGREE OF DOCTOR OF PHILOSOPHY

DEPARTMENT OF PHYSICS

WINNIPEG, MANITOBA

NOVEMBER 1990



National Library
of Canada

Bibliothèque nationale
du Canada

Canadian Theses Service Service des thèses canadiennes

Ottawa, Canada
K1A 0N4

The author has granted an irrevocable non-exclusive licence allowing the National Library of Canada to reproduce, loan, distribute or sell copies of his/her thesis by any means and in any form or format, making this thesis available to interested persons.

The author retains ownership of the copyright in his/her thesis. Neither the thesis nor substantial extracts from it may be printed or otherwise reproduced without his/her permission.

L'auteur a accordé une licence irrévocable et non exclusive permettant à la Bibliothèque nationale du Canada de reproduire, prêter, distribuer ou vendre des copies de sa thèse de quelque manière et sous quelque forme que ce soit pour mettre des exemplaires de cette thèse à la disposition des personnes intéressées.

L'auteur conserve la propriété du droit d'auteur qui protège sa thèse. Ni la thèse ni des extraits substantiels de celle-ci ne doivent être imprimés ou autrement reproduits sans son autorisation.

ISBN 0-315-77010-4

Canada

Magnetic and Electrical Properties of
Dilute
PdNi, PdFe, and (PdFe)Mn Alloys

by

Zhongquan Wang

A thesis submitted to the Faculty of Graduate Studies of the University of
Manitoba in partial fulfillment of the requirements of the degree of

DOCTOR OF PHILOSOPHY

© 1990

Permission has been granted to the LIBRARY OF THE UNIVERSITY OF MANITOBA to lend or sell copies of this thesis, to the NATIONAL LIBRARY OF CANADA to microfilm this thesis and lend or sell copies of the film, and to UNIVERSITY MICROFILMS to publish an abstract of this thesis.

The author reserves other publication rights, and neither the thesis nor extensive extracts from it may be printed or otherwise reproduced without the author's written permission.

Abstract

Detailed measurements of the field and temperature dependent *ac* susceptibility of a number of Pd based alloys, fourteen PdNi alloys containing between 2 and 5 at% Ni, seven PdFe alloys containing between 0.35 and 2.4 at% Fe, and five (PdFe)Mn alloys containing between 0.35 and 2.2 at% Fe, are presented. Attempts are made to analyse these data for Curie temperature and critical exponent values. It is shown that for most of the alloys studied, reliable estimates for critical exponents are precluded by the spin-orbit induced anisotropy, though ferromagnetic Curie temperatures T_c still can be determined.

High-resolution measurements of the *ac* magnetoresistance in the PdNi, PdFe, and (PdFe)Mn alloys have been carried out at low temperature. These data demonstrate the application of magnetoresistance measurements to investigate the onset of magnetic ordering via the appearance of a spontaneous resistive anisotropy (SRA) in low field, leading to the accurate determination of the critical Ni concentration x_0 in PdNi necessary to establish a ferromagnetic ground state. The first demonstration of a power-law relation between the SRA and the reduced composition near x_0 is presented, and the corresponding critical exponent governing this relationship is estimated experimentally.

The effects of hydrogen on a typical sample, 5.0 at% Ni, have also been studied. It is shown that hydrogen has enormous effects on the geometry, susceptibility, and coercive field of the sample.

Acknowledgements

I wish to express my deepest gratitude to Dr. Gwyn Williams who supervised this research project and whose many comments and suggestions contributed immeasurably to the success of this work. His encouragement throughout the course is also greatly appreciated.

I would like to extend special thanks to Dr. Henry Kunkel for invaluable assistance in completing this study.

I would like to thank Dr. A. H. Morrish, Dr. B. W. Southern, and Dr. R. M. Roshko for their instruction and discussions.

I am also indebted to the following people for various reasons: to Dr. J. Page for allowing me the use of the electromagnet in his laboratory, to Mr. M. S. Westmore for generating the effective exponent plots of the dilute PdNi alloys, to Mr. J. Schacter for analysing some of the *ac* susceptibility data of one dilute PdFe sample, and to all the others who have participated either directly or indirectly in shaping this work.

And last, but not least, I would like to express my appreciation to my wife, Xiaoli, for her understanding and encouragement during the study.

Contents

Abstract	I
Acknowledgments	II
Chapter 1: Theories	1
1.1 Introduction	2
1.2 Magnetic Properties	2
1.2.1 Interaction of Magnetic Moments	2
1.2.2 Landau Theory	8
1.2.3 The Scaling Approach and Scaling Laws	12
1.3 Electrical Resistivity and SRA	26
1.3.1 General Properties	26
1.3.2 Localised Model	31
1.3.3 Itinerant Model	33
Chapter 2: Review	40
2.1 Introduction	41
2.2 Pure Palladium	41
2.3 Palladium Based Magnetic Alloys	44
2.3.1 Magnetic Moment and Magnetic Phase Diagrams	44
2.3.2 Magnetization, Susceptibility and Critical Exponents	57

2.3.3 Electrical Resistivity, Magnetoresistivity and SRA	60
Chapter 3: Experimental Methods	67
3.1 Introduction	68
3.2 Sample Preparation	68
3.3 X-Ray Measurements	70
3.4 <i>ac</i> Magnetic Susceptibility Measurements	73
3.4.1 The Measurement System	73
3.4.2 Measurement of Susceptibility	76
3.4.3 Calibration and Corrections	78
3.5 <i>ac</i> Magnetoresistance Measurements	82
3.5.1 Experimental Geometry	82
3.5.2 The Measurement Technique	85
3.5.3 Circuit Diagram	89
3.6 Hydrogen Absorption	94
Chapter 4: Results and Discussion	97
4.1 Introduction	98
4.2 <i>ac</i> Susceptibility Results for the Dilute PdFe System	98
4.2.1 A "Perfect System" – Pd _{98.6} Fe _{1.4}	98
4.2.2 Fe Concentration Dependence	109
4.3 <i>ac</i> Susceptibility Results for the Dilute PdNi System	120
4.3.1 General Features for the Dilute PdNi System	120

4.3.2 Detailed Features of a PdNi Specimen	122
4.3.3 Concentration Dependence of Various Parameters	130
4.4 <i>ac</i> Susceptibility Results for the Dilute (PdFe)Mn System .	140
4.5 SRA Results for the Dilute PdNi System	153
4.5.1 A Typical Alloy – Pd _{95.0} Ni _{5.0}	153
4.5.2 Ni Concentration Dependence	158
4.5.3 Quantitative Estimates from $\rho(H_a^{min})$	172
4.5.4 Power Law Relationship	177
4.6 SRA Results for the Dilute PdFe System	185
4.7 SRA Results for the Dilute (PdFe)Mn System	202
4.8 Effects of Hydrogen	211
4.9 Summary and Conclusions	218
Appendix	225
A. <i>ac</i> Susceptibility Data	226
B. <i>ac</i> Magnetoresistance Data	251
References	266

Chapter 1

Theories

1.1 Introduction

This chapter is intended to discuss some theories and models describing the magnetic and electrical properties of ferromagnets. This field has attracted considerable interest over a long period of time and has grown to such an extent that it is not possible to cover all the concepts and developments completely in a simple short review. Therefore we have decided to focus our attention only on those theories which are directly related to the subjects we have studied experimentally.

1.2 Magnetic Properties

1.2.1 Interaction of Magnetic Moments

The pioneering theoretical work in understanding the magnetic properties of ferromagnets was done by Weiss in 1907. Several important properties of ferromagnets, such as the spontaneous magnetization, the existence of the susceptibility curve and the technical magnetization curve, can be interpreted, at least in principle, by his theory.

In the Weiss approach two assumptions were made; the first was that the constituent magnetic moments interact with one another through a "molecular field"¹ which was proportional to the magnetization of the system; the second assumption was that actual specimens are composed of a number of small regions called magnetic domains. While this latter assumption, the

¹Also called the Weiss field or mean field.

existence of domains, was verified by direct observation of domain structure using the Bitter method as early as 1931, the detailed features of the interacting magnetic moments are still not clear.

Many specific models have been put forward in order to understand this interaction. If the dimensionality of magnetic moment space, or the spin space, is D , then $D = 1, 2, 3$, and ∞ corresponds to the Ising, Planar, Heisenberg, and Spherical models respectively as shown in Figure 1.1. Two of them are particularly interesting, namely the Ising model and the Heisenberg model, as these models appear to represent reasonable theoretical descriptions of certain physical systems.

As shown in Figure 1.1, in the Ising model the magnetic moments are assumed to be classical, one dimensional "sticks" capable of only two orientations, up and down. The interaction Hamiltonian of the system is given by

$$H = -2J_{ex} \sum_j^N S_{zi} S_{zj} \quad (1.1)$$

where J_{ex} is a constant which couples spins on sites at i and at j , S_{zi} and S_{zj} is the z component of spins on the sites at i and j respectively; and the summation is over the nearest neighbors of atom i (Morrish 1965).

Ising (1925) solved this model (which is now named after him) for the case of a one-dimensional lattice (or linear chain) in the absence of an external field; the solution did not display a phase transition.

$\vec{S} = \text{D-Dimensional Classical spins}$

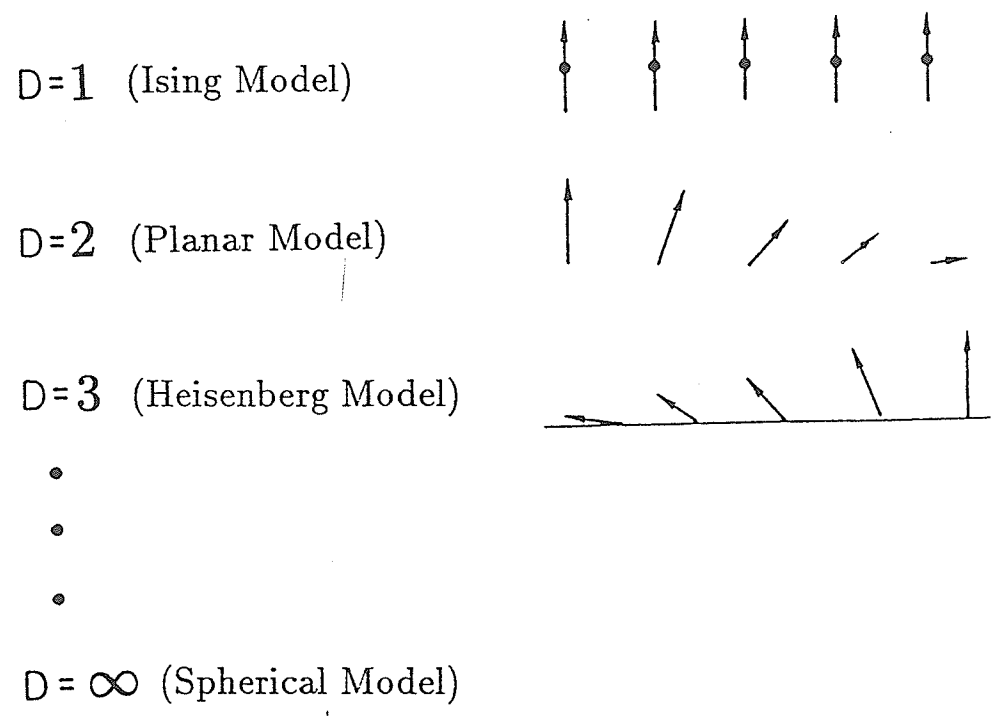


Figure 1.1: Illustration of the concept of interacting D -dimensional spin.

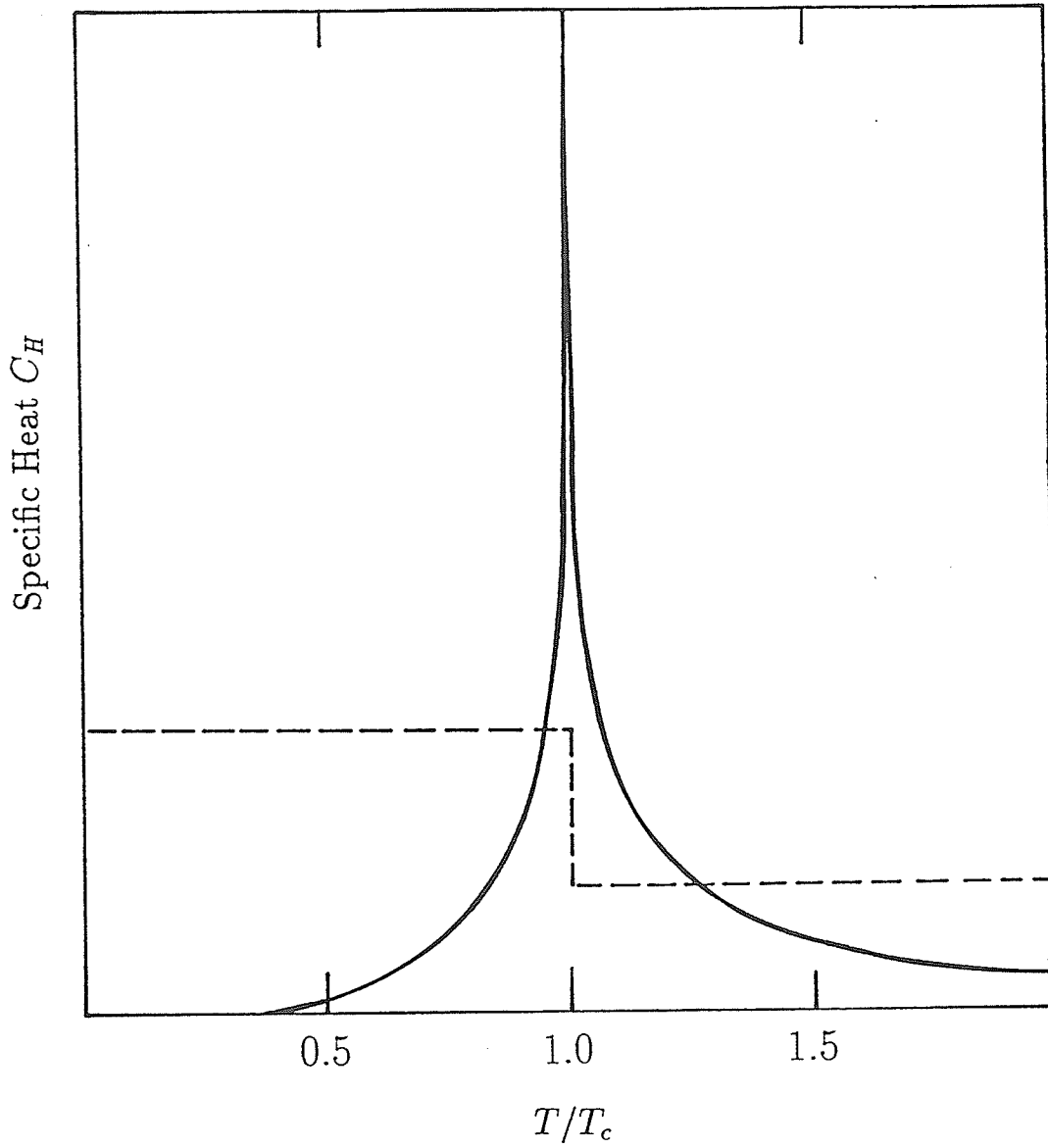


Figure 1.2: The specific heat of the two dimensional Ising model (solid curve) and the mean field theory (dashed curve).

Onsager's exact solution of the two-dimensional Ising model is a landmark in the history of phase transitions and critical phenomena. From the partition function for zero external field, Onsager (1944) was able to show that the specific heat possesses a logarithmic divergence at T_c when approached from both $T < T_c$ and $T > T_c$ as shown in Figure 1.2. In contradiction to the predictions of the other theories such as mean field theory, Onsager's result agrees with most experimental measurements.

The critical-point exponents associated with a magnetic phase transition for a two-dimensional Ising model have also been calculated, but as we will see later the values, in general, do not agree with experimental measurements.

The three-dimensional Ising model has not yet been solved exactly, and some authors claim that it may in fact be an insoluble problem.

On the other hand in the Heisenberg model, the basic idea is that the spin is a three-dimensional vector and the magnetic moments \vec{S}_i and \vec{S}_j situated on sites i and j in the lattice have an exchange interaction of the form

$$E_{ex} = -2J_{ex}\vec{S}_i \cdot \vec{S}_j \quad (1.2)$$

where J_{ex} is the exchange integral. The lowest energy state of Equation (1.2) depends on the sign of the exchange integral. If J_{ex} is positive, E_{ex} is a minimum when the spins are parallel, as in the case of ferromagnets. The exchange energy, the physical origin of the Weiss field, has no classical

analogue, although it is of electrostatic origin. It expresses the difference in Coulomb interaction energy of the system when the spins are parallel or antiparallel, and is a consequence of the Pauli exclusion principle.

If the exchange integral J_{ex} is isotropic then the exchange Hamiltonian for the entire system is

$$H = -2J_{ex} \sum_j^N \vec{S}_i \cdot \vec{S}_j \quad (1.3)$$

Expansion of the scalar product of the above equation gives

$$H = -2J_{ex} \sum_j^N (S_{xi}S_{xj} + S_{yi}S_{yj} + S_{zi}S_{zj}) \quad (1.4)$$

If $(S_{xi}S_{xj} + S_{yi}S_{yj})$ can be neglected, then the Hamiltonian is just

$$H = -2J_{ex} \sum_j^N S_{zi}S_{zj} \quad (1.5)$$

which is just Equation (1.1), the Hamiltonian of the Ising model.

By solving for the properties of a system with either an Ising or Heisenberg model Hamiltonian, we should arrive at a theory of ferromagnetism. Unfortunately, neither the Ising nor the Heisenberg model has yet yielded an exact solution for a three-dimensional lattice. The Heisenberg model is not even solvable for a two-dimensional lattice without making further approximations. Therefore if one wishes to obtain predictions of critical properties

for realistic models, one must resort to numerical approximation techniques. Many approximation techniques, such as the successive approximation methods and the series expansion methods, have been used; some of them are very successful in predicting accurate values of critical temperatures and critical exponents, such as the exponents for the 3d Heisenberg model (as will be seen later in Table 1.1).

1.2.2 Landau Theory

In this and the following subsection we will present some attempts to provide a more realistic equation of state, and discuss the critical behaviour predicted by these theories and models. We begin with the Landau theory.

It is possible to understand a number of important magnetic properties of a ferromagnet in terms of Landau theory (Landau and Lifshitz 1969). This theory, sometimes called mean field theory, is a simple and solvable theory. According to this model, the Helmholtz free energy F of a magnetic system near a critical phase transition temperature can be expressed by a standard Taylor series, as the magnetization M will be small at temperature T close to Curie temperature T_c

$$F(T, M) = F_0(T) + a_2(T)M^2 + a_4(T)M^4 + \dots \quad (1.6)$$

where $F_0(T)$ is a constant term, a_2 and a_4 are two temperature dependent coefficients. Notice that there are no odd terms in the expansion since the free energy must be symmetric under reversal of the magnetization.

At a given temperature T , when

$$\left(\frac{\partial F}{\partial M}\right)_T = 0 \quad (1.7)$$

and

$$\left(\frac{\partial^2 F}{\partial M^2}\right)_T > 0 \quad (1.8)$$

the magnetic system will be in an equilibrium state at zero field. Equation (1.7) and (1.8) lead directly to the following two equations.

$$\left(\frac{\partial F}{\partial M}\right)_T = 2a_2(T)M + 4a_4(T)M^3 = 0 \quad (1.9)$$

and

$$\left(\frac{\partial^2 F}{\partial M^2}\right)_T = 2a_2(T) + 12a_4(T)M^2 > 0 \quad (1.10)$$

Below the Curie temperature, from Equations (1.9) and (1.10) one has $a_4(T) > 0$ as $M^2 > 0$, and therefore

$$a_2(T) < 0 \quad (1.11)$$

as required by Equation (1.9).

Above the Curie temperature, however, from Equation (1.10) as $M = 0$ at $T > T_c$, we have

$$a_2(T) > 0 \quad (1.12)$$

so that the sign of $a_2(T)$ changes at the Curie temperature.

Expanding the coefficients $a_2(T)$ and $a_4(T)$ as a binomial in T near T_c and retaining only the lowest non-zero term, the above results are consistent with

$$a_2(T) = a_{21}(T - T_c) \quad (1.13)$$

and

$$a_4(T) = a_{40} \quad (1.14)$$

where a_{21} and a_{40} are two positive constants.

One can use these solutions to calculate the magnetization, magnetic susceptibility, and specific heat. For zero field, as M is small at T close to T_c , substituting Equations (1.13) and (1.14) into Equation (1.9), we have

$$M = \left(\frac{a_{21}}{2a_{40}}\right)^{1/2}(T_c - T)^{1/2} \quad (1.15)$$

If one defines an exponent β through the relationship $M \propto (-t)^\beta$ with $t = \frac{T-T_c}{T_c}$, then Equation (1.15) predicts the exponent $\beta = 1/2$ in the Landau theory.

Since the isothermal magnetic susceptibility is defined by

$$\chi^{-1} = \left(\frac{\partial^2 F}{\partial M^2}\right) = 2a_2(T) + 12a_4(T)M^2 + \dots \quad (1.16)$$

for temperatures above Curie temperature, where $M = 0$, at $H = 0$ we have the important result

$$\chi = \frac{1}{2a_{21}} \frac{1}{T - T_c} \quad (1.17)$$

This is the well known Curie-Weiss law with $1/(2a_{21})$ equal to the Curie constant, and if one defines a second exponent γ by $\chi \propto t^{-\gamma}$ then Equation (1.17) indicates $\gamma = 1$ in the Landau theory.

For $T < T_c$, $M \neq 0$, it is straightforward² to show

$$\chi(M, T) = \frac{1}{4a_{21}} \frac{1}{T_c - T} \quad (1.18)$$

thus we obtain $\gamma' = 1$ also as $\chi \propto (-t)^{-\gamma'}$ for $T < T_c$.

However experimental results indicate that for most magnetic systems the susceptibility does not follow a Curie-Weiss law when the temperature T is close to T_c . This is just the opposite behavior predicated by the Landau theory, as a standard Taylor series should be most accurate close to the Curie point.

Recall from the thermodynamic state functions that at $T = T_c$, $H = (\partial F/\partial M)_T$ (where H is magnetic field); now differentiating Equation (1.6), expanding the coefficients and setting $T = T_c$, we have

$$H(M, T_c) = 4a_{40}M^3 \quad (1.19)$$

If one defines $H \propto M^\delta$, then $\delta = 3$ in the Landau theory. Experimental

²By substituting M^2 from Equation (1.15) into (1.16)

results have shown that for most of magnetic materials $\delta > 3$.

Using the Landau mean field theory one also can calculate the specific heat of a magnetic system. This theory predicts that the specific heat at zero field has a discontinuity at the Curie temperature, but the discontinuity is predicted to take the form of a step function (dashed line in Figure 1.2) with an amplitude $a_{21}^2/(2a_{40})$, rather than a lambda anomaly as shown in the figure (solid line).

1.2.3 The Scaling Approach and the Scaling Laws

Experimental results have shown that for ferromagnets many magnetic parameters, such as the magnetic susceptibility (χ), the magnetic specific heat (c_H) and the reciprocal of the magnetization (M^{-1}), become very large near the Curie point, and almost all of them seem to obey a simple power law of the form

$$\chi \propto t^{-\gamma} \quad H = 0, T > T_c \quad (1.20)$$

$$M \propto (-t)^\beta \quad H = 0, T < T_c \quad (1.21)$$

and

$$M \propto H^{1/\delta} \quad T = T_c \quad (1.22)$$

In some cases the critical exponents which govern the power law relationships can be calculated with reasonable accuracy from theoretical models,

This is the case for the one and four or more dimensional systems³, the two dimensional Ising model, and the Spherical model ($D = \infty$). However none of the systems indicated above occur in the real world (Stanley 1971, Collins 1989).

As shown in Section 1.2.2 the Landau approach fails to provide a general theory of critical phenomena in the following two respects. First the expansion of the basic equation (Equation (1.6)) is not valid for a system whose specific heat diverges to infinity at $T \rightarrow T_c$; and second the critical exponents values predicated by the theory disagree with most experimental measurements.

So a less rigorous approach called the Scaling approach (Widom 1965, Domb and Hunter 1965, and Kadanoff 1966) has been introduced. The basic assumption⁴ of scaling theory is that when we change the size of a cell, we only change the parameters (such as the magnetic field H and reduced temperature t) that go into the Hamiltonian, but not the form of the Hamiltonian. Scaling theory expresses all the static critical exponents in terms of just two parameters p and q . However the theory does not predict the values of the critical exponents themselves.

This approach can be illustrated as follows. The Gibbs free energy⁵ G of a cell often can be written in terms of two parameters, H and t . According

³As an example one may calculate the temperature dependence of spontaneous magnetization, susceptibility, specific heat etc. based on the linear chain Ising model in the absence of an external magnetic field, as it is a solvable model.

⁴The same basic assumption has been used in the relatively new theory-renormalization group theory which is a theoretical approach which goes further in evaluating the block (renormalized) variables explicitly.

⁵The Gibbs and the Helmholtz free energies are related by $G = F - HM$.

to the basic assumption of the scaling theory, when we change the cell size from La to λLa , the parameters H and t of the free energy G will be changed to \tilde{H} and \tilde{t} , but leave the form of the Gibbs free energy unchanged, so that for any value of λ we have

$$\lambda G(H, t) = G(\tilde{H}, \tilde{t}) \quad (1.23)$$

This means that Gibb's potential energy $G(H, t)$ is a generalized homogeneous function.

Given the assumption that t and \tilde{t} have a linear relationship, and that H and \tilde{H} are also linear when H is small, Cooper (1968) has proved that

$$\tilde{H} = \lambda^q H \quad (1.24)$$

and

$$\tilde{t} = \lambda^p t \quad (1.25)$$

Equation (1.23) now becomes

$$\lambda G(H, t) = G(\lambda^q H, \lambda^p t) \quad (1.26)$$

Differentiating Equation (1.26) gives the transformation for the free energy

$$\lambda \frac{\partial G(H, t)}{\partial H} = \lambda^q \frac{\partial G(\lambda^q H, \lambda^p t)}{\partial (\lambda^q H)} \quad (1.27)$$

From thermodynamics, the magnetization $M(H, T)$ in a small field is given by

$$M(H, T) = -\left(\frac{\partial G(H, T)}{\partial H}\right)_T \quad (1.28)$$

Therefore in zero field, we have

$$\lambda M(0, t) = \lambda^q M(0, \lambda^p t) \quad (1.29)$$

This equation should be valid for any positive value of λ , so we set

$$\lambda^p(-t) = 1 \quad (1.30)$$

For $t \rightarrow 0$ or temperatures below Curie temperature T_c , we have

$$M(0, t) = (-t)^{(1-q)/p} M(0, -1) \quad (1.31)$$

Comparing with the definition of $M(0, t) \propto (-t)^\beta$, we get

$$\beta = \frac{1-q}{p} \quad (1.32)$$

This equation demonstrates that the critical exponent β can be simply expressed in terms of the two unspecified scaling parameters p and q .

Similarly from Equations (1.27) and (1.28), we can derive the variation

of magnetization as a function of H in the form of

$$\lambda M(H, t) = \lambda^q M(\lambda^q H, \lambda^p t) \quad (1.33)$$

This equation is sometimes called the magnetic equation of state; at $T = T_c$, set $\lambda^q H = 1$, when

$$M(H, 0) = H^{(1-q)/q} M(1, 0) \quad (1.34)$$

as shown in Equation (1.22), $M(H, 0) \propto H^{1/\delta}$, then

$$\delta = \frac{q}{1-q} \quad (1.35)$$

This gives another example of using the scaling parameters p and q to define a critical exponent.

From Equations (1.27) and (1.28) we also can derive the isothermal susceptibility, since $\chi = \frac{\partial M}{\partial H}$.

By differentiating equation (1.34), at $T = T_c$ the isothermal susceptibility has the following form

$$\chi(H, 0) = M(1, 0) H^{(1/\delta)-1} \quad (1.36)$$

Differentiating Equation (1.33) with respect to H

$$\lambda \frac{\partial M(H, t)}{\partial H} = \lambda^{2q} \frac{\partial M(\lambda^q H, \lambda^p t)}{\partial (\lambda^q H)} \quad (1.37)$$

let $H = 0$ and $\lambda^p(-t) = 1$, at T below T_c

$$\chi(0, t) = (-t)^{-\frac{2q-1}{p}} \chi(0, 1) \quad (1.38)$$

therefore

$$\chi \propto (-t)^{-\frac{2q-1}{p}} \quad (1.39)$$

Comparing with the definition of γ' gives

$$\chi \propto (-t)^{-\gamma'} \quad (1.40)$$

we get

$$\gamma' = \frac{2q-1}{p} \quad (1.41)$$

Using the same arguments for temperature just above T_c , we find

$$\gamma = \gamma' \quad (1.42)$$

The equality of the unprimed and primed critical exponents is a common feature of static scaling theory.

It is straightforward to show that combining Equations (1.32), (1.35) and (1.41) gives

$$\gamma = \gamma' = \beta(\delta - 1) \quad (1.43)$$

This relationship between critical exponents is called the scaling law, and the above form was first derived by Widom (1965). Equation (1.43) is

a special case of a rigorous inequality among the exponents; specifically the inequality $\gamma' \geq \beta(\delta - 1)$ was proved by Griffiths (1965). As indicated by Equation (1.43), only two of these exponents are independent of each other.

From the definition of the specific heat in constant field (c_H) at $H = 0$ and T just above T_c ,

$$c_H = T \left(\frac{\partial^2 G}{\partial T^2} \right)_H \quad (1.44)$$

and the definition of critical exponent α , $c_H \propto t^{-\alpha}$, we get

$$\alpha = \frac{2p - 1}{p} \quad (1.45)$$

Similarly, assuming the correlation length ξ is also a homogeneous function of H and t , at $H = 0$ and T just above T_c , we have

$$\xi(0, t) = t^{-1/q} \xi(0, 1) \quad (1.46)$$

From the definition of the critical exponent ν

$$\xi(0, t) \propto t^{-\nu} \quad (1.47)$$

we have

$$\nu = q^{-1} \quad (1.48)$$

Using the same arguments for temperature just below T_c , we can show

$$\nu' = \nu \quad (1.49)$$

and

$$\alpha' = \alpha \quad (1.50)$$

Again the primed and unprimed critical exponents have the same value.

As discussed above, the scaling law provides a unified description of magnetic properties near the transition point. It is not only of theoretical importance but has also been used extensively to analyse numerous experimental investigations of magnetic materials, ranging from pure metals and ionic compounds to dilute magnetic alloys.

Starting from the scaling law equation of state (i.e. Equation (1.33)), if we set $\lambda^p = 1/t$, then the magnetization M can be related to the magnetic field H and the reduced temperature $t (= \frac{T-T_c}{T_c})$ via

$$M(H, t) = \lambda^{q-1} M\left(\frac{H}{t^{q/p}}, 1\right) \quad (1.51)$$

or

$$M(H, t) = t^\beta F(H/t^{\gamma+\beta}) \quad (1.52)$$

As shown in this equation, scaling theory specifies only the argument, but not in general, the form of the function F . The above equation, however, leads to the well known asymptotic relationships near the Curie temperature

(T_c) such as the ones shown in Equations (1.31), (1.34), and (1.36). We rearrange and present them in the following way

$$M(0, t) \propto (-t)^\beta \quad (T < T_c) \quad (1.53)$$

$$M(H, 0) \propto H^{1/\delta} \quad (T = T_c) \quad (1.54)$$

$$\chi(H, 0) \propto H^{(1/\delta)-1} \quad (T = T_c) \quad (1.55)$$

$$\chi(0, t) \propto t^{-\gamma} \quad (T > T_c). \quad (1.56)$$

The critical exponents β , δ and γ therefore can be estimated experimentally⁶. As indicated by these equations, the critical exponents can be determined by measuring the slopes of $\log - \log$ plots of experimental data. Although this is a particularly quick method of determining the exponents, it requires an a priori knowledge of the critical temperature, in most of cases, so that in practice one must frequently resort to plotting M or χ for several trial values of β , γ or δ until a value is found which produces a straight line. In addition to these asymptotic dependences, Equation (1.33) predicts that the

⁶It is important to stress (Stanley 1971) that in order to define a critical exponent such as β , the order parameter M does not necessarily have a strict proportional relationship with $(-t)^\beta$ as shown in Equation (1.53), so a more natural definition of the critical exponent β is $\beta = \lim_{t \rightarrow 0} \frac{\ln(M)}{\ln(t)}$.

susceptibility χ has the following form

$$\chi(H, t) = \partial M / \partial H = t^{-\gamma} F'(H/t^{\gamma+\beta}) = H^{-\gamma/(\gamma+\beta)} G(H/t^{\gamma+\beta}) \quad (1.57)$$

where $F'(H/t^{\gamma+\beta})$ is the derivative of the function $F(H/t^{\gamma+\beta})$ with respect to its argument $H/t^{\gamma+\beta}$, and $G(x) = x^{\gamma/(\gamma+\beta)} \cdot F'(x)$. In a fixed field H , the susceptibility is then predicted to have a peak at a reduced temperature t_p given by

$$(\partial \chi / \partial t)_{t=t_p} = 0 \quad \text{i.e.} \quad G'(H/t_p^{\gamma+\beta}) = 0 \quad (1.58)$$

Equation (1.58) is satisfied when the argument of the function G is a constant, thus

$$\frac{T_p - T_c}{T_c} = t_p \propto H^{1/(\gamma+\beta)}. \quad (1.59)$$

Substituting this condition into Equation (1.57) immediately yields

$$\chi(H, t_p) \propto H^{(1/\delta)-1} \quad (1.60)$$

Equation (1.59) demonstrates that the peak ac susceptibility occurs at the reduced temperature t_p , which increases with increasing field, while Equation (1.60) indicates that the peak amplitude decreases with increasing field in the same manner as the susceptibility at T_c . It should be pointed out that unlike the magnetization data, estimates of exponent δ from the field dependence of the peak susceptibility as indicated by Equation (1.60)

are independent of the choice of Curie temperature T_c . These equations have been verified experimentally in many systems (Ho et al 1981 a, b; Gaunt et al 1981; Saran and Williams 1987). These power law relationships also form the basis of the detailed investigation of the dilute PdNi, PdFe and (PdFe)Mn systems carried out here, and it was intended to estimate the critical exponents γ , β and δ from them.

These model independent predictions of the scaling law approach have been confirmed by specific numerical calculations on an Ising model using both high temperature expansion techniques for various lattice structures (Chang and Lee 1980), and within the ferromagnetic phase of the so called SK model (Sherrington and Kirkpatrick 1975, Roshko and Williams 1984, Kunkel et al 1988b). In Figure 1.3 the calculated field and temperature dependent susceptibility, based on the effective field-theory approach due to Southern (1976), is plotted against the reduced temperature in various fields; the calculated susceptibility does indeed behave in the manner predicted by the equations shown above, exhibiting a peak whose height decreases, but the position in temperature of which increases with increasing field.

In Table 1.1 we give a summary of the definition of some magnetic critical exponents, and the predicted values from a number of theories and models. For the Landau, $2d$ Ising, and Spherical models the critical exponents are exact; for the $3d$ Ising, $3d$ planar and $3d$ Heisenberg models the critical exponents are found from approximate calculations, the related uncertainties are also listed.

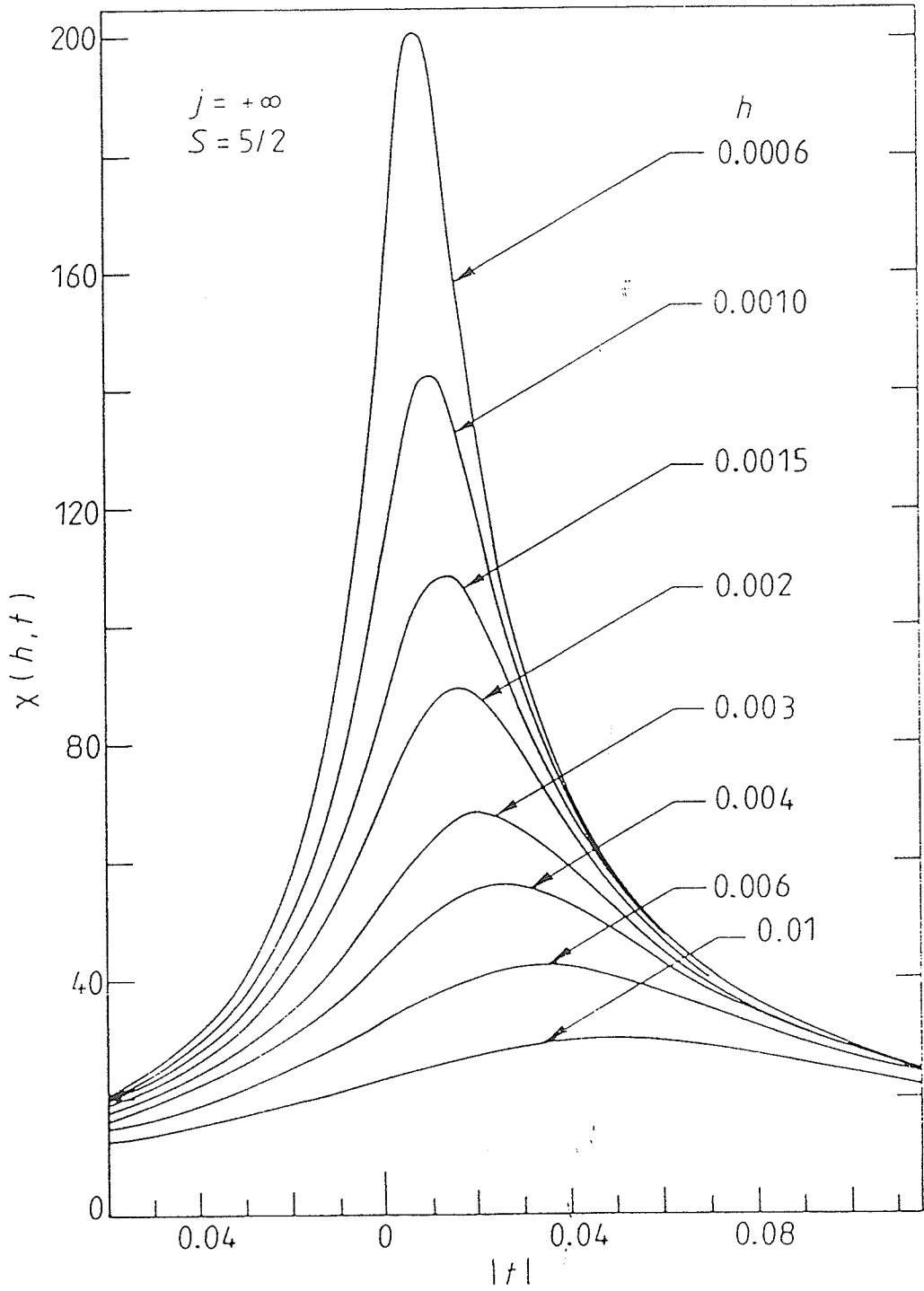


Figure 1.3: The field and temperature dependent susceptibility are plotted against the reduced temperature in various fixed fields calculated based on the SK model (after Roshko and Williams 1984).

The final test of any theory must be determined by experiment, therefore in Table 1.1 the predicted critical exponent values of the various models are compared with the range of values found experimentally. As shown in this table the values given by the solvable theories (Landau, $2d$ Ising, and Spherical) are not quantitatively correct. On the other hand, the predictions of the approximate calculations ($3d$ Ising, $3d$ planar and $3d$ Heisenberg models) do appear to mirror, to a certain extent, the data on ferromagnetic systems. Unfortunately, none of these models has been solved exactly.

Table 1.1: Summary of critical exponents values of models and experiments

Critical Exponent	γ	β	δ	α	ν
Power Law	$\chi \propto t^{-\gamma}$	$M \propto (-t)^\beta$	$M \propto H^{1/\delta}$	$c_H \propto t^{-\alpha}$	$\xi \propto t^{-\nu}$
Conditions	$H = 0$ $T > T_c$	$H = 0$ $T < T_c$	$H \geq 0$ $T = T_c$	$H = 0$ $T > T_c$	$H = 0,$ $T > T_c$
Landau	1	0.5	3	Discont	0.5
2d Ising	1.75	0.125	15	0	1
3d Ising	1.2378 ± 0.0006	0.326	4.78	0.106 ± 0.0003	0.6312
3d Planar	1.316 ± 0.009	0.345	4.81	-0.01 ± 0.007	0.669
3d Heisenberg	1.388 ± 0.003	0.367	4.78	-0.121	0.707 ± 0.003
Spherical	2	0.5	5	-1	1
Experiment	1.3 - 1.4	0.2 - 0.4	3 - 6	-0.3 - 0.3	0.6-0.7

1.3 Electrical Resistivity and SRA

1.3.1 General Properties

One characteristic property of a metal is its electrical conductivity. The calculated resistivity (Bloch 1930) of a pure metal, with electron-phonon coupling and no magnetic scattering, has the following behaviour

$$\rho_h(T) = 4\left(\frac{T}{T_D}\right)^5 f\left(\frac{T_D}{T}\right)\rho_D \quad (1.61)$$

where T_D is the Debye temperature, ρ_D is a constant, and $f\left(\frac{T_D}{T}\right)$ is a Debye integral.

At high temperature the resistivity is proportional to temperature; that is

$$\rho_h(T) \propto T, \quad T > T_D \quad (1.62)$$

as the Debye integral has the behaviour of $\frac{1}{4}\left(\frac{T_D}{T}\right)^4$. This equation agrees with experimental results quite well in a number of cases.

At low temperature $f(\infty) = 124.4$, so the resistivity varies approximately as

$$\rho_h(T) \propto T^5, \quad T < T_D \quad (1.63)$$

When a metal contains impurity atoms which yield additional scattering

its total resistivity ρ_T may sometimes be described by Matthiessen's rule

$$\rho_T(T) = \rho_h(T) + \rho_i(x) \quad (1.64)$$

where $\rho_h(T)$ is the resistivity of the pure host (described by the previous three equations), and $\rho_i(x)$ is the resistivity due to the impurity, which is independent of temperature and concentration x in the case of dilute alloys, specifically those systems in which the impurity is not magnetic (Ziman 1960).

Matthiessen's rule is not always obeyed, particularly when a magnetic transition metal impurity is dissolved in a paramagnetic host, the situation can be considerably more complicated. Various other temperature dependences in the resistivity have been observed, such as $\Delta\rho(T) = \rho_T(T) - \rho_h(T) \propto T, T^{3/2}, T^2$ and $\ln T$. Such dependences have been linked to various models describing scattering from magnetic, or nearly magnetic, impurities. For example, based on the localized spin fluctuation model (LSF model) Lederer and Mills (1968), and Kaiser and Doniach (1970) were able to show that, due to the scattering of conduction electrons in the LSF, the localized spin fluctuation electrical resistivity can exhibit four distinct temperature dependences: $\rho_{LSF}(T) \propto T^2$ at low temperature, becomes linear ($\rho_{LSF}(T) \propto T$) as the temperature increases, above the so called spin fluctuation temperature the resistivity is logarithmic ($\rho_{LSF}(T) \propto \ln T$), and finally the resistivity approaches a unitarity limit as $T \rightarrow \infty$.

When a metal or an alloy is subjected to a magnetic field, the electrical resistivity ρ of the substance will change, a result that has been known for

over a century (Thomson 1851). For many metals the increase in resistivity is proportional to H^2 at low fields, becoming linear at high fields, this result has been summarized by Kohler (1938) through the expression

$$\frac{\Delta\rho}{\rho_0} = f\left(\frac{H}{\rho_0}\right) \quad (1.65)$$

here ρ_0 is the resistivity in zero field, $\Delta\rho$ is the change of the resistivity due to the applied field, and f is a function depending only on the geometrical configuration and on the metal. The field induced increase in $\Delta\rho$ is referred to as the magnetoresistance.

In magnetic materials, additional sources of magnetoresistance cause complex behavior. For a number of ferromagnets, there is a simple relationship between $\Delta\rho/\rho_0$ and the magnetization M at temperatures close to the Curie temperature

$$\frac{\Delta\rho}{\rho_0} = a M^2 \quad (1.66)$$

where a is a constant, and $\Delta\rho$ is the variation in ρ due to the external field. The value of magnetoresistance is extremely small for most substances even at high field (in the order of 0.1% or less), but is relative large for strongly magnetic substances (for nickel, about two percent).

For a magnetic substance, even in the absence of an external magnetic field there will always be a magnetic induction $B = 4\pi M_s$ in the volume of each domain for $T < T_c$. The resistivity measured at zero applied field will

actually still have a magnetoresistance associated with the spontaneous magnetization $4\pi M_s$; in Ni this is 6400 gauss at room temperature. Therefore it is not surprising that substances with magnetic ordering have different resistivity and temperature dependence $\rho(T)$ at $T < T_c$ compared with substances not having magnetic order.

The magnetoresistance phenomenon is important because it throws light on the electronic structure of solids. For example, an extra field vector can resolve the degeneracy of a conductivity tensor with cubic symmetry. The force acting on an electron moving with the Fermi velocity in a magnetic field of a few kOe is much greater than the force extracted by any attainable electric field within the solid, and is thus much more powerful as an instrument for probing the electronic system.

For a polycrystal ferromagnetic conductor⁷, from symmetry arguments. Birss (1964) and Hurd (1974) found the resistivity tensor has the following form:

$$(\rho_{i,j}) = \begin{pmatrix} \rho_{\perp}(B) & -\rho_H(B) & 0 \\ \rho_H(B) & \rho_{\perp}(B) & 0 \\ 0 & 0 & \rho_{\parallel}(B) \end{pmatrix} \quad (1.67)$$

where $\rho_{i,j}(B)$ are functions of the magnetic induction B , which depends in

⁷In the case of single crystal ferromagnets it is found that the resistivity becomes dependent on the direction of current and the magnetization with respect to the crystal axes (Hurd 1974).

turn on the applied field H_a and the demagnetizing factor N of the conductor. Notice that the diagonal elements ρ_{\parallel} and ρ_{\perp} in the equation above are not equal. That means the resistivity depends on the relative orientation of the current \vec{J} and the magnetization \vec{M} .

The electric field \vec{E} is defined by $\vec{E} = \rho\vec{J}$, so with the resistivity tensor indicated above, the electrical field is

$$\vec{E} = \rho_{\perp}(B)\vec{J} + [\rho_{\parallel}(B) - \rho_{\perp}(B)][\vec{\alpha} \cdot \vec{J}]\vec{\alpha} + \rho_H(B)\vec{\alpha} \times \vec{J} \quad (1.68)$$

where $\vec{\alpha}$ is a unit vector in the magnetization direction, ρ_{\parallel} is the resistivity for \vec{J} parallel to \vec{M} , ρ_{\perp} is the resistivity for \vec{J} perpendicular to \vec{M} , and ρ_H is called the extraordinary Hall resistivity. In practice, measurements of the magnetoresistivity are usually made on a wire or strip sample with the measuring current (J) and magnetic field (H) either both parallel to the wire axis or perpendicular to each other. Constraining \vec{J} to flow along the wire axis and calling θ the angle between \vec{J} and \vec{M} , then from Equation (1.68) (Campbell and Fert 1982)

$$\rho_{B=0} = \frac{\rho_{\parallel} + 2\rho_{\perp}}{3} + (\cos^2\theta - \frac{1}{3})(\rho_{\parallel} - \rho_{\perp}) \quad (1.69)$$

For a magnetic substance, the spontaneous resistive anisotropy (SRA) of is particular interest. The spontaneous resistive anisotropy is a measure of the difference in the resistance of a single domain ferromagnetic conductor

in zero magnetic induction (B) when the magnetization lies parallel (\parallel) or perpendicular (\perp) to the current direction. It is usually defined by the ratio

$$\left(\frac{\Delta\rho}{\rho_0}\right)_{B\rightarrow 0} = 3\left(\frac{\rho_{\parallel}(B) - \rho_{\perp}(B)}{\rho_{\parallel}(B) + 2\rho_{\perp}(B)}\right)_{B\rightarrow 0} \quad (1.70)$$

The mechanism responsible for the spontaneous resistive anisotropy (SRA) of the conductor has been a subject of speculation for a considerable period. Based on spin-orbit coupling, two different but complementary approaches to the problem have been introduced, depending on whether the system is best described by a localised or by an itinerant model.

1.3.2 Localised Model

The localised model (Kasuya 1956, Kondo 1962) treats the $3d$ or $4f$ electrons, which tend to form magnetic moments, as localised at the lattice points, interacting with conduction electrons through the exchange interaction. The simplest test of this model, at least in principle, is to dilute rare-earth impurities; here the $4f$ electrons of the rare-earth impurities are completely localized and have a well defined total angular momentum⁸ \vec{J} . Limiting the expansion of the wave functions of the conduction electrons to s and p waves, the interaction between conduction electrons and the electric quadrupole of $4f$ electrons has the form (Kondo 1962)

⁸In order to keep consistent with the common notations frequently used in the literature, we have used \vec{J} to represent both total angular momentum and electrical current vector. For the same reason $\Delta\rho$ has been expressed as resistivity change both in magnetoresistivity and spontaneous resistive anisotropy expressions, as shown in Equations (1.65) and (1.70), respectively.

$$V_Q = -\frac{D}{(k_F)^2} \sum_{\vec{k}'} [(\vec{J} \cdot \vec{k})(\vec{J} \cdot \vec{k}') - \frac{1}{3}J(J+1)\vec{k} \cdot \vec{k}'] a_{\vec{k}'}^+ a_{\vec{k}} \quad (1.71)$$

where \vec{J} is the angular momentum of the rare-earth ion and $a_{\vec{k}'}^+(a_{\vec{k}})$ the creation (annihilation) operator of the conduction electron with wave vector \vec{k} . The total scattering potential then has the form

$$H_{scat} = \sum_{\vec{k}, \vec{k}'} [V + J_{ex} \vec{s} \cdot \vec{J} - \frac{D}{(k_F)^2} \{(\vec{J} \cdot \vec{k})(\vec{J} \cdot \vec{k}') - \frac{1}{3}J(J+1)\vec{k} \cdot \vec{k}'\}] a_{\vec{k}'}^+ a_{\vec{k}} \quad (1.72)$$

As indicated in this equation, in addition to the usual potential (V) and exchange (J_{ex}) scattering terms which are isotropic, at least in a polycrystalline sample, an interaction between the conduction electrons (with spin index \vec{s}) and the electric quadrupole moment (D) of the $4f$ electrons, can also exist. In the case of $V \gg D$, the resistive anisotropy takes the form (Friedrich and Fert 1974)

$$\frac{\Delta\rho}{\rho_0} = \frac{\rho_{||}(B) - \rho_{\perp}(B)}{\rho_0} = \frac{D}{V} \left[\langle J_z^2 \rangle - \frac{J(J+1)}{3} \right] \quad (1.73)$$

where ρ_0 is the zero-induction resistivity and $\langle J_z^2 \rangle$ the mean value of J_z^2 . As indicated in this equation the spontaneous resistivity anisotropy is proportional to the electronic quadrupole moment (D) of the particular rare-

earth ion. It is, therefore, not unexpected that the anisotropy vanishes in the case of zero electrical quadrupole moment ($D = 0$) such as Gd. The anisotropy also vanishes in the paramagnetic limits as $\langle J_z^2 \rangle \rightarrow \frac{J(J+1)}{3}$ when $B \rightarrow 0$.

This model is strongly supported by the observation of the spontaneous resistive anisotropy (SRA) of AuRE and AgRE alloys⁹. It is also confirmed by the result that the SRA of these alloys changes sign at the middle of the heavy rare-earth series (Friedrich and Fert 1974).

It is important to stress, however, that the localised model is not valid for a very wide range of magnetic materials, as it makes the rather stringent assumption of well localised spins. For example, the $3d$ transition metals probably do not satisfy this assumption as their spins are certainly not well localised.

1.3.3 Itinerant Model

In the itinerant model, initially proposed by Mott (1936, 1964) and Smit (1951), and later extended by Campbell et al. (1970), Berger (1978), Campbell and Fert (1982), and Malazemoff (1986), the $3d$ and $4s$ bands were divided into two sub-bands, depending on the spin direction. It is believed that some of the characteristic magnetic and electrical properties of the systems arise from their particular band structure. In Figure 1.4 the band structure of Ni at absolute zero is shown schematically. The $4s$ band is usually thought to contain equal numbers of electrons in both spin orientations; while the two

⁹Where RE stands for rear earth elements.

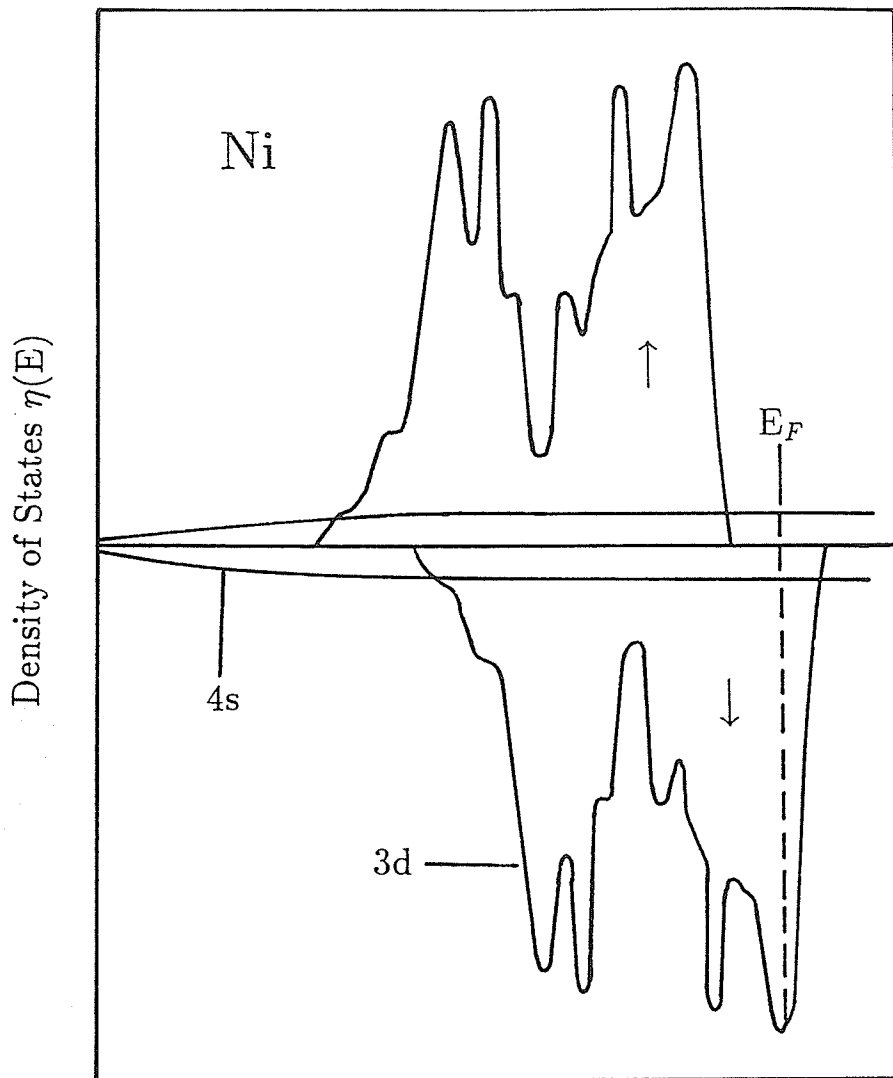


Figure 1.4: Band structure of Ni at absolute zero.

sub $3d$ bands have different numbers of electrons. As shown in this figure the $3d \uparrow$ band while lies below E_F is filled, and the $3d \downarrow$ band which lies partially above E_F is not filled. It is often convenient to speak of the ferromagnetism and the non-integral values of the saturation magnetization of the systems as arising from this band model (Stoner 1933).

The electrical transport properties of the system also can be interpreted by this energy band structure, and in particular the scattering processes can be characterised by a different cross-section in each sub-band with differing associated resistivities ρ_{\uparrow} and ρ_{\downarrow} . As shown in the figure, electrons of the majority sub-band with magnetic moment parallel to the total magnetization are indicated by \uparrow ; while electrons of the minority sub-band by \downarrow . Each of the sub-bands has its own "residual resistivity" which can be measured by comparing low and high temperature resistivities of samples containing a given impurity, or by measurements at low temperatures on samples containing two impurities simultaneously (Fert and Campbell 1968, Farrell and Greig 1968).

In the so called two current model shown in Figure 1.5, the two "resistors", ρ_{\uparrow} and ρ_{\downarrow} , are connected across the same seat of emf , so that the currents in the two branches are

$$i_{\uparrow} = \frac{V}{\rho_{\uparrow}} \quad (1.74)$$

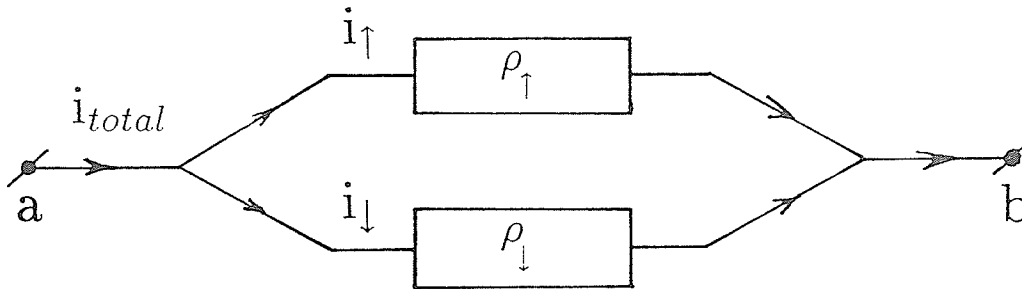


Figure 1.5: Two Current Model

and

$$i_{\downarrow} = \frac{V}{\rho_{\downarrow}} \quad (1.75)$$

Where V is the potential difference that appears between points a and b , and this gives the total observed resistivity of the system

$$\rho = \frac{\rho_{\uparrow}\rho_{\downarrow}}{\rho_{\uparrow} + \rho_{\downarrow}} \quad (1.76)$$

If there is spin-orbit coupling, however, spin mixing scatterings will exist and additional terms should also be included in the general expression of the total resistivity which now becomes (Fert and Campbell 1976):

$$\rho = \frac{\rho_{\uparrow}\rho_{\downarrow} + \rho_{\uparrow\downarrow}(\rho_{\uparrow} + \rho_{\downarrow})}{\rho_{\uparrow} + \rho_{\downarrow} + 4\rho_{\uparrow\downarrow}} \quad (1.77)$$

where $\rho_{\uparrow\downarrow}$ is the resistivity associated with the transfer of electron between sub-bands induced by spin-flip scattering processes (Fert 1969). The microscopic origin of anisotropy in this model is based on the effects of spin-orbit coupling H_{so} (Smit 1951)

$$H_{so} = \lambda \vec{L} \cdot \vec{S} = L_Z S_Z + \frac{\lambda}{2}(L_+ S_- + L_- S_+) \quad (1.78)$$

where the first term lifts the degeneracy of the d states of a given spin, and the off-diagonal terms, $\frac{\lambda}{2}(L_+ S_- + L_- S_+)$, in the coupling result in an admixture between the two $(2l + 1)$ fold orbitally degenerate subgroups that have been split predominantly by the effect of the exchange field H_{ex} on the spin. Specifically, in the case of Ni based alloys without spin-orbit coupling there are no $3d$ band states at the Fermi level for spin \uparrow as shown in Figure 1.4. Without spin-orbit coupling ρ_{\uparrow} is due to $s - s$ scattering only, as there is no d band state at the E_F level for spin \uparrow ; while ρ_{\downarrow} induces both $s - s$ and $s - d$ scattering. In the presence of spin-orbit coupling, however, some $3d \uparrow$ character is mixed into the $3d \downarrow$ density states at the E_F . Since $d \uparrow - d \downarrow$ admixing is anisotropic, the resistivity contribution resulting from the opening of this $s \uparrow - d \downarrow$ scattering channel is also anisotropic, with the magnetization direction defining the axis for spin-orbit coupling. While the underlying physics is thus well understood, calculation of the associated

resistive anisotropy is complicated by the lack of detailed knowledge of such quantities as the scattering potential and realistic band structure. However, with suitable simplifying assumptions applied to the latter Campbell et al (1970) have derived the following expression

$$\frac{\Delta\rho}{\rho} = \frac{\rho_{\parallel} - \rho_{\perp}}{\rho_{\perp}} = \frac{\gamma(\rho_{\downarrow} - \rho_{\uparrow})\rho_{\perp}}{\rho_{\uparrow}\rho_{\downarrow} + \rho_{\uparrow\downarrow}(\rho_{\uparrow} + \rho_{\downarrow})} \quad (1.79)$$

At temperatures low compared with the Curie temperature T_c (so that $\rho_{\uparrow\downarrow} \approx 0$) this leads to the well-known result

$$\frac{\Delta\rho}{\rho} = \gamma(\alpha - 1) \quad (1.80)$$

where γ is a spin-orbit constant and $\alpha = \rho_{\downarrow}/\rho_{\uparrow}$ is the resistivity ratio for spin-down and spin-up which can be derived from the observed deviations from Mattiessen's rule (Campbell et al 1970, Dorleijin 1976). The above equation indicates that at low temperature the spontaneous resistive anisotropy in dilute nickel alloys is an increasing function of the ratio $\alpha = \rho_{\downarrow}/\rho_{\uparrow}$. According to this equation if one were to plot $\Delta\rho/\rho$ as a function of $(\alpha - 1)$, it should result a straight line with a slope of γ . At high temperatures as $\alpha \rightarrow 1$, Equation (1.80) predicates $\Delta\rho/\rho$ should go to zero. Although this equation does not reproduce correctly the detailed behaviour of the SRA (presumably as a result of the numerous simplifying and limiting assumptions made in arriving at the equation) (Dorleijin and Miedema 1976; Malozemoff 1986), it does provide a reasonably good description of the general features of the

spontaneous resistive anisotropy data on Ni-based alloys¹⁰ where the polarizing exchange field is large. The data show an approximately linear increase of $\Delta\rho/\rho$ with $(\alpha - 1)$, the slope of which yields γ ($\gamma \approx 0.0075$).

The itinerant model expression for SRA (Equation 1.80) also can be used to interpret the data of amorphous and hydrogenated FeZr in a semi-quantitative manner (Ma et al 1990). At low temperatures, the spin \uparrow and spin \downarrow subbands are exchange split and a nonzero SRA results. As the temperature increases and thermal fluctuations compete with the exchange splitting, the subband occupations tend to equalize, resulting in a decline in both α and SRA. This process continues until the exchange field collapses at $T = T_c$.

The appearance of a nonzero SRA at low field with hydrogen loading confirms the elevation of T_c above room temperature. While the increase in SRA with increased hydrogen content can be interpreted as an effective transfer of d like electrons from the spin \downarrow to the spin \uparrow band, this leads to an increase in ρ_{\downarrow} and α ; therefore increasing the SRA.

To date, however, no investigation of the spontaneous resistive anisotropy in systems close to the ferromagnetic percolation threshold has been performed, and no specific theoretical predication for its behaviour exists. This has prompted us to do such an investigation in the Pd based dilute alloys.

¹⁰Campbell et al (1970) measured samples of NiTi , NiV , NiCr , NiMn , NiFe , and NiCo at concentrations below 16%.

Chapter 2

Review

2.1 Introduction

Dilute palladium based alloys, especially with Fe, Co, Ni and Mn, have attracted much experimental and theoretical interest. A review of the experimental results on such alloys will be presented in this chapter, with particular emphasis placed on their magnetic and electrical properties.

2.2 Pure Palladium

A number of remarkable effects, such as “giant impurity magnetic moments”, shown by dilute Pd alloys can be ascribed to the particular properties of the host. A brief discussion of pure palladium, therefore, is necessary.

Palladium is one of the few d elements which shows neither magnetism nor superconductivity. Being atomically quite similar to nickel, which has ten electrons outside the argon shell, palladium has ten electrons outside the krypton shell. The ground state configuration of the Pd atom is $4d^{10}$ with the first excited state $4d^9 5s^1$ only 0.813551 eV higher than the ground state (McLennan and Smith 1926). When atoms are brought closer together to form metallic palladium, the energy levels are modified as illustrated in Figure 2.1. The $4d$ levels spread into a narrow $4d$ band, and the $5s$ levels are spread into a much wider $5s$ band. These bands overlap in energy, and the d band contains approximately 0.36 holes per atom, equal to the number of electrons in the s band. This kind of band structure is very similar to that of itinerant ferromagnets such as Ni.

From the band structure, specifically the density of states curve, the

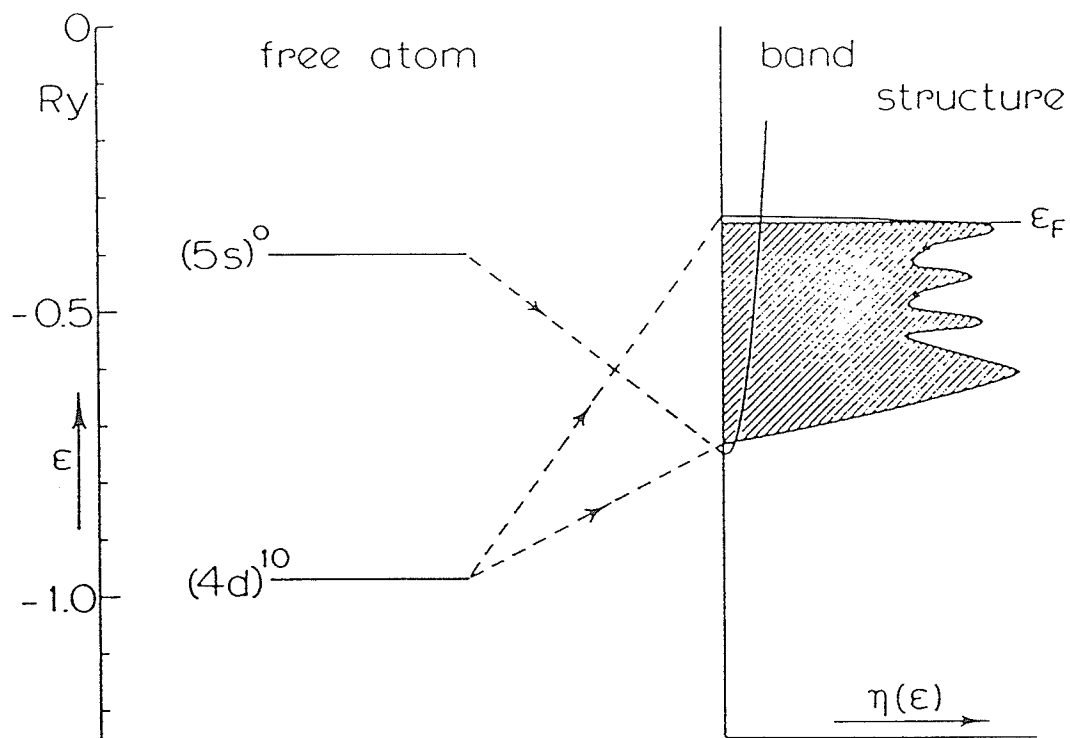


Figure 2.1: Energy levels and energy band structure of Pd (after Nieuwenhuys 1974).

susceptibility of a metal can be estimated via the Pauli spin susceptibility expression

$$\chi_p = 2 \mu_B^2 N(E_F) \quad (2.1)$$

where μ_B is the Bohr magneton, and $N(E_F)$ is the density of state at Fermi energy¹. The calculated susceptibility of pure Pd using this equation is $0.8 \times 10^{-4}(\text{emu/mol})$, which is already much larger than that for other non magnetic metals, but is still approximately an order of magnitude smaller than that measured experimentally. It is possible to resolve this discrepancy in terms of Stoner's theory, in which the effect of the electron interactions is considered. To a first approximation, the susceptibility of an interacting electron system can be calculated from (Stoner 1938)

$$\chi = \frac{2 \mu_B^2 N(E_F)}{1 - \bar{I}} = \frac{\chi_p}{1 - \bar{I}} \quad (2.2)$$

where χ_p is the Pauli susceptibility shown in Equation (2.1), and $(1 - \bar{I})$ is called the Stoner susceptibility enhancement factor². Based on the specific data for pure Pd metal $\bar{I} = 0.9$ (Doniach and Engelsberg 1966), this leads to a calculated susceptibility which agrees with the experimental measurements quite well. As \bar{I} has a value close to one, palladium is sometimes called

¹ $N(E)$ defined as the number of states per unit of energy per spin direction per atom at the energy E .

² $\bar{I} = IN(E_F) > 1$ is called the Stoner ferromagnetism criterion, and I is an effective interaction energy between the electrons; obviously when $\bar{I} = 1$ the susceptibility χ diverges, i.e the system becomes ferromagnet. This condition is referred to us the Stoner criterion for ferromagnetism.

“nearly ferromagnet” (Wohlfarth 1976).

By considering the nonlinear magnetization (Muller et al 1970) of Pd in high field, to a second approximation, Wohlfarth (1976) has shown that the susceptibility of strong paramagnets like Pd has following form

$$\chi = \frac{2 \mu_B^2 N(E_F)}{1 - \bar{I}} \left[1 + \frac{1}{2} \frac{\mu_B^2 N(E_F)}{(1 - \bar{I})^3} H^2 \left\{ \frac{N''}{N} - 3 \left(\frac{N'}{N} \right)^2 \right\} \right] \quad (2.3)$$

where N' is $\frac{\partial N(E)}{\partial E}$, and N'' is $\frac{\partial^2 N(E)}{\partial E^2}$. This equation gives an independent way of estimating the Stoner susceptibility enhancement factor $(1 - \bar{I})$ by estimates of the coefficient of H^2 . There have been several estimates of the coefficient of H^2 for Pd (Lipton and Jacobs 1971, Muller et al 1970). An effect of about 0.5% was observed for $H = 350 \text{ kOe}$, the effect going as H^2 .

2.3 Palladium Based Magnetic Alloys

2.3.1 Magnetic Moment and Magnetic Phase Diagrams

Pd is itself not magnetic at any temperature, but its 3d magnetic alloys $\text{Pd}_{1-x}\text{Fe}_x$, $\text{Pd}_{1-x}\text{Co}_x$, $\text{Pd}_{1-x}\text{Ni}_x$ and $\text{Pd}_{1-x}\text{Mn}_x$ have shown ferromagnetic order for x as small as 0.1 at%. Meanwhile, at low impurity concentration, the magnetic moment associated with the dissolved impurity is very large, typically $10 \mu_B$ per impurity atom. Since in pure transition metals the magnetic moment is about $2.2 \mu_B$ per atom or less, the associated moment with each magnetic impurity in Pd based alloys is called a “giant moment”. The value of the moment is concentration dependent, decreasing with increasing

concentration of magnetic impurities. In the case of PdFe alloys, the magnetic moment per Fe atom first rises from $2.2 \mu_B$ in pure Fe to about $6 \mu_B$ in 10 at% Fe alloy. Below 10 at% Fe, the magnetic moment per Fe atom rises rapidly to a value of about $10 \mu_B$ at 1 at% Fe.

A similar behavior has been found in dilute PdCo, PdNi and PdMn alloys. It should also be pointed out that the "giant moment" has also been observed in the paramagnetic concentration range in these alloys³. Obviously, the observed "giant moment" in dilute Pd based alloys can not possibly be due to the magnetic impurity alone. It is quite natural, therefore, to assume that the "giant moment" in such alloys, in which there is practically no direct exchange interaction between distant impurity atoms, is caused by an indirect exchange mechanism in which an active role is played by the conduction electrons of the host, the *d* hole spins of neighboring Pd atoms are polarised by the localized moments of the dissolved magnetic atoms. Early neutron experiments suggested that the induced Pd moments saturate at low impurity concentration, with polarization ranges up to about 10 \AA (Low and Holden 1966). More recently it has been proposed that saturation occurs only at higher impurity concentration with a polarization range on the order of the nearest-neighbour distance, and ferromagnetism occurs through a percolation process between otherwise isolated polarization clouds at low temperature (Ododo 1985).

³Obtained from the Curie constant.

When the saturation magnetic moment is written as

$$\mu_{sat} = g_{eff} J \mu_B \quad (2.4)$$

the question arises immediately of how to describe the observed "giant moment". Three possible approaches have been suggested.

(a) a large value effective Lande factor g_{eff} and a normal value of the magnetic quantum number J .

(b) a small value of g_{eff} and a large J .

(c) an enhancement of both the effective Lande factor and the magnetic quantum number.

The first approach⁴ has support from measurements of the specific heat (Nieuwenhuys 1975), while the magnetic measurements, in contrast, favour approach (b) (McDougald and Manuel 1968, 1970). Magnetoresistance measurements (Grassie et al 1971, Kleiman and Williams 1982), however, indicate an enhancement of both the quantum number J and the Lande factor g . This latter approach has the advantage that it gives the better description not only the data of PdMn, but also the data of other Pd based dilute alloys such as PdFe and PdCo.

The magnetic phase diagrams of dilute Pd based alloys with Mn, Fe and Co have been studied by many investigators and these are surveyed below.

The magnetic phase diagram of the PdMn system has been investigated

⁴This approach needs to assume a distribution of g values the origin of which is not clearly specified.

using a variety of transport, magnetic and thermal methods (e.g. Ho et al 1981a, b). The following magnetic states have been found from pure palladium to pure manganese, namely paramagnetism, spin glass, ferromagnetism, mixed state, spin glass, and antiferromagnetism. In the limit of very high dilution, Mn impurities possess a stable moment with a Kondo temperature T_k well below 0.01 K. Such a magnetic moment polarizes the Pd $4d$ electrons and results in an impurity giant magnetic moment of about $7.8 \mu_B$ per Mn atom (Star et al 1975). As the Mn concentration is increased from the isolated impurity limit, the exchange coupling between impurities will initially be of RKKY type, and while a spin glass like state exists at very low temperature (Thomson and Thompson 1979), most of the studies of this system have been carried out on samples with Mn impurity concentration more than 0.1 at%, and the corresponding transition temperature is near or above 1 K.

In Figure 2.2, the experimentally determined magnetic transition temperatures of the system have been plotted against the Mn impurity concentration. This figure indicates that the ferromagnetic transition temperature increases smoothly with increasing Mn impurity concentration from 1.65 K for 0.5 at% Mn to 6.0 K at 2.5 at% Mn. Further increases in impurity concentration result in the magnetic transition temperature falling. Still further increases in Mn concentration (from 5.0 at% Mn), produce a spin glass (up to about 25 at% Mn), and the spin glass freezing temperature increases with increasing impurity concentration, i.e. 3.15 K for 5.5 at% Mn and 8.05 K at 10.45 at% Mn alloy, with $\frac{dT_f}{dx} \approx 0.99$ K/at% impurity. The current in-

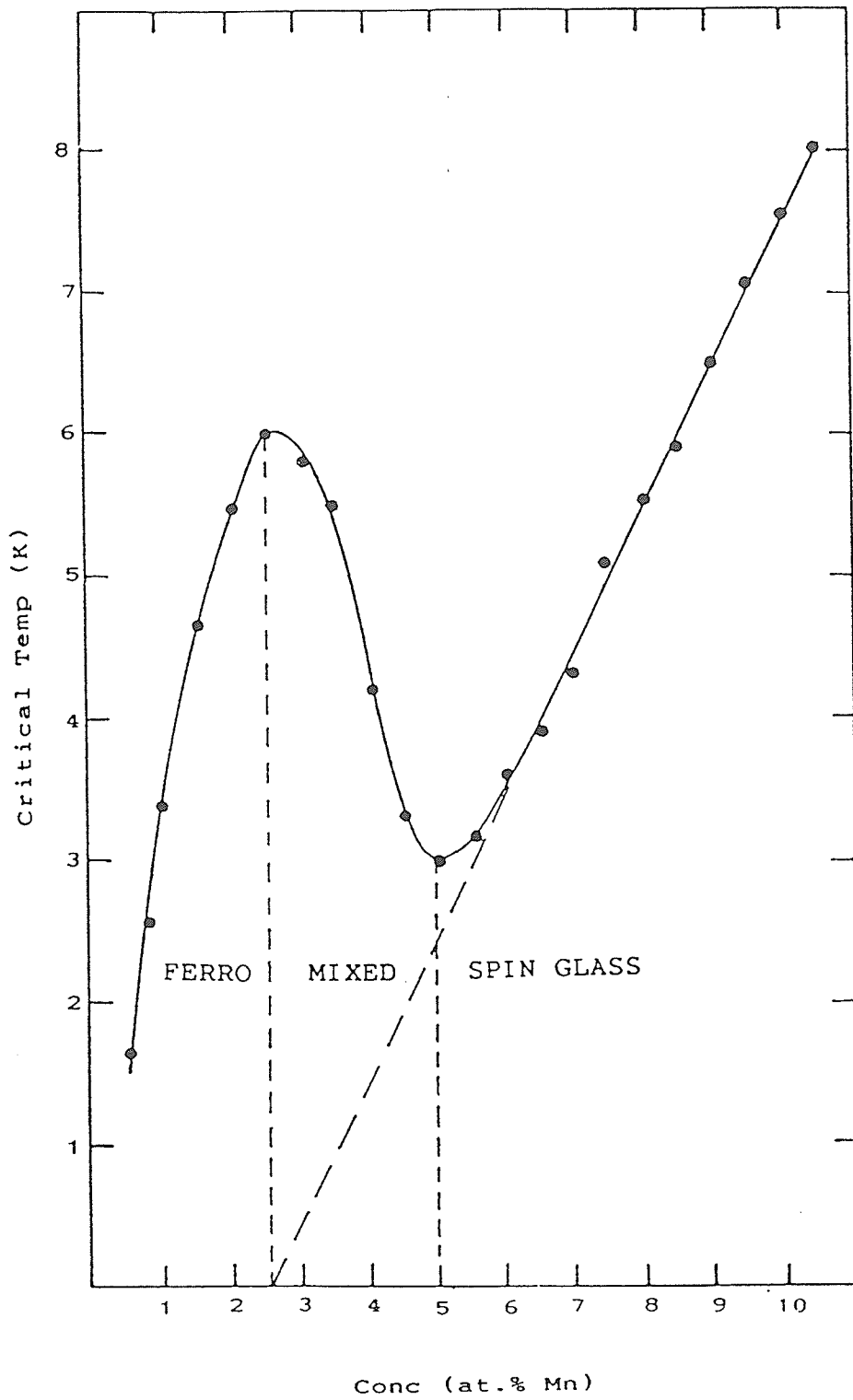


Figure 2.2: Magnetic phase diagram for PdMn alloys (after Ho 1982).

interpretation of the phase diagram discussed above suggests that at low Mn concentration the average Mn separation falls inside the first zero in the modified RKKY polarization as shown in Figure 2.3; direct overlap between giant moments becomes possible and results in a predominantly ferromagnetic ground state. Beyond 5.0 at% Mn, the competition between long range indirect RKKY mediated ferromagnetic coupling and near neighbour coupling, which is antiferromagnetic between the half-filled d -shells appropriate for Mn (Moriya 1967), produces a spin glass ground state with zero spontaneous magnetization. While at the intermediate concentrations (typically 2–5 at% Mn), the mixed state results from the presence of predominantly ferromagnetic Mn–Mn indirect interactions via the polarised Pd d band and the increasing influence of antiferromagnetic Mn–Mn direct coupling (Moriya 1967). The associated spin frustration effects cause a decrease of the ordering temperature as the impurity concentration increases in this region.

Dilute PdFe alloys are soft ferromagnets down to impurity concentrations as low as about a few hundred ppm Fe with $\frac{dT_c}{dx} \approx 40$ K/at% Fe (McDougald and Maunel 1968, 1970). Below approximately 100 ppm Fe, the system becomes a spin glass⁵ (Peters et al 1984), while between the ferromagnetic and spin glass regimes is the so called reentrant regime (Kornik et al 1988). Unlike uniform ferromagnets such as pure Ni, the onset of ferromagnetic ordering in dilute PdFe does not occur at a sharply defined temperature. The transition becomes broader with decreasing Fe concentration.

⁵Pd alloys with as low as 2.2 ppm Fe show the spin glass behavior at ultra low temperature with a freezing temperature 0.19 mK .

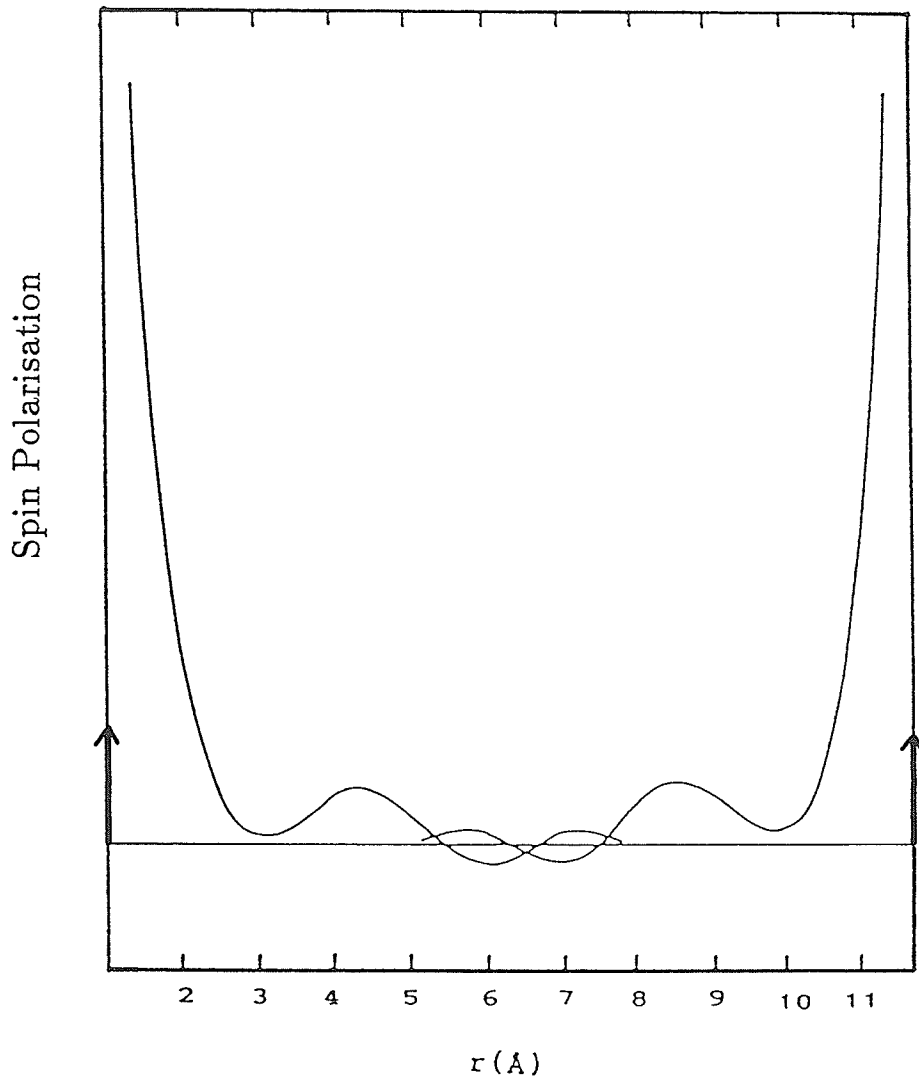


Figure 2.3: Interaction between distant impurity moments through the tails of the associated RKKY polarisations.

A summary of the currently available data, in the form of the experimentally determined magnetic ordering temperatures as a function of Fe concentration for less than 15 at%, is illustrated in Figure 2.4. As this figure indicates, the magnetic phase diagram is simpler than that of PdMn. Much lower impurity concentrations were needed in PdFe alloys to produce similar Curie temperature to PdMn; for example, only 0.25 at% Fe is needed, in contrast to 1.5 at% Mn, in order to have the transition temperature in the liquid helium range. The impurity concentration dependence of the Curie temperature, however, does not exhibit a simple relationship. To give a very rough sketch, we might say the transition temperature is linear at large impurity concentration (above 2 at% Fe), is proportional to the square of Fe concentration at lower concentration (below about 1 at% Fe), and between about 1 and 2 at% Fe is the intermediate range. There is no clear cut ferromagnetic percolation threshold in this system.

Dilute PdCo alloys are, in many respects, very similar to PdFe alloys. Experimental results show that ferromagnetism also exists in PdCo alloys down to very low impurity concentration, about 0.1 at% Co. A "giant moment" of about $10 \mu_B$ is associated with each Co atom, so dilute PdCo alloys must also contain a large induced magnetic polarization of the Pd atoms in the vicinity of the Co atoms, which is analogous to the magnetic role of an isolated Fe in Pd. The value of the magnetic moments is also impurity concentration dependent and decreases with increasing Co concentration. Dilute PdCo alloys have very similar ordering temperatures to dilute PdFe alloys,

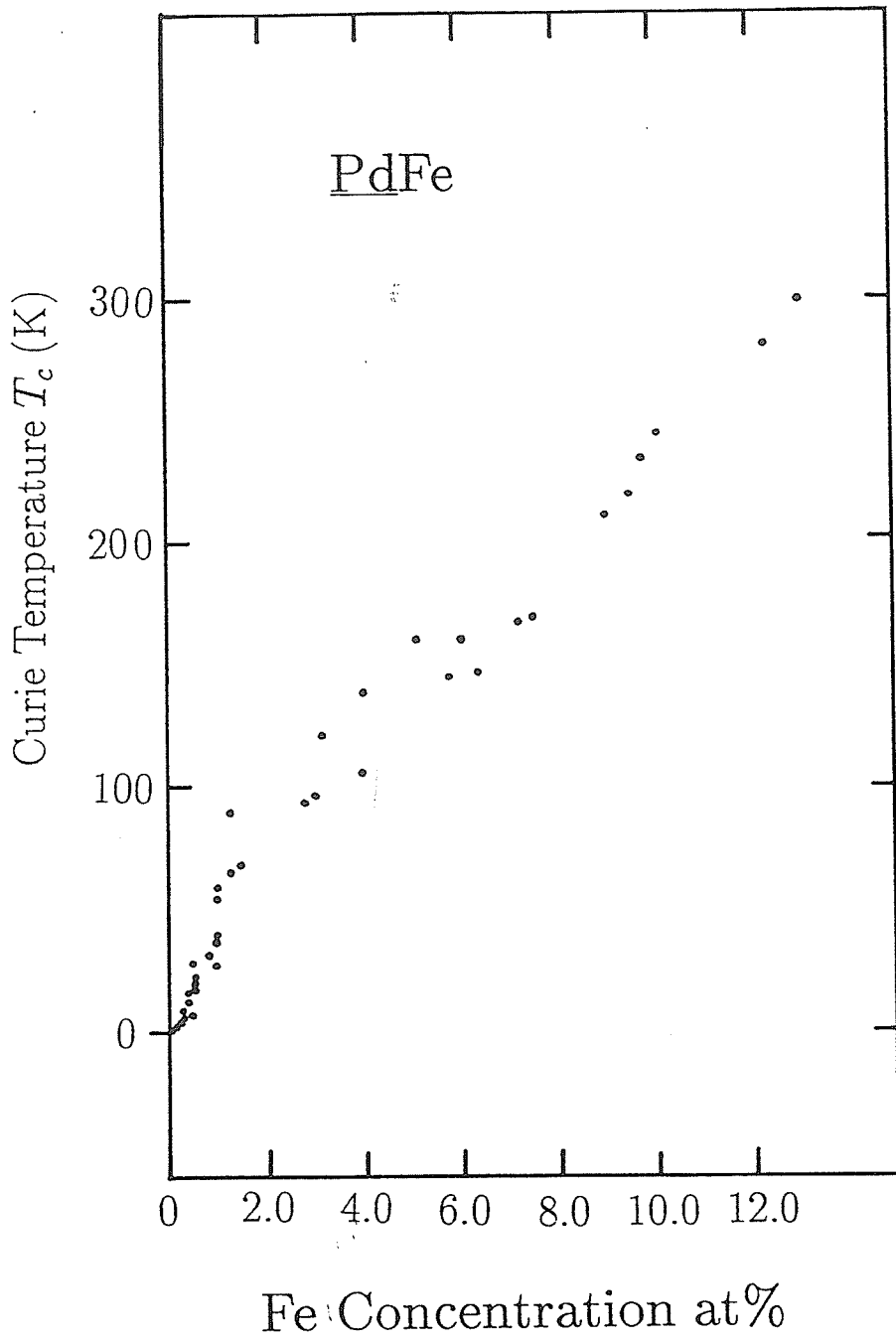


Figure 2.4: Magnetic phase diagram for PdFe alloys (selected data listed in Nieuwenhuys' thesis 1974)

and comparison of the concentration dependence of the transition temperature between them is possible. As shown in Figure 2.5, the ratio $\frac{dT_c}{dx} \approx 40$ K/at% impurity is also evident in the PdCo system, and again no simple relationship exists between transition temperature and Co concentration. The onset of ferromagnetism does not occur at a sharply defined temperature, but rather over a wide temperature range.

Expressions for the Curie temperature of dilute Pd based alloys have been derived by Takahashi and Shimizu (1965), by Kim (1966) and by Long and Turner (1970) based on the molecular field, itinerant and localized theories, respectively. These expressions predicate that T_c is proportional to the impurity concentration of the alloys which is not in agreement with experimental results over all concentration ranges.

PdNi alloys occupy an unique position in the broad spectrum of magnetic solid solution alloys. One question that has been debated is how to correctly describe the state of isolated Ni moments in Pd. There are two main approaches.

Analysis of elastic diffuse neutron scattering measurements (Aldred et al 1970, Parra and Medina 1980) inferred that dilute PdNi is an inhomogeneous system, so that the magnetic properties of the system depends critically up on its local environment. In contrast to Mn, Fe or Co in Pd, isolated Ni atoms are non magnetic. In dilute PdNi some authors claim that only a fraction of the Ni atoms in nearest neighbour pairs (Aldred et al 1970), or clusters of three or more nearest neighbour Ni atoms, are magnetic (Chouteau

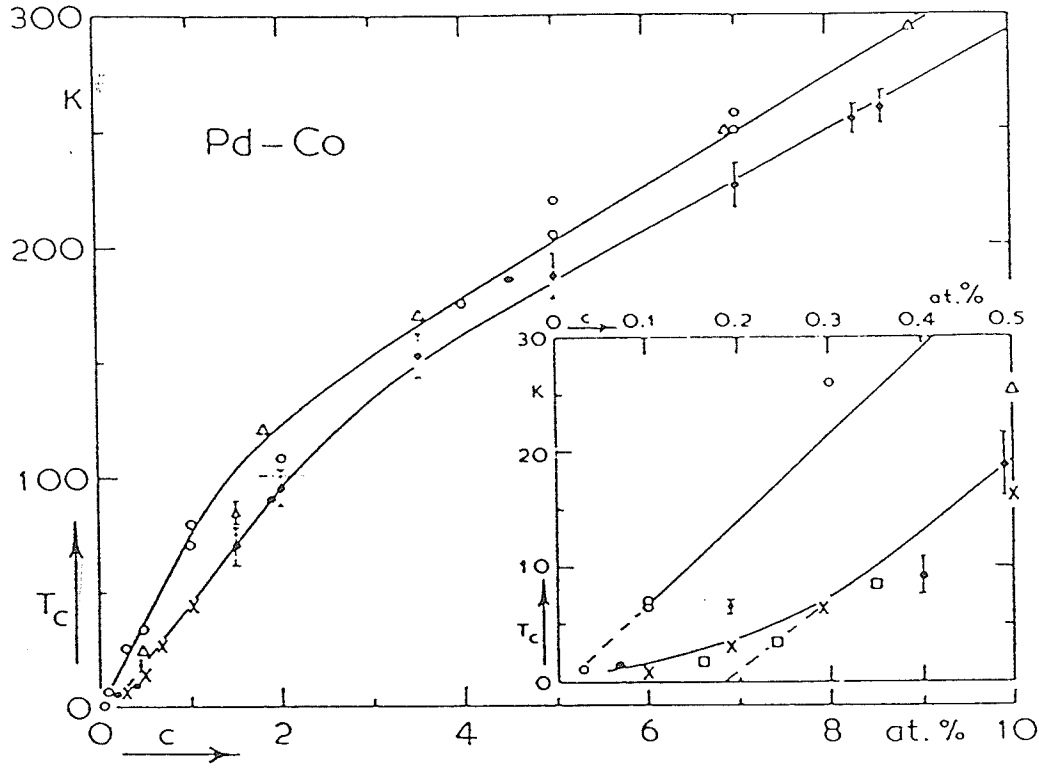


Figure 2.5: Magnetic phase diagram for PdCo alloys (after Boerstael 1970).

et al 1974, Cheung et al 1981). Magnetization measurements reveal strongly curved Arrott plots, and the behaviour of the temperature and field dependence of the susceptibility also support the inhomogeneous model (Murani et al 1974, Sain and Kouvel 1978, Cheung et al 1981). However, the absence of spin glass or micromagnetic order for Ni concentration less than the ferromagnetic percolation threshold has been taken as strong evidence against the inhomogeneous model (Loram and Mirza 1985).

Other approaches agree that local environment plays some role in PdNi alloys, but nevertheless assume the system is magnetically homogeneous. This suggests that all the Ni atoms dissolved in Pd are non magnetic in the static Hartree-Fock sense, but with localized spin fluctuations. This model has been applied to interpret electrical resistivity, magnetostriction and thermal expansion measurements (Lederer and Mills 1968, Fawcett et al 1968). More recently Loram and Mirza (1985) reanalysed the susceptibility and magnetization data quoted above and suggested the results are not inconsistent with the homogeneous model.

Despite the controversy over the correct description of the state of isolated Ni moments in Pd, there is general agreement that the occurrence of long ranged ferromagnetism lies in the range 2 to 5 at% Ni. Figure 2.6 shows the experimental data for the Ni concentration dependence of Curie temperature in PdNi alloys. The $T_c(x)$ for the alloys is, in general, similar to those for PdFe and PdCo alloys; T_c is roughly linear for higher impurity concentrations and proportional to x^2 for small amounts of Ni in Pd. It should be noted

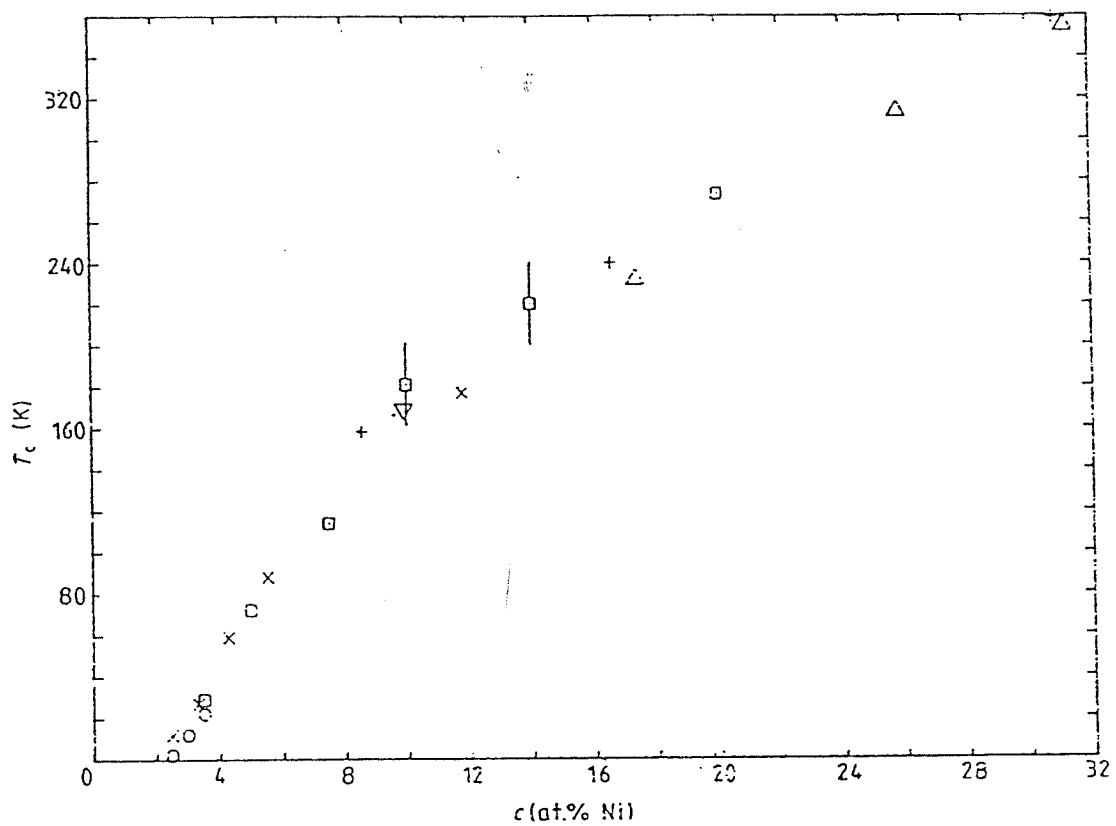


Figure 2.6: Magnetic phase diagram for PdNi alloys (after Loram et al 1985).

that in order to have the same transition temperature as PdFe and PdCo, a higher concentration of Ni is needed; for example, one needs about 22 at% Ni, compared with about 10 at% impurity in the case of PdFe and PdCo, to have T_c near room temperature. It also should be pointed out that unlike PdFe and PdCo alloys, the Curie temperatures of PdNi alloys goes to zero at rather high impurity concentrations.

2.3.2 Magnetization, Susceptibility and Critical Exponents

Magnetization and susceptibility measurements are important in order to determine the magnetic moment, the magnetic quantum number, the transition temperature, the critical exponents and other physical parameters of a specimen. Much of the results shown in the Section 2.3.1 were obtained from these two measurements, in fact magnetization measurements were the first to reveal a "giant moment" in dilute PdFe and PdCo alloys (Bozorth et al 1961).

From measurements of the magnetization and susceptibility it has now been shown that the "giant moment" exists in dilute Pd based systems not only in the ferromagnetic phase, but also in the paramagnetic regime, down to the very dilute limit. These two measurements also show that dilute PdFe is a soft ferromagnet and that the magnetization at $T \ll T_c$ saturates in small applied fields (e.g Chouteau and Tournier 1972). Early susceptibility measurements showed PdFe to have a "giant moment" of about $10 \mu_B/\text{Fe atom}$ (Crangle and Scott 1965). Theoretical predictions (Nieuwenhuys 1975), as

well as the susceptibility measurements (Webb et al 1979), have indicated that very low concentration PdFe alloys are spin glasses. SQUID susceptibility measurements (Peters et al 1984), at ultra low temperatures on Pd with 2.2 to 100 *ppm* Fe, have demonstrated typical spin glass behavior, and shown that these samples have freezing temperatures between 0.19 and 9.0 *mK*, or a ratio of freezing temperature to Fe concentration $\frac{dT_f}{dx} \approx 83 \mu\text{K}/\text{ppm Fe}$.

Measurements of magnetization and susceptibility indicate that dilute PdCo and PdNi alloys are magnetically harder, and they appear to be technically saturated by an applied field on the order of a few hundred *Oe*. However, high field magnetization measurements show that the magnetization does not become truly saturated even in magnetic fields up to 140 *kOe* (e.g. Loram et al 1985).

Dilute PdMn alloys are ferromagnets below about 2.5 at% Mn with a zero field susceptibility peaked at a value close to the limit set by the sample's dimensions (N^{-1}) below a well defined Curie temperature (Ho et al 1981a). Similar to dilute PdNi and PdCo alloys, the magnetization of PdMn alloys only becomes truly saturated when very strong magnetic fields are applied (Star et al 1975).

The detailed critical behavior of a series of dilute PdMn alloys has been investigated previously by Ho et al (1981a, b). For low Mn concentration alloys ($0.5 \leq x \leq 2.5$), the critical exponent δ decreases systematically with increasing Mn concentration from 4.0 (at 0.5 at% Mn), which is close to that obtained for elemental ferromagnets such as Ni, to about 3.3 at 2.5 at%

Table 2.1: Summary of critical exponents values for PdMn alloys (after Ho 1982).

Mn (at%)	δ	γ	μ_{eff} (μ_B/Mn)	T_c or T_f (K)
0.5	4.0 ± 0.15	1.37	12.3	1.65 ± 0.01
0.75	4.0 ± 0.15	1.32	10.2	2.59 ± 0.01
1.0	3.7 ± 0.15	1.34	9.6	3.37 ± 0.01
1.5	3.6 ± 0.15	1.30	9.0	4.65 ± 0.01
2.0	3.4 ± 0.15	1.34	8.3	5.46 ± 0.01
2.5	3.3 ± 0.15	1.36	7.5	6.00 ± 0.01
3.0	$\delta_l = 3.4; \delta_h = 3.4$ ± 0.15			5.8 ± 0.1
3.5	$\delta_l = 3.8; \delta_h = 3.1$ ± 0.15			5.5 ± 0.1
4.0	$\delta_l = 4.0; \delta_h = 2.9$ ± 0.15			4.2 ± 0.1
4.5	$\delta_l = 4.2; \delta_h = 2.8$ ± 0.15			3.2 ± 0.1
5.0	spin glass			2.79 ± 0.05

Mn; the values for critical exponent γ lie in the range 1.30 to 1.37 close to the $3d$ Heisenberg model prediction which is listed in Table 1.1. For Mn concentrations above 2.5 at% no unique critical exponent γ value can be determined. The critical exponent values, together with corresponding μ_{eff} and T_c values deduced from ac susceptibility data, are summarised in Table 2.1; here δ_l and δ_h are δ values extrapolated from low and high field, respectively.

With the exception of dilute PdMn alloys, knowledge of critical exponents in Pd based dilute alloys is still rather limited. To date, no extensive experimental work establishing critical exponent values for dilute PdFe, PdCo or PdNi alloys has been carried out, though Kouvel and Comly (1971) did investigate a small number of dilute PdFe alloys.

2.3.3 Electrical Resistivity, Magnetoresistivity and Spontaneous Resistive Anisotropy (SRA)

Measurements of the electrical resistivity of dilute Pd based alloys have been carried out by many workers so its behaviour has been well established.

Williams and Loram (1969) measured the resistivity of a number of PdFe alloys with Fe contents less than 1 at%. Their results indicate that at temperature well below T_c , the incremental resistivity⁶ $\Delta\rho$ varies with temperature as

$$\Delta\rho \propto Bx^{-1} T^{3/2} \quad (2.5)$$

⁶The incremental resistivity $\Delta\rho$ is defined by $\Delta\rho(T) = \rho_{alloy}(T) - \rho_{Pd}(T)$.

where B is a numerical factor, and x is the impurity concentration. Just below the Curie temperature, however, a linear decrease of the $\Delta\rho$ with temperature (T) was observed. This agrees well with the theoretical prediction made by Long and Turner (1970).

At higher impurity concentrations ($x \geq 2$ at% Fe), a T^2 resistivity variation⁷ replaces the $T^{3/2}$ behaviour (Skalski et al 1970) which is believed to be the result of electron-magnon scattering with and without momentum conservation, respectively.

Dilute PdCo alloys have a very similar behavior of temperature dependence of the resistivity (Williams 1970); that is at low temperatures ($T \ll T_c$) the incremental resistivity $\Delta\rho$ is proportional to $T^{3/2}$ and at higher temperatures $\Delta\rho$ varies with T .

Early resistivity measurements showed that the dilute PdMn alloys exhibit a sudden linear decrease in resistivity below a temperature which varies with Mn concentration and which corresponds approximately to the Curie temperature of the alloy (Sarachik and Shaltiel 1967).

Ho et al (1980a) have shown that the temperature dependence of the resistivity of dilute PdMn alloys is qualitatively similar to that observed in PdFe and PdCo alloys, with a change of slope in $\rho(T)$ at T_c and follows a $T^{3/2}$ limiting form at low temperature. In comparing the width of the transition at the Curie temperature for the PdMn, PdFe and PdCo samples with the same T_c , a decrease in width from PdCo to PdMn was observed (Nieuwenhuys

⁷ $\rho = \rho_0 + pT^2$, where p is a constant.

1975).

Unlike “good moment” systems such as PdFe, the temperature dependence of dilute PdNi alloys has a different feature. It is difficult to interpret the resistivity data in a quantitative way and the Curie temperature is not easy to detect in the $\rho - T$ curve. Nevertheless Tari and Coles (1971) fitted their resistivity measurements to the expression⁸

$$\rho = \rho_0 + AT^n \quad (2.6)$$

and extrapolated the critical concentration for the system by plotting A against Ni concentration as shown in Figure 2.7.

Magnetoresistance measurements have been carried out on dilute Pd based alloys by Williams et al (1973) and Hamzic et al (1978). The isotropic magnetoresistivity⁹ $\bar{\rho}$ against magnetic field for four typical ferromagnetic dilute alloys at low temperature is shown in Figure 2.8.

The PdFe alloys show very little isotropic magnetoresistance which agrees well with the magnetic measurements, as the PdFe is a soft ferromagnet.

The magnetoresistance of PdCo samples is characterized by a negative term at low temperature which is similar in sign to that observed in PdFe

⁸This T^n term with $n = 2$ is attributed to conduction electron scattering by spin fluctuation/spin waves when the Ni concentration x is well below/above the critical concentration necessary for the establishment of a ferromagnetic ground state. Near this critical concentration, n decreases to values near $3/2$ or $5/3$.

⁹Sometimes called the average magnetoresistivity, and is defined by $\bar{\rho}(H) = \frac{1}{3}(\rho_{\parallel}(H) + 2\rho_{\perp}(H))$.

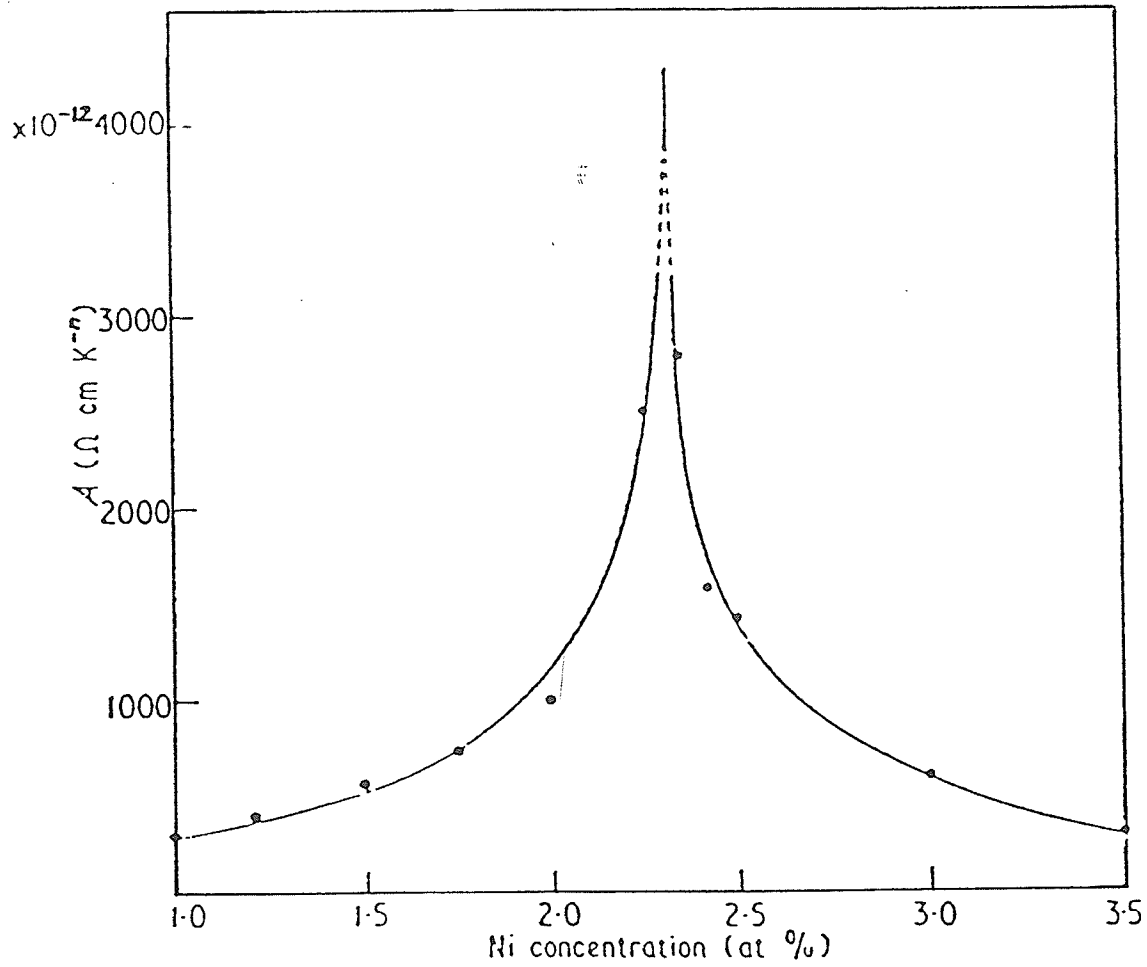


Figure 2.7: The coefficient A against PdNi concentration (after Tari and Coles 1971).

alloys, but the magnitude of the magnetoresistance and the field needed to saturate the magnetoresistance are much larger than that in PdFe alloys. The PdCo alloy saturates in an applied field about 15 *kOe* at 1.2 K.

In contrast to the PdFe and PdCo alloys, the magnetoresistance of PdMn alloy remains strongly negative indicating there is a certain fraction of the magnetic moments which remain disaligned even at low temperature and high field (Hamzic et al 1980). This is in agreement with the magnetic measurements which show the sample does not reach true saturation until very high applied fields (on the order of 200 *kOe* (Smit et al 1979)).

The isotropic magnetoresistance curve of a ferromagnetic PdNi alloy is totally different from those of systems such as PdFe, showing strong positive magnetoresistivity in applied magnetic fields. This can be interpreted as indicating that the Ni local moment increases with increasing applied field (Hamzic et al 1978). The basic character of the isotropic magnetoresistance of dilute PdFe, PdCo, PdMn and PdNi remains unchanged with temperature and impurity concentration.

Spontaneous resistive anisotropy SRA investigations on PdFe, PdCo, PdNi, and PdMn alloys have been carried by Senoussi et al (1977), and Hsu et al (1982). PdFe and PdCo alloys show positive anisotropy ($\rho_{\parallel} > \rho_{\perp}$), while PdNi and PdMn show negative anisotropy. The magnitude of the SRA for these alloys is on the order of a few percent or less. Unfortunately, our knowledge about the SRA of these dilute alloys is still rather poor. There have been no extensive measurements of SRA for the dilute Pd based al-

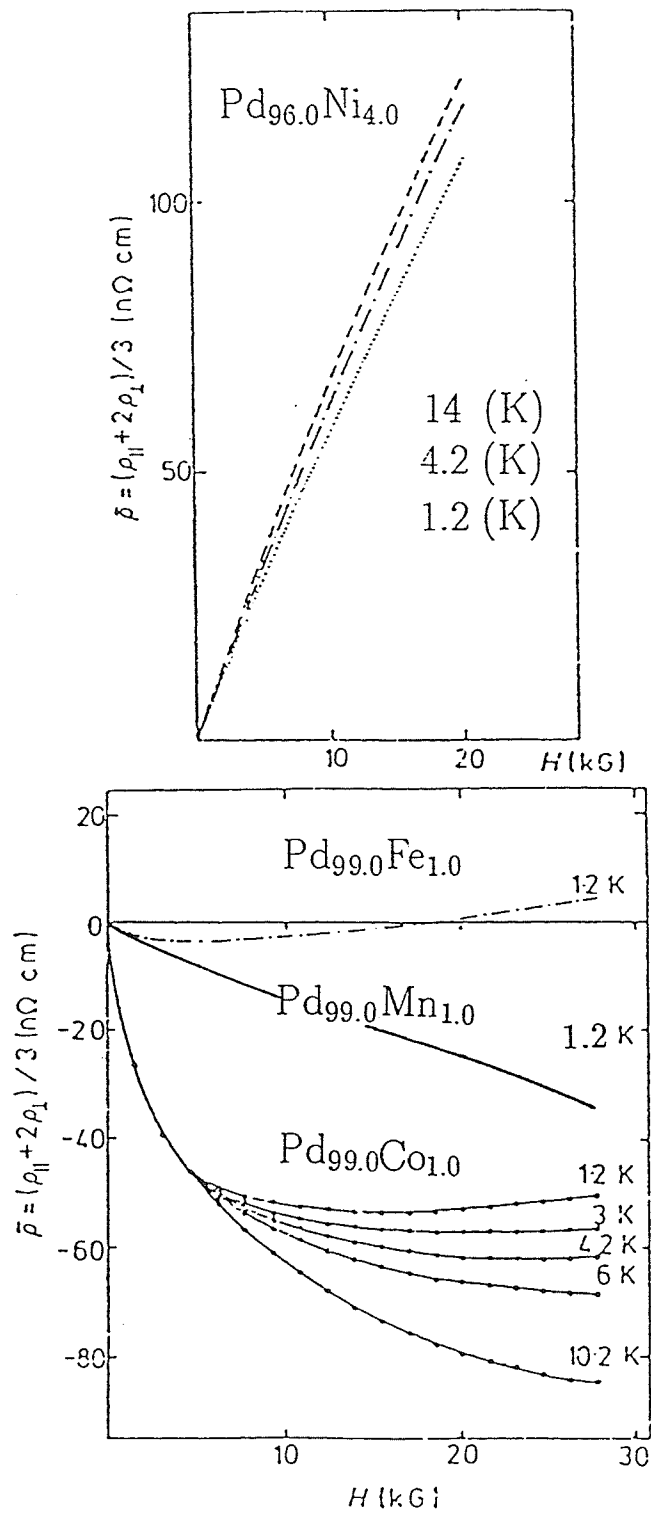


Figure 2.8: Magnetoresistivity for PdFe, PdCo, PdNi and PdMn alloys (data from Hamzic et al 1978, 1980).

loys, since the systems may have ferromagnetic order in as little as 0.1 at% alloy. The data quoted above were obtained from the measurements of the alloys in steps of about 5.0 at% between 0 and 35 at% impurity. Thus an experimental investigation of the SRA in the alloys close to the ferromagnetic percolation threshold has not been performed previously, although some authors (Senoussi et al 1977) mention the problems encountered in attempting to measure the SRA near the critical concentration.

Chapter 3

Experimental Methods

3.1 Introduction

This chapter discusses in detail the experimental methods used along with the necessary corrections required for data analysis.

3.2 Sample Preparation

The PdNi alloys were prepared by melting high purity starting materials 99.999 % pure Pd wire and 99.998 % pure Ni rod in an argon furnace using pressure near 200 torr. Initially a master alloy of Pd + 5.0 at% Ni was prepared, and subsequently fourteen alloys containing between 2.0 and 5.0 at% Ni, in steps of 0.1 between 2.0 and 3.0 at% Ni, and in steps of 0.5 above 3.0 at%, were carefully prepared by dilution from this master alloy. Six PdFe alloys containing Fe between 0.35 and 2.2 at% were prepared by successive dilution of a 2.4 at% Fe master alloy, the latter having been made from 99.999 % pure Pd wire and 99.99 % pure Fe rod by arc melting. Five (PdFe)Mn alloys containing 5 at% Mn were prepared by melting 99.99 % pure Mn flake with five PdFe alloys containing between 0.35 and 2.2 at% Fe in argon atmosphere, respectively. The specimens used in these studies have been listed in Table 3.1; all the starting materials mentioned above (Pd, Fe, Ni, and Mn) were supplied by Johnson Matthey, London.

The importance of proper homogenization, especially in Pd based alloys has been emphasised by other researchers (Zweers 1976). Each alloy was therefore inverted and remelted several times to ensure homogeneity. At each stage in the preparation the melting losses were always negligibly small. Thin

Table 3.1: List of the specimens.

Alloy	Impurity concentration in atomic percent
$\text{Pd}_{1-x}\text{Ni}_x$	0, 2.1, 2.2, 2.3, 2.4, 2.5, 2.6, 2.7, 2.8, 2.9 3.0, 3.5, 4.0, 4.5, 5.0
$\text{Pd}_{1-x}\text{Fe}_x$	0.35, 1.4, 1.6, 1.8, 2.0, 2.2, 2.4
$(\text{Pd}_{1-x}\text{Fe}_x)_{95}\text{Mn}_5$	0.35, 1.6, 1.8, 2.0, 2.2

sheets of material from which magnetoresistance and susceptibility samples were cut were produced by cold-rolling between protective Melinex sheets in order to avoid contamination. The typical dimensions of the magnetoresistance samples were $3.5 \times 0.2 \times 0.01 \text{ cm}^3$, while the susceptibility specimens were typically $1.7 \times 0.2 \times 0.01 \text{ cm}^3$ and on which the corners had been rounded. These samples were then etched for one minute to remove the surface layer (using the etching solution shown in Table 3.2), washed, and then annealed for 24 hours at 1000 C in 10^{-6} torr vacuum and finally quenched in ice water immediately before measuring.

In the case of the zero field susceptibility measurements, a single sample strip of the dimensions indicated above was usually large enough to give a signal of suitable magnitude; when an external dc magnetic field was applied,

Table 3.2: The etching solution.

Acids	Formula	Parts by Volume
Conc.nitric acid	HNO ₃	1
Hydrochloric acid	HCl	3
Water	H ₂ O	1
Hydrogen Peroxide	H ₂ O ₂	A few drops

consequently a number of pieces with very similar dimensions were frequently needed to stack one on top of the other, for such measurements in order to give a signal of suitable magnitude; these pieces were in good thermal contact, but electrically isolated from each other with masking tape.

3.3 X-Ray Measurements

The structure and the related lattice parameters of the dilute Pd based alloys were determined by x-ray measurement. The photographs were taken on a 11.46 *cm* diameter Debye-Scherrer camera which employed Straumanis asymmetrical film loading. The camera had the special feature of automatic compensation for film shrinkage after exposure. The x-ray source was copper, and a Ni filter was used. Typical exposure time was 6 hours, developing time

6 minutes, and fixing time 8 minutes. The film was measured to ± 0.002 cm with a Picker traveling micrometer. The analysis of the films followed the general procedure described in the book entitled "X-Ray Diffraction Methods" (Nuffield 1966).

Figure 3.1 shows a typical x-ray photograph for the case of Pd + 2.8 at% Ni. There are 18 lines in the photograph. From the known wavelengths of x-ray emissions from Cu, the lattice parameter was estimated at 3.8773 ± 0.0002 Å, which agrees well with the extrapolated value from more concentrated PdNi alloys listed in "A Handbook of Lattice Spacings and Structures of Metals and Alloys" by Pearson (1958).

All the alloys and the pure palladium were confirmed to be *fcc* with no superlattice structure. A knowledge of the lattice parameters and structures of the alloys is important since the resistivity ρ is related to the resistance R by

$$\rho = R (A/L) \quad (3.1)$$

where A is the cross section, L is the length, and A/L is called the form factor of the sample. However, the cross section A of the sample is a difficult quantity to determine accurately because of its small thickness and slightly irregular shape. In order to determine the resistivity accurately an indirect method, based on the following two equations, was used:

$$Density = M/V = \frac{M}{L^2} \times \left(\frac{L}{A}\right) \quad (3.2)$$

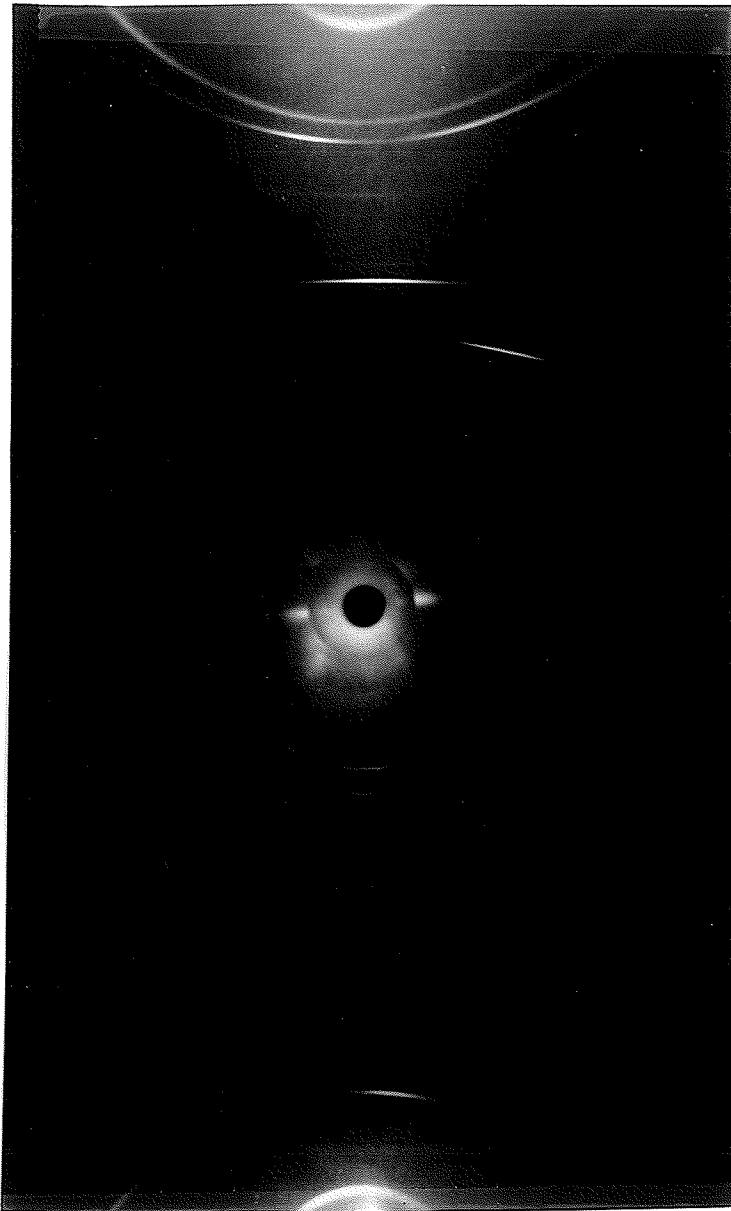


Figure 3.1: X-ray pattern of the Pd_{97.2}Ni_{2.8} alloy.

and

$$Density = \frac{4(k_1X + k_2Y)}{N \times a^3} \quad (3.3)$$

where V is the sample volume, M its mass, k_1 is the atomic mass of Pd, k_2 is the atomic mass of Ni or Fe, X is the atomic percent of Pd, Y that of Ni or Fe, N is the Avogadro's number and a is the concentration-dependent lattice parameter. The factor 4 indicates there are four atoms per unit cell in an *fcc* structure. The formula for the density of *fcc* substitutional alloys was first used to calculate the density from the measured lattice parameter. From this density and accurate measurements of the mass (M) and the length (L) of the sample (mass were accurate to ± 0.0001 g, and lengths were measured to ± 0.001 cm with a Picker traveling micrometer) the form factor and then the resistivity for the sample were accurately determined. This technique for measuring the form factor is applicable even if there are significant irregularities in the cross sectional area of the sample.

3.4 *ac* Magnetic Susceptibility Measurements

3.4.1 The Measurement System

Figure 3.2 shows the general arrangement of the sample probe, sensing coils and external field coils forming the main components of the susceptibility measuring system. The sample probe consists of a machined copper block and a large bundle of thin copper wires (32 gauge) soft-soldered to it. The

sample was mounted inside the bundle, but electrically insulated from it with masking tape, thus ensuring good thermal contact through the Cu bundle to the block which is 10 *cm* above it. A calibrated Germanium resistance and a Au + 0.03 at% Fe vs. chromel P thermocouple used as temperature sensors are also located inside the same bundle close to the sample. Temperatures below about 10 K are measured using the resistance thermometer, while at higher temperatures the thermocouple is used. The Cu block also has a non-inductive wound nichrome heater (50 Ω) attached to it, which is capable of warming the sample up to 300 K. The Cu block is connected to a thin wall stainless steel tube with a diameter of about 0.8 *cm*, which, in turn, is connected to the top of the apparatus. Stainless steel has relatively low thermal conductance and this helps reduce heat leak from room temperature. The sample probe is inserted into a narrow liquid He filled dewar, surrounded by an outer dewar filled with liquid N₂. The narrow-tailed glass He dewar is 82 *cm* long, 8 *cm* in internal diameter narrowing to 1 *cm* diameter in the tail.

Two isolated sensing coils L_1 and L_2 , with measured inductances of 205 and 202 *mH*, respectively are placed in the liquid nitrogen dewar, concentric with the tail of the inner He dewar, shown in Figure 3.2. The *dc* biasing coils are also placed inside the liquid N₂ dewar. The biasing coils have two functions. One is to cancel the vertical component of the earth's field which is about 0.4 *Oe* so that true zero field measurements can be made, and the other is to produce a 0-1000 *Oe* biasing magnetic field to be applied to the sample. Unless otherwise stated these fields were applied parallel to the longest di-

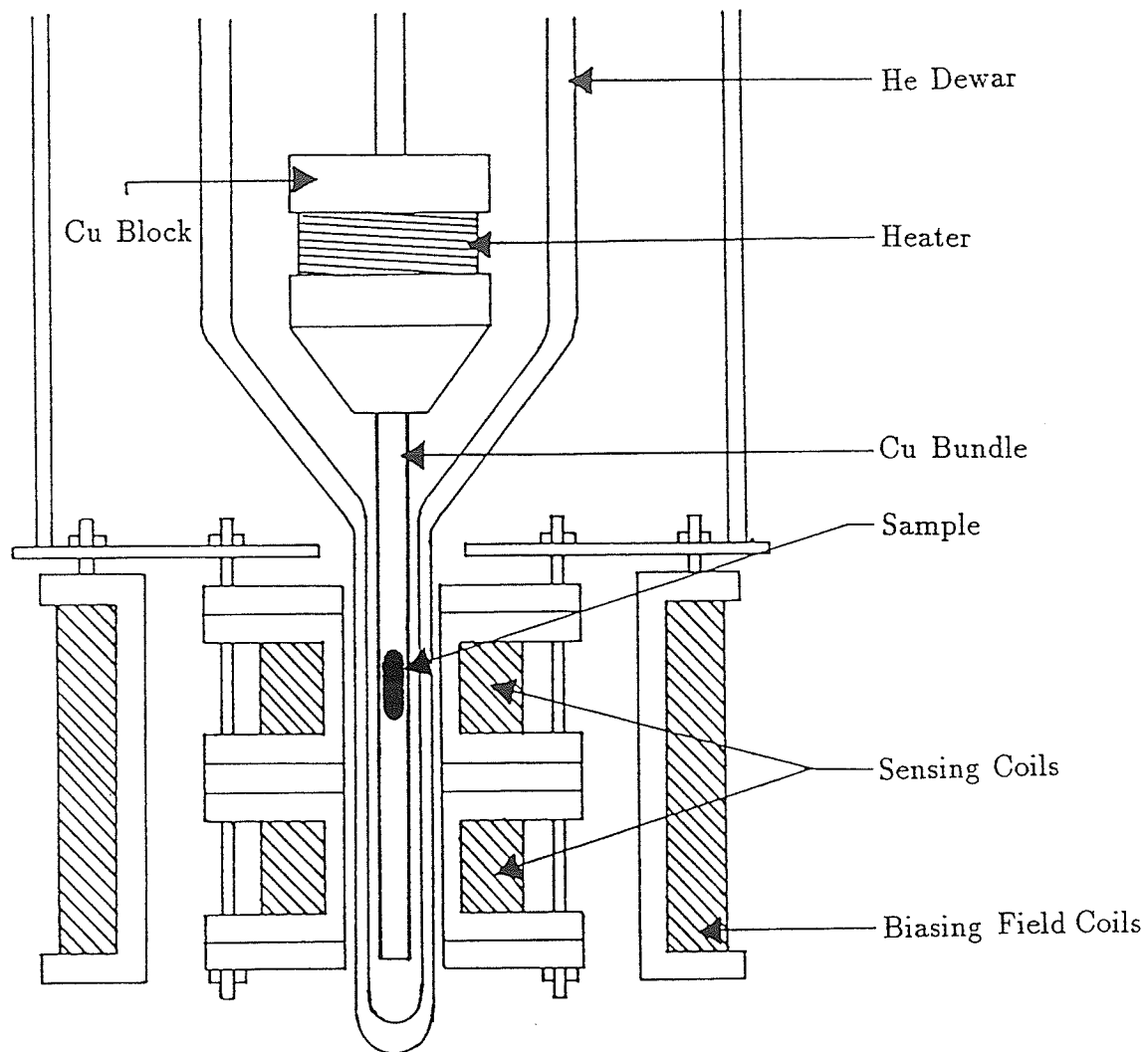


Figure 3.2: Sample probe, sensing coils and external field coils.

mension of the samples (the corresponding demagnetizing factor being about 0.07-0.50). The liquid N_2 bath not only cools and maintains the temperature stability of the sensing and field coils, but also provides additional thermal isolation for the liquid helium contained in the inner dewar.

3.4.2 Measurement of Susceptibility

The magnetic susceptibility was measured using a phase locked susceptometer (Maartense 1970) operating at 2.4 kHz with a driving field of 50 mOe. Figure 3.3 shows a block diagram of the basic susceptibility apparatus. The central part of the apparatus is a phase detector. When a magnetic material is inserted into one of the two identical isolated sensing coils, both of which are components of separate LC oscillators, a differential change in inductance, ΔL , is produced. The signals are compared in the phase detector, and a voltage proportional to the phase difference is used to control the resonant frequency of the oscillator by means of a voltage dependent reactive element. The voltage, therefore, is a measure of the effect of the magnetic material and is directly proportional to the susceptibility. It is connected to the Y-input of an X-Y recorder, while the signal, monitored by a digital multimeter, from the calibrated germanium resistance or the Au + 0.03 at% Fe vs. chromel P thermocouple, is connected to the X-input. The susceptibility as a function of changing temperature can therefore be recorded continuously by the X-Y recorder, with a typical Y-output signal of a few volts. The general procedure adopted for susceptibility measurements consisted of

- (1) cooling the sample from above the Curie temperature, T_c , to the

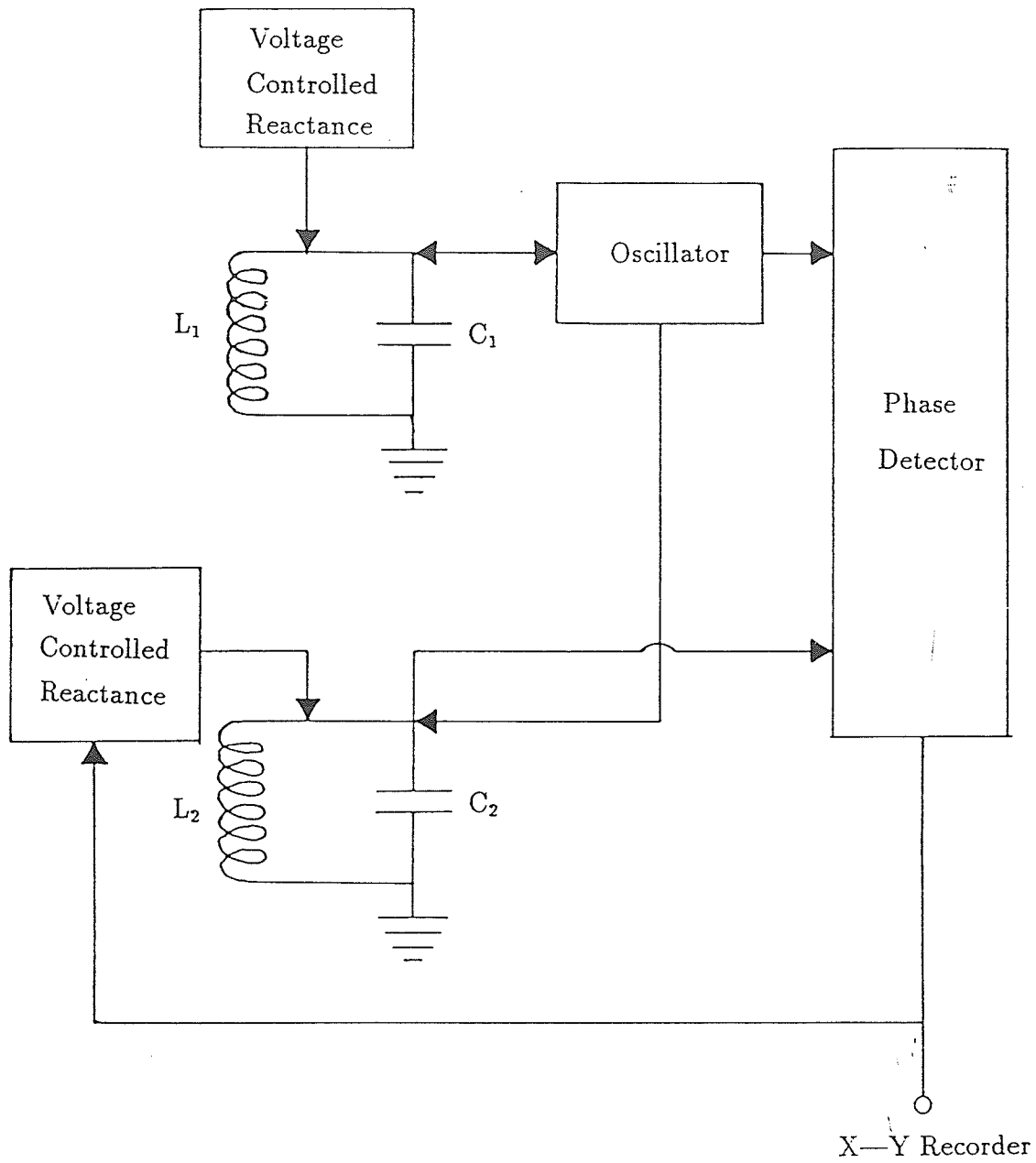


Figure 3.3: Block diagram of the bias susceptibility apparatus.

temperature of interest in zero field.

(2) Maximizing the signal at a fixed temperature by positioning the sample at the center of the sensing coil L_1 .

(3) Applying a magnetic field of a predetermined value.

(4) Recording the data as the sample is warmed. The usual warming rate was approximately 1.5 K per hour for the temperatures below 4.2 K, and about 4.0 K/hour above 4.2 K.

The sample temperature may be reduced to approximately 1.8 K by pumping on the helium bath using a mechanical rotary pump. Temperature between 1.8 and 4.2 K can be controlled by a combination of the use of the nichrome heater and the pumping speed. Temperatures above 4.2 K were achieved by controlling the thermal link between the sample space and liquid nitrogen bath around it and/or using the nichrome heater. The magnetic susceptibility measurement can thus be carried out as a function of temperature (between 1.8 K and room temperature) and external magnetic field (from 0 to 1000 Oe).

3.4.3 Calibration and Corrections

The output voltage from the phase detector circuit of the magnetometer is proportional to the change of inductance and therefore susceptibility. Thus, the signal amplitude in volts can be converted to susceptibility with a simple calibration factor. The magnetometer was calibrated using Gd_2O_3 powder whose filling factor was approximately the same as the Pd based alloy samples. Gd_2O_3 was used as a calibration substance for the magnetometer because

of the high value of its susceptibility and the supposed simple Curie-Weiss behaviour. At a given temperature its susceptibility is given by

$$\chi = \frac{N\mu_{eff}^2}{3k_B(T - \theta)} \quad (3.4)$$

where θ is a constant, with the dimensions of temperature, in the case of Gd_2O_3 , $\theta = -13$ K (Schinkel and Van Amstel 1973)¹, so the magnetic susceptibility at a given temperature T can be calculated using known values for the number of gadolinium atoms per gram N , the Boltzmann's constant k_B , and $\mu_{eff} = (7.70 \pm 0.04)\mu_B$. The calibration factor, which was done at 77 K (fresh liquid N_2), of the magnetometer was found to be $6.95 \times 10^{-7} (emu/gOemV)$. This is expected to be reliable to within 10 % in absolute value (due to the non-uniformity of the sample shapes), although relative susceptibility values can be measured to 1 part in 10^4 .

Three corrections are necessary when analysing the measured susceptibility data in order to obtain the true susceptibilities. The first one is simply the background correction. This correction amounts to a small temperature and applied magnetic field dependent diamagnetic (negative) signal which could be detected in the absence of a sample. The typical magnitude is about -0.025 V at 4.2 K. Whatever the reasons causing the negative signal (non-uniformities in the Cu bundle, small construction differences between the two sensing coils as well as possible contribution from the Ge thermome-

¹At temperature between 20 K and 300 K these susceptibility data could be fitted with a relative accuracy better than 0.5% (1% absolute) to this equation.

ter and/or the AuFe thermocouple), the true sample signal should be the difference between the measured signal and the background. The correction was done by measuring the background signal in the temperature range of interest. These values were then added (because they are negative) to the measured susceptibilities.

The second correction is due to the sample shape. If a magnetic body of finite size is magnetized, free magnetic poles are induced on both its ends. These, in turn, produce a demagnetizing field H_d , which is proportional to the intensity of magnetization M , but in a direction opposite to that of the magnetization. For a regularly shaped magnetic sample the internal field H_i is always less than the applied field H_a by the amount equal to the demagnetizing field, that is

$$H_i = H_a - H_d = H_a - NM \quad (3.5)$$

where N is the demagnetizing factor, which is a function of the shape of the sample. In general, the calculation of the demagnetizing factor of a sample is very complex, and for irregular samples is impossible. The demagnetizing factors N in this investigation were estimated by treating each sample as an ellipsoid (the edges of the samples were rounded), with principal axes equal to the sample's dimensions, and then evaluating the corresponding elliptic integral (Osborn 1945)². The magnetization M was found by a simple

²In the case of an ellipsoid of revolution, the sample having a length a and with $b = c =$ diameter of the solid then $N_a = (\frac{1}{e^2} - 1) [\frac{1}{2e} \log(\frac{1+e}{1-e}) - 1]$ where the eccentricity of the ellipse $e = (1 - b^2/a^2)^{1/2}$.

numerical summation of available *ac* susceptibility data at various fields, viz.

$$M(T) = \sum_{i=1}^n \chi_i(T) \times \Delta H_i \quad (3.6)$$

From the relation between the magnetization M and the field H , it is straightforward to show that Equation (3.5) can be expressed as

$$\chi_t = \frac{\chi_m}{1 - N\chi_m} \quad (3.7)$$

where χ_t and χ_m are true and measured susceptibilities (after background correction) defined as $\chi_t = \partial M / \partial H_i$, and $\chi_m = \partial M / \partial H_a$. The true value of the sample susceptibilities were then calculated using the above equation. It should be noticed that the term "true" susceptibility has only a qualitative meaning here. As Equation (3.7) suggests that the maximum susceptibility is limited by the demagnetizing factor N as the samples examined here have positive susceptibility.

An additional correction was needed for all the temperature measurements just above the boiling point of the cooling liquid in use. The correction is based on the result that since the Germanium resistor and AuFe thermocouple are placed a few millimeters higher than the sample on the sample probe, the temperature reading of the Germanium resistance can be slightly higher than the true sample temperature. This is particularly true just above 4.2 K, although the typical corrections required were not more than a tenth of one degree. As the He level falls below the level of the sensor, the sensor beg-

ings to warm while the sample remains immersed in He temporarily. A “dead range” was observed in the susceptibility measurements at the temperatures just above 4.2 and 77 K. One way to approach the temperature correction is to shift the germanium resistor readings obtained above the boiling point temperatures using a height and slope matching technique as illustrated in Figure 3.4, and which has been described in detail previously by Saran (1986).

3.5 *ac* Magnetoresistance Measurements

3.5.1 Experimental Geometry

Figure 3.5 shows the experimental geometry for the *ac* magnetoresistive measurements. The electrical current I is constrained to flow along the Y direction, and whatever the applied field H_a or magnetization M direction, the resistivity is proportional to the voltage V between the knife-edges c and d . Currents on the order ten mA were usually applied and resulted in typical voltages of a few tens of mV .

The magnetoresistance is not a simple scalar quantity, as it depends on the relative orientations of the current and the magnetic field. However it is usual to consider just two configurations, the longitudinal position where magnetic field H and current I are parallel to each other which is Y direction in the figure, and the transverse position where the applied field and current are perpendicular as in the conventional Hall geometry. It seems that both longitudinal and transverse effects are of about the same order of magnitude in metals. The corresponding spontaneous resistivity anisotropy (SRA) can

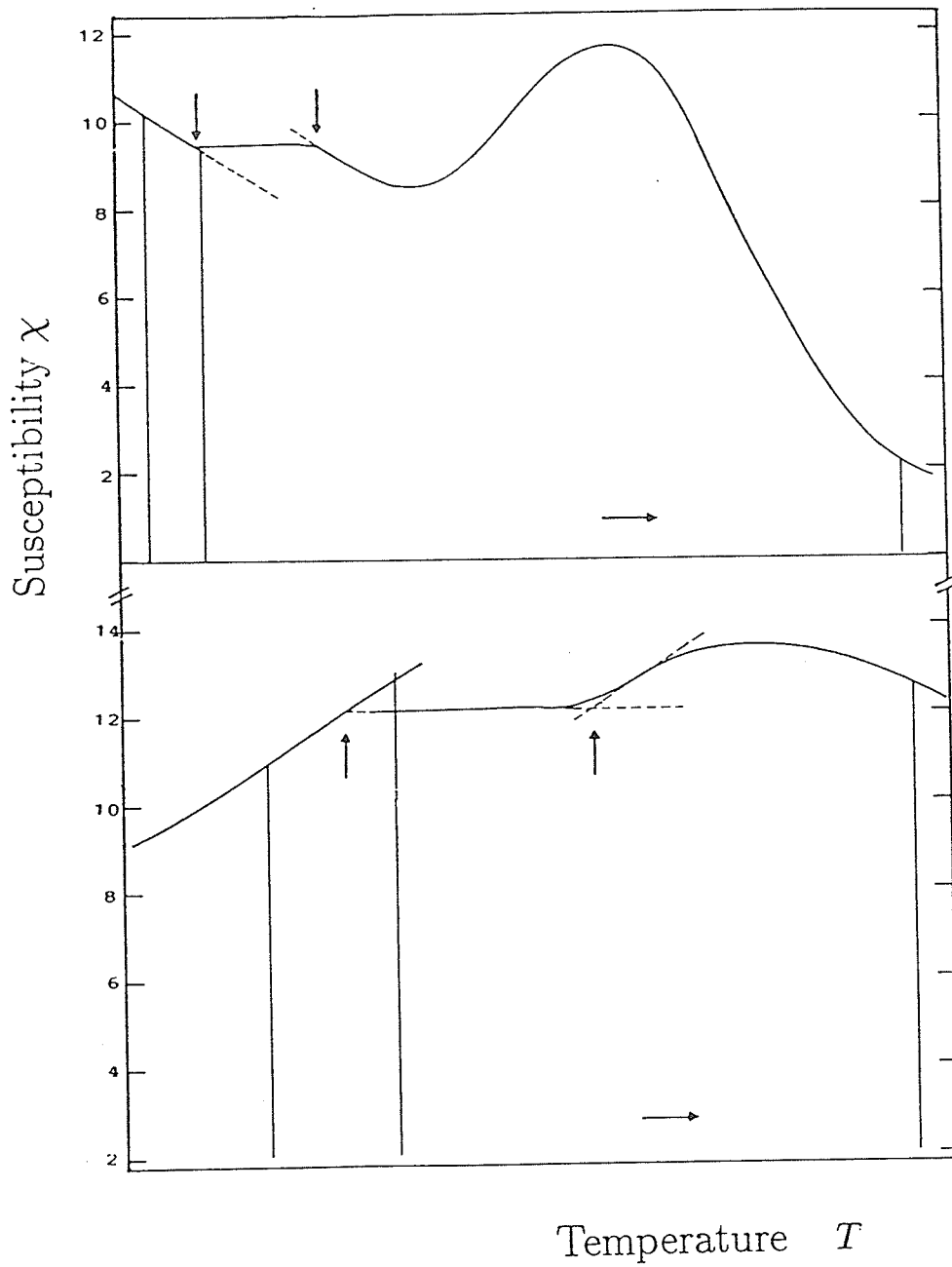


Figure 3.4: Temperature correction of the susceptibility measurement by slope matching technique as illustrated.

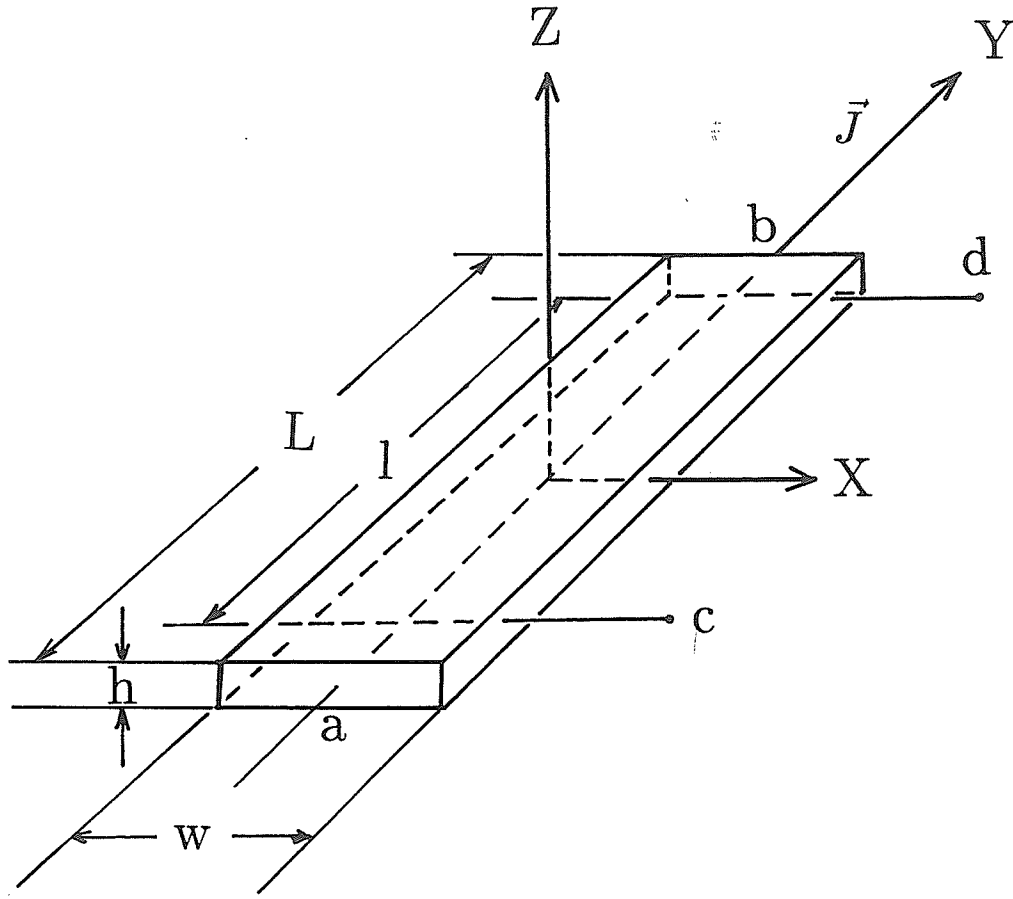


Figure 3.5: The experimental geometry for the *ac* magnetoresistive measurement.

have either sign, with values generally of a few percent or less although some magnetic alloys (such as *fcc* nickel-rich NiFe and NiCo alloys) may have an SRA as high as 20% (Smit 1951).

3.5.2 The Measurement Technique

Figure 3.6 shows the arrangement of the sample block, dewar system and electromagnet for measurement of *ac* magnetoresistance. The sample block illustrated in Figure 3.7 was made of high thermal conductivity oxygen-free copper, and the approximate dimensions were $7.4 \times 3.5 \times 0.6 \text{ cm}^3$. As many as six specimens, three on each side, could be mounted on the knife-edge supports for each run. The knife-edge supports were electrically insulated from the copper block by condenser paper impregnated with generous amounts of General Electric (G. E.) varnish. The varnish provided reasonably good thermal contact between the knife-edge supports and the sample block. The samples were tightly clamped into place with fibre glass yokes positioned by brass screws, but were electrically insulated with mylar insulating strips.

Six samples were connected in series and therefore carried the same current, this current being applied along the largest specimen dimension. Knowing the current, the resistance of each sample could then be deduced by measuring the voltage between the knife-edges, and using Ohm's law ($R = V/I$). The knife-edge supports leave impressions on the samples and the distance (L) between these marks was measured with a travelling microscopy. This measurement, as well as the precise measurement of the sample form factor (A/L) discussed in Section 3.3, are necessary to convert resistance to

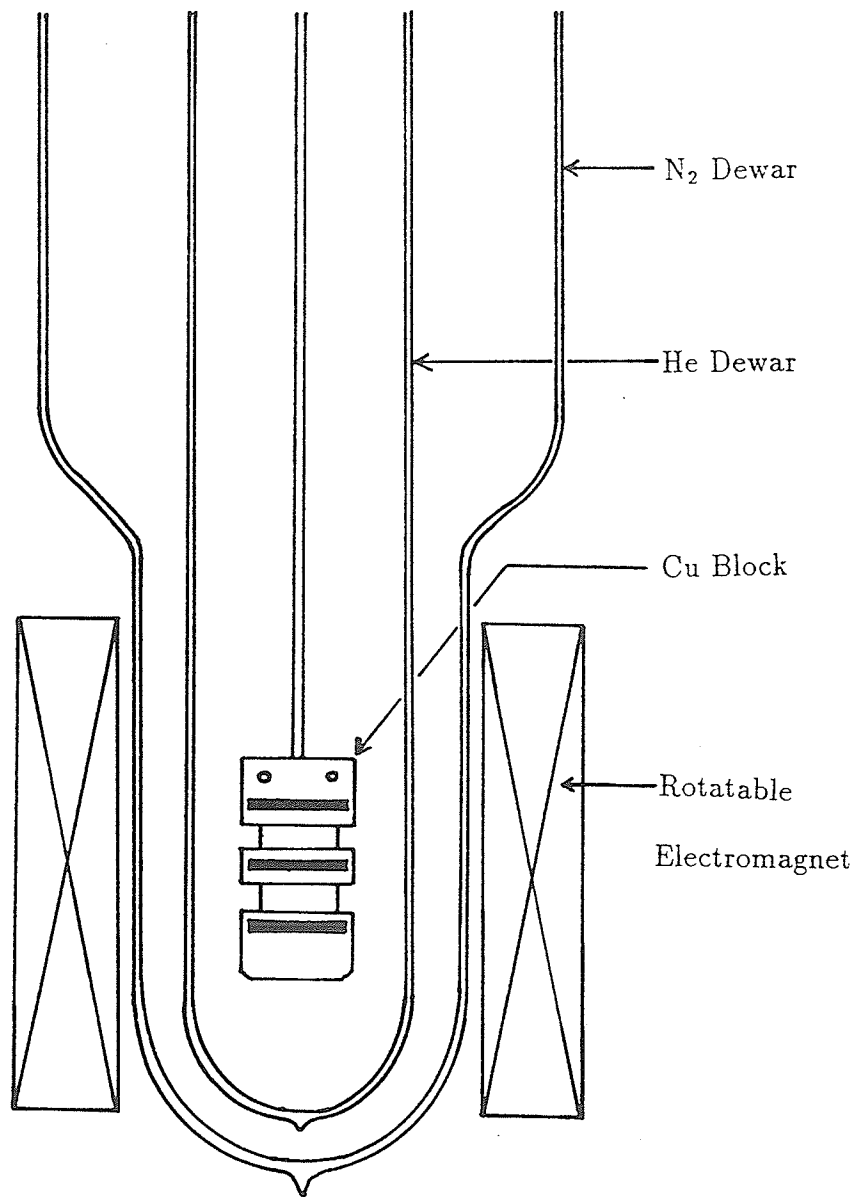


Figure 3.6: Arrangement of sample block dewar system and electromagnet.

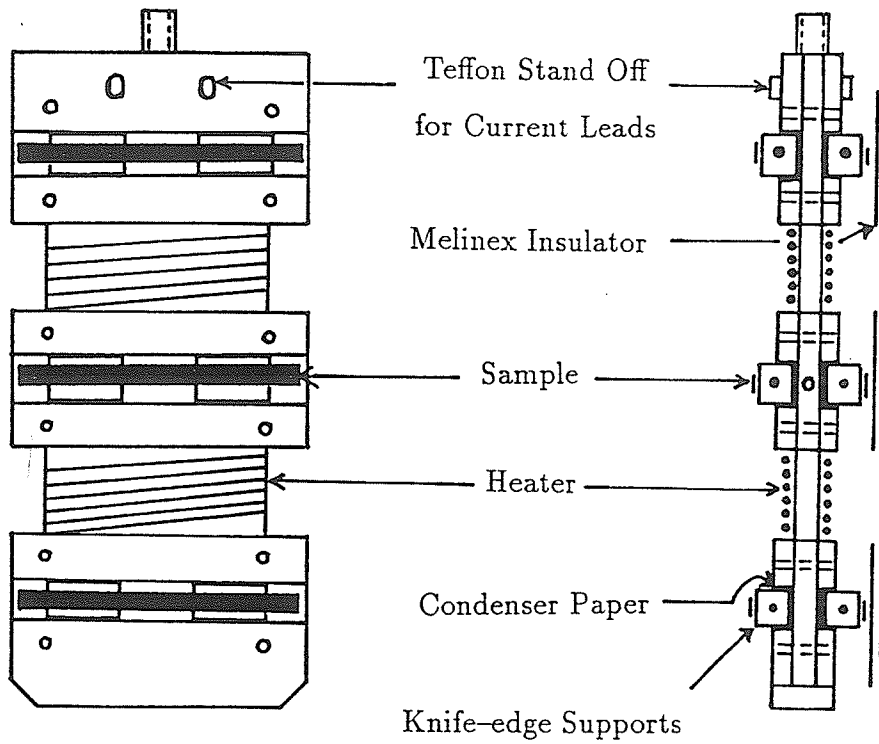


Figure 3.7: Face and edge view of sample holder.

resistivity.

The sample block was immersed in liquid helium contained in a dewar located between the pole pieces of a conventional electromagnet. Temperatures below 4.2 K were achieved by pumping on the He bath, and were estimated from the measured bath vapour pressure.

Fields up to 10 kOe were applied parallel or perpendicular to the current direction by a rotatable electromagnet (Model Fieldial Mark I, manufactured by the Varian Magnet Company) which surrounded the dewar system. The field produced by this electromagnet was calibrated using a F. W. Bell Gaussmeter (Model 615) with an estimated error of $\pm 0.5\%$ of full scale. The electromagnet has two pole faces, 24 cm in diameter, with a separation of 8 cm . The field homogeneity was also measured, the estimated error being about $\pm 1\%$ over the sample volume.

A double dewar system was used in the experiment, an inner dewar contained liquid helium and an outer dewar to contain liquid nitrogen. The narrow tails of the dewars allows the the use of a smaller pole-gap for the magnet producing higher fields for the same magnet current. The top section of the dewar is enlarged to give greater liquid-storage capacity. The liquid helium dewar is 80 cm in length, 12 cm in internal diameter and 5.5 cm at the tail. Typical He consumption is about one litre per hour.

The effect of an applied magnetic field up to 85 kOe , on the longitudinal resistivity, was measured in another system illustrated in Figure 3.8. Surrounding the sample chamber (12.7 cm long), is the gas thermometer bulb

(G. T. Bulb) used for monitoring the temperature of the sample space. Outside the G. T. Bulb a vacuum chamber separates the sample space from the Helium bath.

The whole assembly could be placed inside a superconducting solenoid (SHE Manufacturing Co., U. S. A.) which produced a 0 – 85 kOe biasing magnetic field parallel to the longest dimension of the samples.

The sample holder, shown in Figure 3.9, is a rectangular Cu plate, with the approximate dimensions $10.5 \times 2 \times 0.2 \text{ cm}^3$. As many as four samples, two on each side, could be mounted on the knife-edge supports for each run. The sample holder was soldered to the end of a long, narrow stainless steel tube which carried various current and voltage leads to the samples mounted on the holder.

3.5.3 Circuit Diagram

In order to study the onset of magnetic order in dilute magnetic materials at low temperature using magnetoresistance measurements, a technique with high differential sensitivity but limited absolute accuracy was used. This was based on an *ac* difference technique (originally proposed by Muir and Strom-Olsen 1976), and capable of measuring the fractional change in the magnetoresistance to better than a few parts in 10^6 .

Figure 3.10 shows a circuit diagram of the system used. In order to limit skin depth problems in systems with low resistivity, a low operating frequency (37 Hz) is employed. An alternating current from a General Radio 1311-A audio oscillator is applied to both the sample under observation

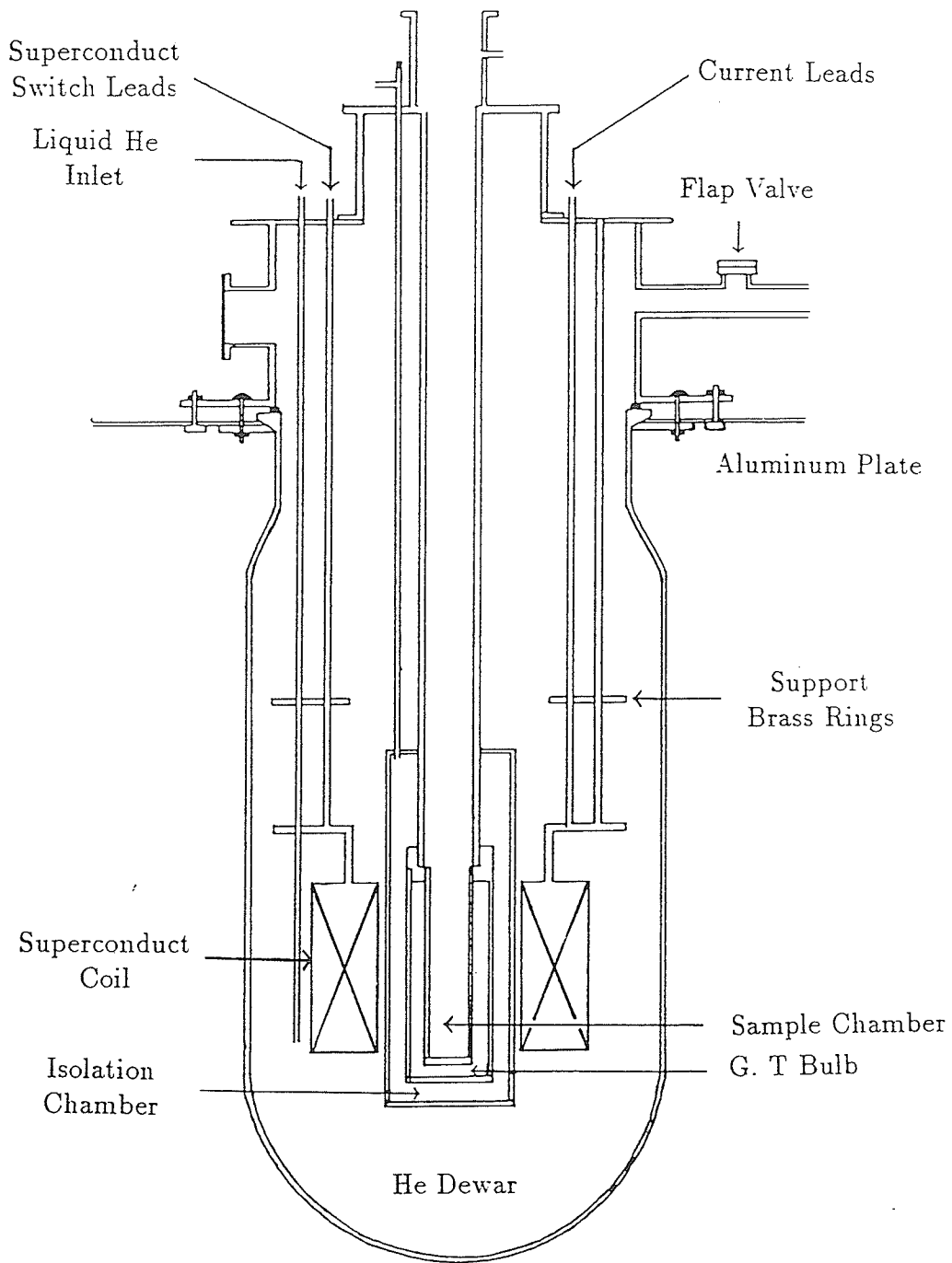


Figure 3.8: Arrangement of higher field longitudinal resistivity measurement.

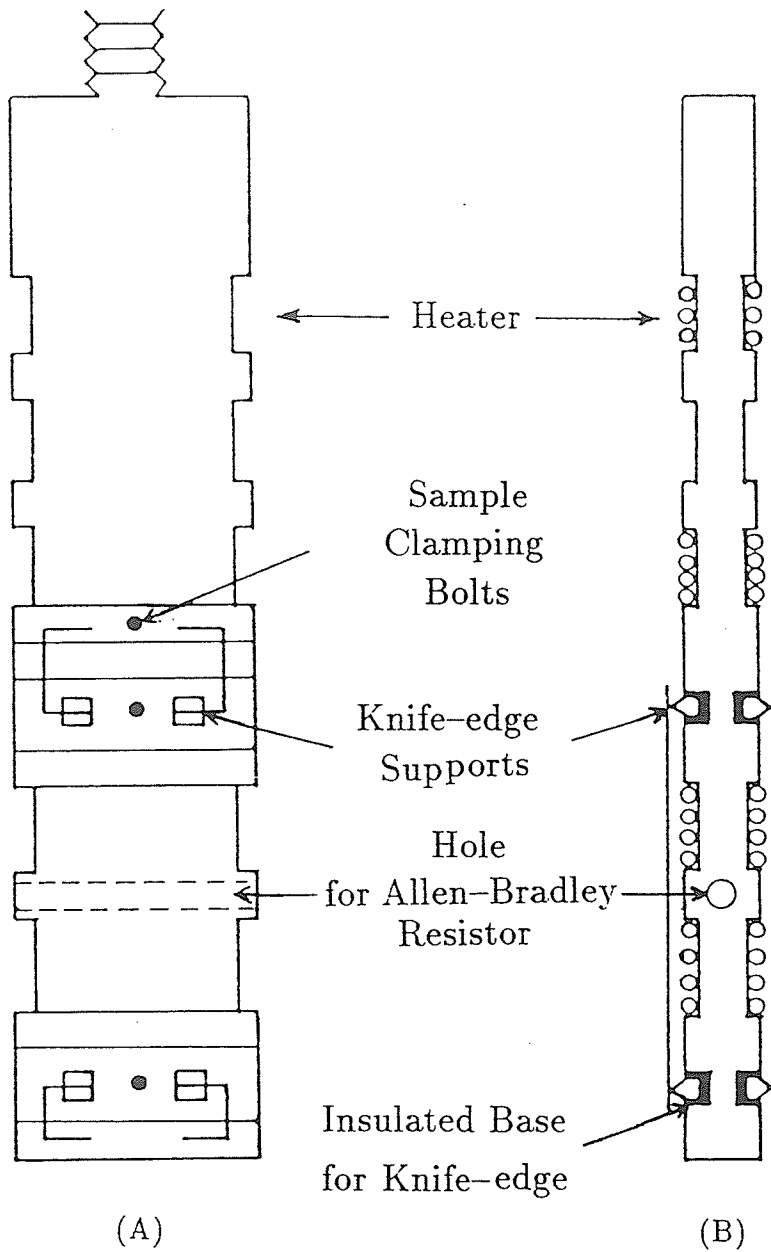


Figure 3.9: Face (A) and edge (B) views of a sample holder for higher field longitudinal magnetoresistivity measurements.

and a series connected variable resistance (Kelvin Varley type DP1211). The voltage difference between the two is then measured accurately with a precision lock-in amplifier (Princeton Applied Research model HR-8) tuned to the driving frequency of the oscillator. Because the variable series resistance can be accurately adjusted, the above difference can be kept small. The variation of this signal with small change in applied magnetic field can then be observed using the lock-in amplifier. In order to obtain high sensitivity in the measurements, a variometer is used to eliminate the interference from stray quadrature components in the signal across the sample. The variometer consists of three coils. One of them is a stationary primary coil of 150 turns and the other two are rotatable secondary coils (250 turns and 10 turns respectively). The variometer not only produces an accurate quadrature signal for setting the phase of the lock-in amplifier, but also produces a nulling signal used to cancel any stray quadrature signals present. After nulling, switch *A* is opened and the total in-phase voltage V_0 read on the lock-in amplifier. Closing the switch *A* and applying a magnetic field H_a allows the differential sample voltage V to be read. From V , the sample current I , and the sample geometry, the magnetoresistance can be calculated. The absolute resistivity could be most accurately determined by measuring the same sample with a conventional four-probe *dc* potentiometric method. In the four-probe method, a known current I is applied to a specimen, and the voltage V across the sample can be measured accurately using a potentiometer. The resistance of the specimen is calculated from Ohm's law, $R = V/I$, and then knowing

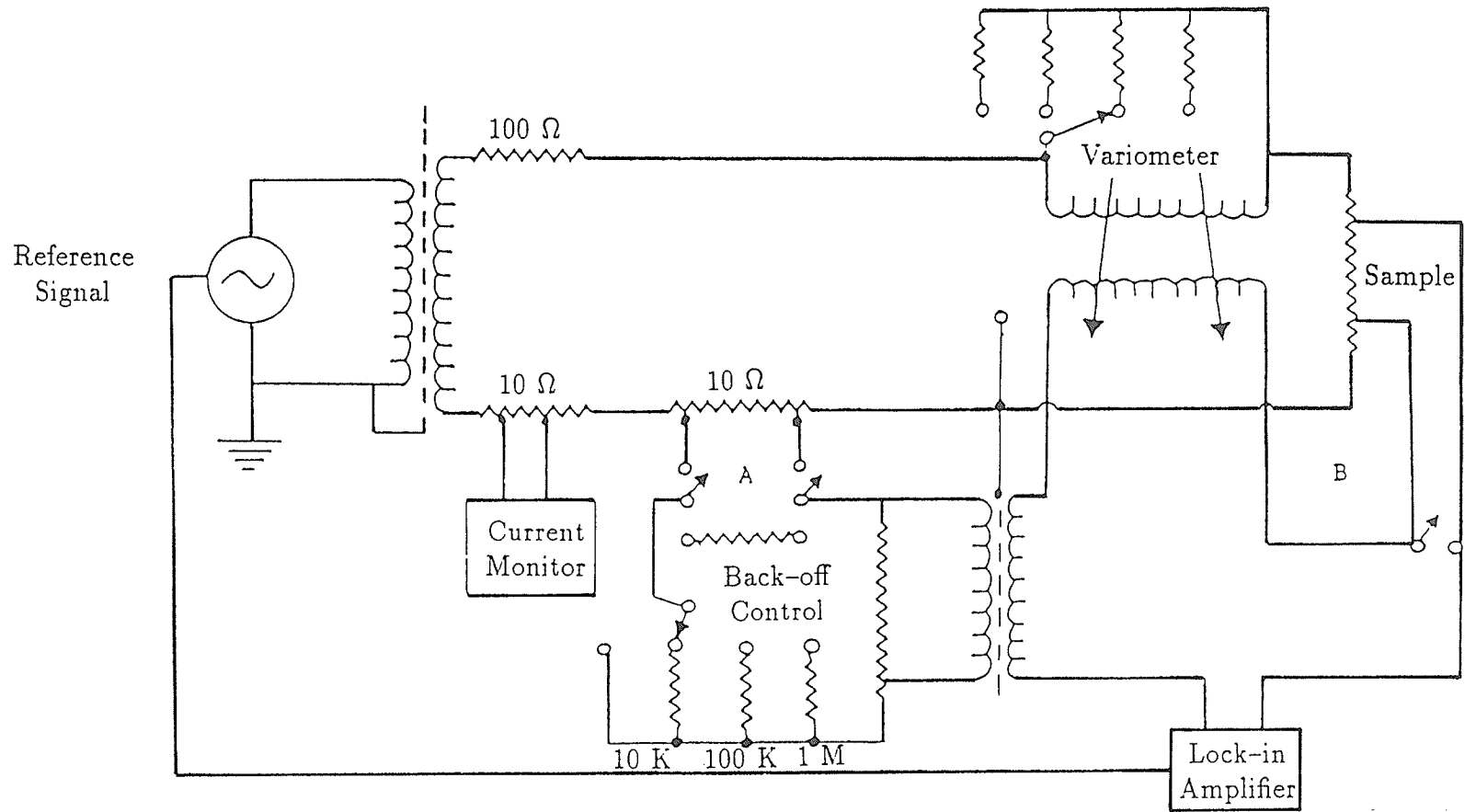


Figure 3.10: Circuit diagram of magnetoresistive measurement.

the form factor (A/L), the electrical resistivity of the sample can be precisely determined using $\rho = R (A/L)$.

3.6 Hydrogen Absorption

Hydrogen can bring about important modifications in the interatomic distance, electronic structure and magnetic properties of transition metal alloys. Dilute Pd based alloys are especially good candidates for the study, as the host itself is a very good hydrogen absorber.

There are several methods that can be used to load hydrogen, such as hydrogen ion bombardment or by exposing a sample to hydrogen pressure. In our investigation however, hydrogen was introduced from an electrolyte by cathodic polarization of a sample at room temperature, using the device illustrated in Figure 3.11. A large platinum plate was used as anode (the sample and platinum plate had an area ratio about 1 : 30). The electrolyte was 0.1 M Na_2CO_3 , with distilled water used as the electrolyte solvent. This method is very simple and cost effective, furthermore this electrolyte does not dissolve the sample. Current densities on the order of 100 (mA/cm^2) of sample were used. The amount of hydrogen can be controlled by setting a constant current and adjusting the exposure time; a typical exposure time being a few minutes. The hydrogen can diffuse throughout the sample shortly after loading. In the case of dilute PdNi , the sample became brittle after loading with hydrogen, although they could still be mounted and measured without breaking if handled carefully. The effect of hydrogen on the dilute

PdNi alloys is dramatic since the dilation it induces is readily measured using a Picker traveling micrometer to observe length changes, and these changes can influence the magnetic response.

The hydrogen absorbed can be discharged by annealing the sample in vacuum or reversing the polarity in the electrochemical cell. The effects of repeated hydrogen charging and discharging on the physical properties of samples can also be studied.

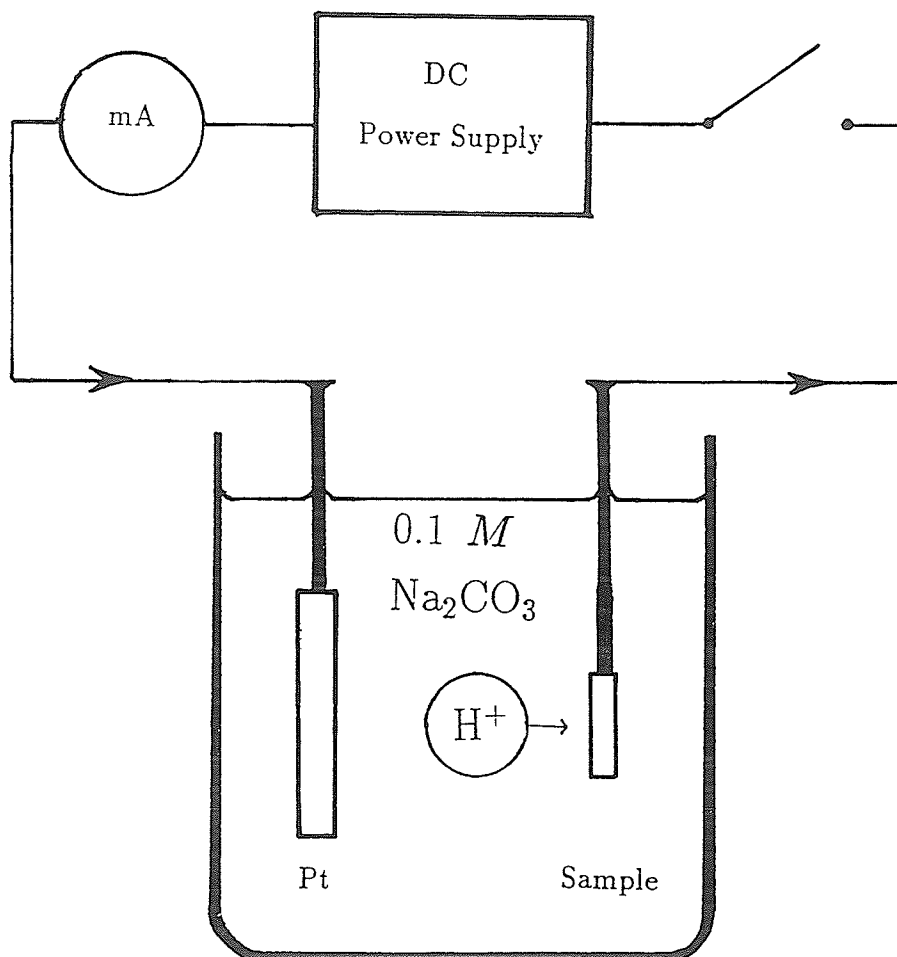


Figure 3.11: Hydrogen absorption device.

Chapter 4

Results and Discussion

4.1 Introduction

The experimental results and their interpretation will be presented in this chapter, which is divided into four major parts. The first part deals with the detailed *ac* susceptibility measurements on three dilute alloy systems namely PdFe, PdNi, and (PdFe)Mn. The second part describes the SRA results on these three systems, while the third part contains a short report of hydrogen effects on a typical dilute PdNi alloy. The conclusions are presented at the end of the chapter.

4.2 *ac* Susceptibility Results for the Dilute PdFe system

4.2.1 A "Perfect System" – Pd_{98.6}Fe_{1.4}

The data reported below are low temperature *ac* susceptibility measurements of seven PdFe alloys containing between 0.35 and 2.4 at% Fe. In the vicinity of the ordering temperature T_c , the zero field susceptibility increases rapidly as the temperature decreases which agrees with the prediction of Equation (1.56). The susceptibility peaks at the temperature T_H (T_H – the Hopkinson maximum (Chikazumi 1964)) which is slightly below Curie temperature T_c . The typical measured maximum zero field susceptibility value was 1.0 (*emu/gOe*), and that represents about 50% of the value set by the dimension of the sample (that is N^{-1} , where N is the demagnetising factor was found by treating the sample as an ellipsoid with the principal axes equal to

the sample's dimensions and evaluating the corresponding elliptic integrals). That latter value is comparable with the maximum zero field susceptibility measured in systems like PdMn, which is known to be a soft ferromagnet, at least for those alloys containing between 0.5 and 2.5 at% Mn (Ho et al 1981a). Indeed the analysis of field susceptibility on the PdFe alloys will further confirm the soft ferromagnetic property of these alloys.

Figure 4.1 shows a detailed examination of the temperature dependence of the *ac* susceptibility for a Pd + 1.4 at% Fe sample in various internal fields (over the range of 0 to 602 *Oe*). The presence of a cross-over line is clear (a line along which the susceptibility in a fixed field exhibits a maximum, that is $(\partial\chi/\partial t)_h = 0$), and the effects described by Equations (1.59) and (1.60) are verified; that is the peak susceptibility decreases as the field increases and the peak temperature (T_p) increases with increasing field. It should be pointed out that a critical peak (corrected for background and demagnetising effects) is observed in a field as low as one *Oe* (shown in Figure 4.2). This means that the measured magnetic response is dominated by contributions arising from critical fluctuations, which is a requirement for any of the power law relations to be valid. The regular contribution to the response (e.g domain wall motion and/or coherent rotation) is removed in low fields.

A quantitative analysis of the field dependence of the peak susceptibility is carried out in Figure 4.2 where the peak susceptibility is plotted against the internal field H_i , where H_i is defined by Equation (3.5), on a double logarithmic plot for the Pd_{98.6}Fe_{1.4} alloy. As can be seen from this plot a

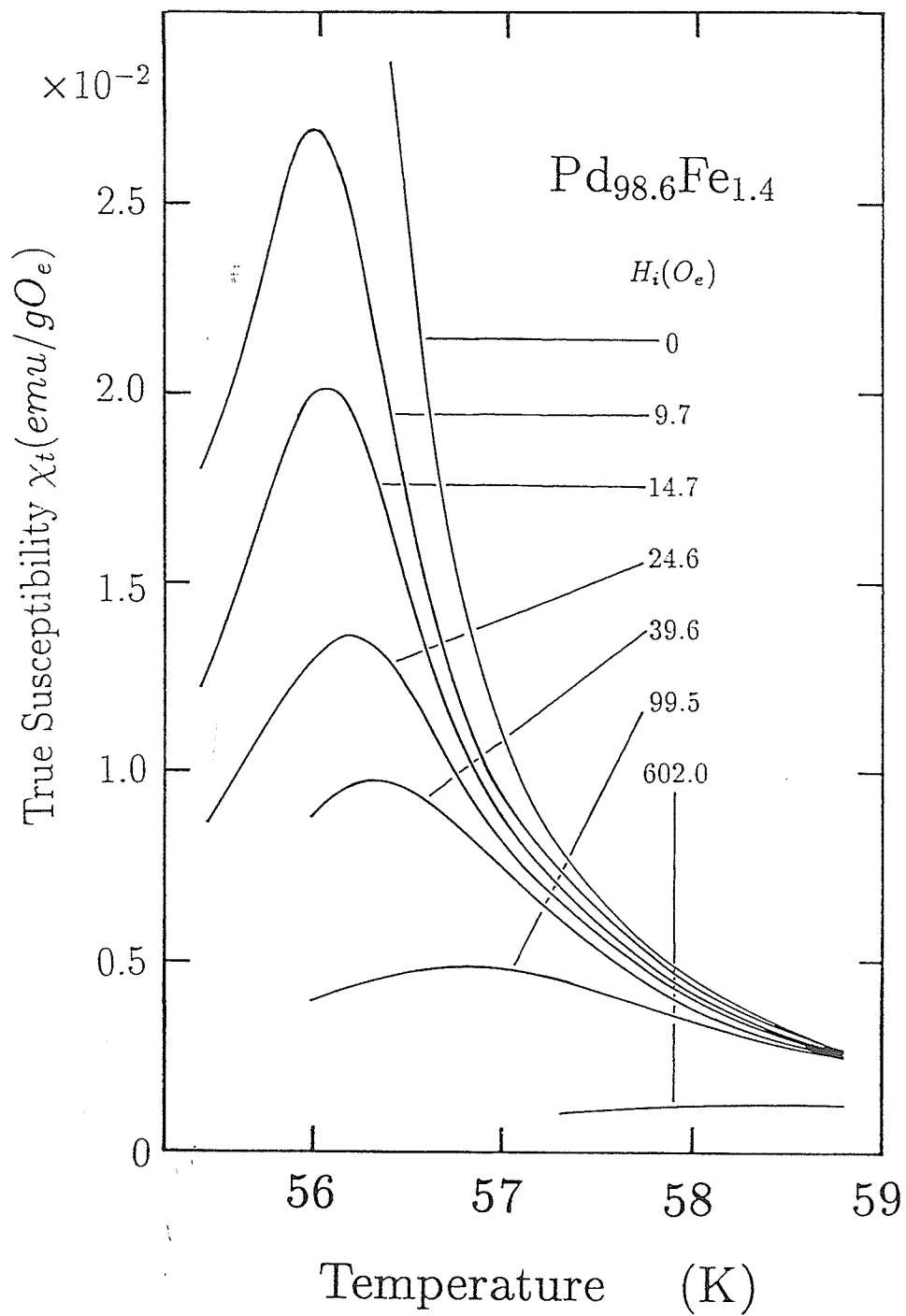


Figure 4.1: The *ac* susceptibility versus temperature for $\text{Pd}_{98.6}\text{Fe}_{1.4}$. The numbers marked against each curve represent the internal field.

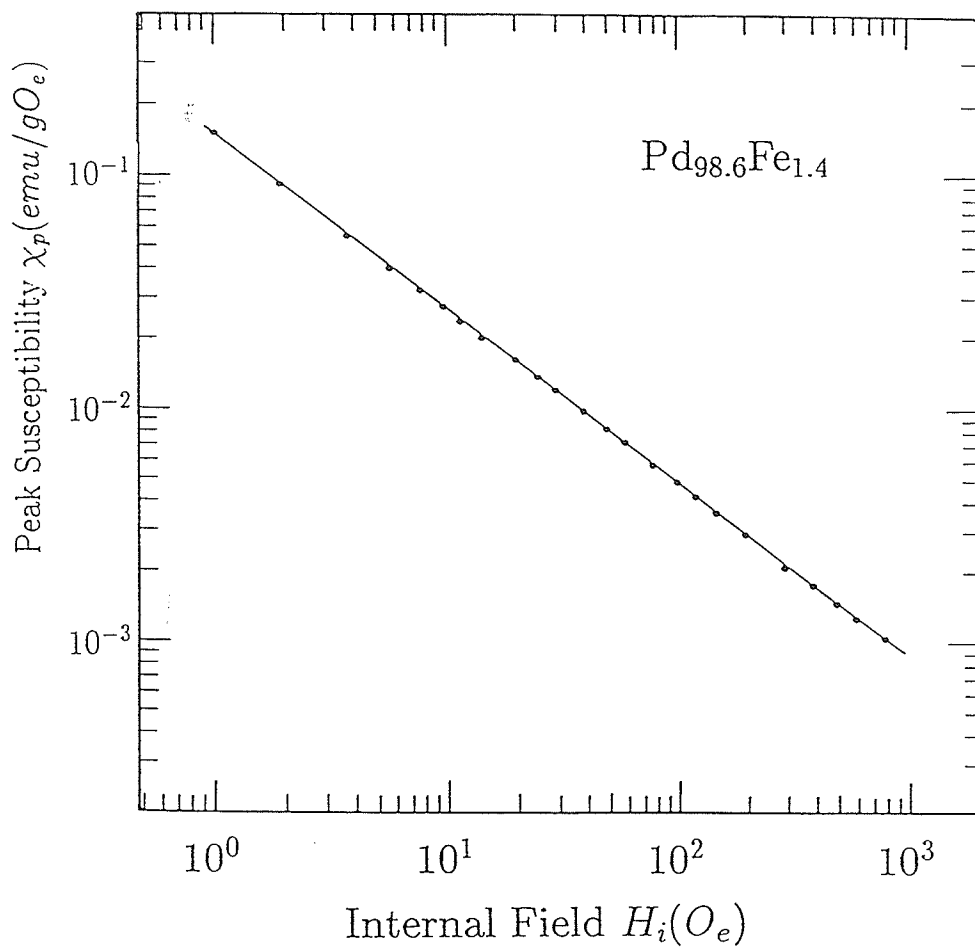


Figure 4.2: The peak susceptibility versus internal field H_i on a double log plot for Pd_{98.6}Fe_{1.4}.

straight line is obtained over the field range between 1 and 800 Oe . A value for the index δ can be obtained from the slope of the plot by using Equation (1.60), which yields $\delta = 4.0 \pm 0.1$. This is close to that found in elemental ferromagnets like pure Ni ($\delta = 4.2$ Kouvel and Fisher 1964). It should be noted that unlike the analysis of magnetization data, the value of δ found from this method is independent of the choice of T_c .

By contrast an estimate for the exponent γ does need a prior knowledge of the critical temperature T_c , which was estimated in the following manner. In Figure 4.3 the critical peak temperature T_p has been plotted against a reasonable power¹ (0.50 in the case of $Pd_{98.6}Fe_{1.4}$) of H_i in order to obtain a first estimate of T_c (Equation 1.59). Such a plot yields a straight line, and the Curie temperature (T_c) was estimated by extrapolating the straight line to $H_i = 0$, the value obtained from such plot is 55.6 ± 0.1 K.

With a value of the Curie temperature so obtained, the reduced peak temperature (t_p) is plotted against the internal field (H_i) on a double logarithmic scale for the $Pd_{98.6}Fe_{1.4}$ sample. According to Equation (1.59), such a plot should produce a straight line with a slope of $1/(\gamma + \beta)$, and the result is shown in Figure 4.4. As can be seen from the plot, the behaviour predicted by the equation is confirmed, namely the temperature of the critical peaks increases with increasing field, and the value for $1/(\gamma + \beta)$ obtained in the above manner is 0.54 ± 0.02 .

¹If the exponents γ and β are assumed to be close to the theoretical values predicated by the isotropic three-dimensional Heisenberg model, as listed in Table 1.1, then $(\gamma + \beta)^{-1} = 0.57$.

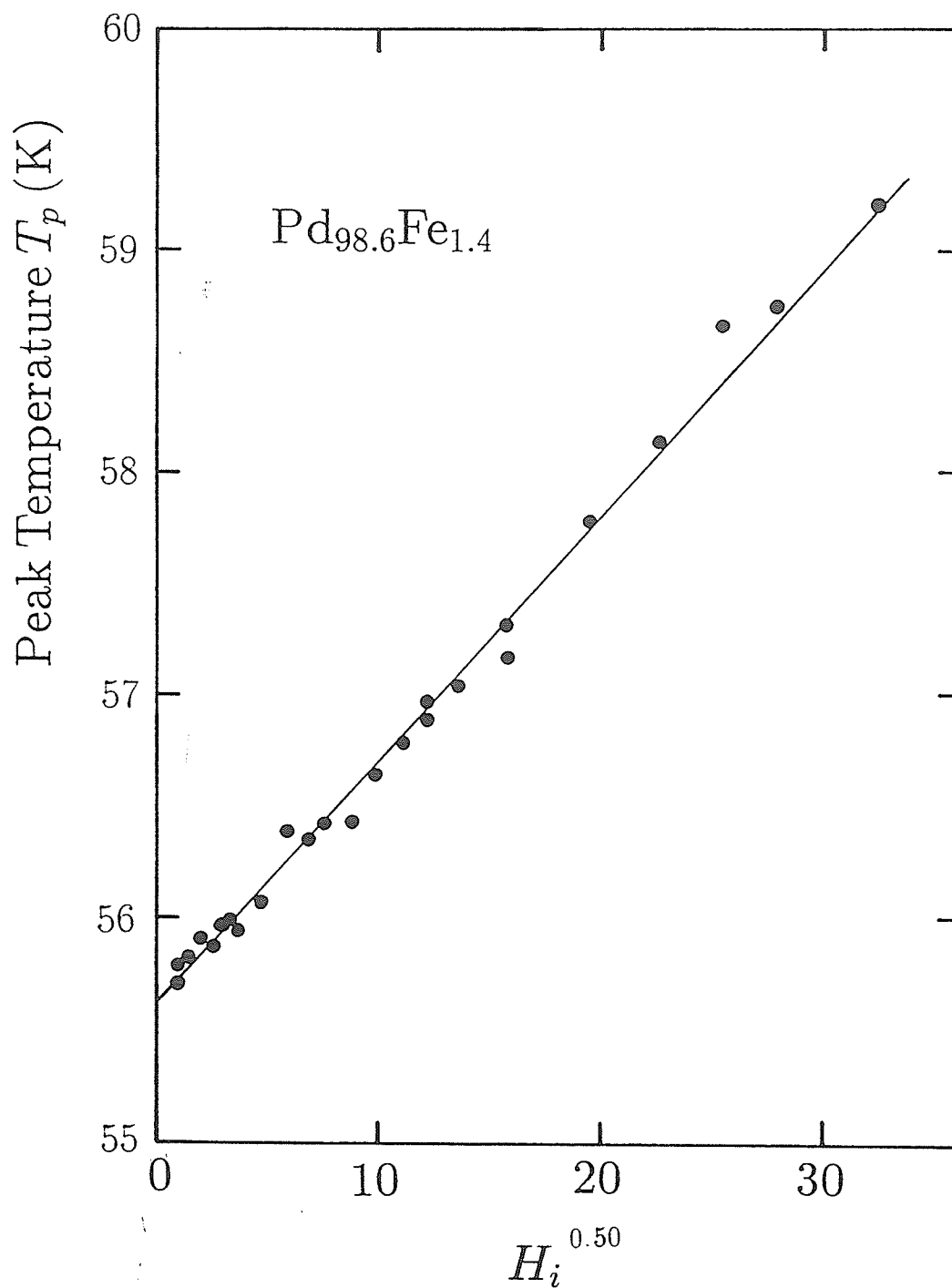


Figure 4.3: The peak temperature versus $H_i^{0.50}$ for $\text{Pd}_{98.6}\text{Fe}_{1.4}$, the intercept of the straight line fit gives T_c .

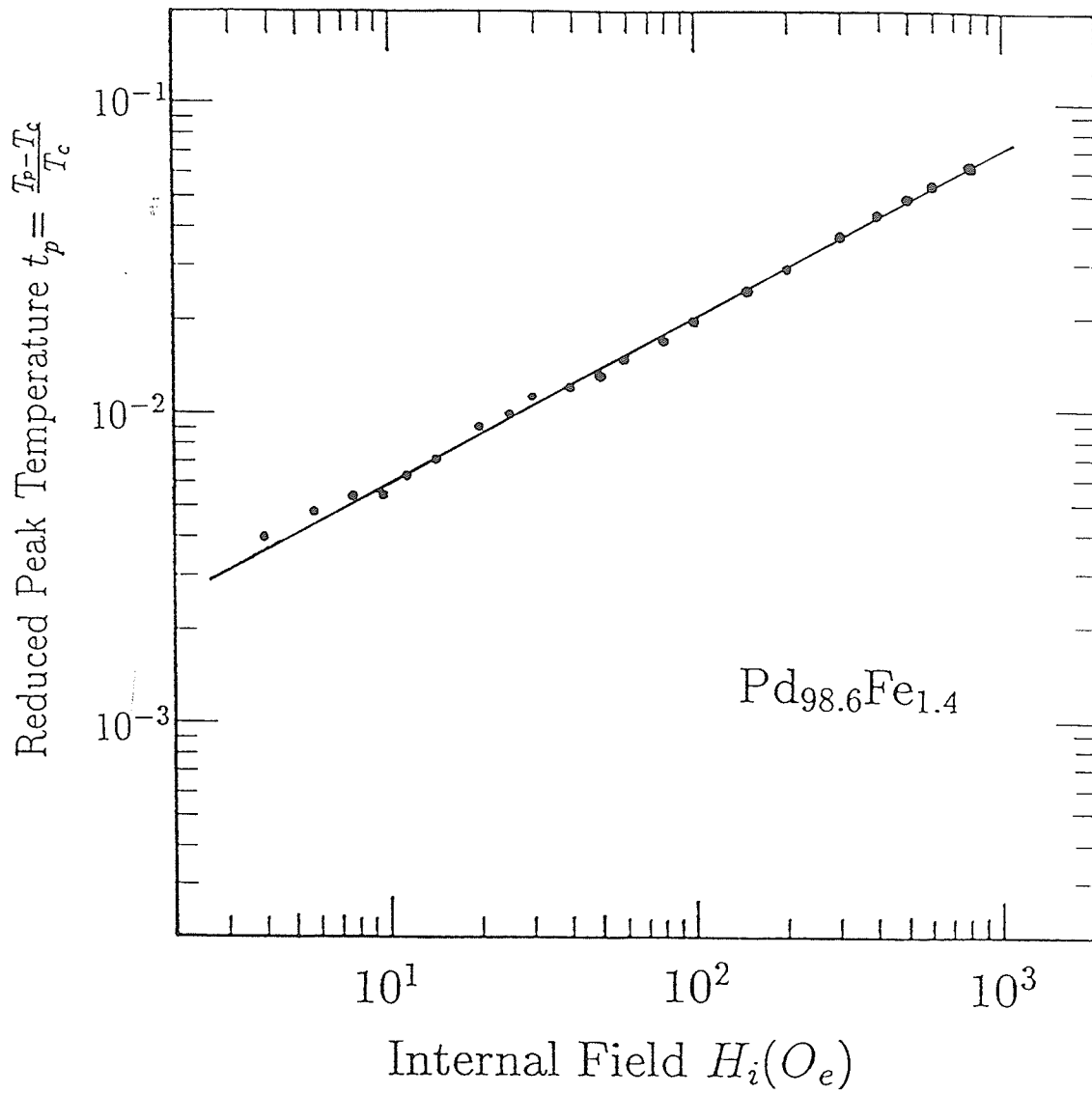


Figure 4.4: The reduced peak temperature versus internal field H_i on a double log plot for Pd_{98.6}Fe_{1.4}.

Using zero field susceptibility data, it is possible to deduce a value for the critical exponent γ by using Equation (1.56). This was done by plotting the susceptibility on a double logarithmic scale against the reduced temperature t as shown in Figure 4.5. In order to obtain the best straight line fit to the data for $t \approx 10^{-2}$, a small adjustment in T_c of a few tenths of a degree is sometimes necessary. The value for γ estimated from these data is 1.36 ± 0.05 which is close to the value of 1.388 quoted for the three dimensional Heisenberg ferromagnet as listed in Table 1.1. Substituting this γ value into the cross-over exponent, $1/(\gamma + \beta)$, yields a β value of 0.49. The exponent values obtained above satisfy the Widom relationship ($\gamma = \beta(\delta - 1)$).

Kouvel and Fisher (1964) have defined the effective exponent $\gamma^*(T)$ as

$$\gamma^*(T) = (T - T_c)/T^* = (T - T_c)(d/dT)\ln(\chi_0^{-1}) \quad (4.1)$$

where T is temperature and χ_0 is initial susceptibility. An alternative extrapolation procedure to deduce a value for the critical exponent γ is to plot the effective exponents γ^* (from the local slopes on the log-log plot of the zero field susceptibility data as indicated in the above equation) as a function of reduced temperature t , as showed in the inset of Figure 4.5. Excluding² the temperature region very close to T_c the effective susceptibility exponent γ^* shows very little change with changing temperature, and the extrapolated γ^* value at $T = T_c$, is 1.36 ± 0.02 which agrees very well with that (1.36 ± 0.05)

²As the susceptibility does not reach the demag limit, presumably due to the anisotropy effect, the effective exponent $\gamma^*(T)$ must eventually fall at temperature close to T_c .

previously deduced from the plot of zero field susceptibility versus reduced temperature by using Equation (1.56).

A final appraisal of the ferromagnetic transition can be carried out by summarizing the entire field and temperature dependence of the susceptibility in a scaling plot. Equations (1.57), (1.59) and (1.60), when combined, yield

$$\frac{\chi(h, t)}{\chi(h, t_p)} = \frac{G(h/t^{\gamma+\beta})}{G(h/t_p^{\gamma+\beta})} \propto G(h/t^{\gamma+\beta}) \quad (4.2)$$

since the denominator is a constant. Equation (4.2) predicts that the normalized susceptibility plotted against $h/t^{\gamma+\beta}$ should produce a universal curve. The dependence of the scaling function G on its argument for arbitrary values of h and t (i.e. the form of the curve) can only be specified by experimental data, not from general scaling considerations.

In Figure 4.6 the field and temperature dependence of the *ac* susceptibility of the $\text{Pd}_{98.6}\text{Fe}_{1.4}$ sample has been plotted against the argument $(t/h^{1/(\gamma+\beta)})$ of the scaling function G using the Curie temperature $T_c = 55.6$ K and $\frac{1}{\gamma+\beta} = 0.55$ (Equation 4.2). As shown in the plot, the susceptibility data normalized to its peak value and measured in a number of fixed non-zero fields h as a function of temperature collapses onto a single universal curve. Similar results have been previously obtained for the ferromagnet $(\text{Pd}_{99.25}\text{Mn}_{0.75})$ as well as the re-entrant system $((\text{Pd}_{99.65}\text{Fe}_{0.35})_{95}\text{Mn}_5)$ (Kunkel and Williams 1988a, b).

The scaling law only describes that part of the susceptibility that arises

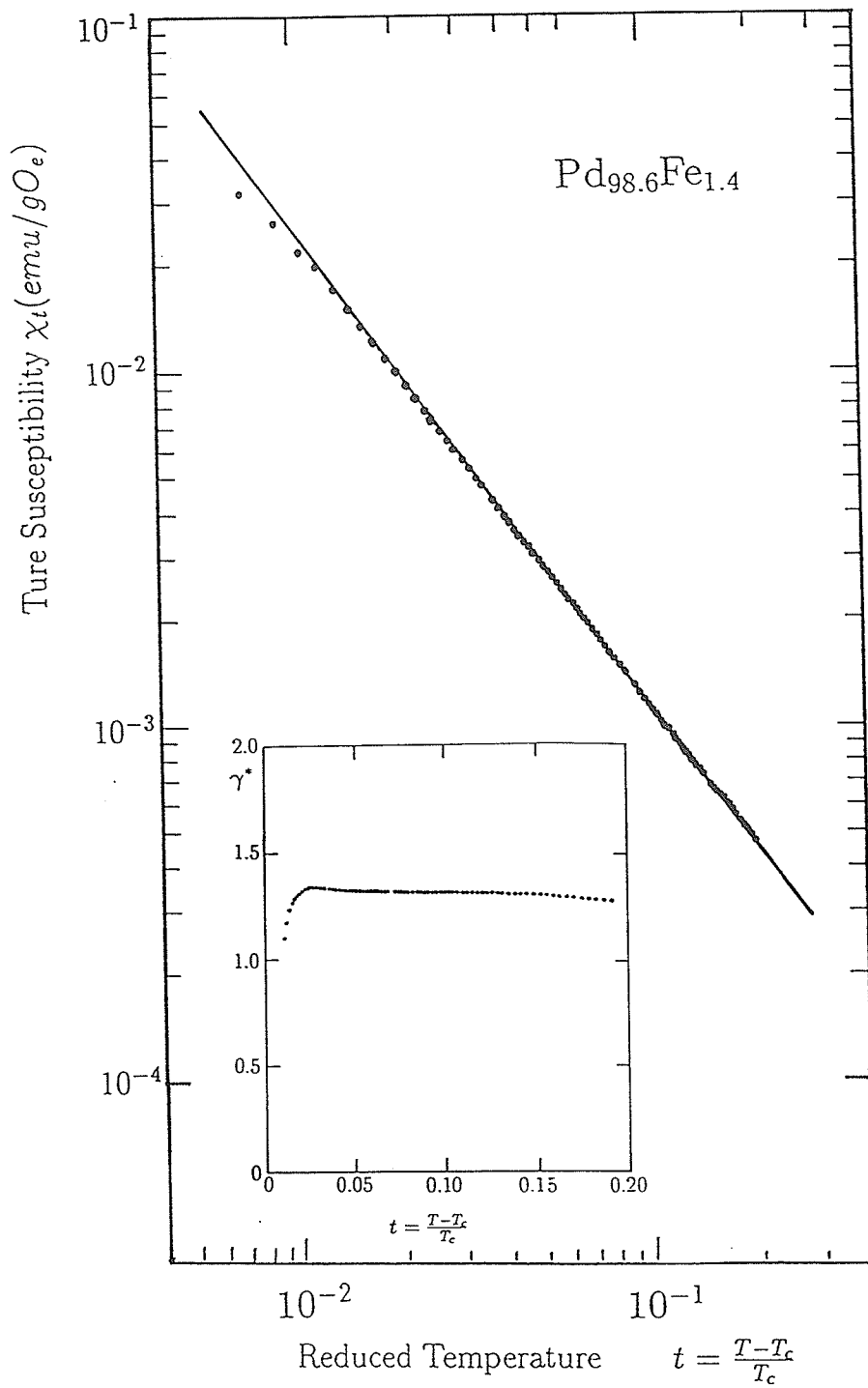


Figure 4.5: The zero field susceptibility versus the reduced temperature t near T_c on a double log plot for the $\text{Pd}_{98.6}\text{Fe}_{1.4}$ specimen. The inset shows the temperature dependence of the effective exponent γ^* .

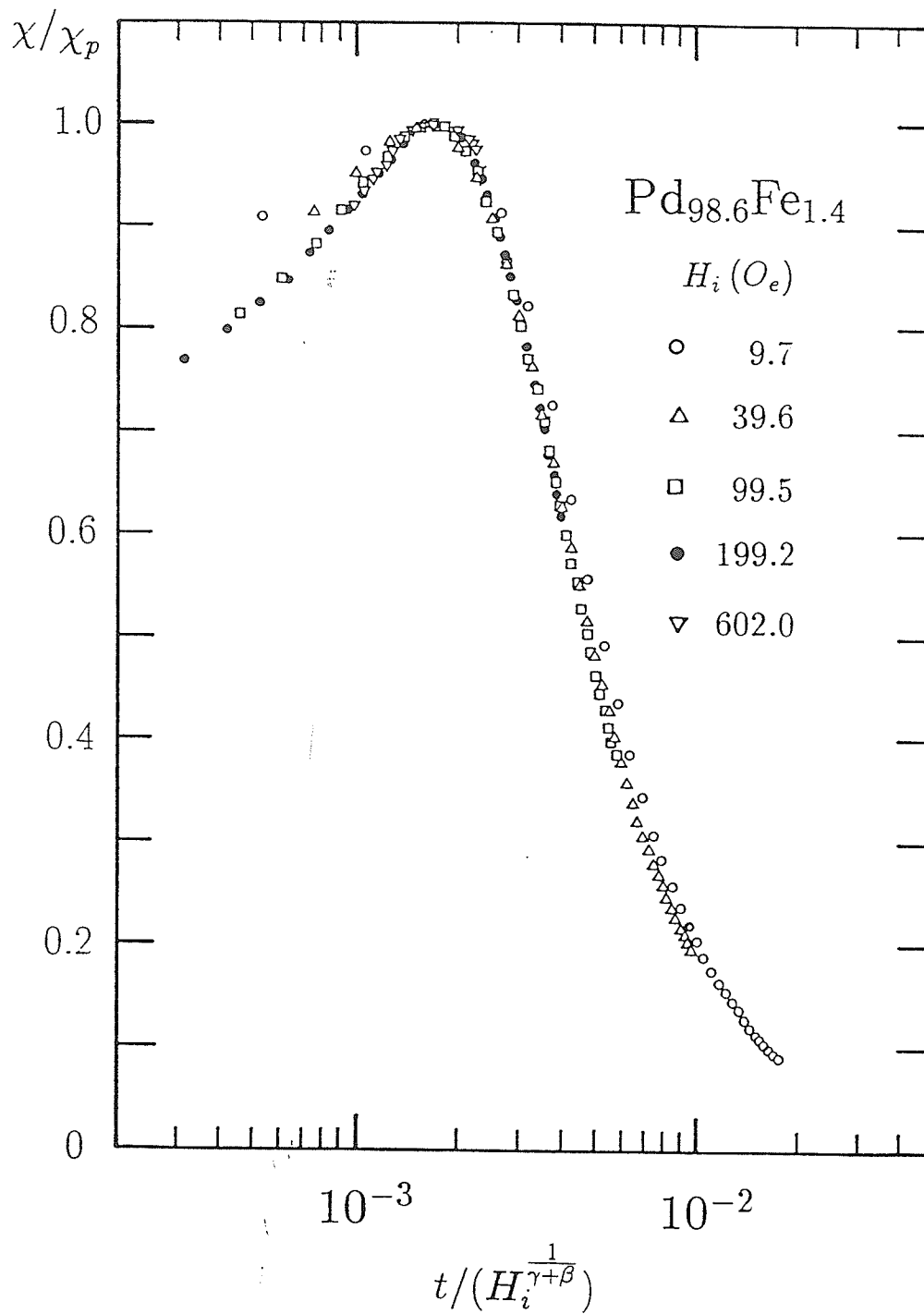


Figure 4.6: A scaling plot for Pd_{98.6}Fe_{1.4} in various fields.

from critical fluctuations. In situations where an anisotropy exists, which typically might occur if an orbital moment were present on the impurity site, and results in spin-orbit coupling, an additional non-critical component in the susceptibility may also exist. Basically this would, for example, consist of domain wall contributions, since the applied field would no longer saturate this "technical" contribution in low fields. This complicates the determination of the critical exponents as the magnitude of this "technical" contribution would not generally be known. This complication was not observed in the case of the $\text{Pd}_{98.6}\text{Fe}_{1.4}$ alloy, and indeed the Fe impurity does not have a substantial orbital moment in this host at this composition (Senoussi et al 1977). We conclude therefore that $\text{Pd}_{98.6}\text{Fe}_{1.4}$ is a good ferromagnet, with near Heisenberg critical exponent values. However in the case of dilute PdNi alloys (where Ni is known to have a substantial orbital moment (e.g. Kunkel et al 1987), and also in higher composition PdFe alloys, an anisotropy exists which complicates the magnetic measurements, although at the same time, it is essential for the presence of a spontaneous resistive anisotropy (SRA) (discussed in Sections 4.3 and 4.5).

4.2.2 Fe concentration Dependence

Figures 4.7 and 4.8 present a closer examination of the temperature variation of true susceptibility in various internal fields for the $\text{Pd}_{99.65}\text{Fe}_{0.35}$ and $\text{Pd}_{97.6}\text{Fe}_{2.4}$ alloys which typify the results that have been obtained in this concentration range; i.e. from one of the most dilute to one of the most Fe concentrated samples studied. The effects of applied fields are quite strik-

ing as a field as small as the earth's field can reduce the susceptibility substantially, thus facilitating the observation of smaller secondary peaks in the vicinity of the transition temperature. Basically all the seven PdFe alloys studied exhibit similar behaviour in various collinear biasing fields. External fields rapidly suppress the susceptibility in the ordered state, allowing the critical peak to be observed in applied fields as low as about 0.3 Oe (in the case of 0.35 at% Fe alloy), although the minimum field necessary to resolve an emerging critical peak climbs to about 10 Oe for the Pd + 2.4 at% Fe alloy. Nevertheless, these results confirm the alloys are soft ferromagnets. The expected maximum in the susceptibility at temperature T_p increases as the field increases. The detailed temperature and field variation for all the PdFe alloys studied are shown in Appendix A.

A quantitative analysis of the field dependence of the peak susceptibility for two PdFe alloys (0.35 and 2.4 at% Fe) is carried out in Figure 4.9 using Equation (1.60). The peak susceptibility is plotted against the internal field H_i on a double logarithmic plot. As shown in this figure the peak susceptibility is indeed proportional to the $H_i^{-\delta}$ over the range $10\text{ }Oe \leq H_i \leq 1000\text{ }Oe$ (down to 0.3 Oe in the case of Pd_{99.65}Fe_{0.35} alloy). The estimates for exponent δ then can be made from the slopes of these curves, and these values combine with the ones obtained for other PdFe alloys studied are listed in Table 4.1.

The δ values obtained range from 2.4 to 3.1 for the samples we have investigated (the Pd_{98.6}Fe_{1.4} is an exception as it has a δ value 4.0 as discussed in Section 4.2.1.). Most of these values for δ are substantially less than that

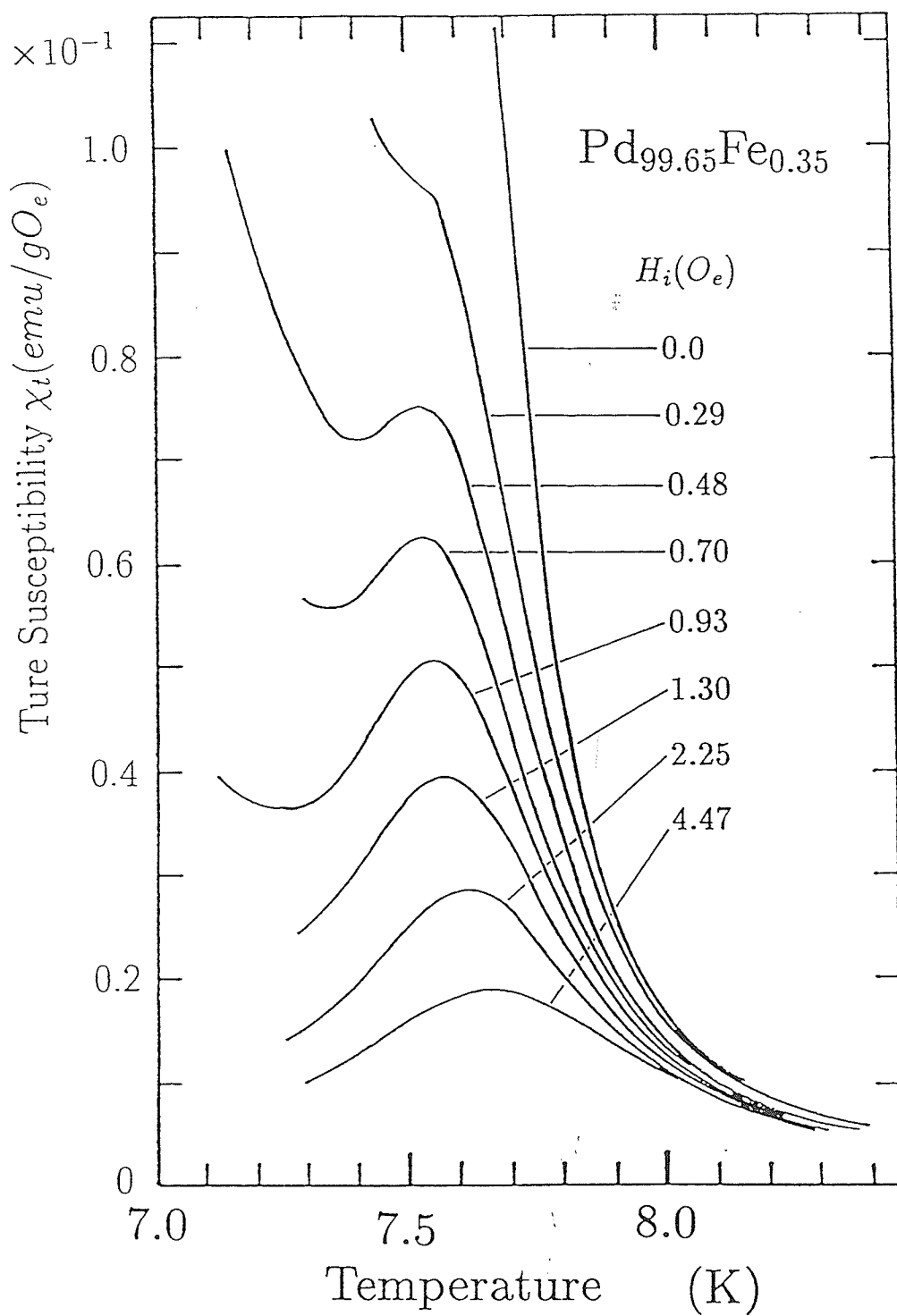


Figure 4.7: The true susceptibility versus temperature for $\text{Pd}_{99.65}\text{Fe}_{0.35}$ in various internal fields.

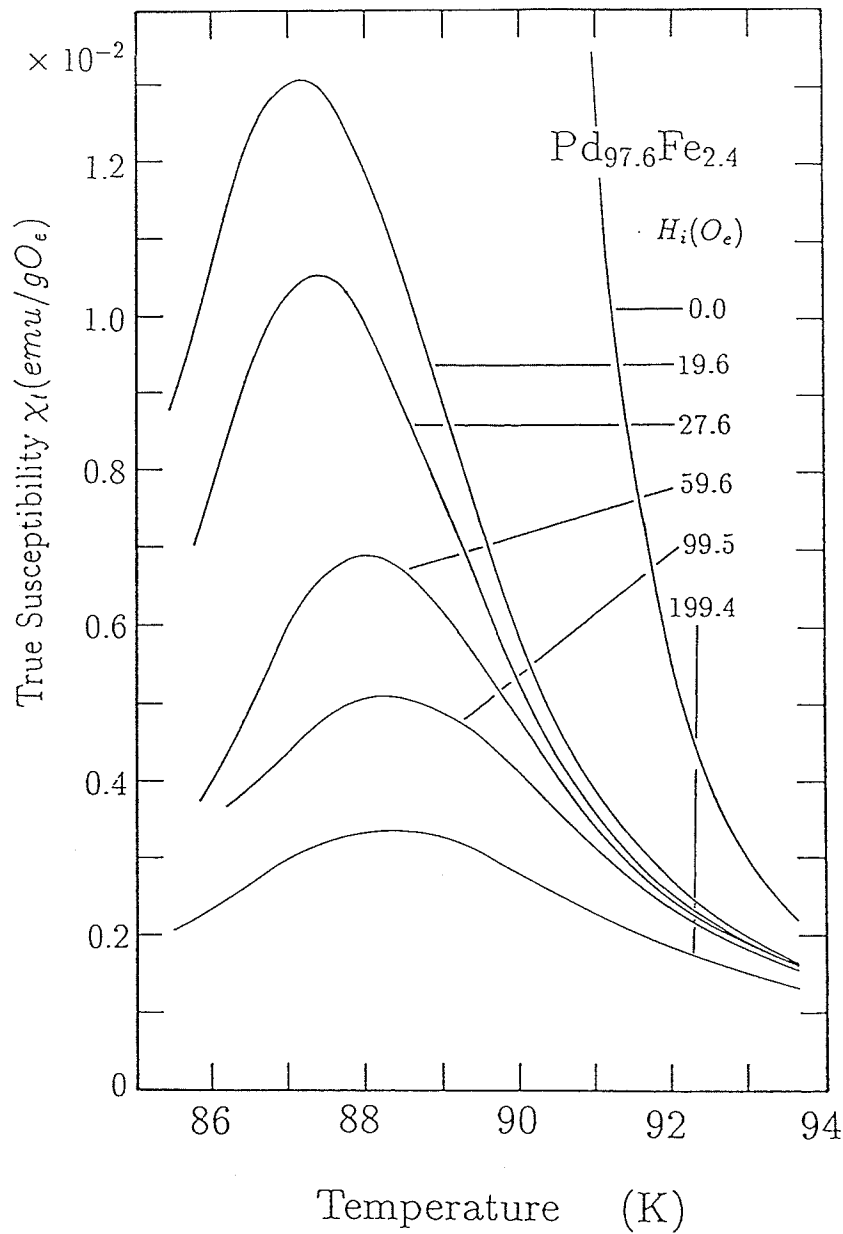


Figure 4.8: The true susceptibility versus temperature for $\text{Pd}_{97.6}\text{Fe}_{2.4}$ in various internal fields.

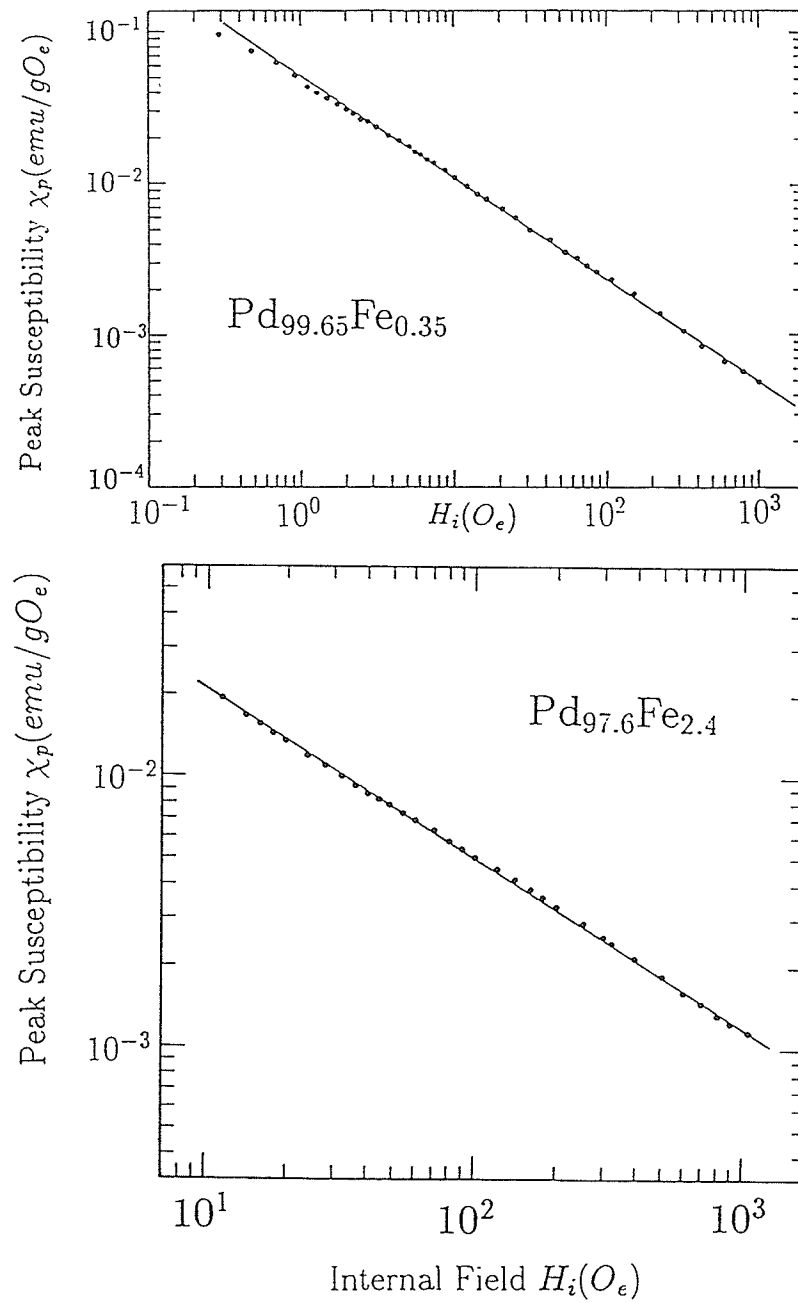


Figure 4.9: Peak susceptibility versus internal fields for the Pd_{99.65}Fe_{0.35} and Pd_{97.6}Fe_{2.4} alloys.

Table 4.1: Summary of parameters taken from the *ac* susceptibility data for the PdFe specimens.

Alloy Fe at%	T_c (K)	δ	γ_{max}^*
0.35	7.50 ± 0.03	3.1 ± 0.1	1.8 ± 0.1
1.4	55.6 ± 0.1	4.0 ± 0.1	1.36 ± 0.02
1.6	61.5 ± 0.2	2.8 ± 0.1	3.5 ± 0.1
1.8	69.1 ± 0.2	2.5 ± 0.1	3.2 ± 0.1
2.0	75.4 ± 0.3	2.4 ± 0.1	3.3 ± 0.1
2.2	80.6 ± 0.5	2.4 ± 0.1	3.2 ± 0.1
2.4	86.6 ± 0.5	2.7 ± 0.1	3.6 ± 0.1

found for elemental ferromagnets as quoted in Chapter 1, but are comparable with the δ values obtained in some other Pd based dilute alloys such as intermediate concentration PdMn alloys.

These δ values decrease initially with Fe concentration above 1.4 at% Fe, passing through a minimum at about 2.0 at% Fe, and then increase with further increases in Fe content. A similar concentration dependence has been observed in the dilute (PdFe)Mn alloys (discussed later).

Using data similar to that shown in Figure 4.9, it is possible to estimate the peak position of the susceptibility in zero field, that is a value for T_c . In Figure 4.10 the peak susceptibility temperatures of the Pd_{99.65}Fe_{0.35} and Pd_{97.6}Fe_{2.4} alloys have been plotted against $H_i^{1/2}$ for the entire field range studied. This figure indicates that the approximate relationship³ between peak temperature and field does exist. This approach enables estimates for T_c to be made; and the results are also listed in Table 4.1.

The Curie temperature exhibits a nearly linear dependence on Fe concentration between 1.4 and 2.4 at% with a ratio $\frac{dT_c}{dx} \approx 32$ K/at% Fe. The 0.35 at% Fe sample has a $T_c = 7.50$ K, substantially less than the value estimated by extrapolation from higher concentration samples. That is not unexpected, as discussed in Section 2.3.1; the transition temperature is roughly proportional to the square of Fe concentration in the case of low concentration PdFe alloys.

Using the estimated value for the Curie temperature mentioned above,

³We will give more details about the approximate relationship in Section 4.3.2.

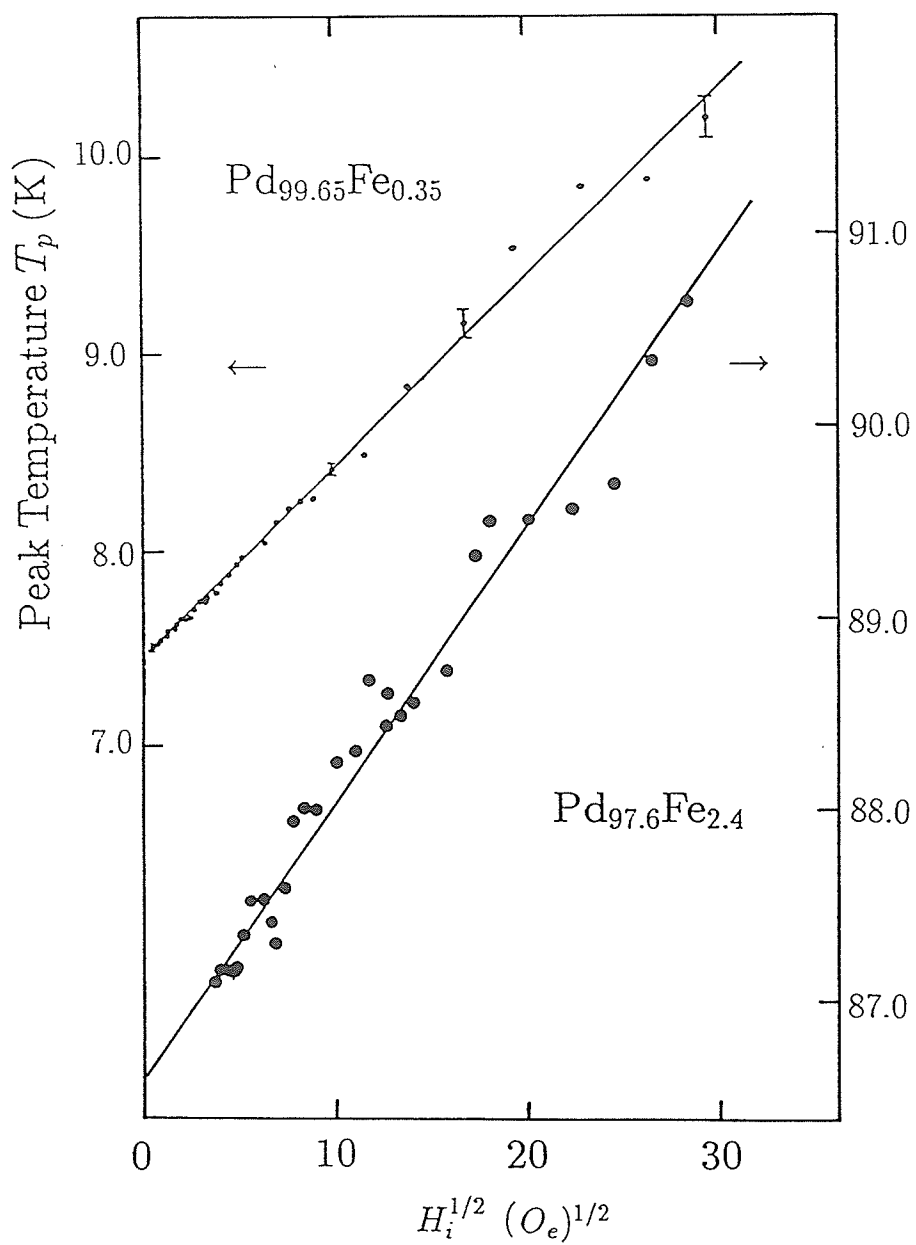


Figure 4.10: Peak temperature T_p versus $H_i^{1/2}$ for $\text{Pd}_{99.65}\text{Fe}_{0.35}$ and $\text{Pd}_{97.6}\text{Fe}_{2.4}$ alloys.

an attempt was made to estimate the critical exponent γ by plotting the zero field susceptibility values (for $T \geq T_c$) on a double logarithmic plot against reduced temperature t . As shown in Figure 4.11, at low reduced temperatures a severe flattening is observed; while at higher temperatures close examination reveals considerable curvature with large local slopes, and no extended power law regime is seen.

The insets of Figure 4.11 show the temperature dependence of the effective exponent γ^* . Unlike the $\text{Pd}_{98.4}\text{Fe}_{1.4}$ alloy, at intermediate temperature the effective susceptibility exponents increase with increasing temperature, and achieves a maximum value γ_{max}^* (1.8 ± 0.1 in the case of 0.35 at% Fe, and 3.5 ± 0.1 in 2.4 at% Fe alloy). Thus the effective susceptibility exponents γ^* are strongly temperature dependent as indicated by the “S” shaped γ plot shown in the Figure 4.11. The γ_{max}^* values for all the PdFe alloys studied are also listed in Table 4.1.

High γ_{max}^* values coupled with low δ values in more concentrated PdFe alloys are not unexpected since the smallest field required to first resolve a critical peak increases with increasing Fe concentration (from about one Oe for 1.4 at% Fe to about ten Oe for 2.4 at% Fe alloy,⁴ as shown in Figures 4.2 and 4.9). This indicates an additional non-critical component in the susceptibility of PdFe alloys, which plays some role in complicating the determination of the critical exponents. This situation becomes much more pronounced in the case of PdNi alloys, as Ni is known to have a substantial orbital moment.

⁴This field is less than 0.5 Oe in the case of 0.35 at% Fe alloy.

This latter conclusion receives support from the observation of non-zero SRA in both PdNi and PdFe alloys discussed in Section 4.5 and 4.6.

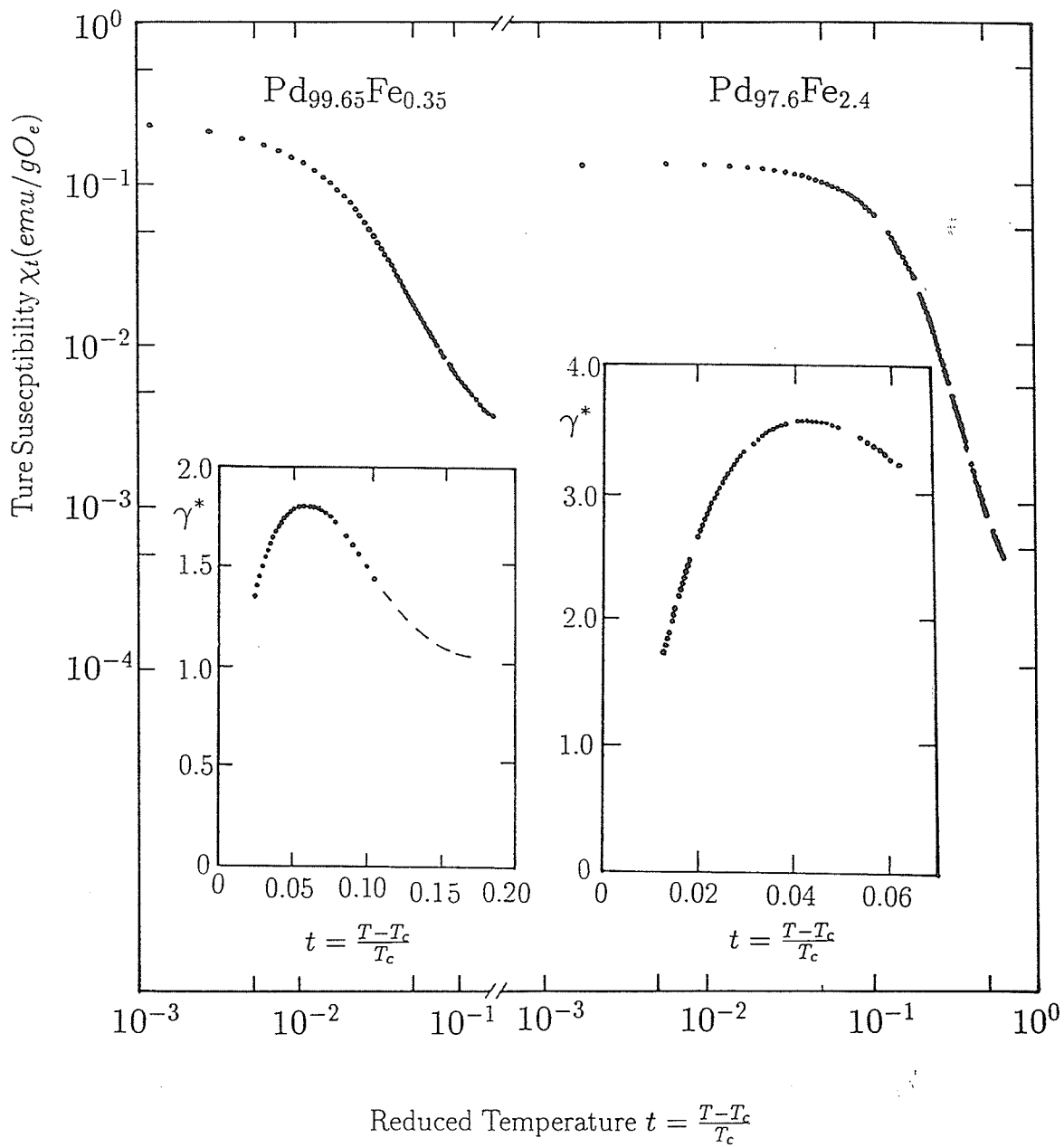


Figure 4.11: The zero field susceptibility versus the reduced temperature t near T_c on a double log plot for $\text{Pd}_{99.65}\text{Fe}_{0.35}$ and $\text{Pd}_{97.6}\text{Fe}_{2.4}$ alloys. The insets show the temperature dependence of the effective exponent γ^* .

4.3 *ac* Susceptibility Results for the Dilute PdNi System

4.3.1 General Features of the PdNi System

Figure 4.12 shows the behaviour of the zero field *ac* susceptibility for a typical sample Pd + 3.5 at% Ni. In the vicinity of the ordering temperature T_c the susceptibility, $\chi(H_a = 0, T)$, increases rapidly with decreasing temperature. It peaks at about 30 K (Hopkinson peak, Chikazumi 1964), with a maximum susceptibility of about $3 \times 10^{-2}(\text{emu/gOe})$. This latter value represents only a few percent of the limit set by demagnetising constraints, and it is up to a factor of 50 smaller than that observed in soft ferromagnetic alloys based on the same host, such as PdMn (Ho et al 1981a), and PdFe alloys as discussed in Section 4.2.2. It is, however, comparable with the maximum susceptibility observed in systems like (PdNi)Mn (Hall et al 1984; Kunkel et al 1988b), and PdCo (Maartense and Williams 1976), systems in which the impurity is known to carry an orbital moment (Senoussi et al 1977). Below the peak temperature, the susceptibility then decreases rapidly with decreasing temperature, an effect which is often attributed to the presence of anisotropy (actually due to a strong temperature dependence of the anisotropy/coercivity (Morrish 1965)).

The effects of various external applied fields H_a are illustrated in Figure 4.13. The Hopkinson peak height decreases rapidly and its position moves downwards in temperature as H_a increases, allowing a secondary peak (i.e. the critical peak) to be resolved at a temperature close to the Curie tempera-

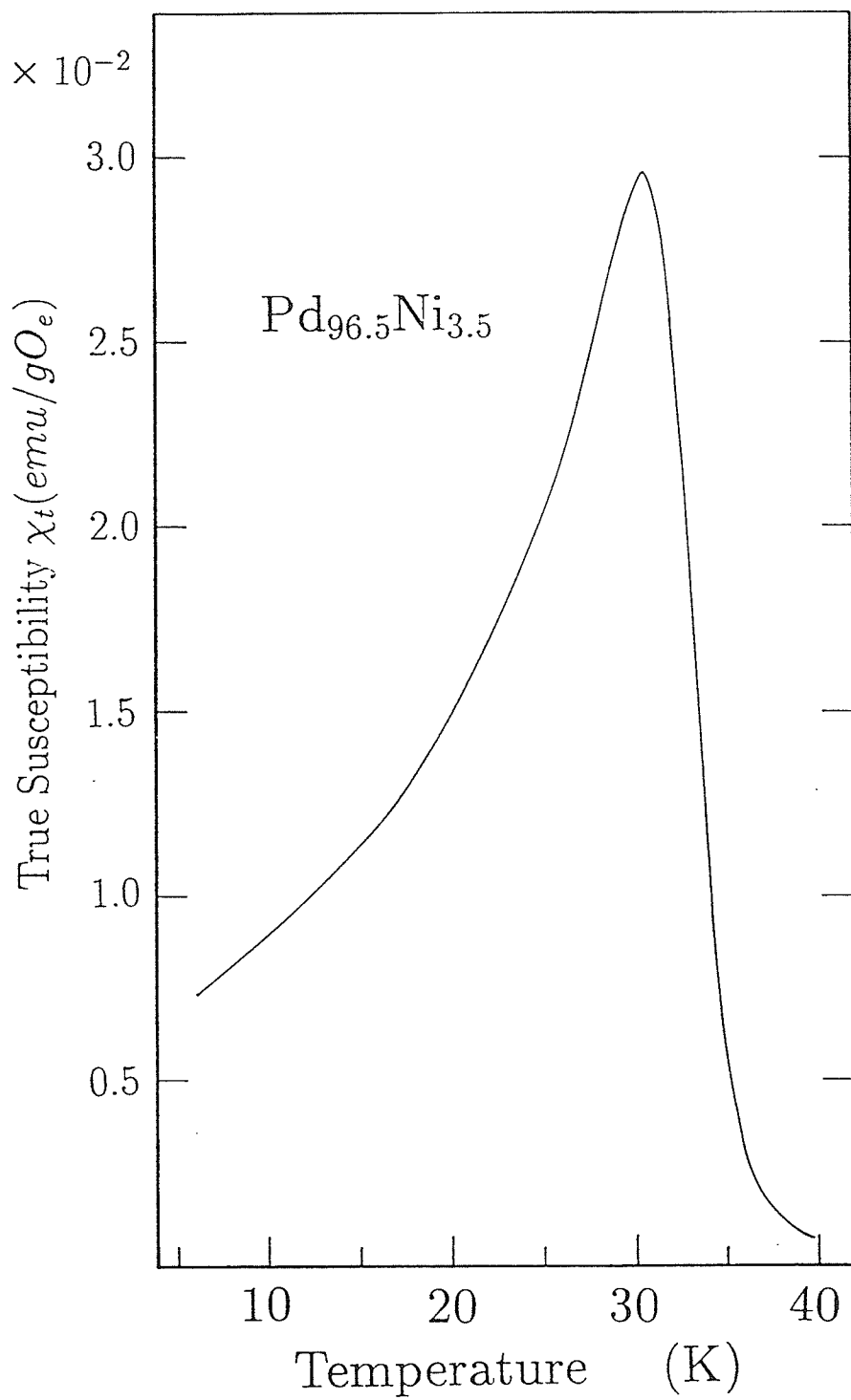


Figure 4.12: Zero field true Susceptibility versus temperature of Pd_{96.5}Ni_{3.5} alloy.

ture T_c and somewhat higher in temperature than the Hopkinson maximum; the critical peak amplitude though is much smaller than that of the Hopkinson maximum. As can be seen from this figure the behaviour of the critical peak described by Equations (1.59) and (1.60) is basically followed, namely the critical peak is rapidly suppressed in amplitude with increasing dc biasing field, while the peak position T_p increases slightly in temperature with increasing field. In all the ferromagnetic samples examined, ($2.4 \leq x \leq 5.0$ at% Ni), the qualitative behaviour of the ac susceptibility in both zero and various applied fields is very similar, and it will be further detailed below.

4.3.2 Detailed Features of a PdNi Specimen

Figures 4.12, 4.13, as well as the detailed data shown in Appendix A present a closer examination of the temperature variation of the true susceptibility (corrected for background and demagnetising effects) in a number of applied fields (between 0 and 900 Oe) for the Pd + 3.5 at% Ni sample. As indicated in these figures, similar to the PdFe samples, the qualitative behaviour described by Equations (1.59) and (1.60) is followed, namely the experimentally observed peak susceptibility χ_p decreases as field increases and secondly the peak temperature T_p increases with increasing field. Notice, however, that unlike the PdFe samples, the critical peak cannot be resolved until the applied field reaches about 40 Oe , that is about 50 times the field required for a soft ferromagnet such as Pd_{98.6}Fe_{1.4} (about 100 times the field required in Pd_{99.65}Fe_{0.35}). This is strong evidence that the regular contribution (basically the result of anisotropy which is essential to explain the non-zero spontaneous

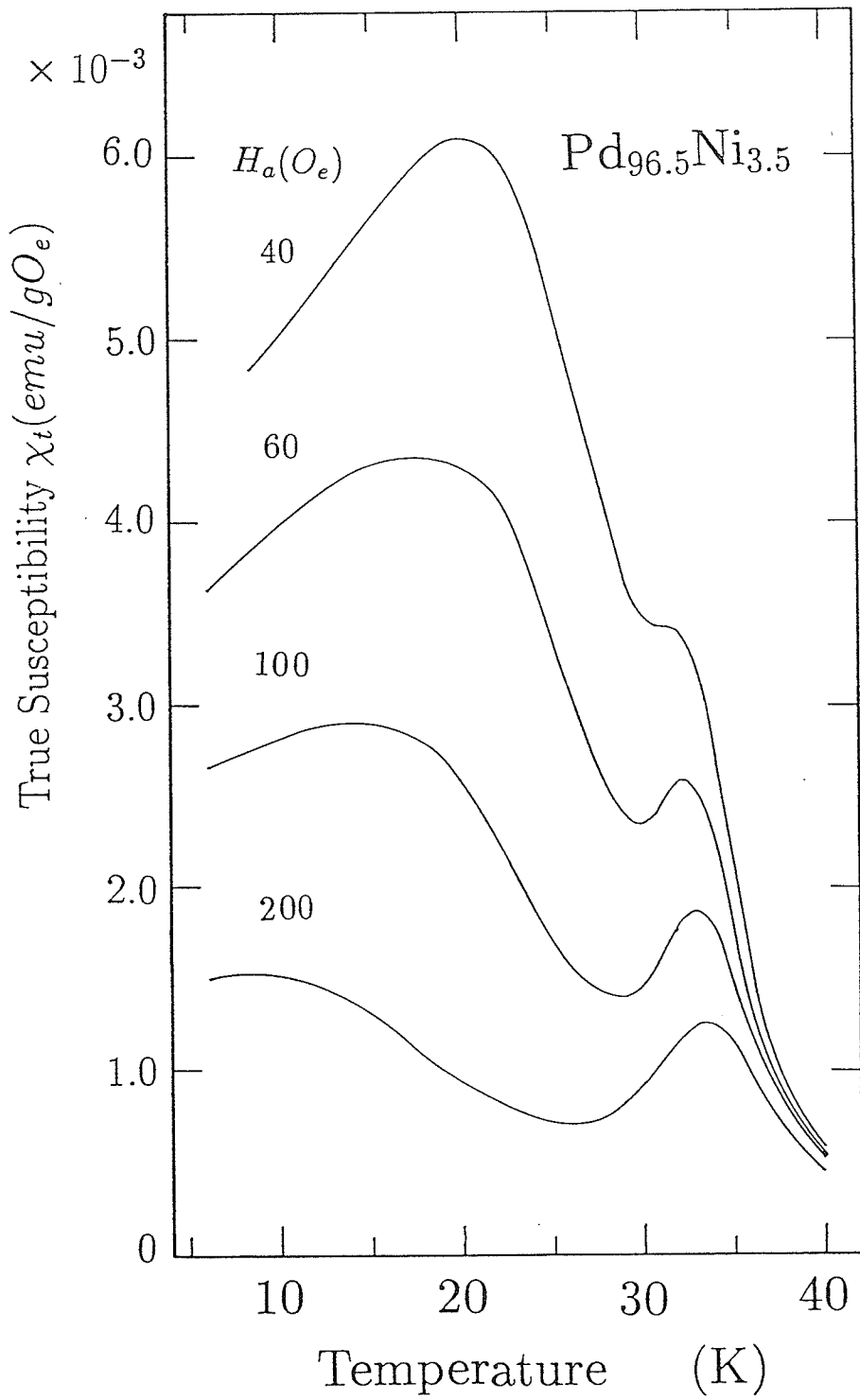


Figure 4.13: Susceptibility versus temperature for $Pd_{96.5}Ni_{3.5}$ at various static biasing fields.

resistive anisotropy (SRA) as we will discuss in Section 4.5) makes a significant contribution to the susceptibility in this system. This latter statement is further supported by the following observation. Even in an applied field up to 100 Oe , the slope of the susceptibility curve reverses quite rapidly just below the critical peak temperature indicating a large background susceptibility, which means that non-critical response is much more difficult to saturate.

In Figure 4.14 the peak susceptibility χ_p has been plotted against the internal field H_i (estimated from $H_i = H_a - NM$) on a double logarithmic plot for the $Pd_{96.5}Ni_{3.5}$ sample. As the plot shows, the power-law behaviour predicted by Equation (1.60) is not followed over the entire field range measured. The peak susceptibility against the internal fields plot exhibits a visible curvature and therefore no unique critical exponent δ could be deduced from the plot. This situation was not observed in soft ferromagnetic materials such as $Pd_{98.6}Fe_{1.4}$ (Figure 4.2). The extent of the curvature can be seen from the two straight lines drawn at low and high field, which yield two corresponding effective exponents, δ_l^* and δ_h^* , (from the low and high field slopes respectively), which are 3.3 and 2.2 respectively. These values are much lower than that for a typical ferromagnet.

As shown earlier, the zero field susceptibility and the field dependence of the critical peak temperatures in soft ferromagnets such as $Pd_{98.6}Fe_{1.4}$ can be well described by Equations (1.56) and (1.59). Reliable critical exponents γ and β can then be obtained from double logarithmic plots of reduced peak temperature t_p against internal field H_i and the true zero-field susceptibility

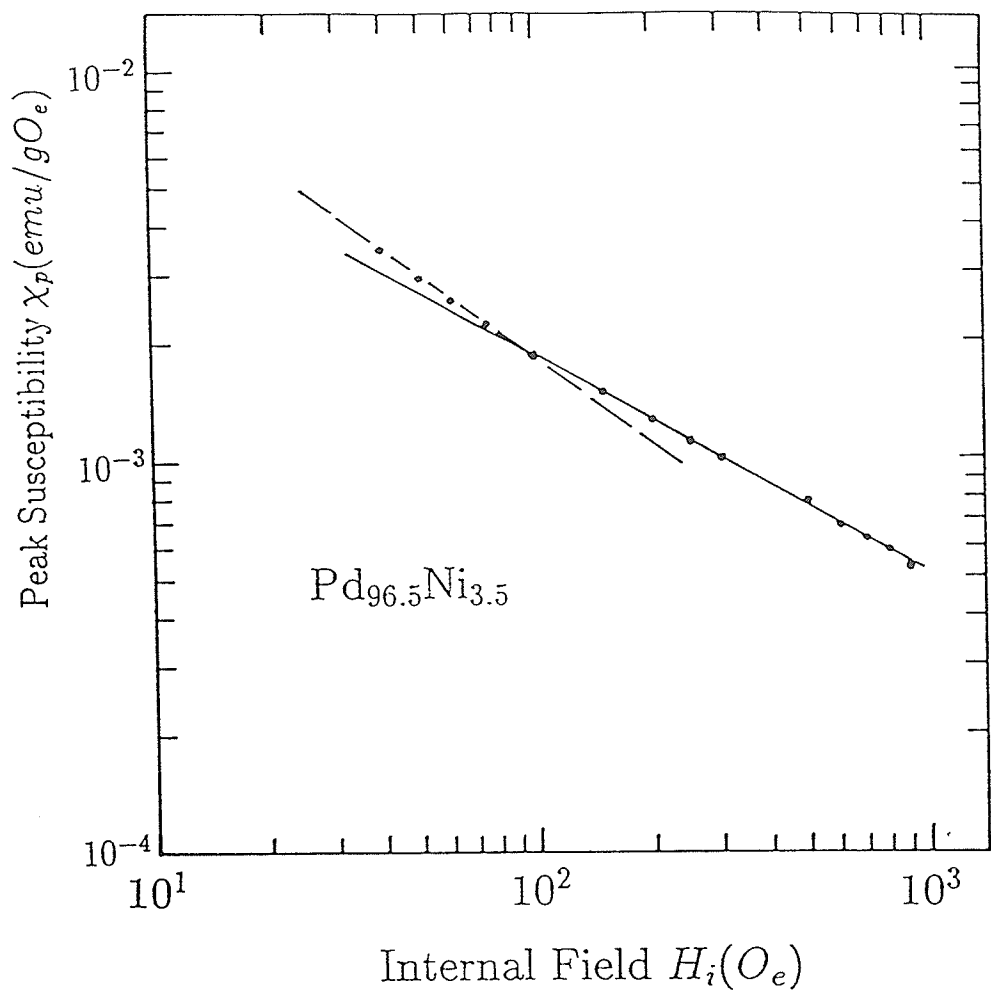


Figure 4.14: Double log plot of the peak susceptibility versus internal field for $\text{Pd}_{96.5}\text{Ni}_{3.5}$.

χ_i against the reduced temperature t ; the Curie temperature T_c can be extracted from a plot of peak temperature as a function of a reasonable power of H_i .

In the case of the PdNi system, however, due to the substantial effect of the regular contribution (attributed to the presence of an anisotropy), estimates of the critical exponents (γ and β) based on the plot of reduced peak temperature t_p versus the internal field H_i on a double logarithmic scale becomes very questionable. First of all an applied field in excess of 40 *Oe* is required in order to resolve a critical peak; this field is more than one order of magnitude larger than that required to produce similar effects in soft ferromagnets. On a logarithmic scale, this means the loss of data covering more than one decade. In addition, the critical peaks are rather broad compared with soft ferromagnets (this is also the result of the anisotropy, and its effect on the low temperature side of the critical peak), which increasing the uncertainty in the peak temperature. This is particularly noticeable on a logarithmic plot, so no reliable critical exponent could be extracted from it.

An approximate method can, however, be used to analyse the field dependence of the critical peak temperature T_p which has been previously adopted for the (PdNi)Mn system (Hall et al 1984). In Figure 4.15 the peak temperature T_p has been plotted on a linear scale against the square root of the internal field H_i for the sample Pd_{96.5}Ni_{3.5}. Such a plot is based on the assumption that the critical exponents (γ and β) have values, listed in Table 1.1, close to those predicated by the Heisenberg model (LeGuillon and

Zinn-Justin 1980); then Equation (1.59) can be approximated by a simple power law relationship

$$T_p \approx H_i^{1/2}. \quad (4.3)$$

As shown in the plot based on this equation (Figure 4.15) a reasonable straight line is obtained, from which the Curie temperature T_c can be determined by measuring the vertical axis intercept of the straight line. The value so obtained is 31.0 ± 0.5 K.

With the Curie temperature determined by the plot of T_p vs $H_i^{1/2}$, the zero field susceptibility for the $\text{Pd}_{96.5}\text{Ni}_{3.5}$ sample is plotted in Figure 4.16 on a double logarithmic scale against the reduced temperature t . The simple power law relationship predicted by Equation (1.56) ($\chi(0, t) \approx t^{-\gamma}$) does not hold for this system, unlike the behaviour in many soft ferromagnets. Some adjustments in the choice of T_c (up to a few tenths of a degree which resulted in the choice of T_c moving above or below the temperature of the zero field inflection point) have been made in an attempt to obtain a better straight line fit to these data; this procedure was not successful in the PdNi system, and no extended power law regime could be observed.

Figure 4.16 shows that the zero field susceptibility increases with decreasing reduced temperature, but not as fast as predicted by the scaling hypothesis because of severe flattening that is observed at low reduced temperature. At higher reduced temperature, double logarithmic plots exhibit marked curvature in this sample, with large local slopes (effective exponent

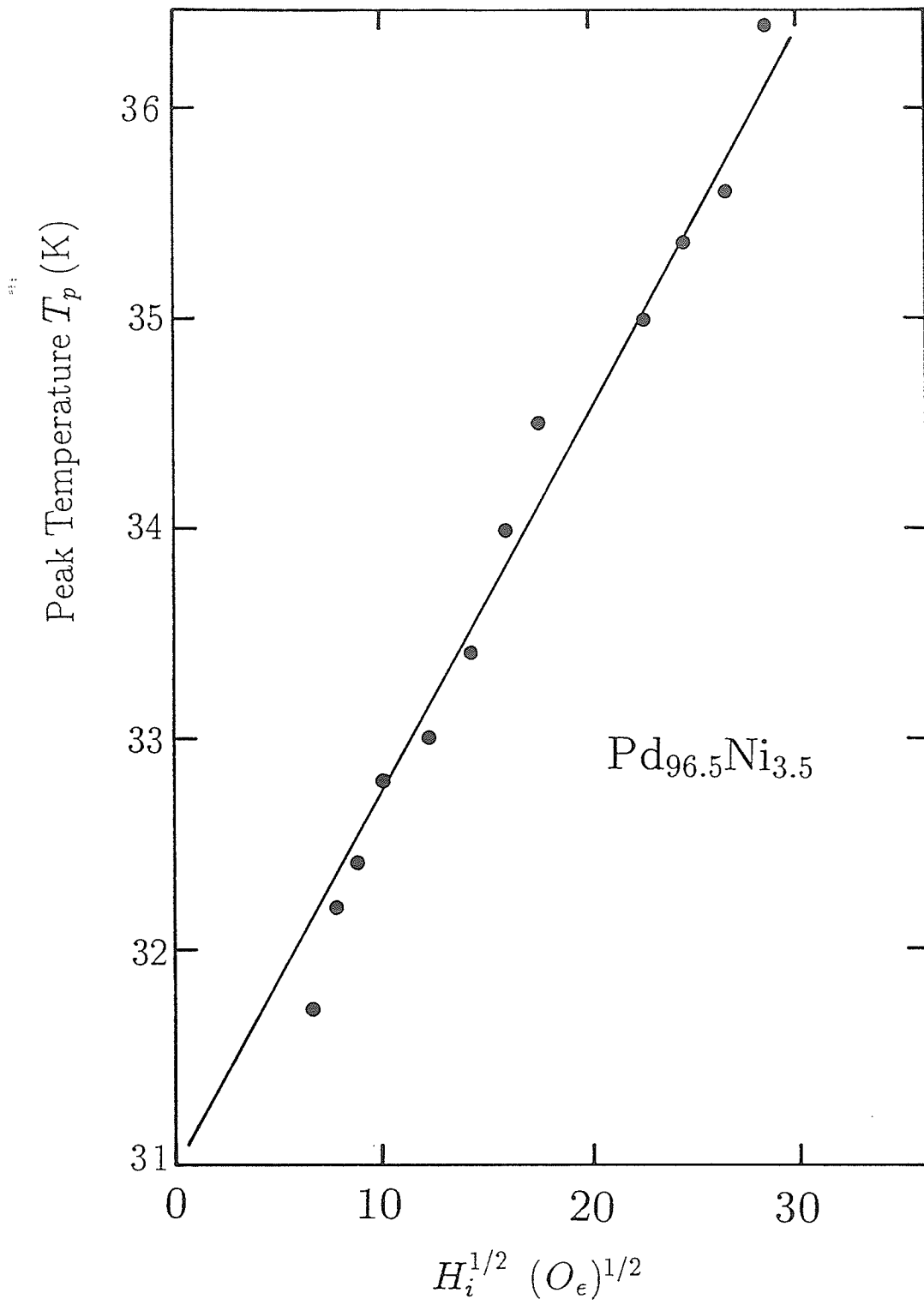


Figure 4.15: The peak temperature versus $H_i^{1/2}$ for $\text{Pd}_{96.5}\text{Ni}_{3.5}$.

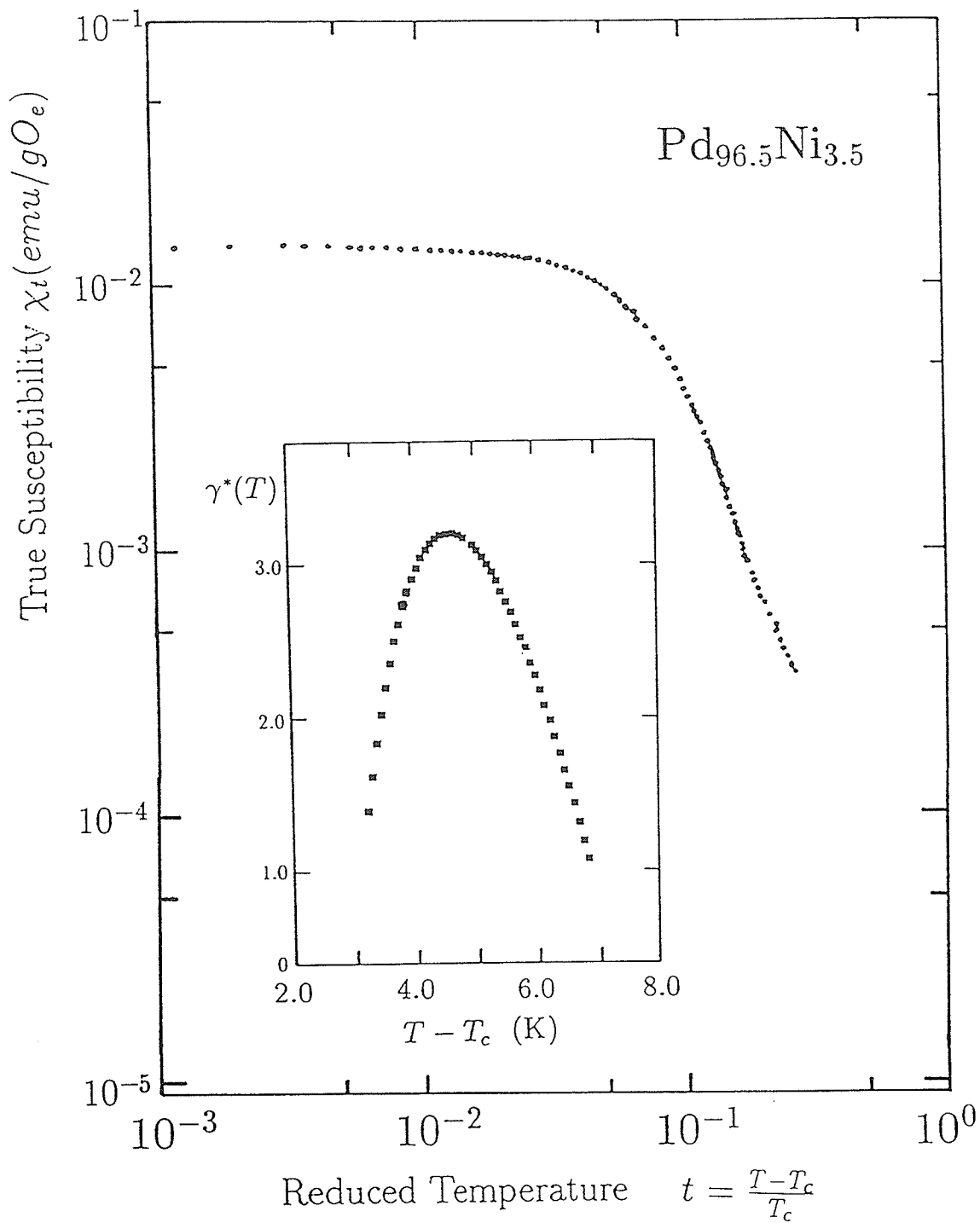


Figure 4.16: The zero field susceptibility versus the reduced temperature t near T_c for the $\text{Pd}_{96.5}\text{Ni}_{3.5}$ specimen. The inset shows the temperature dependence of the effective exponent γ^* .

γ^*). This result is quite similar to that observed in other disordered systems (Gaunt et al 1981, Kaul 1985, Fahnle et al 1988, Seegar and Kronmuller 1989), and so we have adopted a similar approach to analyse our data.

The effective exponents γ^* of 3.5 at% Ni alloy (from the local slopes on the log-log plot of the zero field susceptibility data) have been plotted against the temperature above the Curie temperature $\Delta T (= T - T_c)$ in the inset of Figure 4.16. Above the Curie temperature the effective exponent $\gamma^*(T)$ first increases (presumably from a value $\gamma^* \approx 1.30$ close to that predicted theoretically)⁵, with a peak effective exponent $\gamma_{max}^* = 3.2$ at $\Delta T = 4.5$ K, and then decreases with increasing temperature. This effective exponent value is much larger than the predicted value from Monte Carlo or renormalization calculations ($(\gamma(T)_{max} = 1.55)$ (Seeger and Kronmuller 1989). The concentration dependence of the effective exponent, γ^* , as well as of other effective exponents for the PdNi system will be discussed below, in greater detail.

4.3.3 Concentration Dependence of Various Parameters

In Figure 4.17 the critical peak susceptibility χ_p has been plotted on a double logarithmic scale against the internal field H_i based on Equation (1.60) for three selected samples. The 2.4 at% Ni sample is the most dilute alloy which still exhibits long range magnetic order at low temperature in this system.

⁵In the temperature region very close to T_c such plots remain unreliable due to the severe flattening of the zero field susceptibility plot (Figure 4.16), and its associated failure to climb towards the demag limit.

The 4.5 at% Ni sample is the second most concentrated specimen, and has a T_c comparable with the 1.4 at% Fe alloy discussed earlier, while the 2.9 at% Ni has an intermediate concentration. As can be seen from this figure, a power law relationship with a unique index (as predicted by Equation (1.60)) is not observed over the entire field range examined in this system. There are, however, some features that should be noticed. First, the alloys with intermediate Ni concentration require larger fields (about 40 *Oe* compare with about 20 *Oe* for lower and higher Ni concentrated alloys) to first resolve a critical peak. Second, the critical peak amplitude at a particular field increases with increasing Ni concentration. Third, the curvature of the double logarithmic plot is noticeable for all the samples examined, but the amount of curvature decreases with decreasing Ni composition. Furthermore, the effective exponent δ_h^* found at high field ($H_i \geq 100$ *Oe*) varies little (the values range between 2.2 and 2.5) for all the specimens investigated. At lower field, however, the effective exponent δ_l^* (estimated for $H_i < 100$ *Oe*) decreases monotonically with decreasing Ni concentration from 4.1 at 4.5 at% to 2.7 at 2.4 at% Ni (also seen Table 4.2). The low-field value, $\delta_l^* = 4.1$ of $\text{Pd}_{95.5}\text{Ni}_{4.5}$ is very close to that found by Kouvel and Fisher (1964) in pure Ni.

Having presented these observations, we next discuss the field dependence of the effective exponents (δ^*). As can be seen from Figure 4.17 as well as in Table 4.2, the effective exponent δ_l^* is always larger than δ_h^* for all the samples studied; that means the δ^* value decreases with increasing

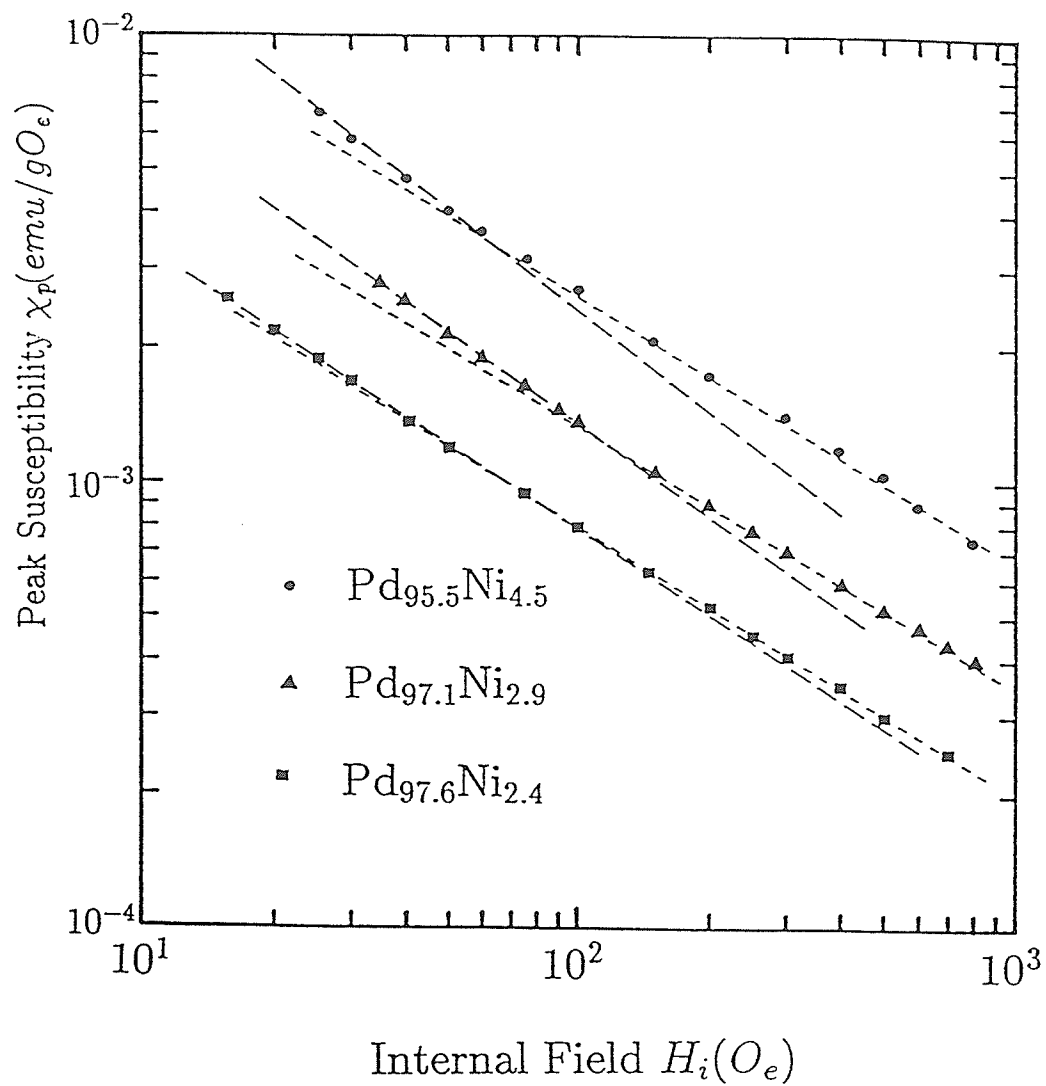


Figure 4.17: The peak susceptibility versus H_i for several PdNi alloys on a double log plot.

Table 4.2: Summary of parameters deduced from *ac* susceptibility data for the PdNi alloys.

Composition Ni at%	T_c (K)	δ_i^*	δ_h^*	Slope of T_p vs $H_i^{1/2}$ plot (K/Oe ^{1/2})
5.0	62.7 ± 1	4.1 ± 0.1	2.4 ± 0.1	0.100 ± 0.003
4.5	57.5 ± 1	4.1 ± 0.1	2.5 ± 0.1	0.150 ± 0.005
4.0	44.3 ± 0.5	4.0 ± 0.1	2.2 ± 0.1	0.190 ± 0.005
3.5	31.0 ± 0.5	3.3 ± 0.1	2.2 ± 0.1	0.180 ± 0.005
3.0	12.5 ± 0.5	3.0 ± 0.1	2.5 ± 0.1	0.170 ± 0.005
2.9	11.0 ± 0.3	3.2 ± 0.1	2.4 ± 0.1	0.160 ± 0.005
2.7	6.0 ± 0.2	3.0 ± 0.1	2.5 ± 0.1	0.130 ± 0.004
2.6	4.05 ± 0.1	2.8 ± 0.1	2.4 ± 0.1	0.105 ± 0.003
2.5	3.85 ± 0.1	2.7 ± 0.1	2.2 ± 0.1	0.100 ± 0.003
2.4	1.95 ± 0.1	2.7 ± 0.1	2.5 ± 0.1	0.085 ± 0.003

field. This latter behaviour has been observed previously in other dilute systems such as PdMn and PdGd (Ho et al 1981b, Saran et al 1987). Such a result can be explained by the so-called SK like model (Sherrington and Kirkpatrick 1975, Southern 1976). As shown by Roshko and Williams (1984), when the ratio η declines toward one, ($\eta = J_0/J$, where J_0 is the mean value of the impurity-impurity exchange bond distribution and J is the width of the Gaussian exchange bond distribution), the effective exponent δ^* shows a pronounced reduction with increasing field, although its asymptotic value ($h \rightarrow 0$) remains unchanged. Thus the data shown in Figure 4.17 and Table 4.2 can be interpreted as indicating an effective exchange field distribution between impurities (between Ni sites in the case of present system) which becomes broader as the Ni concentration is lowered towards the critical composition, x_0 , necessary to produce a ferromagnetic ground state when the ratio η decreases towards one. This latter interpretation is consistent with previous model calculations (Yeung et al 1986) as well as with magnetization measurements for PdNi (Murani et al 1974) which show that the Arrott plots exhibit increasing curvature at low field when the impurity concentration is reduced towards the critical composition.

Next we would like to make an interesting observation on the comparison of the critical peak amplitudes among the different magnetic ions in Pd. Specifically, for internal fields near 100 Oe, the ratio of the critical peak amplitudes for PdNi, PdMn and PdGd containing comparable amounts of impurity (about 3 at%) is 1:3:5. This ratio is remarkably close to that

predicted, if the spin value used for the impurity sites is $1/2$, $5/2$ and $7/2$ respectively, by calculations (Kunkel et al 1990) based on the same effective field approach discussed above. This argues not only for stable half-filled shell configurations in the case of Mn and Gd, but also supports indirectly the spin assignment $S = 1/2$ for Ni made by Loram et al (1985).

In Figure 4.18 the behaviour of the critical peak temperature T_p as a function of H_i for the samples with Ni concentrations between 2.4 and 4.5 at% is presented. As in the 3.5 at% Ni sample, the approximate relationship predicted by Equation (4.2) ($T_p \approx H_i^{1/2}$) is reasonably well obeyed for all other samples in the present system. Estimates for T_c were again obtained by extrapolating these plots to $H_i = 0$, and these results are listed in Table 4.2. The results indicate that the Curie temperature T_c drops rapidly as the Ni composition decreases, from 62.7 K at 5.0 at% to a value of 12.5 K at 3.0 at% Ni sample with $\frac{dT_c}{dx} \approx 25$ K/at% Ni. Below 3.0 at% the Curie temperature drops much more slowly as the Ni composition decreases. As a rough approximation, the Curie temperature T_c is linear in x for the samples with Ni concentrations between 3.0 and 5.0 at%, but is proportional to x^2 for the specimens with less than 3.0 at% Ni. To give a rough estimate, we might say the critical composition necessary to produce a ferromagnetic ground state at zero temperature lies between 2.2 and 2.4 at% Ni. In contrast with the SRA measurements, no precise critical composition x_0 for ferromagnetic long range order could be obtained from these data.

One additional feature concerning Figure 4.18 that is of interest is the

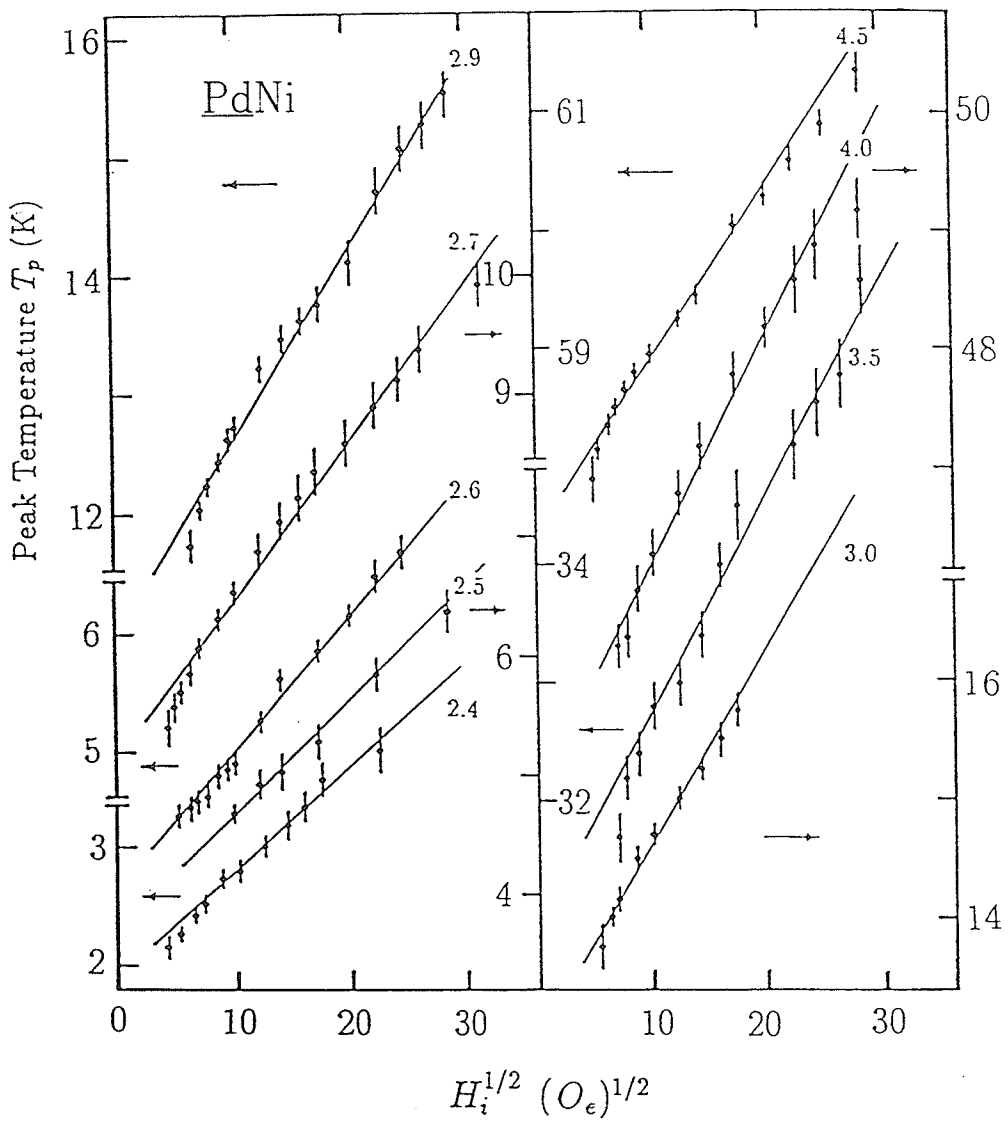


Figure 4.18: The peak temperatures versus $H_i^{1/2}$ for a number of PdNi alloys.

concentration dependence of the slopes. The slopes increase markedly from 8.5×10^{-2} (K/Oe^{1/2}) for the 2.4 at% Ni sample to 19.0×10^{-2} (K/Oe^{1/2}) for the 4.0 at% Ni alloy, then decrease above this concentration. This latter behaviour is very similar to the concentration dependence of the slopes of the high field magnetoresistance in the same system as will be presented in Section 4.5, although the physical origin for this is not clear at present.

With T_c estimated using the above power law approximation ($T_p \approx H_i^{1/2}$), the critical index γ governing the temperature dependence of the zero field susceptibility immediately above T_c has been examined. The power law relationship predicted by Equation (1.56) (i.e. $\chi(0, t) \approx t^{-\gamma}$ ($T > T_c$)) does not exist over any significant range for any of the samples examined here. When the zero field susceptibility is plotted against reduced temperature on a double logarithmic scale it does not result in a straight line but instead the plots exhibit marked curvature with the following additional characteristics. The values of the maximum effective exponent, γ_{max}^* , as well as the temperature at which the peak effective exponent occurs, are Ni concentration dependent. These latter characteristics are apparent in Figure 4.19. The data shown in this plot (γ^* against $(T - T_c)$) have been selected from the measurements carried out on all the ferromagnetic alloys.

This figure shows a non-monotonic temperature dependence for each of the five selected samples. At an intermediate Ni concentration the sample shows a much stronger increase of $\gamma^*(T)$ with increasing temperature. Meanwhile the maximum value of the effective exponent γ_{max}^* and the corre-

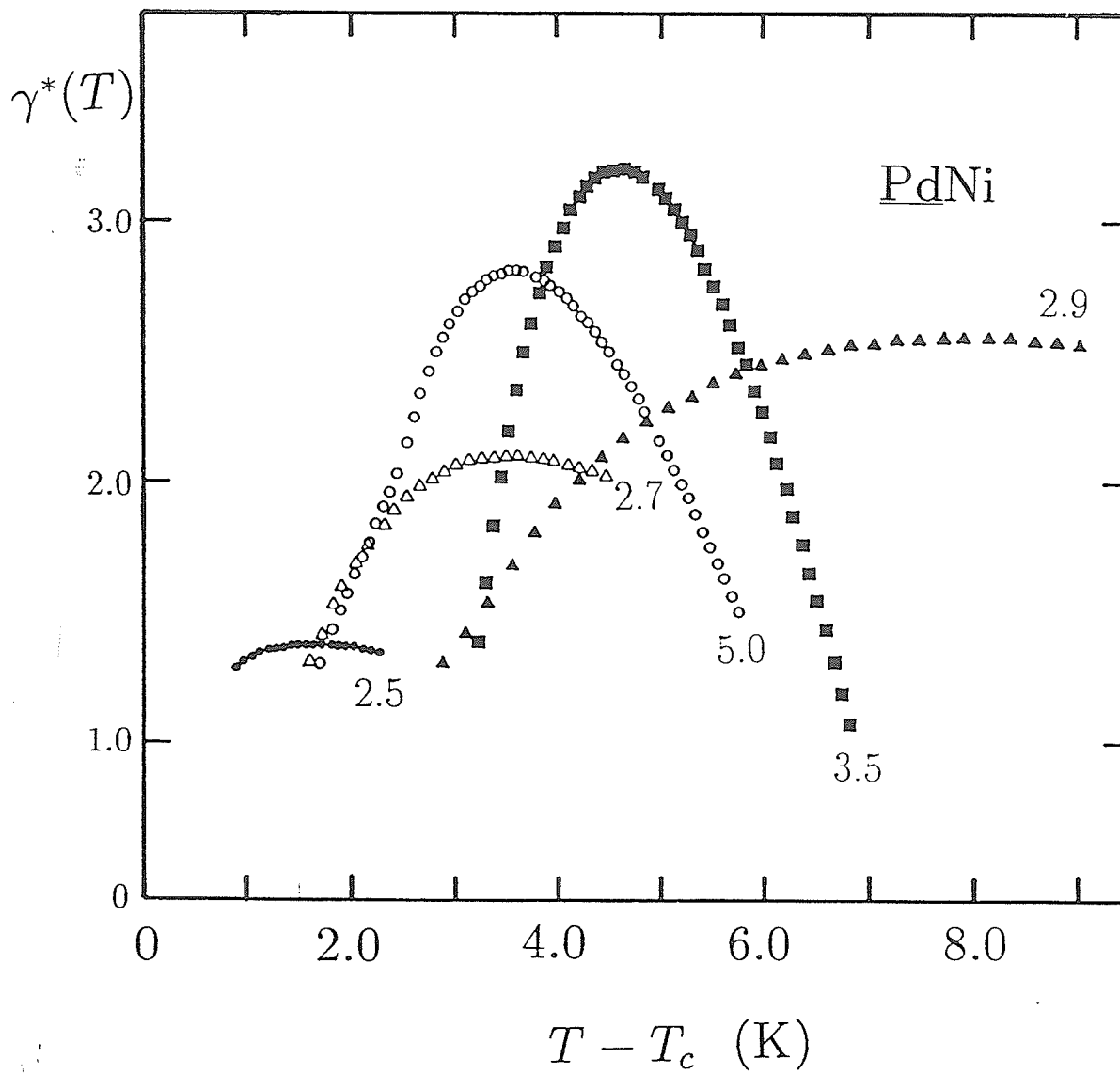


Figure 4.19: The effective exponent γ^* vs $T - T_c$ for a number of the PdNi alloys in the range of 2.4 to 5.0 at% Ni.

sponding temperature T_m at which this maximum value occurs also exhibit some systematic variation with Ni concentration. In fact they have a similar behaviour to the slopes of T_p versus $H_i^{1/2}$ and the high field magnetoresistance.

Near the Curie temperature γ^* is close to the value predicted for the isotropic three dimensional Heisenberg model, whereas at a temperature much higher than T_c the value of the effective exponent γ^* falls towards the mean field value of one. In the intermediate temperature range the effective exponent achieves a maximum value for each sample studied. For most of the samples the maximum value of the effective exponent lies between 2 and 3.2, which is equal to or larger than the maximum value of 2 reported in amorphous systems (e.g Kaul 1985), but is comparable with the estimated value for intermediate-concentration PdMn (3–5 at% Mn) alloys (Ho et al 1981b). For the sample with Ni concentration very close to the critical composition, x_0 , the maximum effective exponent γ_{max}^* has a value close to but slightly higher than the predicted 3d Heisenberg value 1.388. Despite the difficulties in estimating critical exponents, the *ac* susceptibility data are shown to be consistent, not only with a previous suggestion that a spin-glass ground state would appear at low Ni concentration if complications due to the Kondo effect were not present⁶, but also with assigning a low spin value ($S = 1/2$) to the Ni site (Kunkel et al 1990).

⁶i.e. $\eta = J_0/J$ decreases towards a value of 1 as the Ni concentration is decreased towards 2.4 at%. If this trend were to continuity, η should fall below 1 for concentrations between 1 and 2 at% Ni, when a spin-glass state should emerge at low temperature.

4.4 *ac* Susceptibility Results for the Dilute (PdFe)Mn System

The magnetic properties of the dilute PdFe alloys containing between 0.35 and 2.4 at% Fe were discussed in detail in Section 4.2, and here we present *ac* susceptibility measurements of some of these alloys with an additional 5 at% Mn. We will focus on the magnetic properties of these (PdFe)Mn alloys in this section, and leave the SRA results until Section 4.7.

At temperatures near the ferromagnetic Curie point, the qualitative features of the *ac* susceptibility of these samples are similar to those acquired previously on the other Pd based alloys. The zero field susceptibility increases rapidly with decreasing temperature in the vicinity of the Curie temperature and peaks at a temperature somewhat below T_c . Typical, the measured maximum zero field susceptibility value was 0.5 (*emu/gOe*), and that represents about 30 % of the value set by the dimension of the sample, compared with a ratio of 50 % for dilute PdFe but only a few percent for dilute PdNi alloys.

In Figure 4.20 the behaviour of the true susceptibility χ_t for a (PdFe)Mn alloy with 1.6 at% Fe in various fields is examined in detail in the vicinity of the ordering temperature. As can be seen the qualitative behaviour expressed in Equations (1.59) and (1.60) is again followed; namely the peak height decreases rapidly with increasing field whereas the peak position increases slightly in temperature with increasing field.

Figures 4.21 and 4.22 present plots of the peak susceptibility against the internal field for the 0.35 at% Fe sample and the other (PdFe)Mn alloys

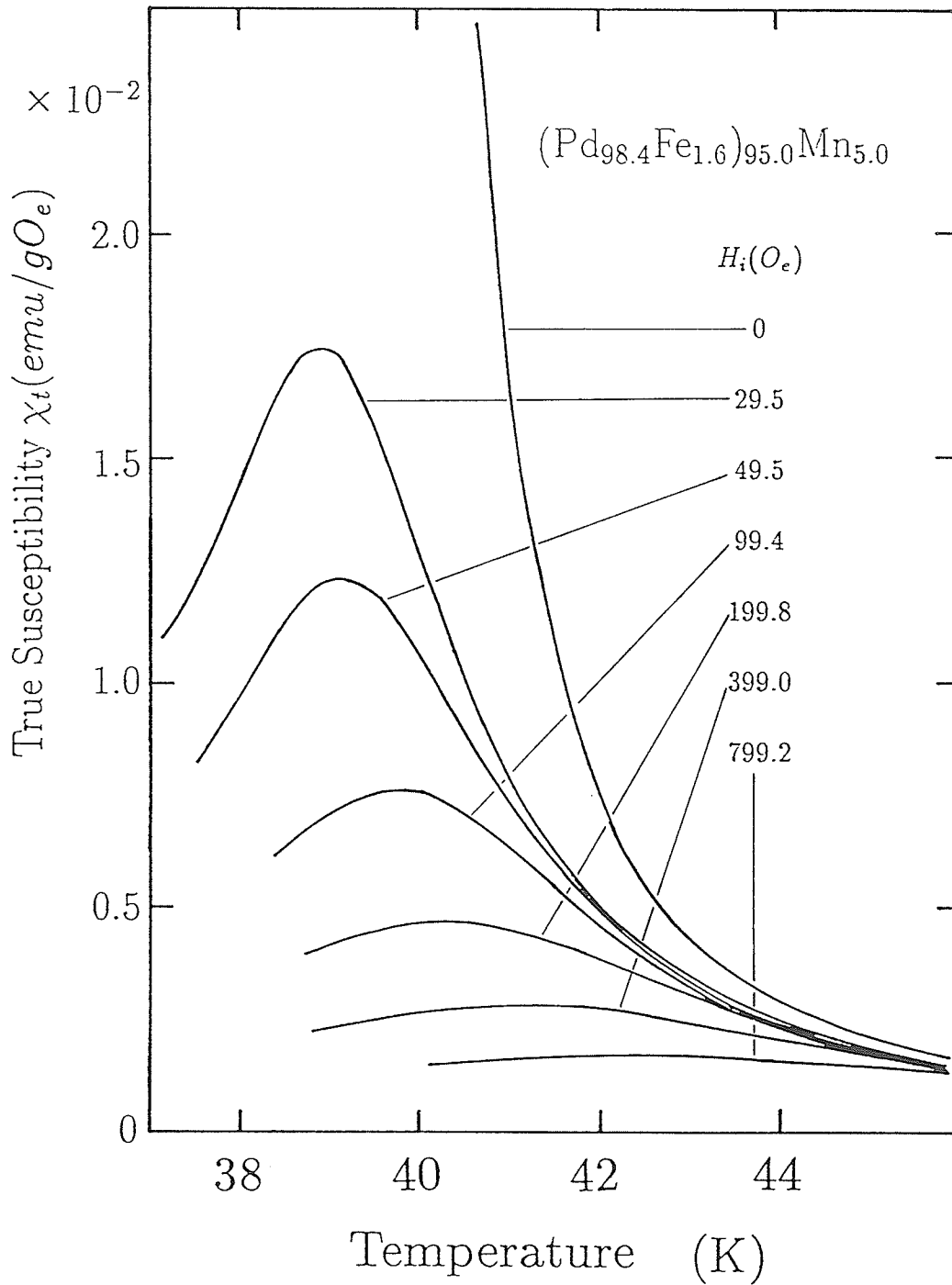


Figure 4.20: The *ac* susceptibility versus temperature for (Pd_{98.4}Fe_{1.6})₉₅Mn₅ in various internal fields.

on a double logarithmic scale. For all the (PdFe)Mn samples studied a power law behaviour with a unique critical exponent δ is observed.

The slope of the plot for the $(\text{Pd}_{99.65}\text{Fe}_{0.35})_{95}\text{Mn}_5$ sample yields a δ value of 4.1 ± 0.1 , while for the more concentrated Fe alloys δ values range from 2.9 ± 0.1 to 3.3 ± 0.1 which are again less than those found for elemental ferromagnets. For the alloys with between 1.6 and 2.2 at% Fe, the concentration dependence of the δ values measured for (PdFe)Mn is similar but less dramatic compared to that found in PdFe, first the δ value decreases with increasing Fe concentration and has a minimum at about 2.0 at% Fe.

As shown in Figure 4.22, for the (PdFe)Mn alloys with 1.6 to 2.2 at% Fe applied fields in excess of about 20 *Oe* are required before the emerging critical peaks can be resolved and this is about an order magnitude larger than those required to produce similar effects in the PdFe alloys with comparable amounts of Fe. The minimum field required to emerge the critical peak for the $(\text{Pd}_{99.65}\text{Fe}_{0.35})_{95}\text{Mn}_5$ alloy was only about 3 *Oe* (as shown in Figure 4.21), but it is still one order of magnitude larger than that required to produced similar effects for the $\text{Pd}_{99.65}\text{Fe}_{0.35}$ (about 0.3 *Oe*).

In Figure 4.23 the peak temperatures T_p were plotted against $H_i^{1/2}$ on a linear plot in order to estimates T_c for the (PdFe)Mn alloys with 1.6 to 2.2 at% Fe. As these data indicate, the Curie temperatures of the system are rapidly suppressed, and are much smaller than those observed in PdFe alloys; for example, Pd + 1.6 at% Fe has $T_c = 61.5$ K, which is lowered to 38 K by the addition of 5 % Mn.

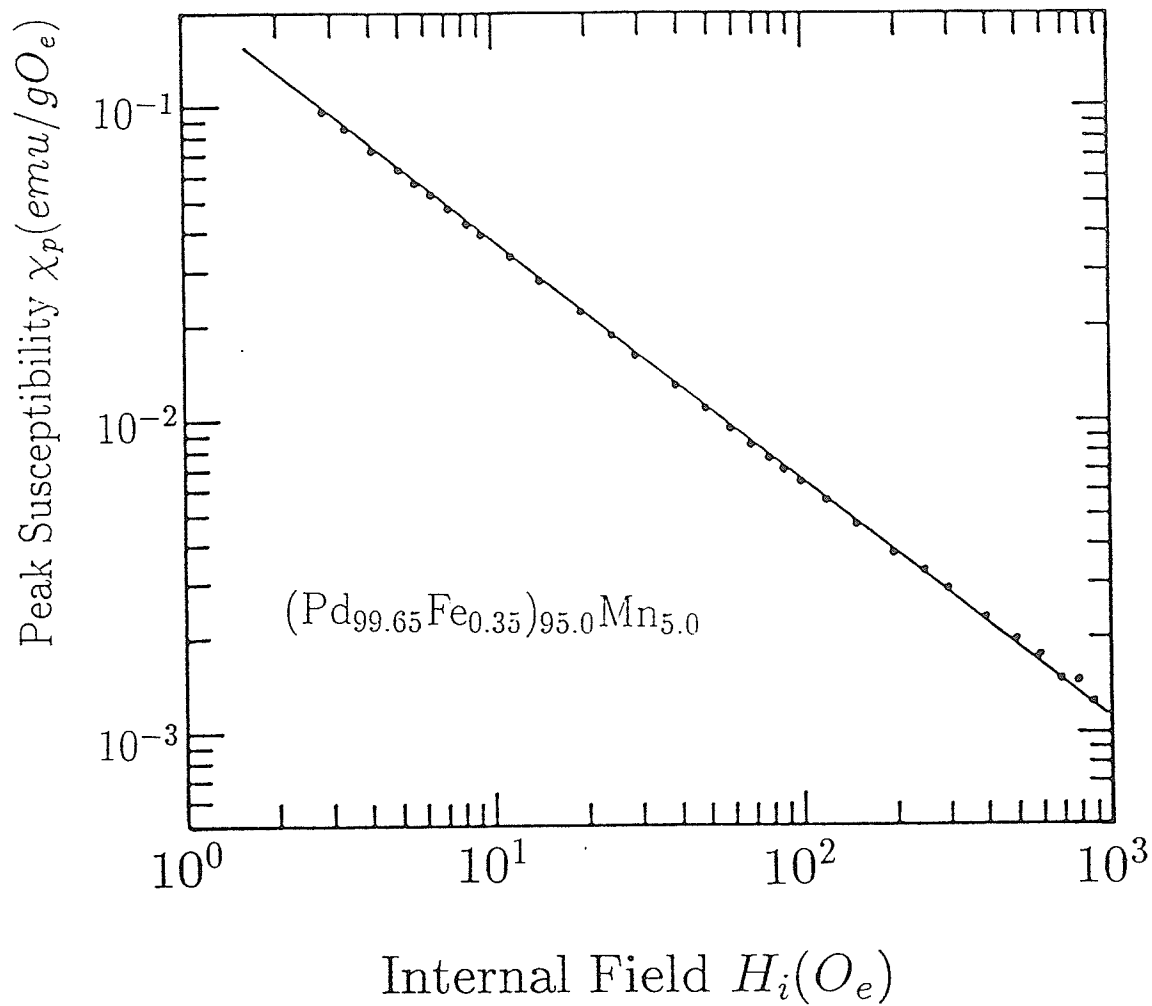


Figure 4.21: The peak susceptibility versus various internal field H_i on a double log plot for the $(\text{Pd}_{99.65}\text{Fe}_{0.35})_{95}\text{Mn}_{5}$ sample.

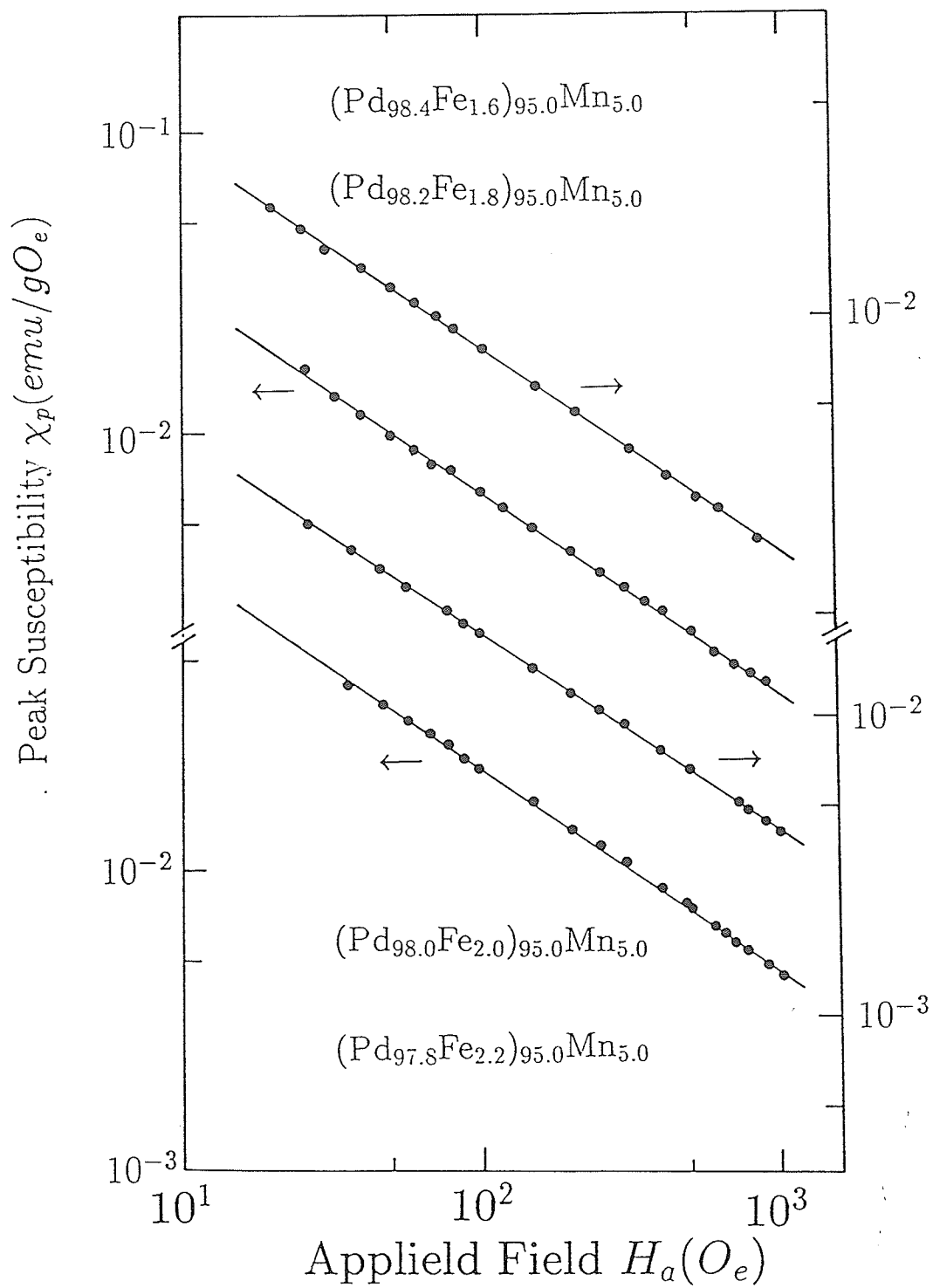


Figure 4.22: The peak susceptibility versus internal field H_i on a double log plot for the (PdFe)Mn alloys.

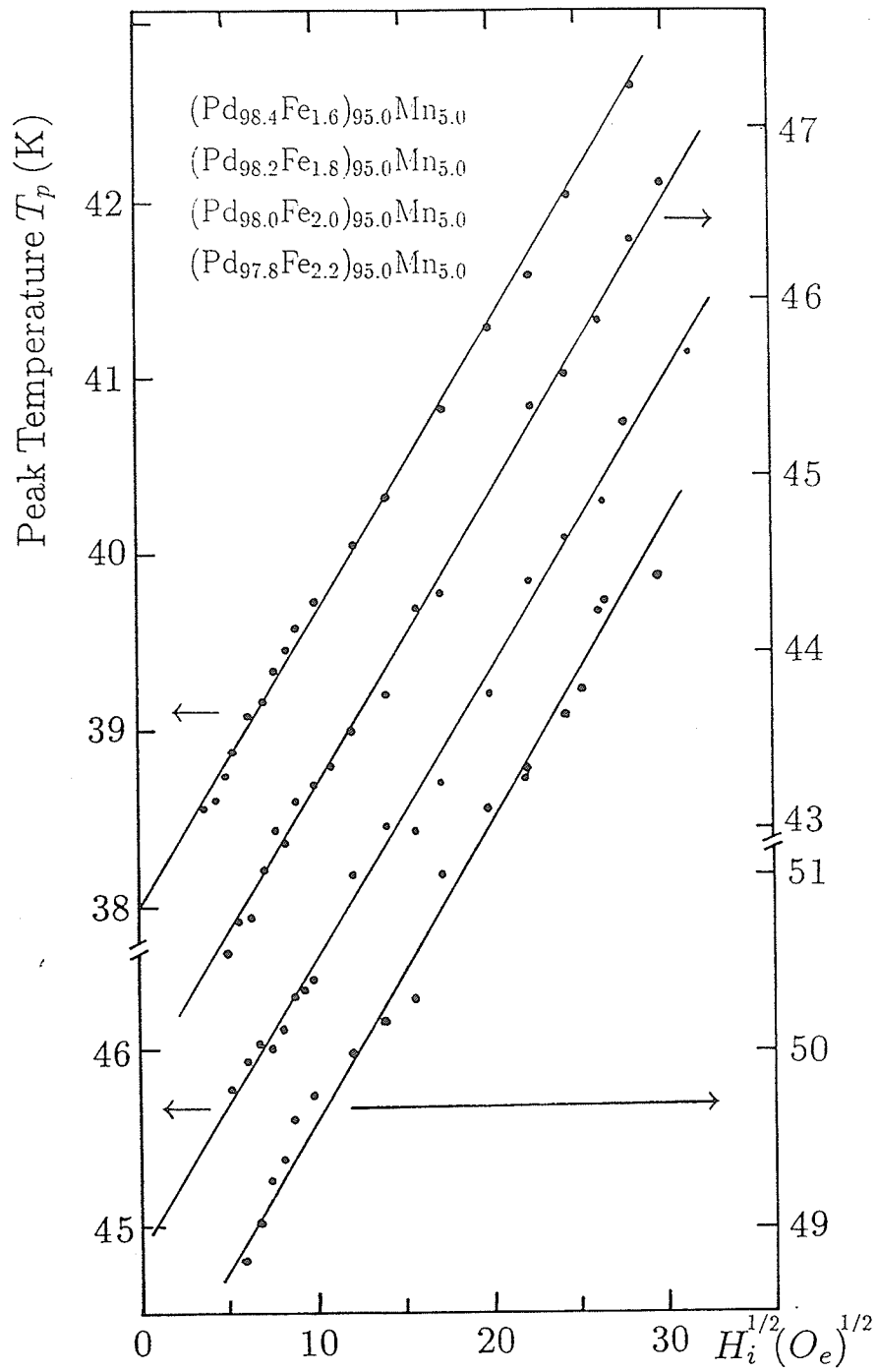


Figure 4.23: The peak temperature versus $H_i^{1/2}$ for (PdFe)Mn alloys.

The impurity concentration dependence of the Curie temperature displays a simple linear relationship, with $\frac{dT_c}{dx} \approx 16$ K/at%Fe for the alloys with Fe concentration between 1.6 and 2.2 at%. This latter ratio is also much smaller than that of the measured ratio for the PdFe alloys (≈ 32 K/at%Fe).

With a value specified for T_c , it is usual to examine the remaining scaling prediction by attempting to fit the zero field susceptibility to Equation (1.56) on a double logarithmic scale (the γ plot). Figure 4.24 shows such a plot for a $(\text{Pd}_{98.0}\text{Fe}_{2.0})_{95}\text{Mn}_5$ sample. As can be seen in this figure there is a severe flattening of the plot at low reduced temperature (that is, as $T \rightarrow T_c$), this is due to the failure of zero field susceptibility to approach the value set by the dimension of the sample. No extended power law regime is seen. The inset of the figure shows the temperature dependence of the effective exponent $\tilde{\gamma}$. This effective susceptibility exponent is strongly curved and has a maximum value $\tilde{\gamma}_{max} = 3.3 \pm 0.2$. This situation is very similar to that seen in the PdNi and the more Fe concentrated PdFe alloys discussed in the last two sections. The $\tilde{\gamma}_{max}$ value so obtained for the other (PdFe)Mn alloys are all listed in Table 4.3.

It should be pointed out that the $(\text{Pd}_{99.65}\text{Fe}_{0.35})_{95}\text{Mn}_5$ sample is particularly interesting because it is a re-entrant system⁷. Previous measurements have shown this latter alloy to have a ferromagnetic Curie temperature T_c about 10 K and a spin glass temperature T_f near 4 K (Verbeek et al 1978). From the susceptibility data (Kunkel and Williams 1988b), a well defined

⁷We believe that the other (PdFe)Mn alloys studied are also re-entrant systems, but with the lower transition temperatures well below 1 K.

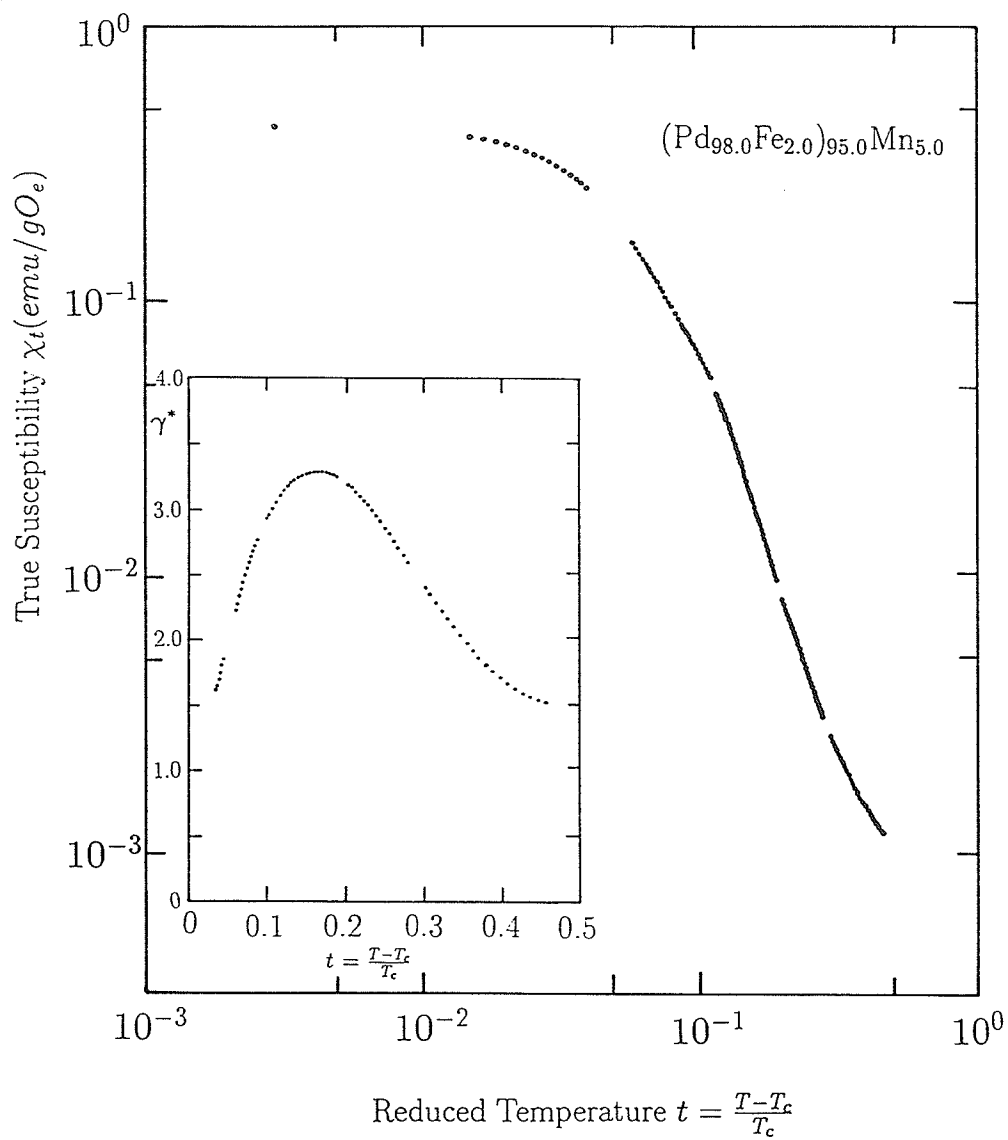


Figure 4.24: The zero field susceptibility versus reduced temperature t for the $(\text{Pd}_{98.0}\text{Fe}_{2.0})_{95}\text{Mn}_{5.0}$ sample. The inset shows the temperature dependence of the effective exponent γ^* .

Table 4.3: Summary of parameters taken from the *ac* susceptibility data for the (PdFe)Mn specimens.

Alloys Fe (at%)	T_c (K)	T_f (K)	δ	γ_{max}
0.35	9.30 ± 0.02	4.07 ± 0.02	4.1 ± 0.1	1.9 ± 0.2
1.6	38.0 ± 0.2		3.3 ± 0.1	3.1 ± 0.2
1.8	41.6 ± 0.2		3.0 ± 0.1	3.4 ± 0.2
2.0	44.9 ± 0.5		2.9 ± 0.1	3.3 ± 0.2
2.2	47.9 ± 0.5		3.1 ± 0.1	2.4 ± 0.2

ferromagnetic Curie temperature $T_c = 9.30 \pm 0.02$ K has been found, and it characterised by critical exponent values

$$\delta = 4.1 \pm 0.1, \gamma = 1.64 \pm 0.07, \text{ and } \beta = 0.53(5) \pm 0.08.$$

The non-linear magnetic response of the re-entrant system $(\text{Pd}_{99.65}\text{Fe}_{0.35})_{95}\text{Mn}_5$ has also been studied in the vicinity of both transitions based on the following two equations

$$\chi_{ferro}(H, t) = t^{-\gamma} - \frac{H^2}{t^{3\gamma+2\beta}} + \frac{H^4}{t^{5\gamma+4\beta}} \quad (4.4)$$

for the upper transition⁸.

In terms of the non-linear response, the coefficient of the H^2 term $\frac{\chi(H,t)}{H^2}$ is plotted against the reduced temperature t in Figure 4.25 on double logarithmic scale for the upper transition. The coefficient predicted by scaling theory is confirmed as a straight line results with the slope being 6.2 ± 0.6 compared with the predicated value of $3\gamma + 2\beta = 6.0 \pm 0.4$ from more conventional data listed above this section.

For the lower transition substantial experimental effort has been expended in attempts to verify predictions of singular components in the non-linear magnetic response (Binder and Young 1986), i.e. predictions that the susceptibility of spin glasses can be written

$$\chi_{s.g}(H, t) = \chi_0(t) - \frac{H^2}{t^{\gamma'}} + \frac{H^4}{t^{2\gamma'+\beta'}} \quad (4.5)$$

⁸Expanding the static scaling law equation (i.e. Equation (1.57)) in terms of the field H , and retaining only the lowest non-linear terms.

where primes are used to distinguish the exponents in spin glasses from those in ferromagnets.

The coefficient of the H^2 term has also been measured near the spin-glass temperature T_f . Figure 4.26 summarizes the temperature dependence of this coefficient over the range 2 to 4.2 K. An anomaly in the non-linear response has been clearly shown for the first time. It is located near the temperature at which the initial susceptibility falls abruptly. This peak is not divergent, but clearly exhibits a distinct maximum at 4.07 K. This peak structure is believed to be a strong indication of a true re-entrant ferromagnetic-spin glass transition.

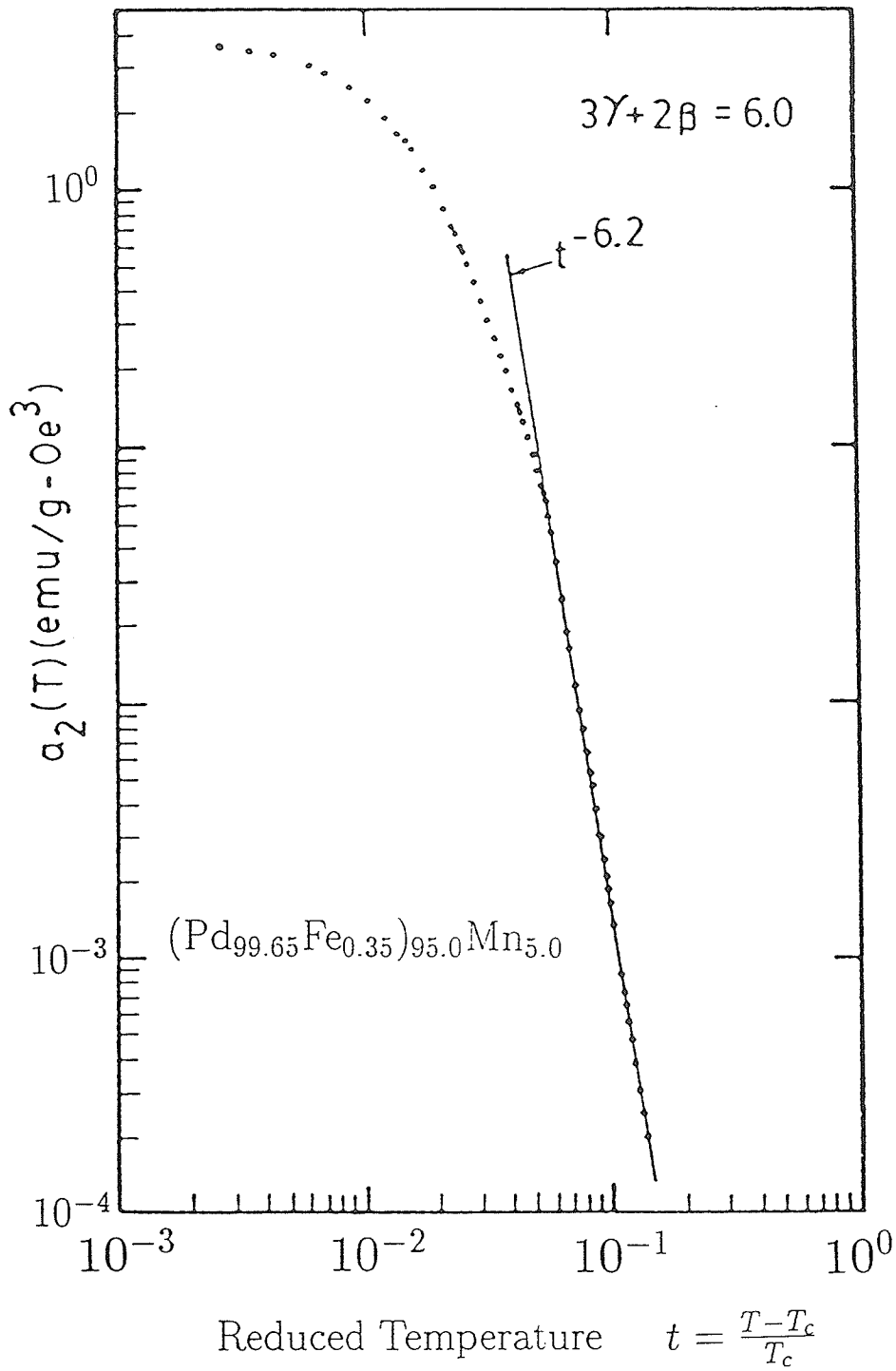


Figure 4.25: Coefficient of the H^2 term in susceptibility immediately above the ferromagnetic transition.

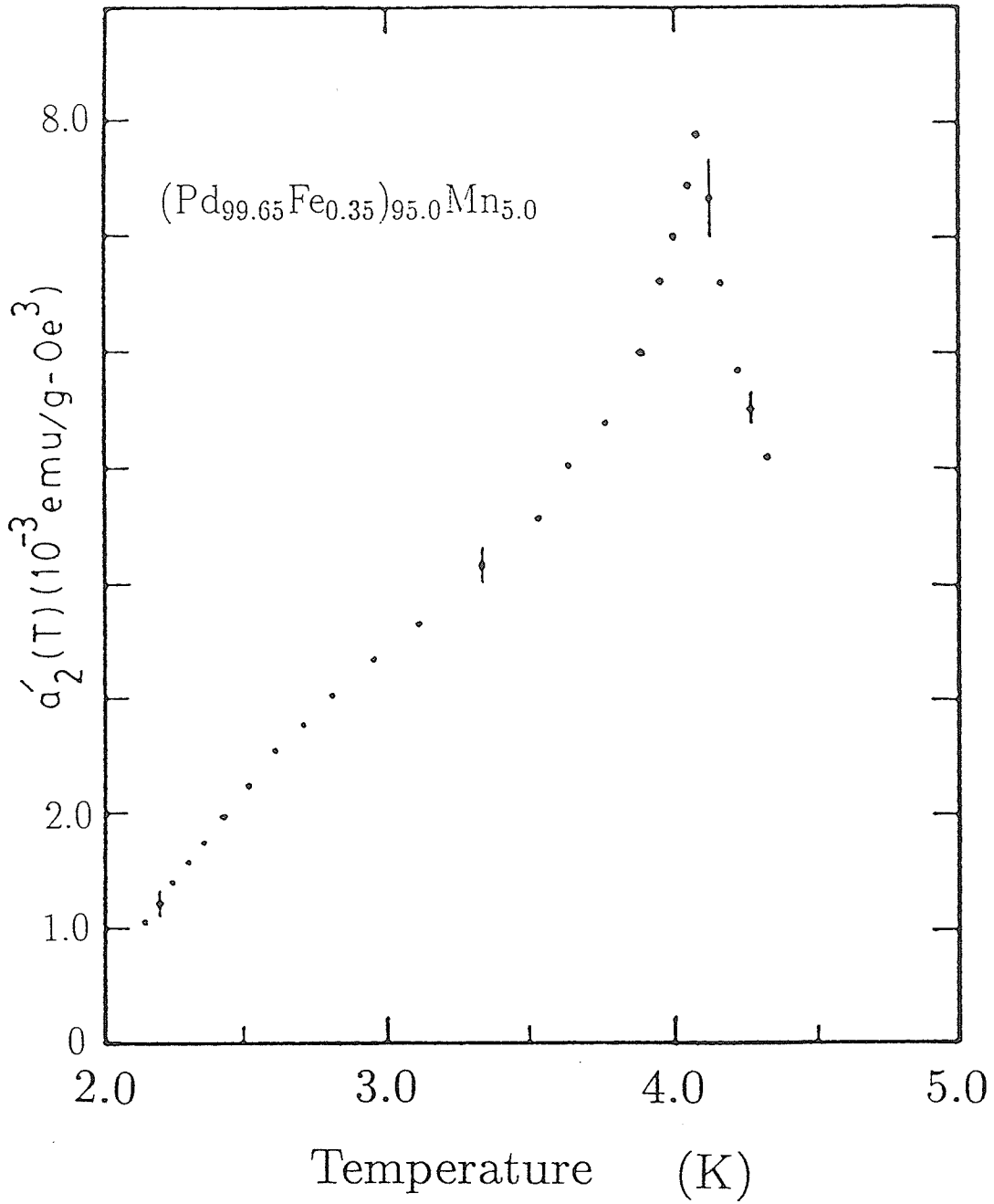


Figure 4.26: Coefficient of the H^2 term in susceptibility near the re-entrant transition.

4.5 SRA Results for the Dilute PdNi System

As mentioned in Section 2.3.3, no previous experimental investigation of the SRA on Pd based dilute alloys close to the ferromagnetic instability has been carried out nor does there exist any specific theoretical prediction for it. Here we present the results of the first such investigation. We begin with the dilute PdNi system.

4.5.1 A Typical Alloy—Pd_{95.0}Ni_{5.0}

The resistivities of fourteen dilute PdNi samples containing 2.1 and 5.0 at% Ni at fixed temperature T of 1.5 and 4.2 K in various applied fields were measured using the *ac* technique described in Chapter 3.

In Figure 4.27 the longitudinal ($\rho_{||}$) and transverse (ρ_{\perp}) magnetoresistivities of a typical sample, 5.0 at% Ni, are plotted against the applied field H_a at 1.5 K (this alloy has a Curie temperature of 62.7 K)⁹. This figure indicates that the transverse magnetoresistivity (ρ_{\perp}) increases monotonically with increasing applied field H_a up to 10 *kOe*, with a value of $\rho_{\perp} = 2.3058$ ($\mu\Omega cm$)¹⁰ in zero applied field and increasing to 2.3454 ($\mu\Omega cm$) at $H_a = 10$ *kOe*, with an inflection point (at about 1.0 *kOe*) and a substantial high-field slope

⁹It should be pointed out that the resistivities of the zero and low field states are domain configuration dependent; they depend on the sample history and magnetizing process. Therefore we usually have to apply magnetic fields large enough to technically saturate the sample in order to estimate the spontaneous resistivity anisotropy of a sample at zero induction.

¹⁰While the absolute value of ρ_{\perp} (1.5 K, $H_a = 0$) = 2.3058 ($\mu\Omega cm$) is accurate to $\pm 0.5\%$ (due to shape factor uncertainties), relative values can be determined to a precision of 1 in 10^6 ; thus the value of ρ_{\perp} (1.5 K, $H_a = 10$ *kOe*) = 2.3454 ($\mu\Omega cm$) shows a change in the resistivity of 39.8 ($n\Omega cm$) relative to the zero field value and this change can be accurately specified.

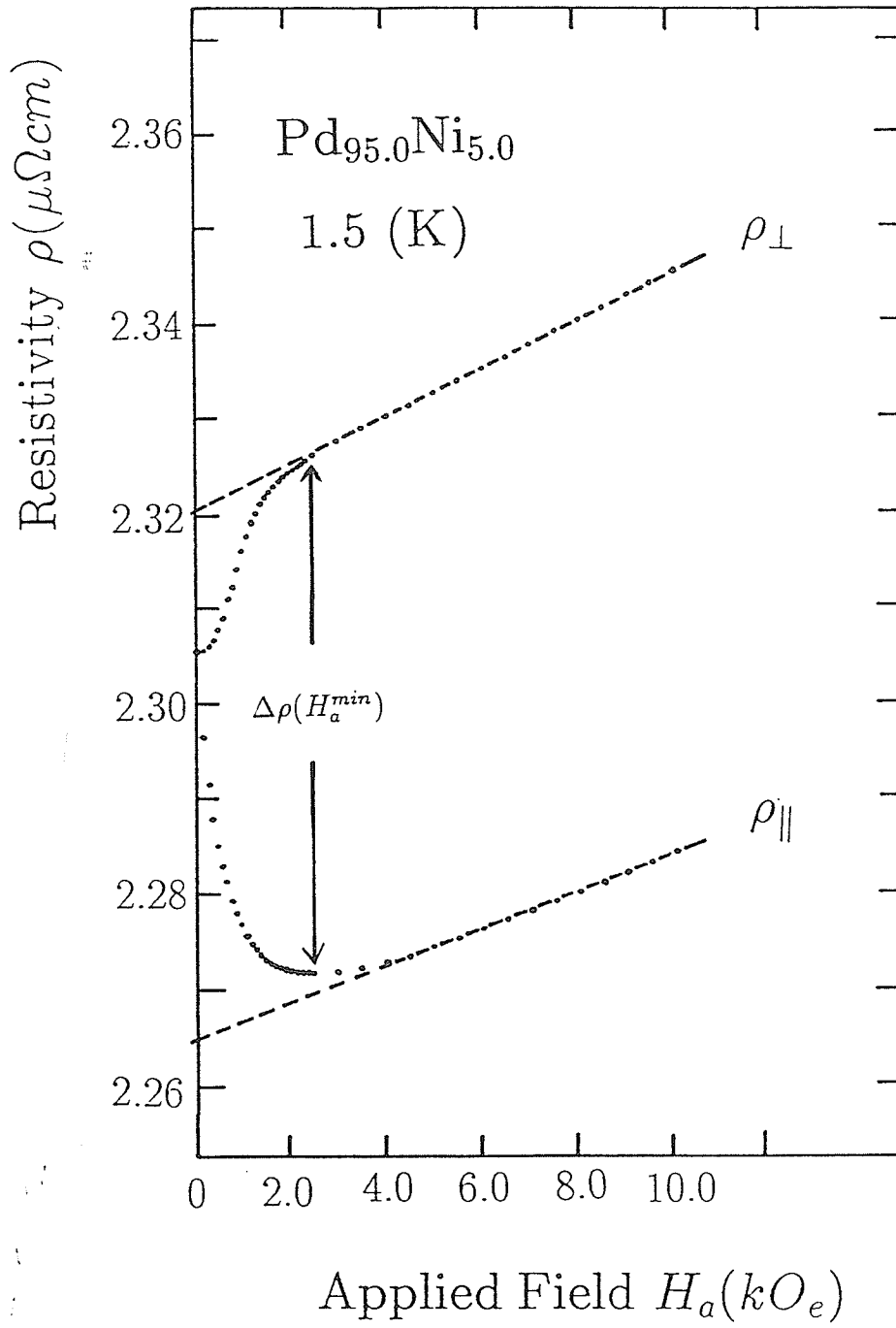


Figure 4.27: Resistivity versus applied field for a Pd_{95.0}Ni_{5.0} sample at 1.5 K.

($d\rho_{\perp}/dH_a = 2.48 (n\Omega cm/kOe)$). The longitudinal magnetoresistivity (ρ_{\parallel}), in contrast, displays a negative component at low field, but also has a substantial positive high field slope ($d\rho_{\parallel}/dH_a = 1.95 (n\Omega cm/kOe)$), so that it is basically U shaped with a minimum at about $2.5 kOe$. At this minimum ρ_{\parallel} drops to $2.2716 (\mu\Omega cm)$ and then gradually increases to $2.2846 (\mu\Omega cm)$ at $H_a = 10 kOe$, a value lower than $\rho(H_a = 0)$. Both $\rho_{\parallel}(H_a)$ and $\rho_{\perp}(H_a)$ are linear in the field between 3.0 and $10 kOe$.

Figure 4.27 clearly demonstrates the appearance of some anisotropy ($\Delta\rho \neq 0$) not only at higher fields, but also at low fields ($H_a < 0.1 kOe$). This is a result which we want to exploit. A non-zero anisotropy in such low applied field provides strong evidence for the presence of a significant exchange field in this sample, which produce a rapid increase in the anisotropy $\Delta\rho$ with increasing field as domain effects are overcome. Applied fields can certainly induce an anisotropy in paramagnetic system as discussed by Friederich and Fert (1974), but such fields have to be sufficiently large in order to induce a significant polarization of the scattering moments, typical $H_a/T \geq 10 kOe/K$ is required, that is far in excess of the values quoted above.

The result of the non-zero SRA observed in the PdNi (due to the presence of an orbital moment) is consistent with results obtained from ac susceptibility measurements. Specifically, the suppression of the zero field susceptibility peak amplitude, the increasing magnitude of the minimum field required to resolve a critical peak, and indeed the inability to extract reliable critical exponents for the system, can all be attributed to an anisotropy

(arising probably from spin-orbit coupling).

As illustrated in Figure 4.27, a simple linear field dependence represents the higher field data in the 5.0 at% Ni sample very well; various other field dependences (namely H^2 , \sqrt{H} etc) have been attempted for the higher field data, but they do not reproduce these data as well as the simple linear form shown¹¹. The extrapolation procedure implicit in Equation (1.70) has therefore been taken as a simple linear form, and this enables a quantitative estimate of SRA to be made. There are nevertheless two equivalent linear extrapolation procedures, and the other is illustrated Figure 4.28.

In Figure 4.27, by using this linear extrapolation for both sets of data from high field (shown by broken lines), the anisotropy ($\Delta\rho$) is found to be $-56.0 \pm 0.7(n\Omega cm)$, and the corresponding spontaneous magnetoresistive anisotropy ratio (SRA) is $-2.43 \pm 0.03\%$; this agrees well with the one previous measurement at this composition (Senoussi et al 1977). It is also comparable with the SRA observed in a system like PdCo near the same concentration, although it has the opposite sign. The negative sign of the anisotropy observed here agrees with that predicted to arise from spin-orbit scattering from either a d^8 or a d^9 configuration at the Ni site (Kondo 1962).

An alternative extrapolation procedure is to plot $\Delta\rho$ ($\Delta\rho = \rho_{||} - \rho_{\perp}$) directly as a function of H_a , as shown in Figure 4.28. Again it is apparent that the simple linear form reproduces the high field data well and a quantitative estimate of the SRA from the extrapolation procedure based on Equation

¹¹In the case of dilute (PdNi)Mn system the higher field data of the sample can be represented by H_i^2 field dependence (Kunkel et al 1988a).

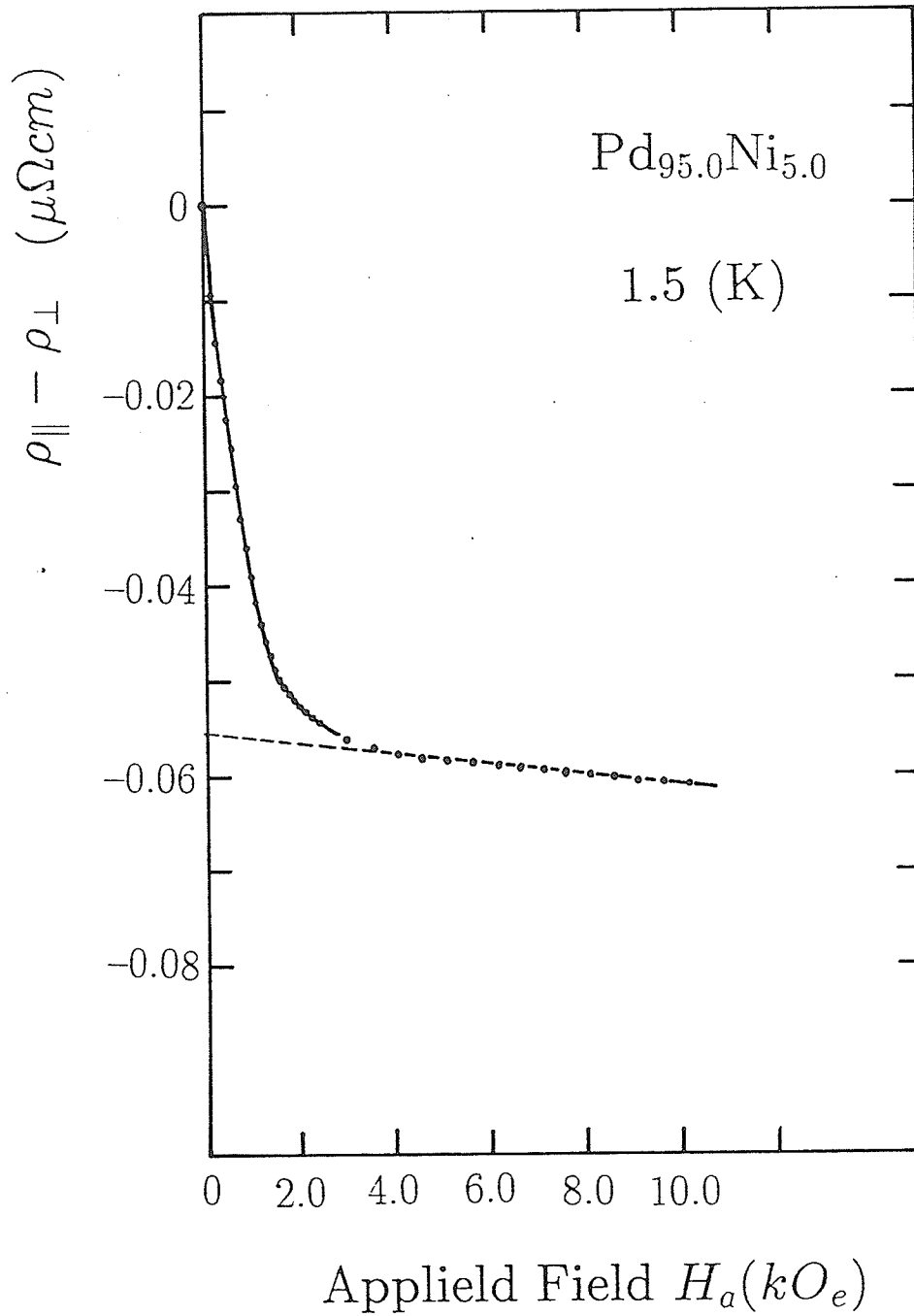


Figure 4.28: $\Delta\rho$ versus applied field for Pd_{95.0}Ni_{5.0} alloy at 1.5 K.

(1.70) is again possible. The value so obtained is $(-2.43 \pm 0.03\%)$ in excellent agreement with that obtained using the first technique.

The spontaneous resistive anisotropy (SRA) shows virtually no change between 1.5 and 4.2 K in this sample, because of the large T_c in comparison with the difference between the two measuring temperatures.

4.5.2 Ni Concentration Dependence

Having presented the SRA results on the $\text{Pd}_{95.0}\text{Ni}_{5.0}$ sample (the most concentrated Ni sample studied), we next discuss the data acquired at lower Ni concentration. Figures 4.29 to 4.31 illustrate the resistivities measured in longitudinal and transverse applied fields at 1.5 K for three samples with 4.5, 4.0, and 3.5 at% Ni, respectively. The simple linear field dependence is again the best fit to the higher field resistivity data.

The field dependent resistivity of these three samples have several features in common with the $\text{Pd}_{95.0}\text{Ni}_{5.0}$ sample. Namely the change of the transverse magnetoresistance ($\rho_{\perp}(H_a)$) is positive everywhere (that is $d\rho_{\perp}/dH_a > 0$), with an inflection point (i.e. $d\rho_{\perp}/dH_a$ has a maximum) in low applied field; the longitudinal magnetoresistance $\rho_{\parallel}(H_a)$ also displays a consistent behaviour, $d\rho_{\parallel}/dH_a$ is negative at low field (ρ_{\parallel} decreases with increasing field), ρ_{\parallel} exhibits a minimum, although the field at which this minimum occurs is dependent on the Ni concentration. The anisotropy and the associated SRA are negative in all the samples studied as $\rho_{\parallel}(H_a) < \rho_{\perp}(H_a)$. There is no virtually change in resistivity between 1.5 and 4.2 K in these three alloys.

A quantitative estimate for the SRA for these three samples was made

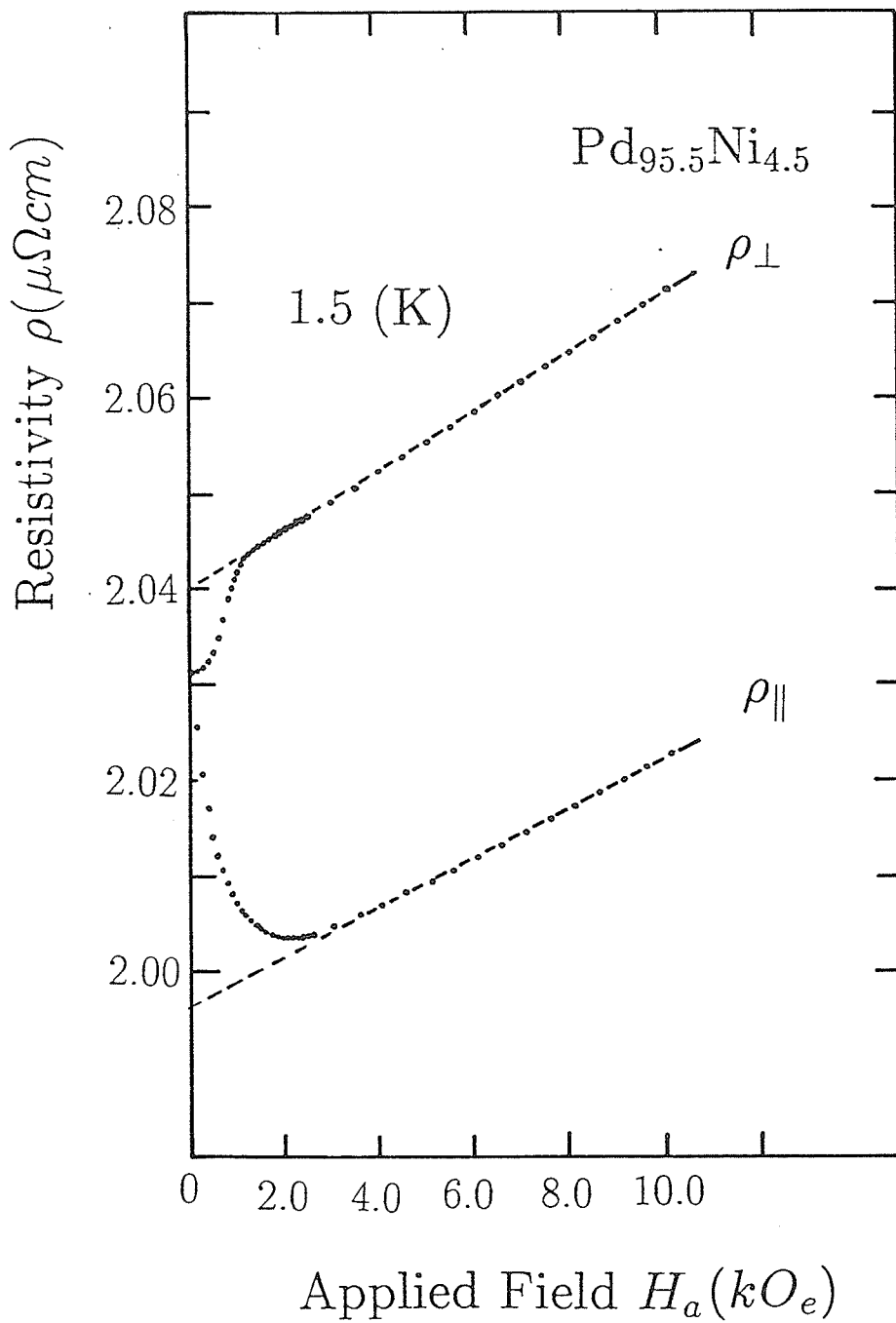


Figure 4.29: Resistivity versus applied field for Pd_{95.5}Ni_{4.5} at 1.5 K.

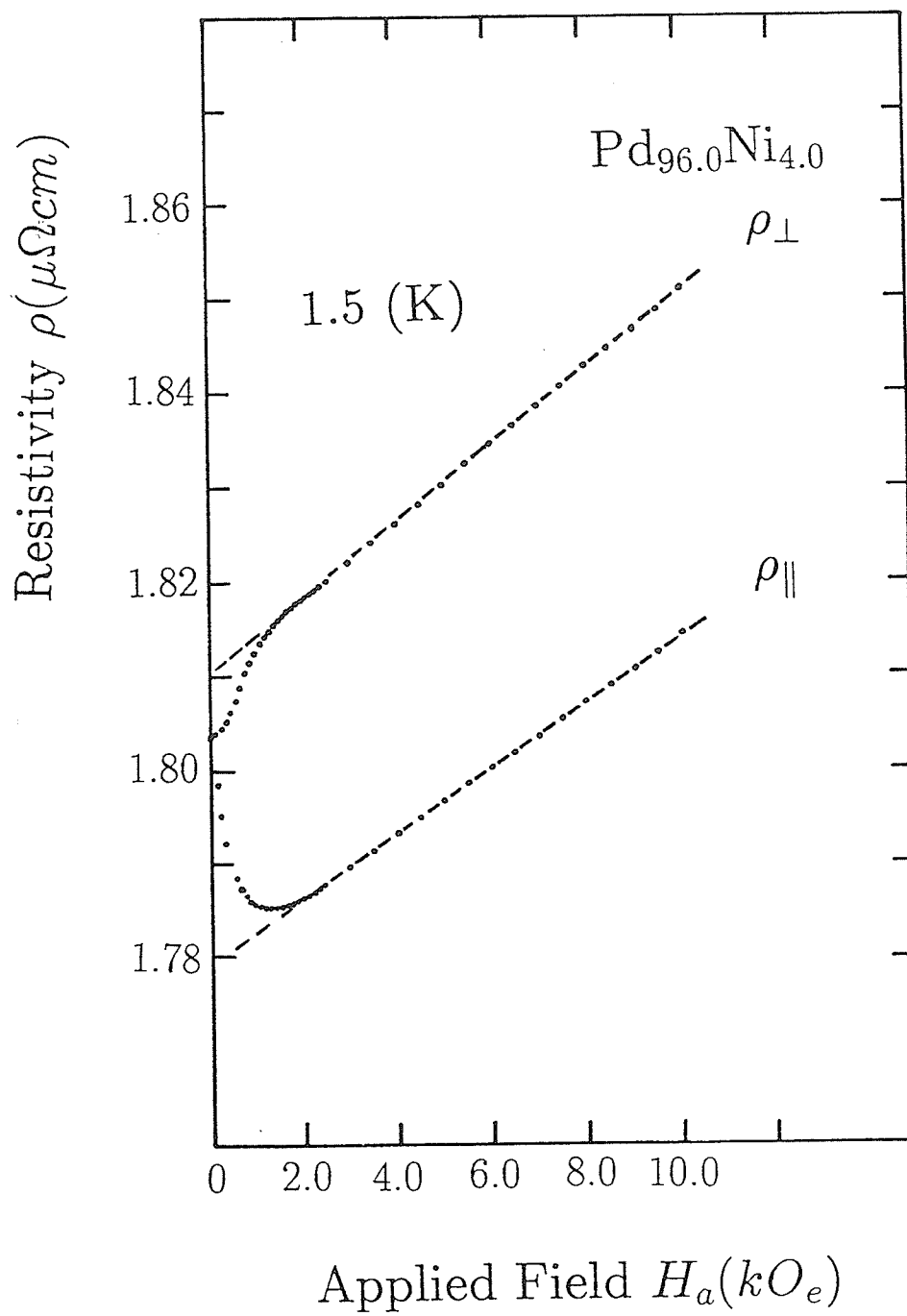


Figure 4.30: Resistivity versus applied field for Pd_{96.0}Ni_{4.0} at 1.5 K.

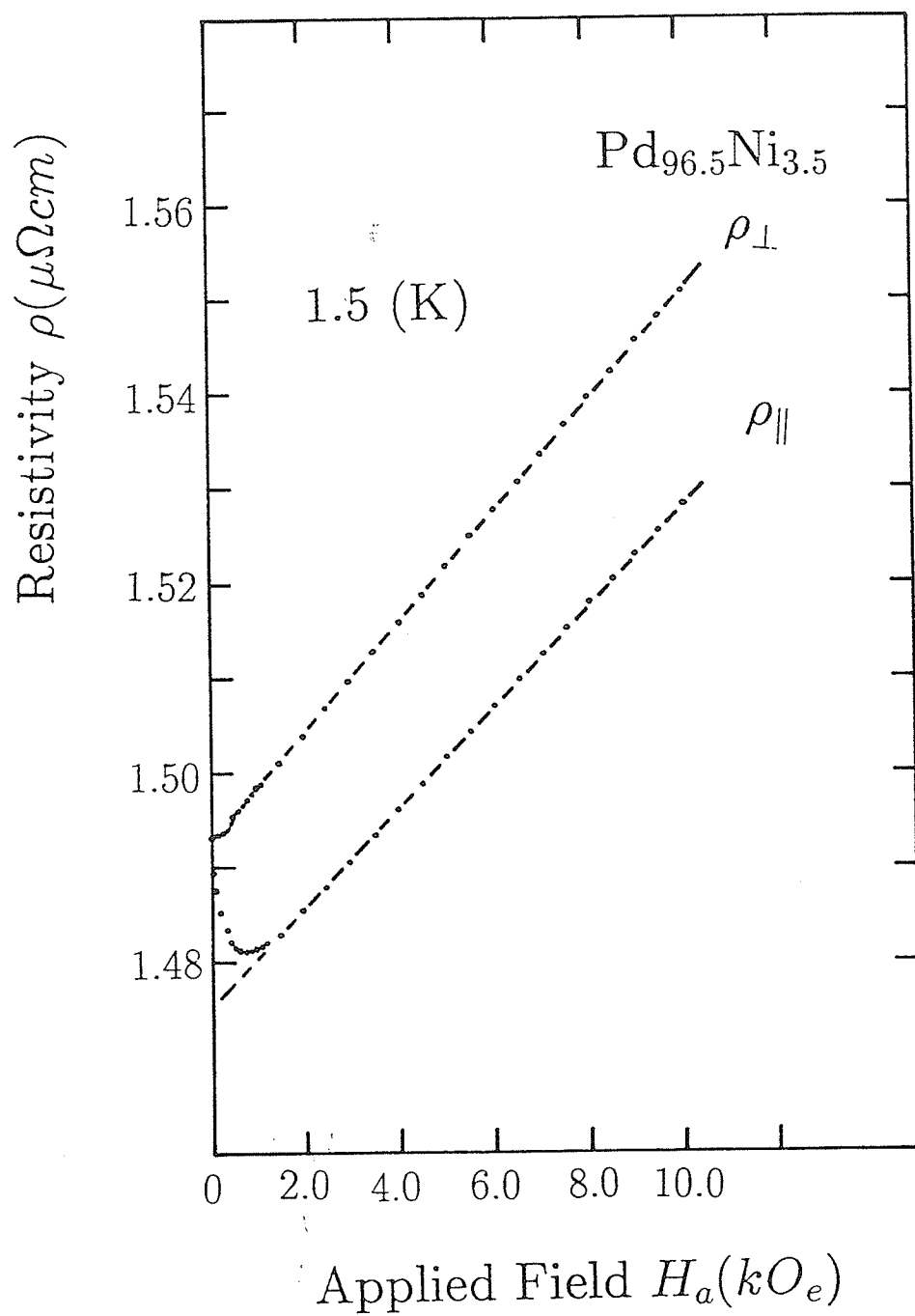


Figure 4.31: Resistivity versus applied field for Pd_{96.5}Ni_{3.5} at 1.5 K.

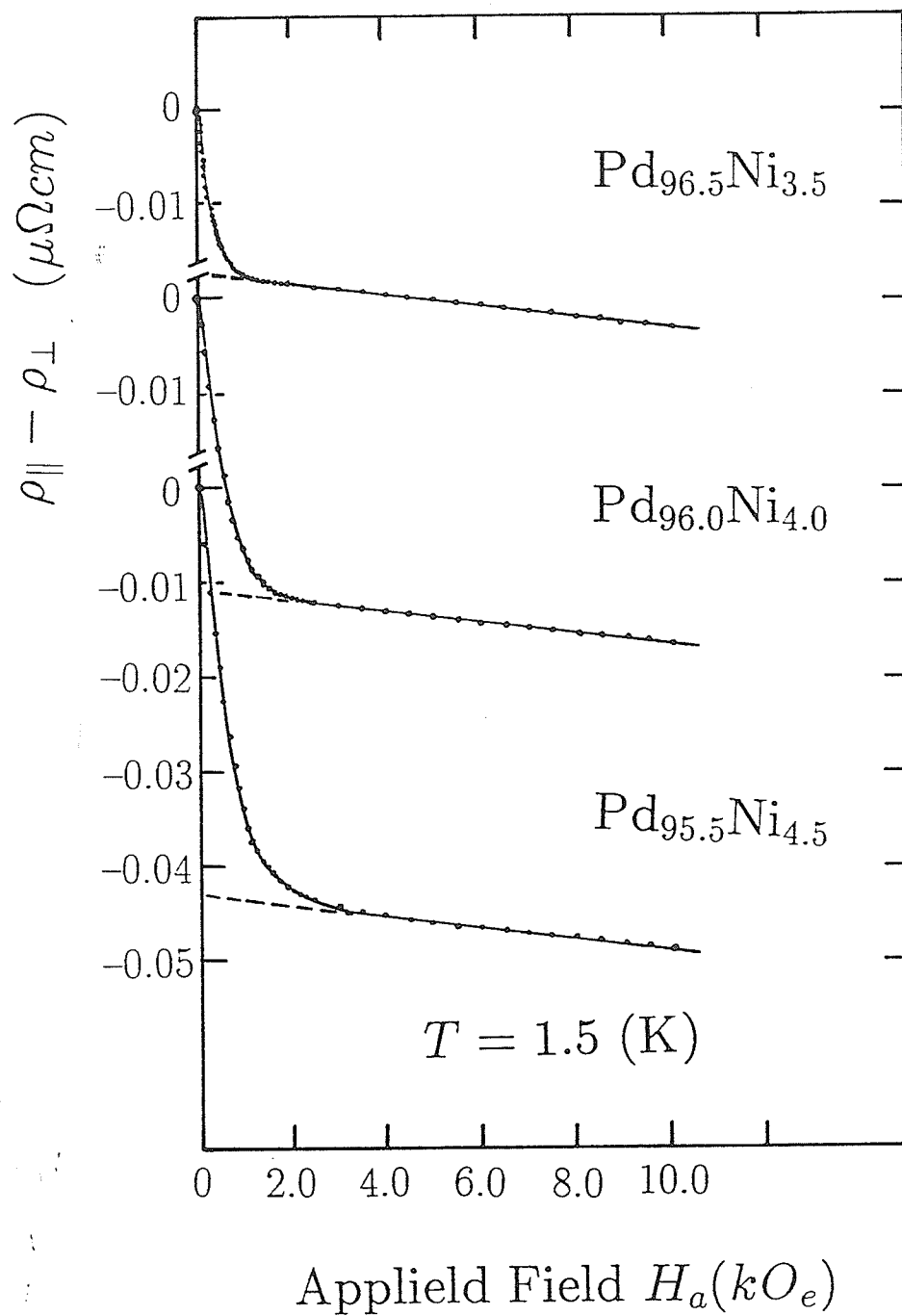


Figure 4.32: $\Delta\rho$ versus applied field H_a for the Pd alloys with 4.5 at%, 4.0 at% and 3.5 at% Ni at 1.5 K.

using a linear extrapolation, while the equivalent technique (extrapolation from the plot of resistivity difference ($\rho_{\parallel} - \rho_{\perp}$) at a given applied field against the field) is illustrated in Figure 4.32. The values so obtained are -2.12% for 4.5 at% Ni, -1.72% for 4.0 at% Ni, and -1.14% for 3.5 at% Ni sample, showing that the magnitude of the SRA decreases rapidly as the Ni concentration decreases (the SRA value for the 3.5 at% Ni sample is only about half that of the 5.0 at% Ni alloy). The high field slope, however, displays the reverse trend, being much larger at 3.5 at% ($d\rho_{\parallel}/dH_a = 5.17(n\Omega cm/kOe)$ and $d\rho_{\perp}/dH_a = 5.75(n\Omega cm/kOe)$) than at 5.0 at% Ni ($d\rho_{\parallel}/dH_a = 1.95(n\Omega cm/kOe)$ and $d\rho_{\perp}/dH_a = 2.48(n\Omega cm/kOe)$). This leads to estimates of the SRA based on the high field extrapolation procedure being subject to increasing uncertainty as the Ni concentration is lowered and the critical composition is approached (that is also confirmed by the data listed in Table 4.4). These will be discussed further for samples with Ni concentration very close to the ferromagnetic instability.

As pointed out in Section 1.3, in order to extract numerically reliable estimates for the spontaneous resistive anisotropy (SRA), the longitudinal (ρ_{\parallel}) and transverse (ρ_{\perp}) magnetoresistivities should be plotted against the magnetic induction B , rather than the applied field H_a . In Figure 4.33, the longitudinal (ρ_{\parallel}) and transverse magnetoresistivities (ρ_{\perp}) of the Pd + 3.5 at% Ni sample are plotted against both the applied field H_a and the magnetic induction B at 1.5 K. The magnetization M used to determine B was estimated by simple numerical integration of available ac susceptibility

data at various applied fields. The appropriate demagnetizing factors (N_{\parallel} and N_{\perp}) were found by treating the sample as an ellipsoid with principal axes equal to the sample's dimensions and evaluating the corresponding elliptic integrals as discussed in Chapter 3. As shown in this figure there are virtually no differences between $\rho_{\perp}(B)$ and $\rho_{\perp}(H_a)$ for this sample, since $N_{\perp} = 12.07 \approx 4\pi$. There are some differences between $\rho_{\parallel}(B)$ and $\rho_{\parallel}(H_a)$ since $N_{\parallel} = 0.011$, but this difference is rather small compared with the fields used. Therefore, estimating the SRA from the higher field slopes of the $\rho(H_a)$ curves instead of $\rho(B)$ is acceptable and introduces little error. Similar conclusions apply to all the PdNi samples examined.

Figure 4.34 displays the magnetoresistance of a 2.9 at% Ni sample ($T_c = 11$ K) at 1.5 and 4.2 K. The measurement was performed in applied magnetic fields up to 11.0 kOe. The higher field slopes $d\rho/dH_a$ ($d\rho_{\parallel}/dH_a = d\rho_{\perp}/dH_a = 6.91(n\Omega cm/kOe)$) here are some three times larger than those exhibited by the 5.0 at% Ni alloy ($d\rho_{\parallel}/dH_a = 1.95(n\Omega cm/kOe)$ and $d\rho_{\perp}/dH_a = 2.48(n\Omega cm/kOe)$) at 1.5 K, but the difference between ρ_{\parallel} and ρ_{\perp} is very small, and this makes the higher field extrapolation procedure very questionable. One can clearly see, however, from enlarged low field data (in Figure 4.35) that a magnetoresistance anisotropy does exist and the sign of the SRA is definitely negative. This latter behaviour emphasizes the necessity of using a high resolution technique to measure the anisotropy near the critical composition. In this figure there is also a clear change in both longitudinal (ρ_{\parallel}) and transverse magnetoresistivity (ρ_{\perp}) between 1.5 and 4.2 K in this

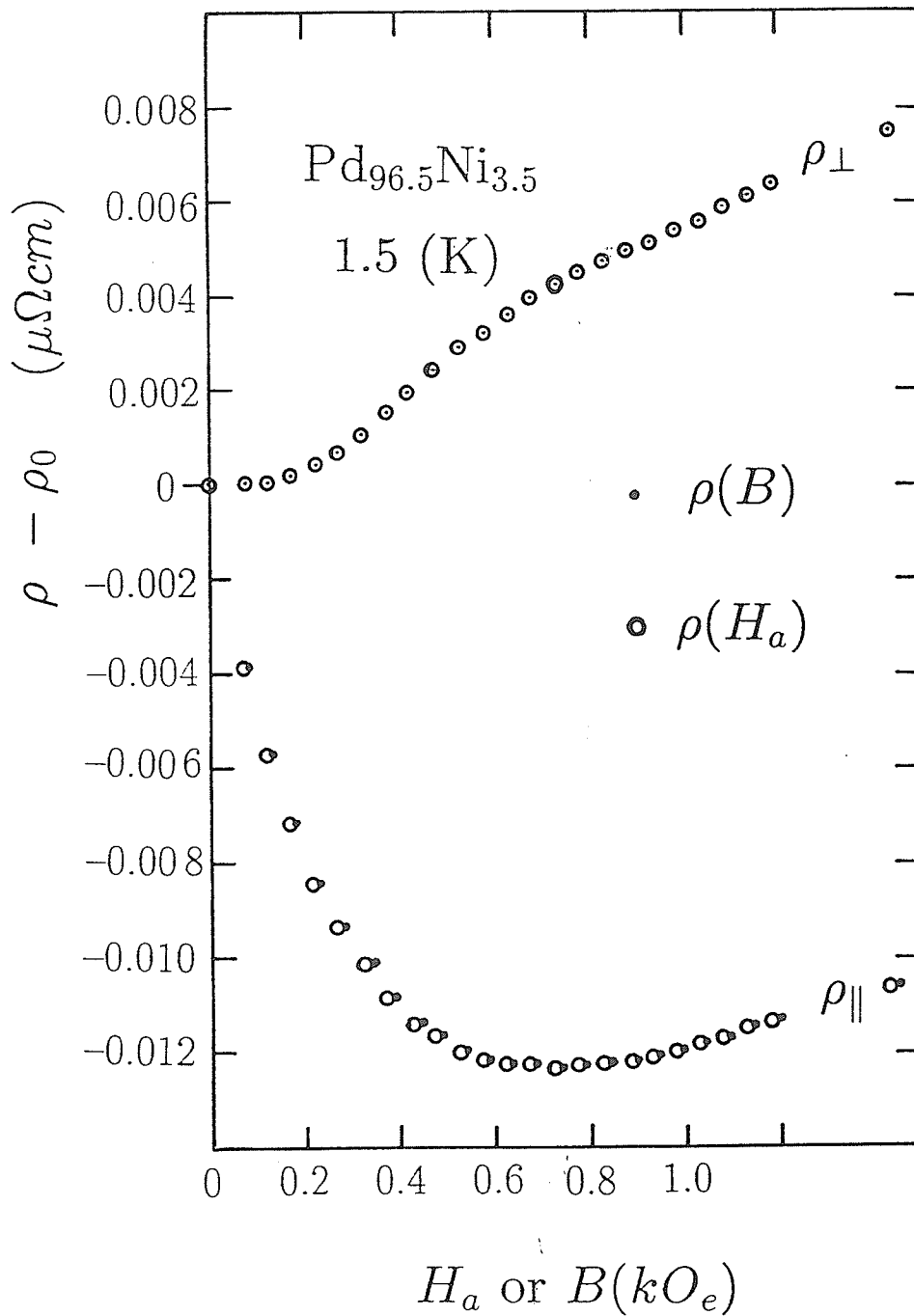


Figure 4.33: Resistivity versus induction B or applied field H_a for Pd_{96.5}Ni_{3.5} at 1.5 K.

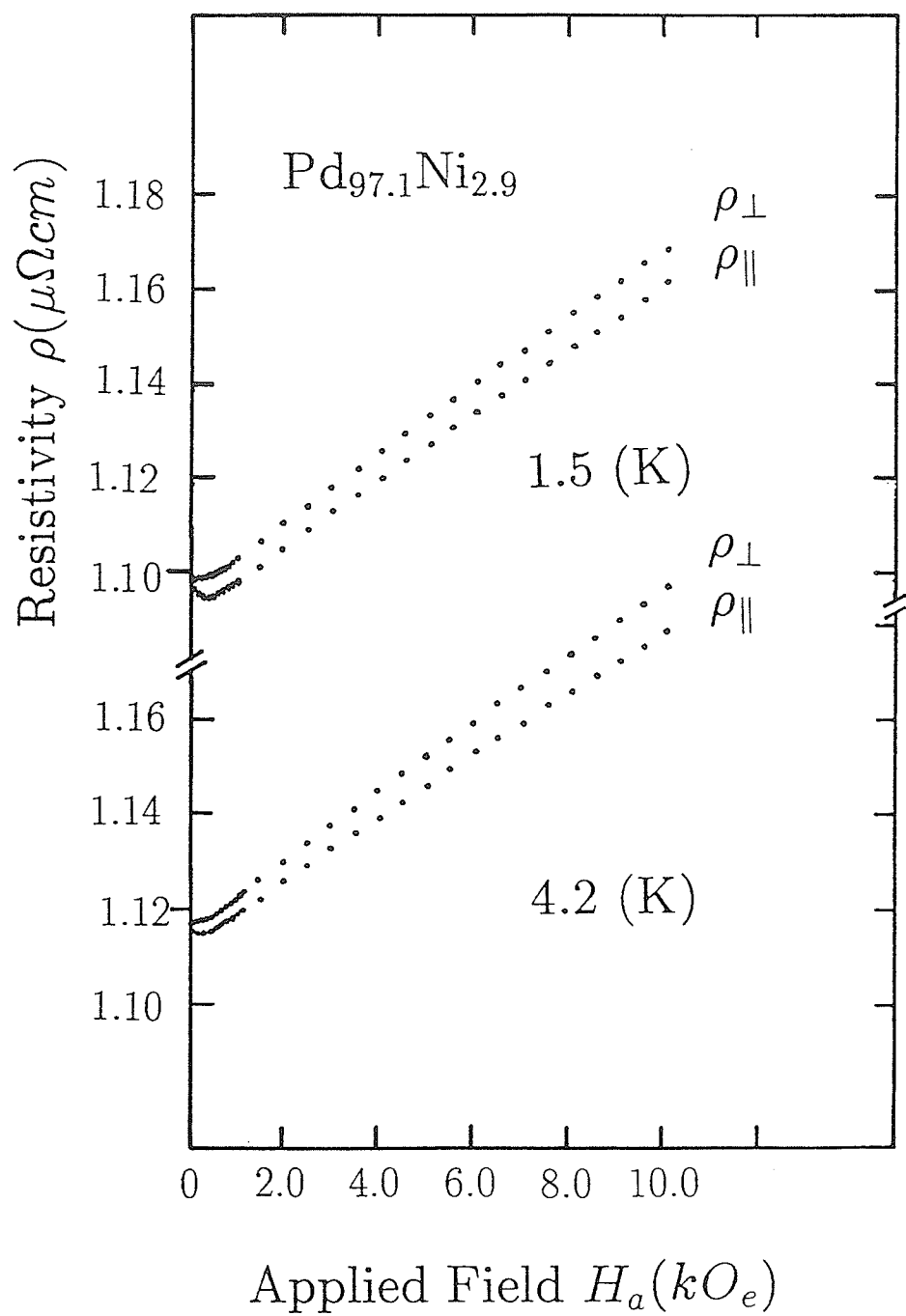


Figure 4.34: Resistivity versus applied field of $\text{Pd}_{97.1}\text{Ni}_{2.9}$ at 1.5 and 4.2 K.

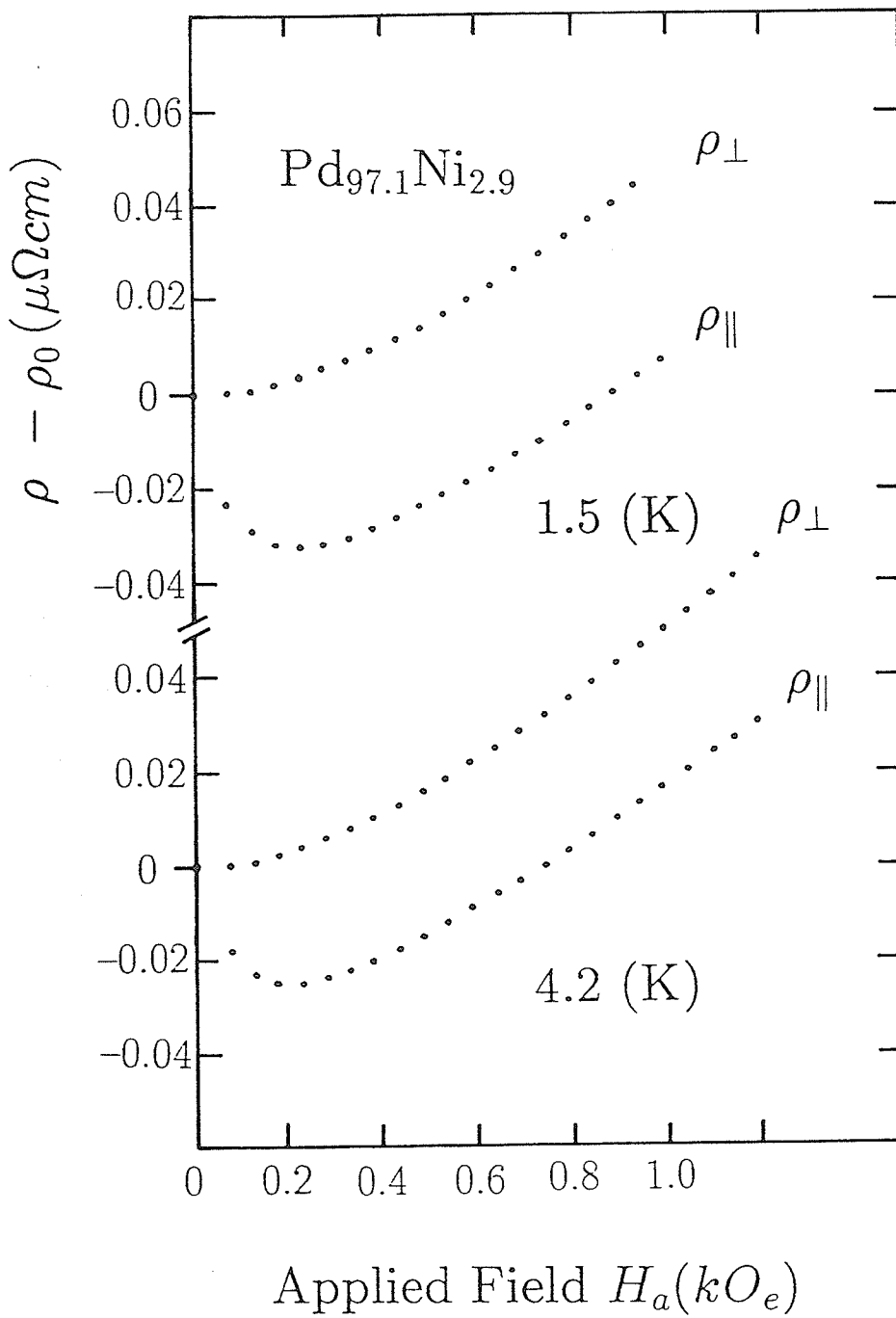


Figure 4.35: Resistivity versus applied field of Pd_{97.1}Ni_{2.9} at 1.5 and 4.2 K (the low field data).

sample. The anisotropy $\Delta\rho$ decreases with increasing temperature, which is anticipated result because the exchange splitting competes with thermal fluctuations and the difference between the measuring temperatures is no longer negligible compared to T_c for this low Curie temperature sample. Magnetic measurements are, by contrast, quite ambiguous when the Ni concentration is lowered towards the critical composition. In alloys containing less than 3.0 at% Ni, the low field Arrott plots become strongly curved making the associated ordering temperature difficult to identify (Murani et al 1974).

The experimental results on a 2.4 at% Ni sample at 1.5 and 4.2 K in full and low fields are shown in Figures 4.36 and 4.37, respectively. Figure 4.36 demonstrates that due to the decrease of the magnitude of the difference between ρ_{\parallel} and ρ_{\perp} , and the increase of higher field slopes, an estimate of the SRA based on the higher field extrapolation procedure is not reliable. By contrast, the low field data is unambiguous (see Figure 4.37). It indicates the presence of a negative SRA at 1.5 K (although it is very small), but not at 4.2 K. Notice the much enlarged scale, emphasizing the necessary of a high resolution technique.

Low applied field magnetoresistance data for a 2.3 at% Ni sample at 1.5 and 4.2 K are presented in Figure 4.38. Despite the high relative precision of the *ac* technique ($\Delta\rho \approx 10 \text{ p}\Omega\text{cm}$), no anisotropy could be resolved at either 1.5 or 4.2 K.

The above results indicate that the 2.4 at% Ni sample possesses long range magnetic order at 1.5 K but not at 4.2 K, while the 2.3 at% Ni sample

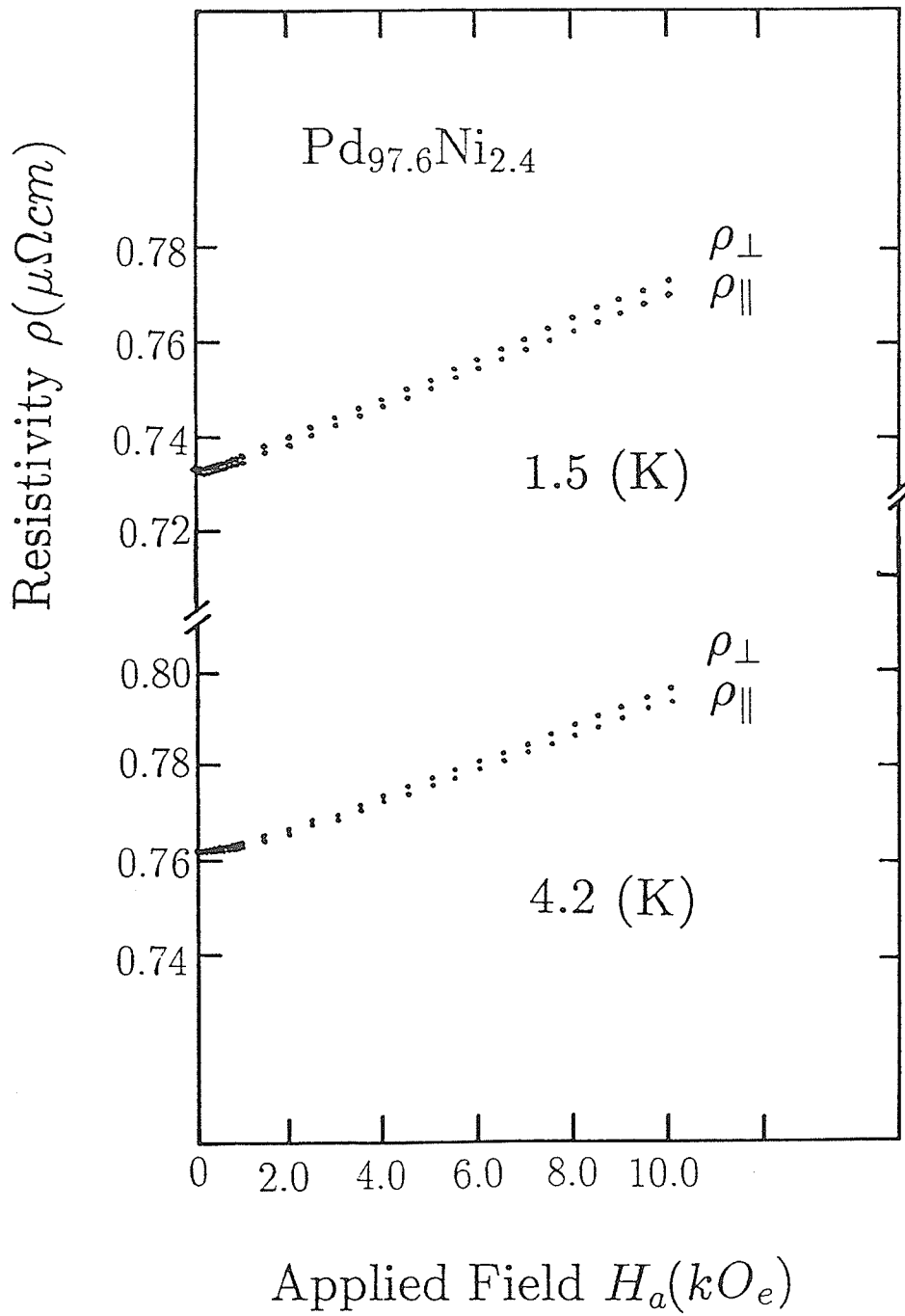


Figure 4.36: Resistivity versus applied field of Pd_{97.6}Ni_{2.4} at 1.5 and 4.2 K.

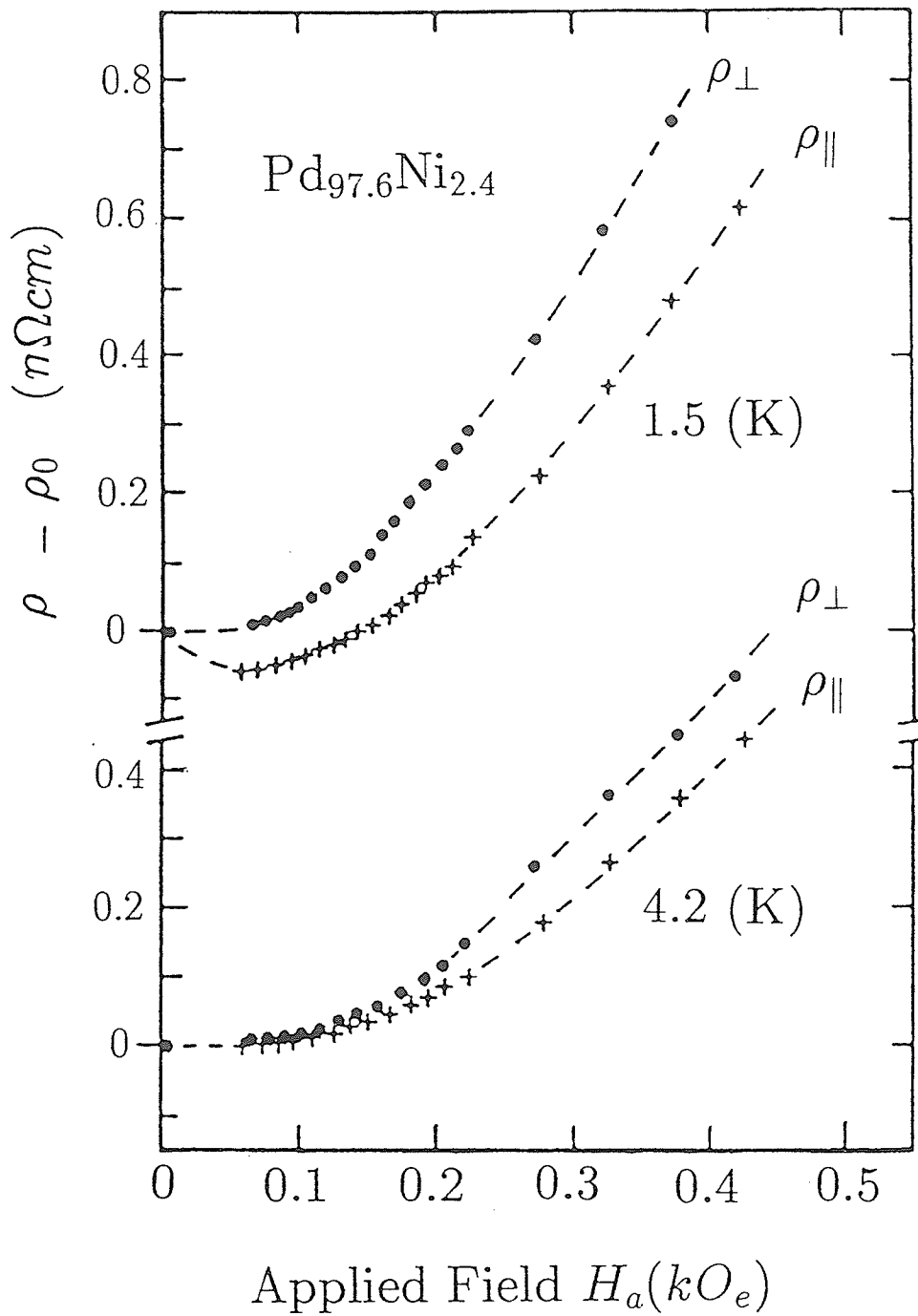


Figure 4.37: Resistivity versus applied field of Pd_{97.6}Ni_{2.4} at 1.5 and 4.2 K (low field data).

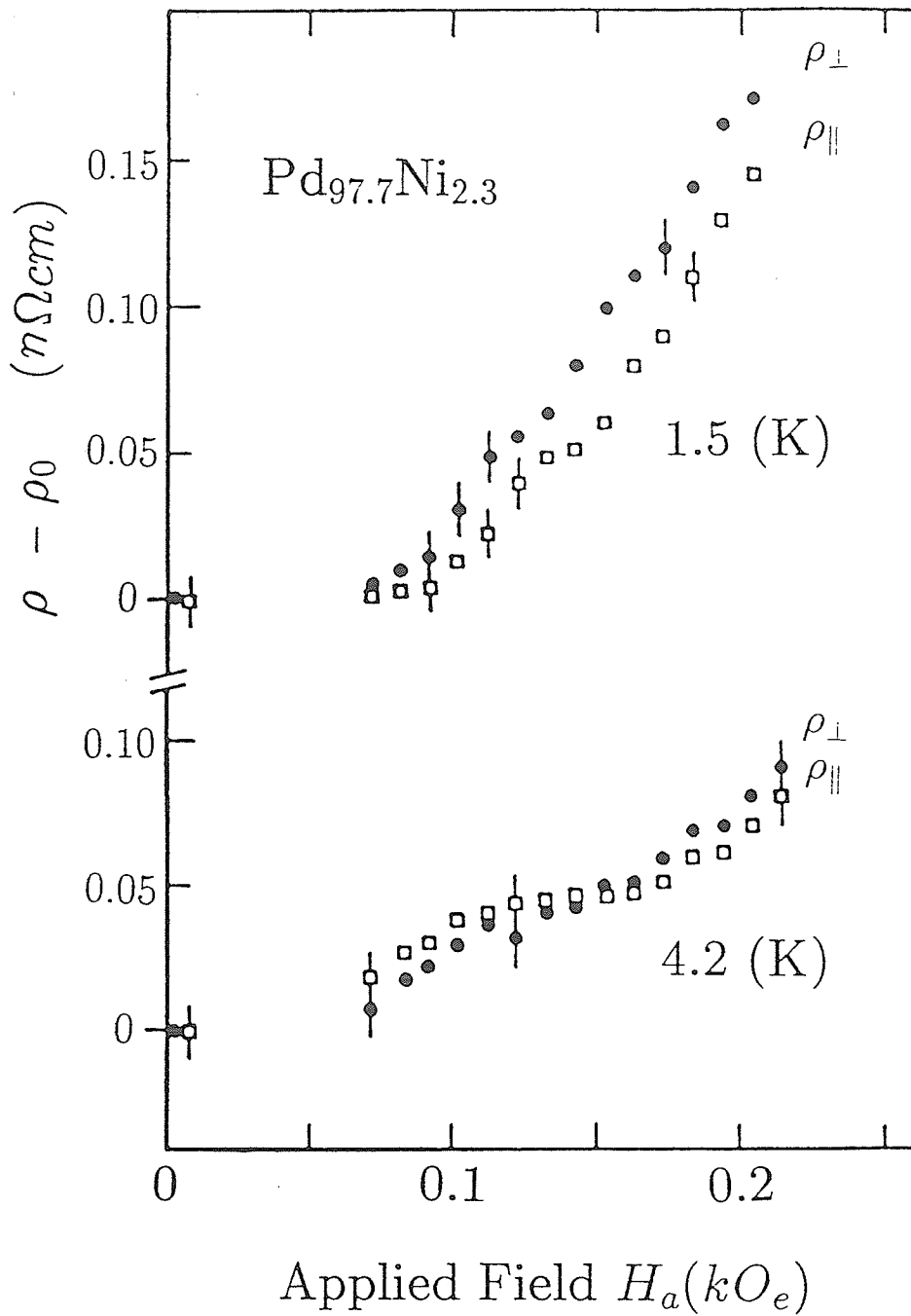


Figure 4.38: Resistivity versus applied field of Pd_{97.7}Ni_{2.3} at 1.5 and 4.2 K.

does not order at 1.5 K or above. These measurements confirm a critical concentration of $2.3 < x_0 < 2.4$ at% Ni at 1.5 K, and also indicate that while many of the estimates for x_0 are based on extrapolation procedures which can be complex, x_0 can be found by direct observation from the appearance of a SRA in applied fields of less than 1.0 kOe .

4.5.3 Quantitative estimates from $\rho(H_a^{min})$

As pointed out earlier, when the Ni concentration is lowered towards the critical composition, the SRA decreases and the high field slope not only becomes progressively larger but it is also no longer strictly linear in field. For those samples with Ni concentration less than 3.0 at%, the high field extrapolation procedure is subject to increasing difficulties, and for those samples with Ni concentrations very near the critical composition, the estimates of SRA based on the high field extrapolation techniques are impossible. The second higher field extrapolation procedure can reliably estimate the SRA value for samples with Ni concentration as low as 2.7 at% (these SRA values are also listed in Table 4.4 under column (b)). However as with the first technique, estimates of the SRA based on this extrapolation procedure are also subject to increasing uncertainty when the critical concentration x_0 is approached. This behaviour indicates that an alternative method is needed in order to obtain quantitative data on the SRA on approaching the critical composition, where the higher field extrapolation is very questionable. Indeed under these conditions the high field extrapolation techniques of the type used on

the more concentrated samples cannot, in our opinion, be relied upon to predict correctly the sign, let alone the magnitude, of the SRA for these low Ni concentration samples. By contrast, all the resistivity figures shown in previous subsections demonstrate that the low-field data are unambiguous; they indicate a negative sign for the SRA and a magnitude which decreases as the Ni concentration x is lowered towards x_0 . Further, a new method, based on this low field behaviour, has been developed in order to make quantitative estimates for the SRA when the latter is small. Notice that there is a minimum in $\rho_{\parallel}(H_a)$ for all samples with Ni concentration greater than 2.3 at% at 1.5 K. If one defines

$$\frac{\Delta\rho(H_a^{min})}{\rho_0} = \frac{\rho_{\parallel}(H_a^{min}) - \rho_{\perp}(H_a^{min})}{\rho_0} \quad (4.6)$$

the SRA can be measured in each sample at a unique field ($\rho(H_a^{min})$) without extrapolation from higher fields, therefore avoiding the complications inherent in the latter process. Furthermore, as is evident from Figures 4.27 to 4.37, this characteristic field $\rho(H_a^{min})$, at which the ratio is measured, shows the desirable property of approaching zero as $x \rightarrow x_0$. This means that the potential perturbing effects of an external field are minimized in this sensitive composition range. This is confirmed by the failure to observe an anisotropy at low fields in samples below the critical composition x_0 . However, estimates of the SRA based on the use of Equation (4.6) must agree with those obtained using established extrapolation techniques which is based on Equation (1.70) (at least, in situations where comparisons are possible). In the case of the 5.0 at%

Ni sample at 1.5 K, the quantitative estimate from $\rho(H_a^{min})$ is $-2.41(\pm 0.01)\%$ which has been indicated in Figure 4.27, while from the higher field extrapolation procedure the SRA is $-2.43(\pm 0.03)\%$. This shows that these two estimates are in excellent agreement. We have estimated the SRA using both methods in all the samples containing 3.0 at% Ni or more where this comparison is possible. The results at 1.5 K have been summarized in Table 4.4. As one can see from the table, for those samples having Ni concentrations > 3.0 at%, the SRA obtained using the magnetoresistance minimum is in excellent agreement with the established extrapolation methods¹² (the SRA estimated from data obtained at 4.2 K is summarized in Table 4.5). As Table 4.4 shows, Equation (4.6) indeed provides a prescription for measuring the SRA in each sample at a unique field (H_a^{min}), thus avoiding the complications inherent in extrapolation procedures. Having demonstrated the applicability of this low-field method in PdNi alloys, it is now possible to use it to find the SRA in samples with Ni concentration close to x_0 where the extrapolation method is not reliable. The corresponding SRA estimates are also listed in Table 4.4. As is clear from this table, over the entire composition range examined, the SRA is negative and its absolute value decreases rapidly as Ni concentration is lowered, from -2.41% for 5.0 at% Ni at 1.5 K to -0.009% for the 2.4 at% Ni sample, as determined by the low-field method.

¹²Where (a) contains the values extrapolated directly from higher field slope, (b) stands the values extrapolated from higher field $(\Delta\rho(H_a))/\rho_0$, and (c) measured values from $\Delta\rho(H_a^{min})$.

Table 4.4: Summary of parameters taken from the *ac* magnetoresistance data for the PdNi alloys at 1.5 K.

Ni at%	Anisotropy ($\mu\Omega cm$)	SRA (a)	SRA (b)	SRA (c)	ρ_0 ($\mu\Omega cm$)
5.0	-0.0560	-0.0243	-0.0243	-0.0241	2.3058
4.5	-0.0430	-0.0212	-0.0212	-0.0212	2.1055
4.0	-0.0310	-0.0172	-0.0172	-0.0168	1.8038
3.5	-0.0170	-0.0114	-0.0114	-0.0111	1.4932
3.0	-0.0060	-0.0053	-0.0042	-0.0036	1.1273
2.9			-0.0038	-0.0032	1.0977
2.8			-0.0024	-0.0020	0.9835
2.7			-0.0015	-0.0013	0.9459
2.6				-0.00069	0.7808
2.5				-0.00034	0.7615
2.4				-0.00009	0.7331
2.3				≤ 0.000014	0.7002
2.2				≤ 0.000014	0.6685
2.1				≤ 0.000014	0.6321
0					0.0508

Table 4.5: Summary of parameters taken from the *ac* magnetoresistance data for the PdNi alloys at 4.2 K.

Ni at%	Anisotropy ($\mu\Omega cm$)	SRA (a)	SRA (b)	SRA (c)
5.0	-0.0550	-0.0239	-0.0243	-0.0239
4.5	-0.0430	-0.0212	-0.0212	-0.0209
4.0	-0.0310	-0.0172	-0.0172	-0.0163
3.5	-0.0160	-0.0107	-0.0114	-0.0104
3.0	-0.0030	-0.0027	-0.0042	-0.0027
2.9			-0.0038	-0.0025
2.8			-0.0024	-0.0014
2.7			-0.0015	-0.00076
2.6				-0.00017
2.5				-0.000046
2.4				≤ 0.000014
2.3				≤ 0.000014
2.2				≤ 0.000014
2.1				≤ 0.000014

4.5.4 Power Law Relationship

As shown in Tables 4.4 and 4.5, the 2.5 at% Ni sample is ordered just above 4.2 K, while in the case of the 2.4 at% alloy, the anisotropy has collapsed to zero at that temperature. For those samples with Ni concentrations less than 3.0 at%, the resistive anisotropy is observed to decrease when the temperature is changed from 1.5 to 4.2 K as thermal fluctuations begin to compete effectively with the exchange splitting, as shown in Figures 4.34 to 4.38; for those alloys with higher Ni concentrations no temperature dependence in the SRA could be measured between 1.5 and 4.2 K because of the higher T_c .

For the samples with Ni compositions close to the critical concentration, one can thus still estimate the SRA quantitatively using the new method. Notice that the SRA decreases rapidly as $x \rightarrow x_0$; there is a reduction by a factor of 250 between 5.0 and 2.4 at% Ni at 1.5 K. This has prompted us to search for a possible power law relationship between the SRA and Ni concentration such that

$$\frac{\Delta\rho}{\rho_0} \propto \left(\frac{x - x_0}{x_0}\right)^n \quad (4.7)$$

We have carefully examined the data listed in the tables, using the critical Ni concentration, $x_0 = 2.3 \pm (0.05)$ at% Ni, which was deduced from previous measurements (Tari and Coles 1971, Murani et al 1974) and confirmed recently by Kunkel et al (1987). The results are shown in Figures 4.39 and 4.40, respectively. This is the first such attempt to fit this type of data,

and it indicates that the power law relationship does reproduce the SRA data both at 1.5 and 4.2 K respectively with the following parameters

$$\eta = 2.25 \pm 0.1 \quad \text{when } x_0 = 2.25 \text{ at\% Ni}$$

$$\eta = 2.00 \pm 0.1 \quad \text{when } x_0 = 2.30 \text{ at\% Ni.}$$

Considering the temperature dependence of the SRA at low Ni concentration, as clearly shown in Figure 4.35 (the SRA increases as the temperature decreases to 1.5 K), measurements at still lower temperature would be expected to produce increased SRA. Therefore we argue for the first estimate i.e. $x_0 = 2.25$ at% Ni and $\eta = 2.25$. This choice for x_0 is in excellent agreement with previously reported estimates listed above; however, by contrast there is no previous measurement or theoretical prediction for the exponent η . Lower and higher values of x_0 have been attempted but they do not reproduce the data as well as this choice for the critical Ni concentration.

A summary of the zero-field resistivity at 1.5 K over the entire Ni concentration range examined is also presented in Table 4.4. As shown in this table, the magnitude of the resistivity increases with increasing Ni concentration from 0.0508 ($\mu\Omega cm$) for the pure Pd to 2.3058 ($\mu\Omega cm$) for the 5.0 at% Ni sample.

The higher field slopes, $d\rho_{\parallel}/dH_a$ and $d\rho_{\perp}/dH_a$ have also been estimated in the field range $5.0 kOe < H_a < 10 kOe$ for all the PdNi samples studied. As shown in Table 4.6, the magnitude of $d\rho_{\perp}/dH_a$ for each sample is usually a few percent larger than $d\rho_{\parallel}/dH_a$, and both $d\rho_{\parallel}/dH_a$ and $d\rho_{\perp}/dH_a$ increase with increasing Ni concentration from 2.1 at% to approximately 3.0 at% Ni.

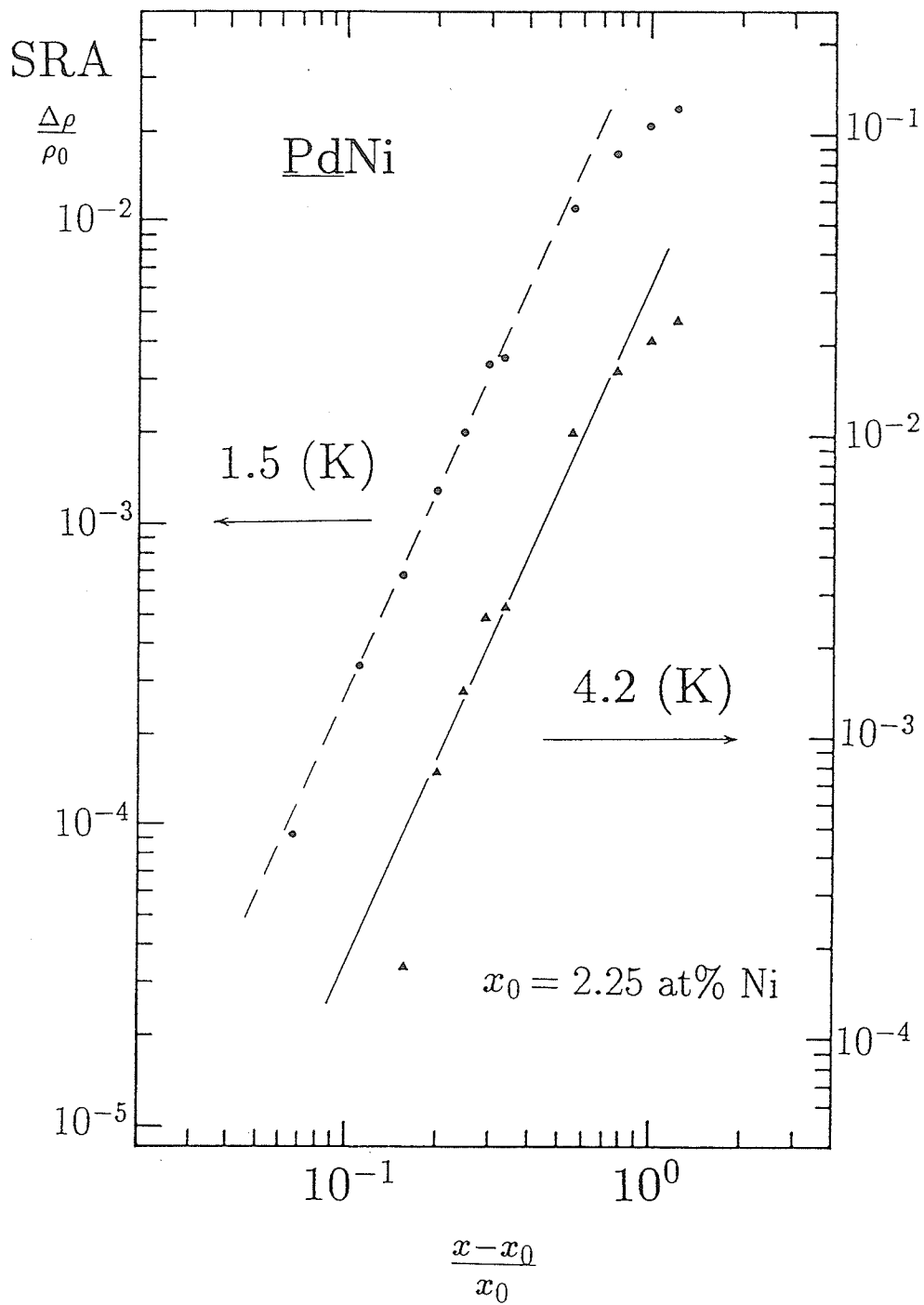


Figure 4.39: SRA versus reduced Ni concentration on a double log plot at 1.5 and 4.2 K with $x_0 = 2.25$ at% Ni.

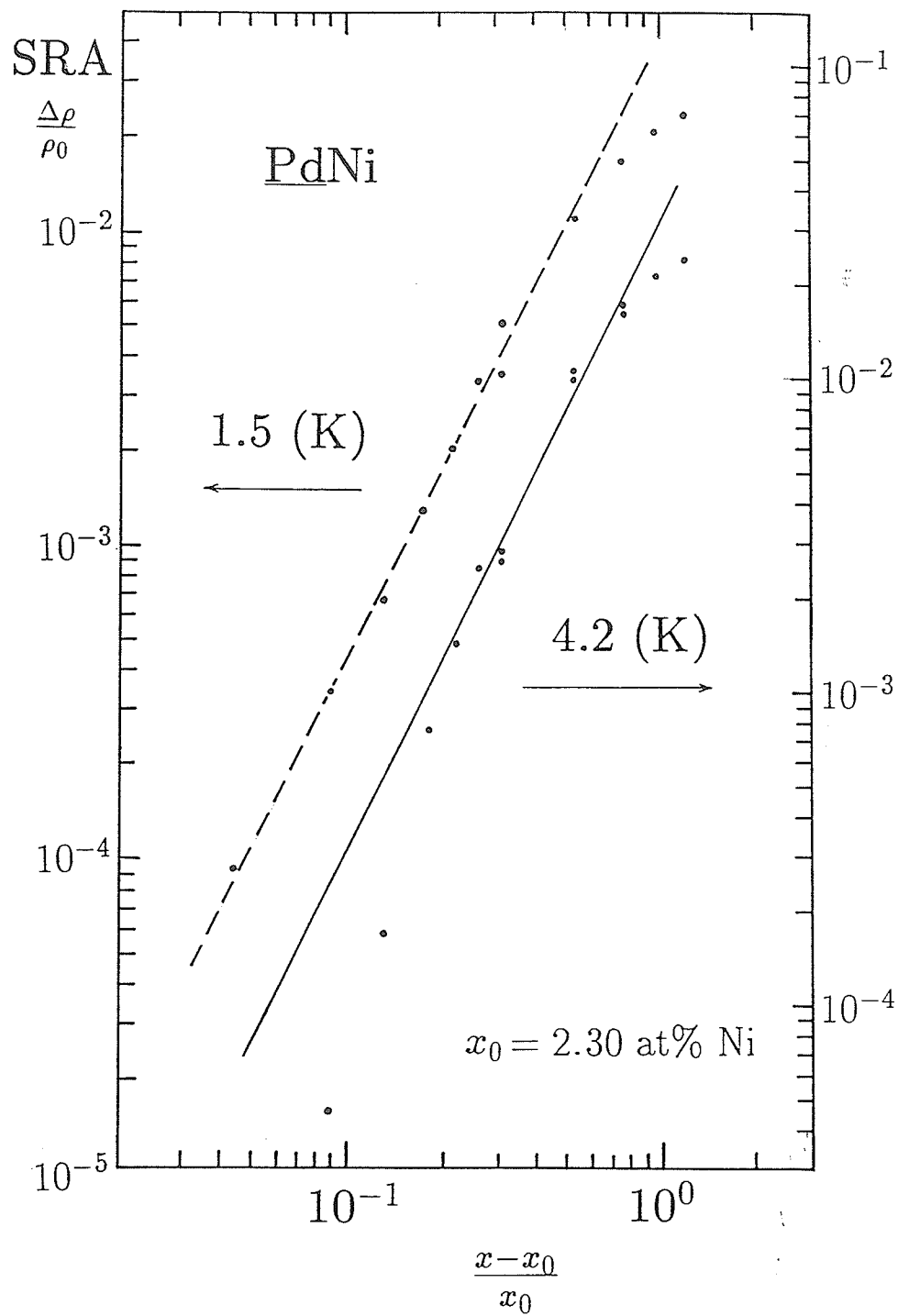


Figure 4.40: SRA versus reduced Ni concentration on a double log plot at 1.5 and 4.2 K with $x_0 = 2.30 \text{ at\% Ni}$.

The magnitude of the slopes at 3.0 at% Ni ($d\rho_{\parallel}/dH_a = 7.00(n\Omega cm/kOe)$, $d\rho_{\perp}/dH_a = 6.70(n\Omega cm/kOe)$) are about three times as big as for 2.1 at% Ni ($d\rho_{\parallel}/dH_a = 2.60(n\Omega cm/kOe)$, $d\rho_{\perp}/dH_a = 2.35(n\Omega cm/kOe)$). The magnitude of both $d\rho_{\parallel}/dH_a$ and $d\rho_{\perp}/dH_a$ peak at about 3.0 at% Ni at both 1.5 and 4.2 K, and then decrease with increasing Ni concentration up to 5.0 at% Ni. While these slopes themselves do not have an anomaly in the vicinity of the critical composition estimated above, they nevertheless support the above estimate for the critical concentration x_0 . The identification of x_0 as a critical concentration means that plots of quantities such as $(1/\rho_0)(d\rho_{\perp}/dH_a)(1/T_c)$ against Ni concentration should diverge at x_0 . This is simply equivalent to stating that $T_c \rightarrow 0$ as $x \rightarrow x_0$. Measurements of Curie temperatures close to the critical concentration in PdNi are difficult not only for the technical reasons outlined above, but also because T_c falls well below 1 K. Plotting the quantity indicated above has the following advantages: first, it uses data acquired from the sample for which the SRA was estimated, and second, it allows the data on paramagnetic samples to be included by the conventional replacement of the Curie temperature T_c by the measuring temperature T . Thus, not only can data for samples with Ni concentrations above x_0 measured above their ordering temperature be included, but samples with concentrations below x_0 can also be assessed (Loewen et al 1986). These data are reproduced in Figure 4.41. The ordinate in this figure increases by a factor of 100 over the concentration range examined (necessitating the use of a log-linear plot). In comparison there is less than a factor of 3 in the variation

Table 4.6: Summary of the high field slopes for PdNi alloys at 1.5 and 4.2 K.

Ni at%	$T = 1.5$ K $d\rho_{\parallel}/dH_a$ ($n\Omega cm/kOe$)	$T = 1.5$ K $d\rho_{\perp}/dH_a$ ($n\Omega cm/kOe$)	$T = 4.2$ K $d\rho_{\parallel}/dH_a$ ($n\Omega cm/kOe$)	$T = 4.2$ K $d\rho_{\perp}/dH_a$ ($n\Omega cm/kOe$)
5.0	1.95	2.48	1.94	2.44
4.5	2.55	3.12	2.53	3.02
4.0	3.55	4.15	3.47	4.04
3.5	5.17	5.75	5.14	5.66
3.0	6.70	7.00	6.56	6.71
2.9	6.91	6.91	6.55	7.05
2.8	6.29	6.75	6.21	6.70
2.7	5.75	6.28	5.82	6.25
2.6	4.89	5.17	4.53	4.90
2.5	4.40	4.70	4.02	4.28
2.4	3.95	4.20	3.63	3.81
2.3	3.43	3.70	3.19	3.42
2.2	3.15	3.40	2.83	3.15
2.1	2.35	2.60	2.11	2.59

for the unscaled slopes. Notice that this scaled plot peaks between 2.2 and 2.3 at% Ni, thus providing indirect confirmation of our choice for x_0 .

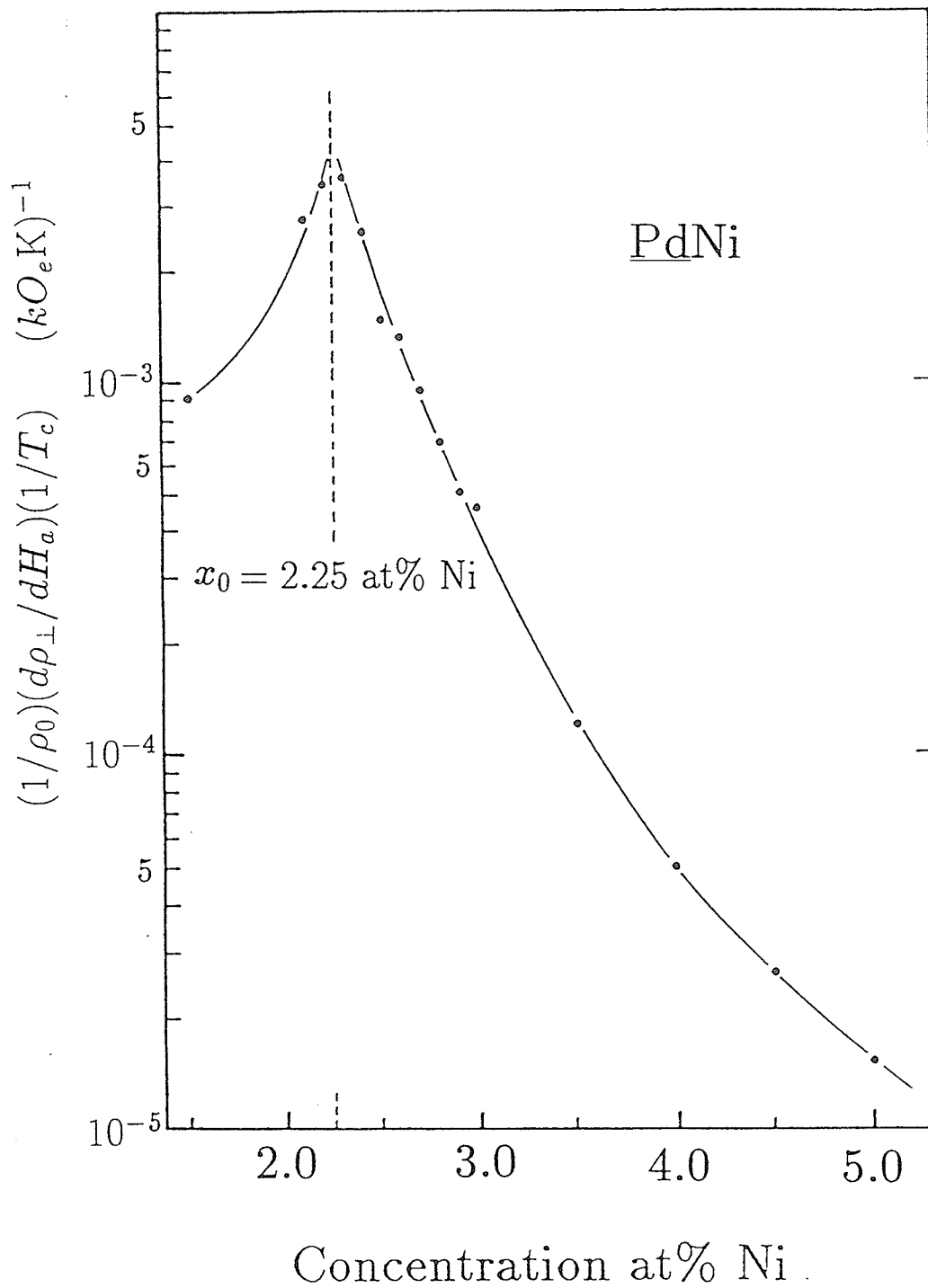


Figure 4.41: the scaled slopes versus Ni concentration at 1.5 K.

4.6 SRA Results for the Dilute PdFe System

The results reported below have been selected from measurements carried out on six dilute PdFe alloys containing between 0.35 and 2.2 at% Fe.

Figure 4.42 reproduces data from a 1.4 at% Fe sample (this alloy has a Curie temperature of 55.6 K) at 1.5 K in the form of plots of resistivity ρ against applied field H_a with fields up to 10 kOe, and these data typify the results obtained from all the PdFe alloys studied. This figure indicates that while the longitudinal resistivity ρ_{\parallel} increases substantially in low field, the transverse resistivity ρ_{\perp} first increases slightly with increasing field, and exhibits a maximum at about 0.4 kOe, then decreases rapidly as the field increases; above 1 kOe both the longitudinal resistivity ρ_{\parallel} and the transverse resistivity ρ_{\perp} display saturation. This clearly demonstrates a difference between ρ_{\parallel} and ρ_{\perp} , thus confirming the presence of a resistive anisotropy in this alloy, and provides clear evidence of a considerable exchange field in this sample. The positive sign of the anisotropy ($\rho_{\parallel} - \rho_{\perp} > 0$) observed here agrees with that predicted to arise from spin-orbit scattering from either a d^5 or a d^6 configuration at the Fe site (Kondo 1962). As shown in this figure, however, a reliable quantitative estimate for the spontaneous resistive anisotropy using the same linear field extrapolation method we used in samples containing more than 3.0 at% Ni samples is not suitable because of the curvature of the magnetoresistance at higher fields, particularly in the transverse direction.

Since the functional dependence of the resistivity on field in the magnetically saturated regime is dictated by the field dependence of the Kohler

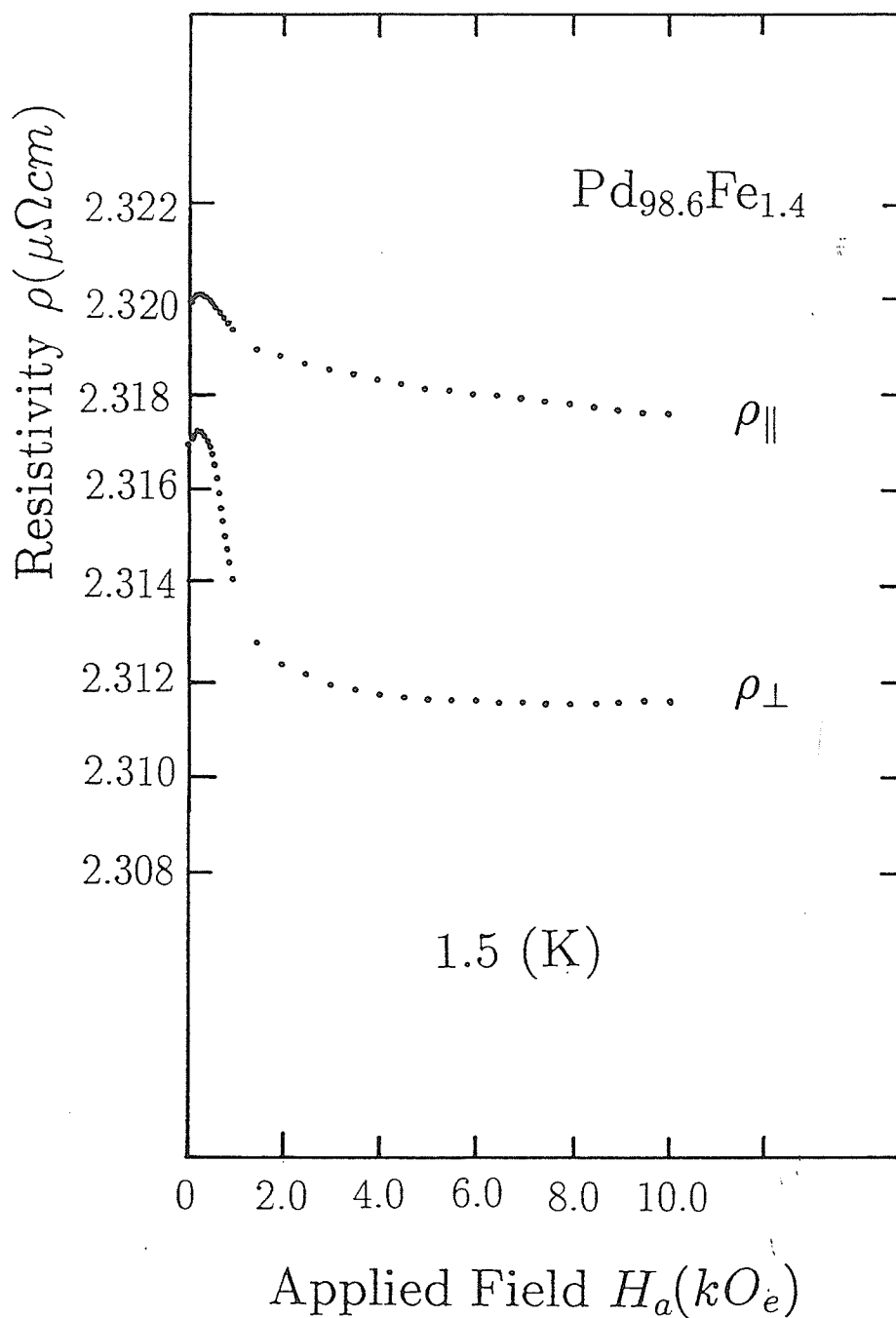


Figure 4.42: Resistivity versus applied field for $\text{Pd}_{98.6}\text{Fe}_{1.4}$ at 1.5 K.

magneto-resistance, the latter thus determines the functional form (of H) against which ρ_{\parallel} and ρ_{\perp} plotted. Various field dependences have been attempted for the higher field data, and it is found that H_a^2 field dependence reproduce the data best.

Figure 4.43 illustrates that the conventional high field extrapolation procedure can be used to find the SRA, based on plots of the resistivity against the square of the applied field; the value so obtained ($0.29(6) \pm 0.01$ %) represents only about 14% of the absolute value (-2.12 ± 0.03 %) measured in a $\text{Pd}_{95.5}\text{Ni}_{4.5}$ sample with a comparable Curie temperature (58 K). This is not unexpected as the *ac* susceptibility data have shown that dilute PdFe alloys are magnetically softer than dilute PdNi samples.

As we pointed out before, to extract numerically reliable estimates for the anisotropy ratios, the longitudinal resistivity ρ_{\parallel} and transverse resistivity ρ_{\perp} , should be plotted against magnetic induction B , rather than applied field H_a or the internal field H_i . However such changes cannot modify the conclusions reached above.

In Figure 4.44, the longitudinal resistivity ρ_{\parallel} and the transverse resistivity ρ_{\perp} of the Pd + 1.4 at% Fe sample are plotted against both the induction B and the square of the induction (B^2) at 1.5 K. The zero temperature saturation magnetization ($M_s = 6.85$ emu/g) of the $\text{Pd}_{98.6}\text{Fe}_{1.4}$ sample obtained by Kouvel and Comly (1971) was used here to determine B and B^2 . The appropriate demagnetizing factors (N_{\parallel} and N_{\perp}) were found by treating the sample as an ellipsoid with the principal axes equal to the sample's dimensions and

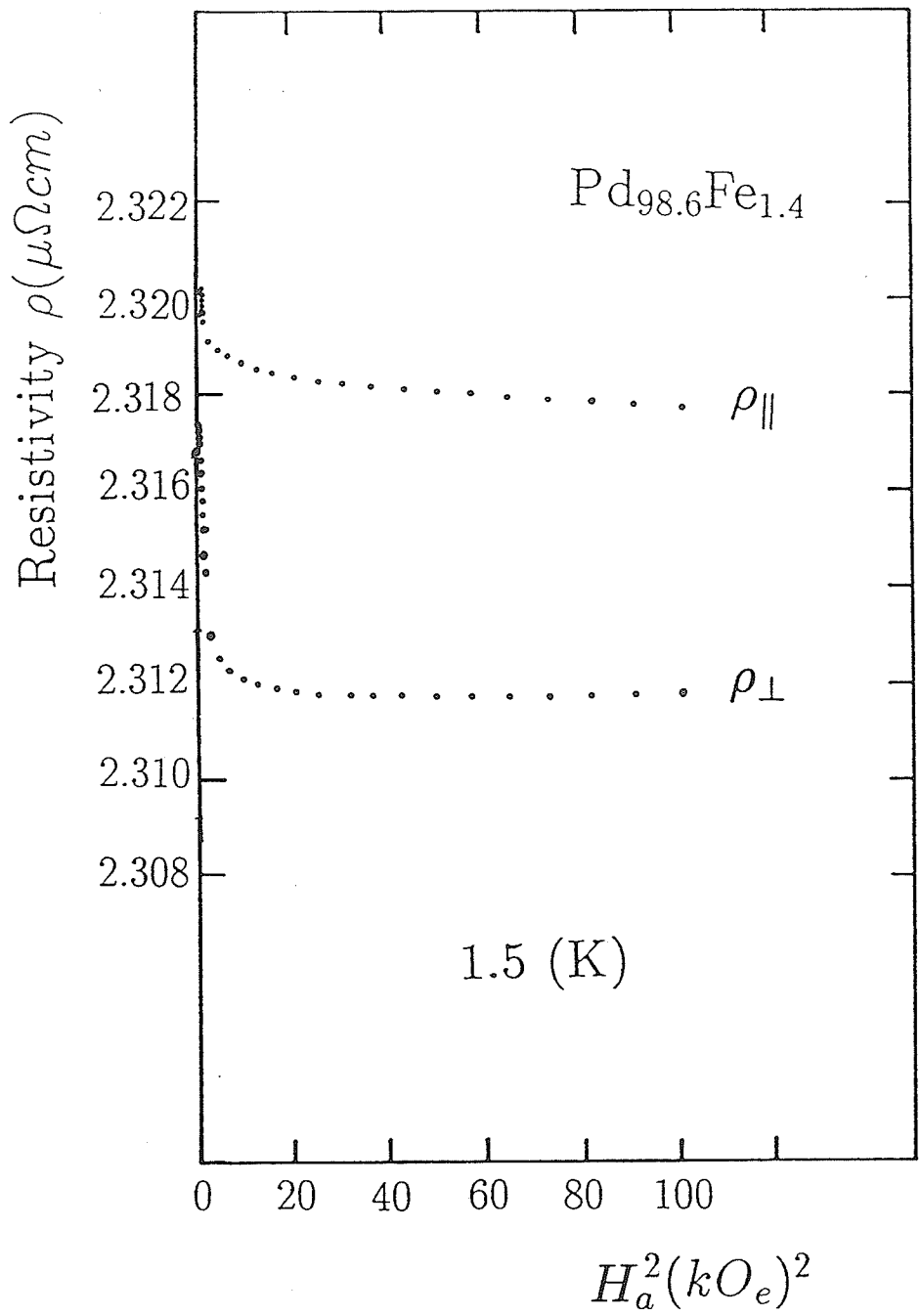


Figure 4.43: Resistivity versus the square of applied field for the Pd_{98.6}Fe_{1.4} alloy at 1.5 K.

evaluating the corresponding elliptic integrals. There are virtually no differences between $\rho_{\perp}(B)$ and $\rho_{\perp}(H_a)$ on the scale shown for this sample since the demagnetizing factor $N_{\parallel} = 12.16 \approx 4\pi$. There are some differences between $\rho_{\parallel}(B)$ and $\rho_{\parallel}(H_a)$ because N_{\parallel} is very small ($N_{\parallel} = 0.006$). The additional terms $(4\pi M_s - N_{\parallel} M_s)$ in the magnetic induction expression have a value of 1.012 kOe for this Pd + 1.4 at% Fe alloy. As shown in this figure for the longitudinal geometry there is a difference of 20 (kOe)^2 between the square of the induction (B^2) and the square of the applied field (H_a^2). However one can clearly see from this figure, that the basic character of magnetoresistivity as a function of induction or applied field is similar, and that the conventional higher field extrapolation procedure can be used to find the SRA. The value so obtained (0.29(5) %) agrees well with the estimate for this sample from the $\rho(H_a^2)$ plots. This agreement is expected since the higher field slopes ($d\rho/dH_a$) are very small (e.g. $d\rho_{\parallel}/dH_a = -0.09 \text{ (n}\Omega\text{cm/kOe)}$) compared with $2.55 \text{ (n}\Omega\text{cm/kOe)}$ for the PdNi sample which has a comparable Curie temperature. Also, plotting resistivity against the applied field H_a , rather than the induction B , does not modify the result substantially. Therefore estimating the SRA from the higher field slope of the $\rho(H_a^2)$ instead of $\rho(B^2)$ is acceptable, and introduces little error. Similar conclusions apply to all the PdFe samples studied.

In Figure 4.45 the longitudinal resistivity ρ_{\parallel} and the transverse resistivity ρ_{\perp} of the Pd_{98.6}Fe_{1.4} sample are plotted against both the applied field H_a and the square of the applied field H_a^2 at 4.2 K. These plots are similar

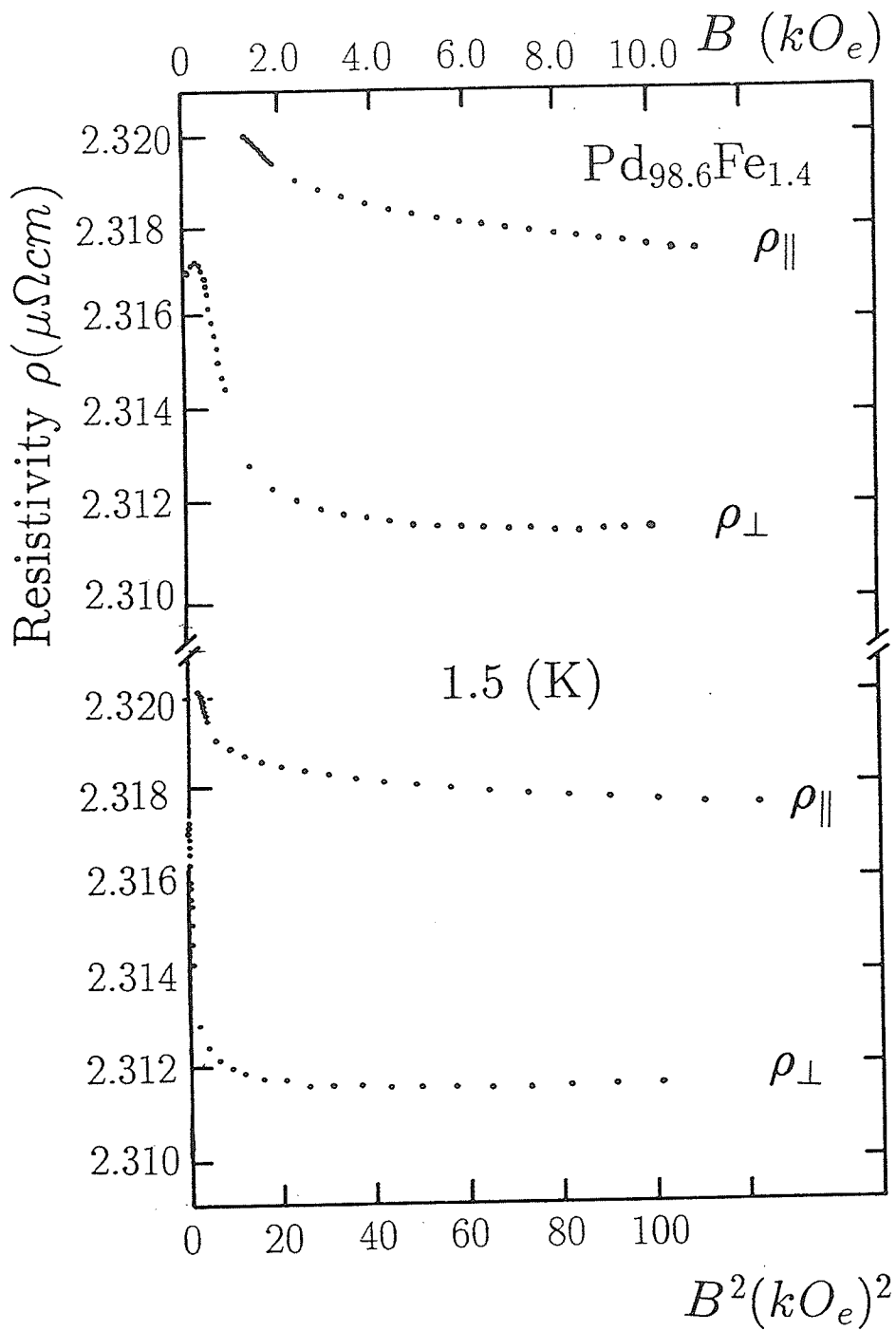


Figure 4.44: Resistivity versus magnetic induction and the square of the induction for the Pd_{98.6}Fe_{1.4} alloy at 1.5 K.

to those for the same sample at 1.5 K, specifically, the shapes of the curves and the sign of the anisotropy. However the magnitude of the SRA (0.28(1) %) is smaller than that at 1.5 K (0.29(6) %), and the absolute value of the high field slope is larger than that exhibited by the sample at 1.5 K.

Figures 4.46 to 4.50 reproduce data acquired at 1.5 K for the other five PdFe samples studied. These data are presented in the form of the longitudinal and transverse resistivities (ρ_{\parallel} and ρ_{\perp}) plotted against the square of the applied field H_a^2 ; which is the best fit of the higher field resistivity data. The higher field extrapolations used for conventional estimates of the SRA for the alloys.

A non-zero anisotropy ($\Delta\rho \neq 0$) in the low field provides clear evidence of a considerable exchange field in these alloys, as domain effects are overcome, and the anisotropy $\Delta\rho$ increases rapidly. It also indicates that these alloys, including the most dilute Pd_{99.65}Fe_{0.35} alloy, possess long-range order at 1.5 K.

As shown in these figures (also confirmed by the data listed in Table 4.7), the estimated SRA values drop rapidly with decreasing Fe concentration from 0.49% for the 2.2 at% Fe to 0.09% for the 0.35 at% Fe sample. The possibility of a power-law relationship, as discussed in Section 4.5 (see Equation 4.7), between SRA and the reduced concentration has also been examined for the dilute PdFe alloys studied. As shown in Figure 4.51 the power-law relationship does reproduce the SRA estimates at 1.5 K for all the samples studied with parameters

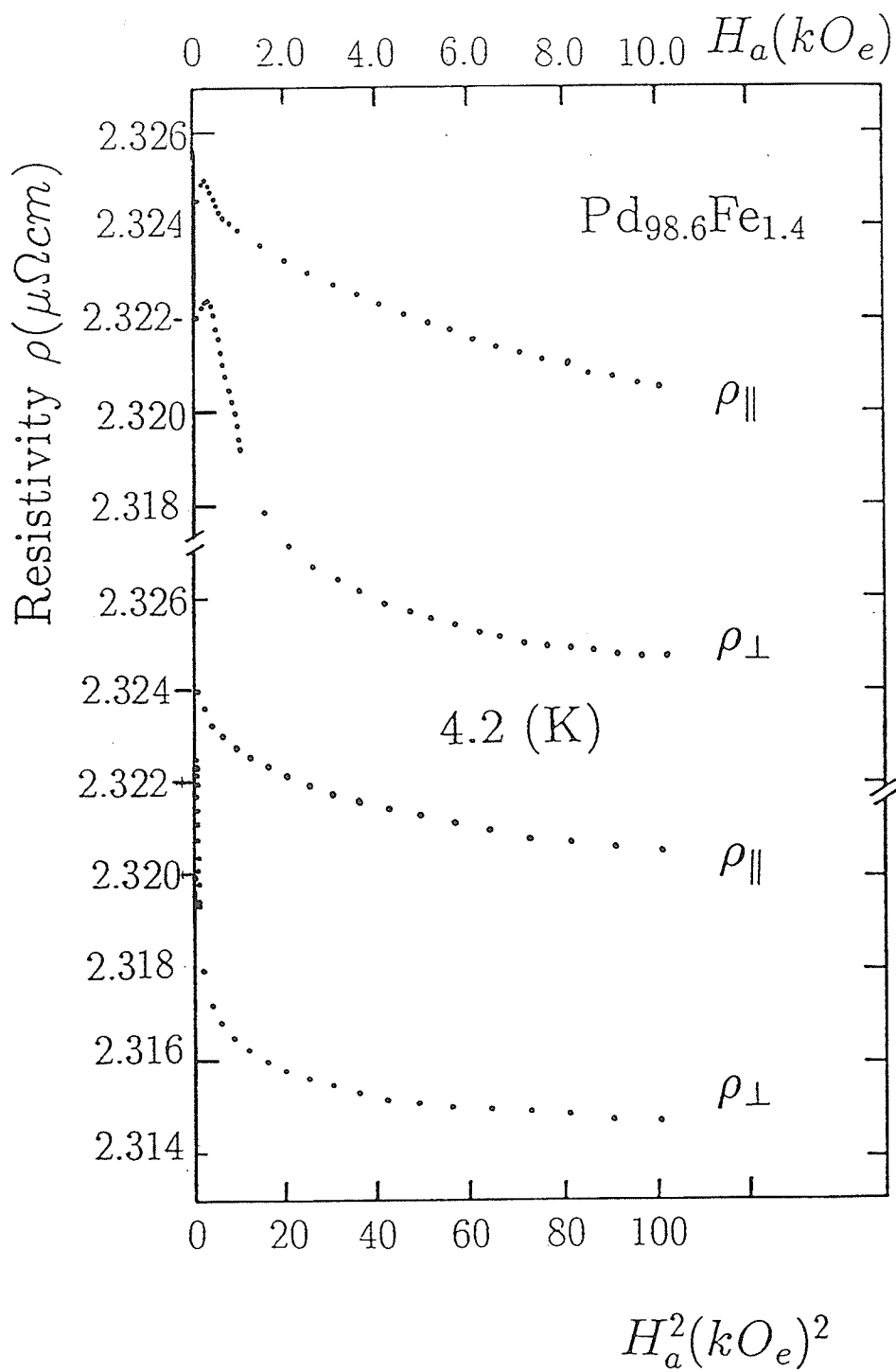


Figure 4.45: Resistivity versus the applied field and the square of the applied field for the Pd_{98.6}Fe_{1.4} alloy at 4.2 K.

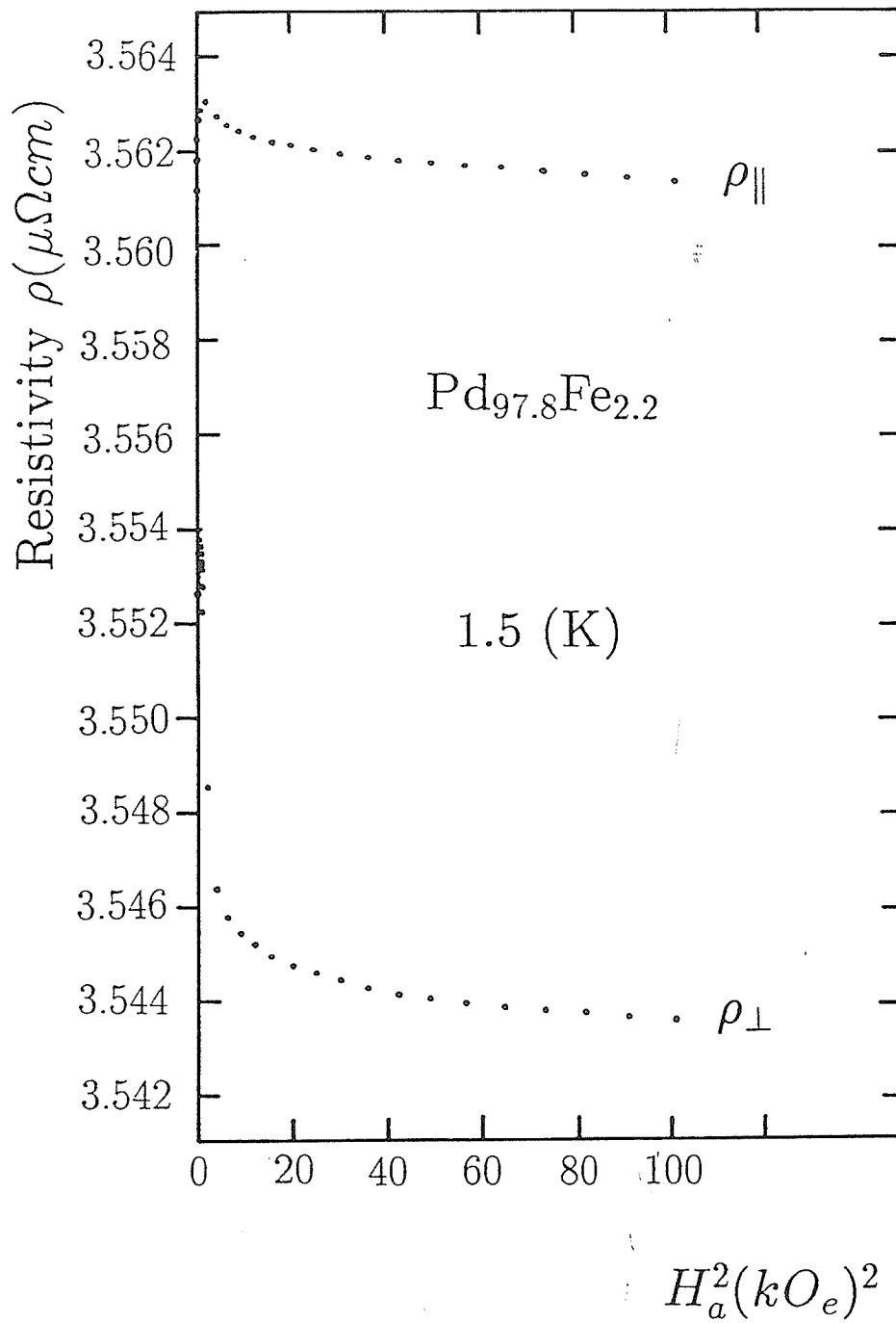


Figure 4.46: Resistivity versus the square of the applied field for the Pd_{97.8}Fe_{2.2} alloy at 1.5 K.

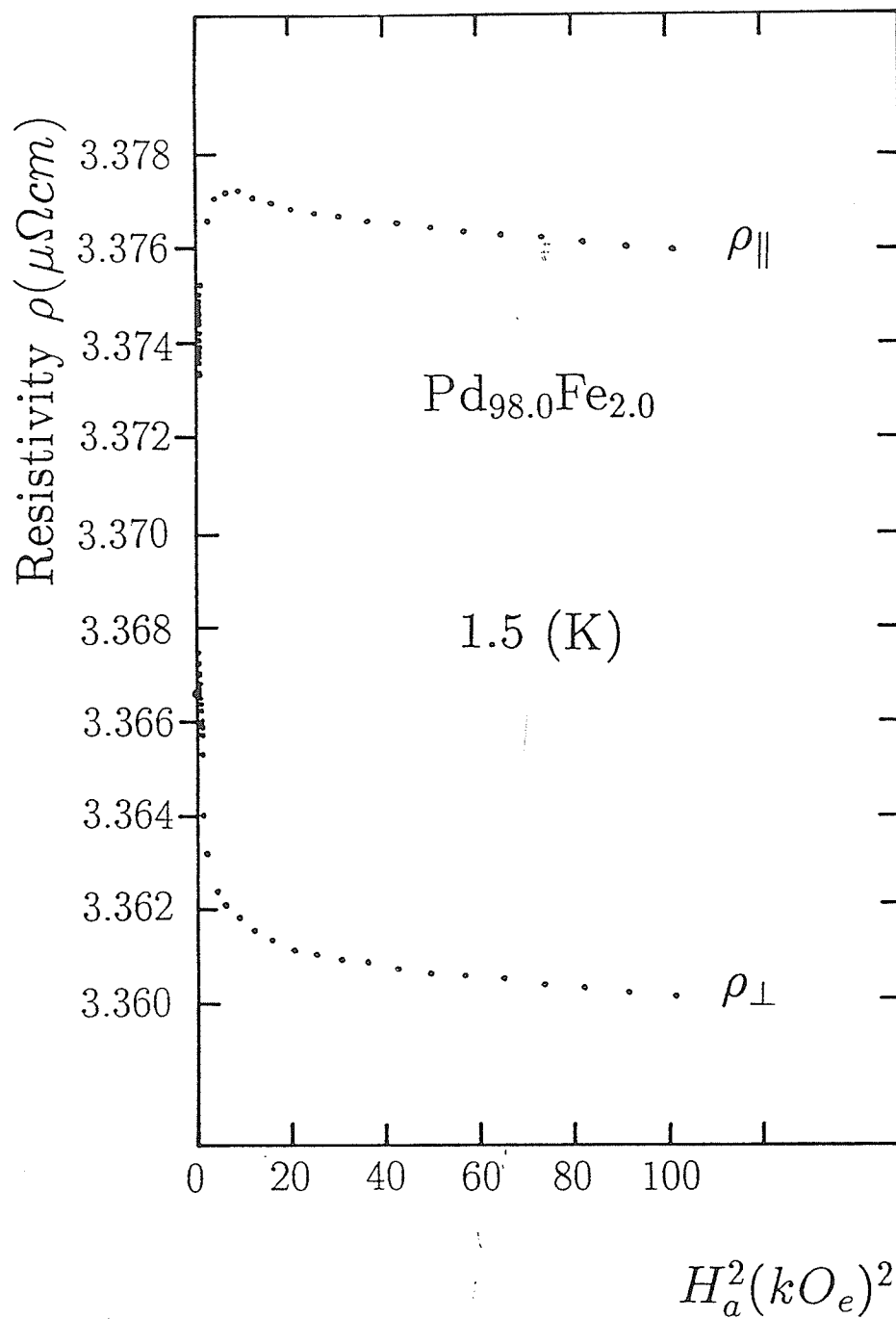


Figure 4.47: Resistivity versus the square of the applied field for the Pd_{98.0}Fe_{2.0} alloy at 1.5 K.

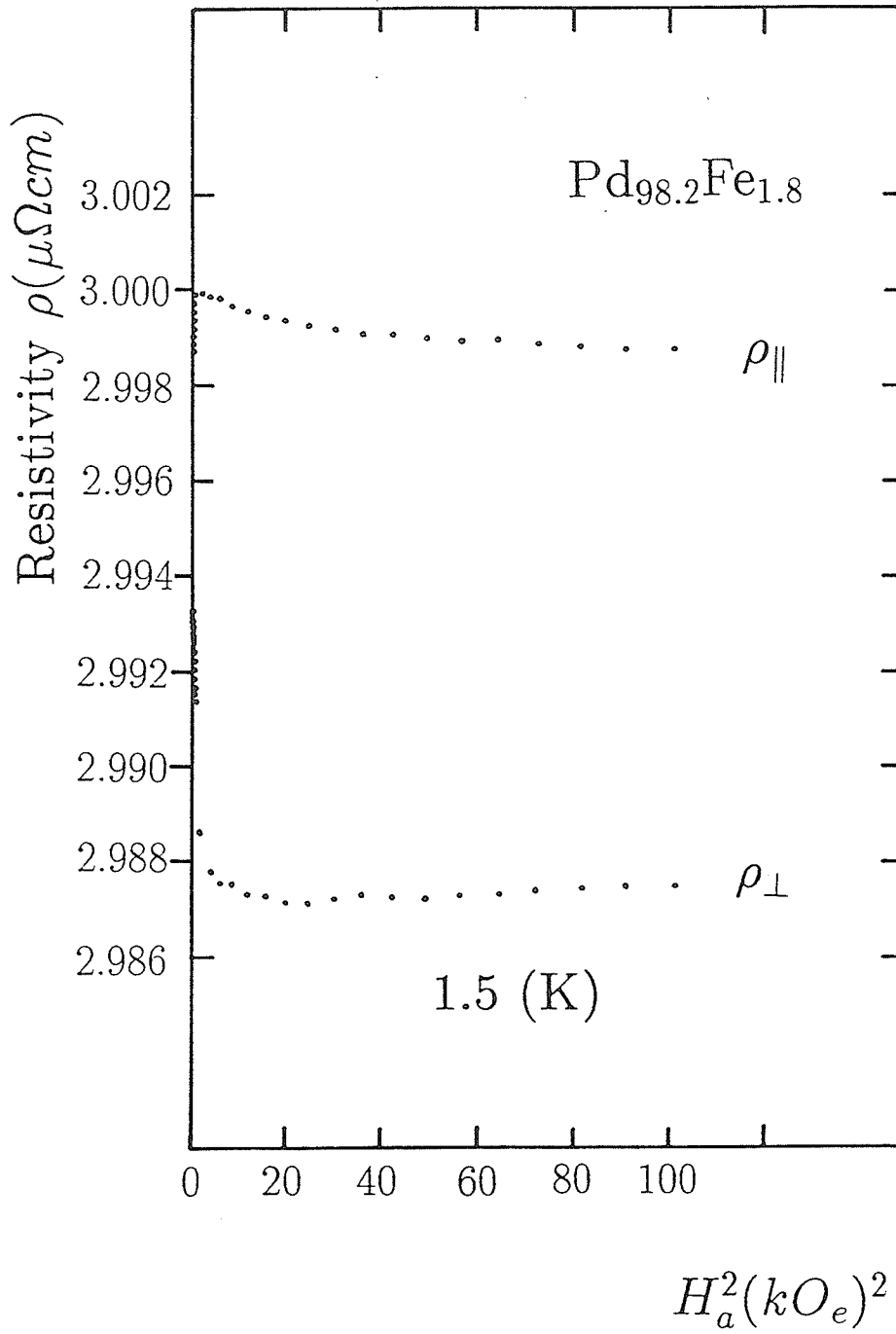


Figure 4.48: Resistivity versus the square of the applied field for the Pd_{98.2}Fe_{1.8} alloy at 1.5 K.

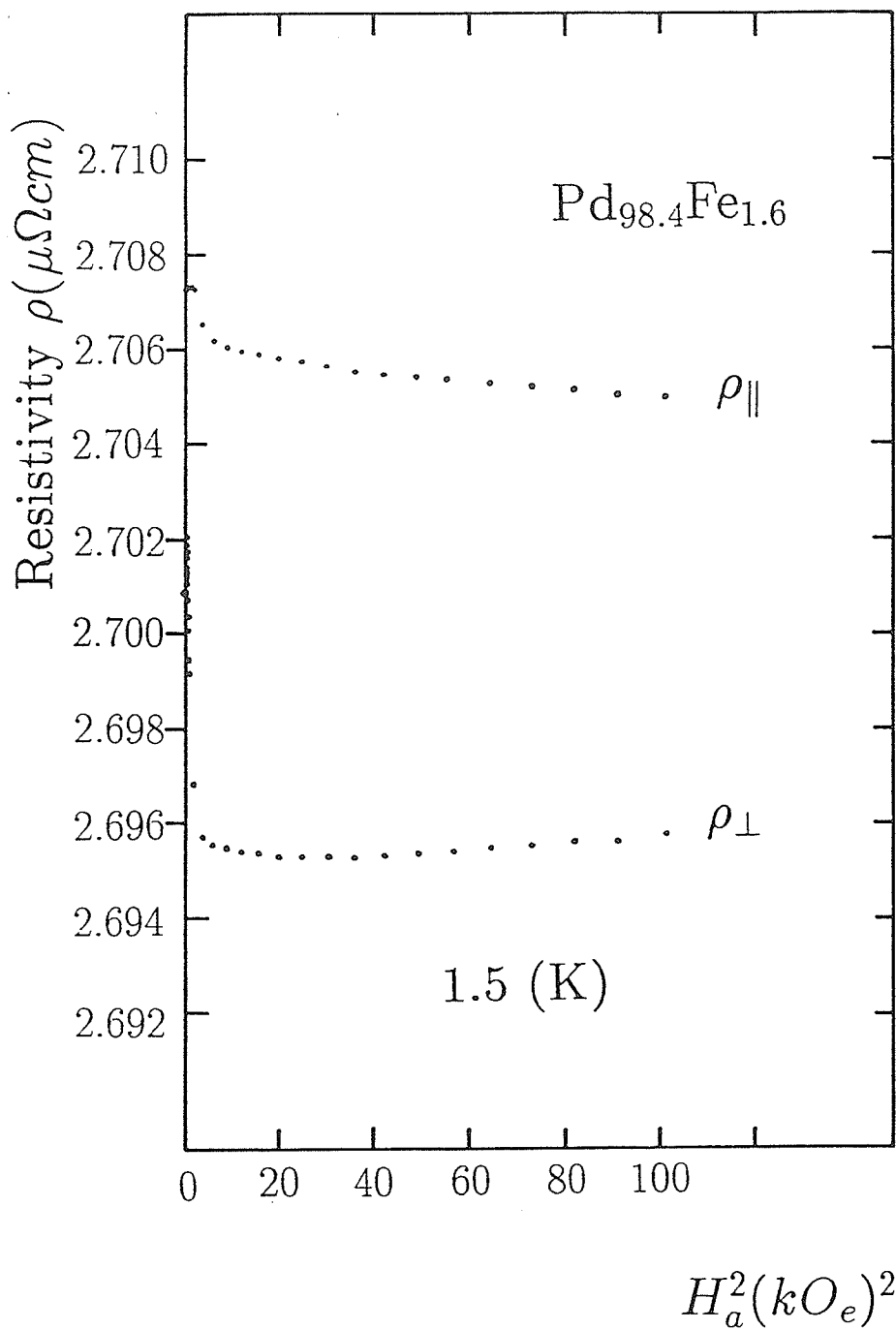


Figure 4.49: Resistivity versus the square of the applied field for the Pd_{98.4}Fe_{1.6} alloy at 1.5 K.

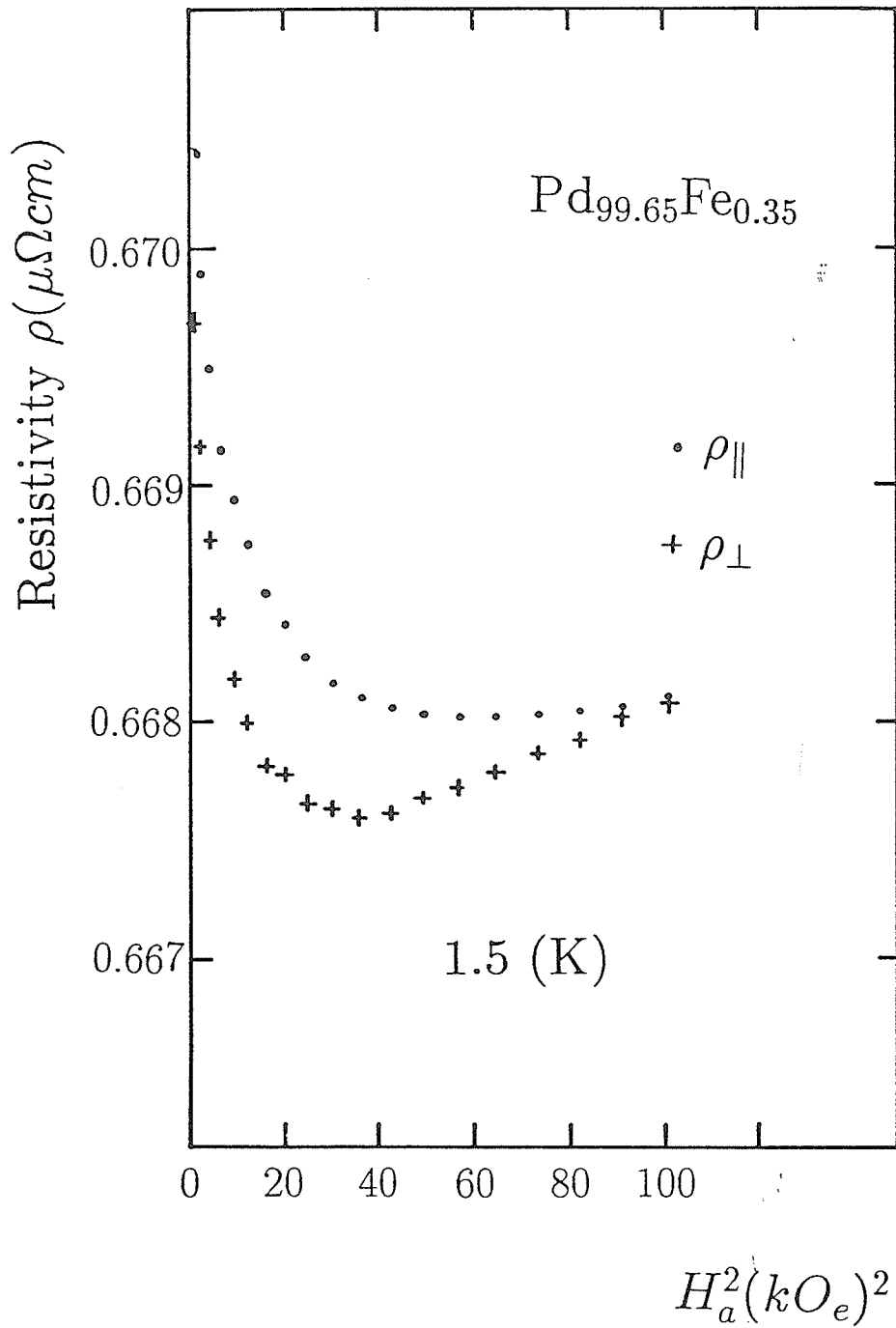


Figure 4.50: Resistivity versus the square of the applied field for the $\text{Pd}_{99.65}\text{Fe}_{0.35}$ alloy at 1.5 K.

$x_0 = 0.010 \pm 0.005$ at% Fe, and $\eta = 0.9 \pm 0.1$.

This result confirms a critical Fe concentration (x_0) necessary to establish a ferromagnetic ground state by magnetoresistance anisotropy measurements. By contrast no previously measurement or theoretical prediction exist for the exponent η . For Fe concentrations less than the critical concentration, the system becomes a spin glass.

Between 1.5 and 4.2 K, we find a decrease in SRA for all the PdFe samples measured. For the alloy with Fe concentration 0.35 at% the decrease in the SRA becomes more marked, as indicated by the data listed in Table 4.7, this is an anticipated result since thermal fluctuations compete with the exchange splitting; while for more Fe concentrated samples the decrease in SRA is less rapid as the measuring temperatures are far below the samples' ordering temperatures.

The zero field resistivities ρ_0 of the PdFe alloys at 1.5 K are also listed in Table 4.7. The data reproduced in Figure 4.52 indicate a linear increase in ρ_0 with x at a rate of about $1.57 \mu\Omega cm/at\%$ Fe (similar behaviour was observed for the PdNi samples studied which had a rate of about $0.65 \mu\Omega cm/at\%$ Ni); furthermore there is an interesting correlation between ρ_0 and T_c in PdFe and PdNi; notice that those samples with comparable Curie temperatures have similar values of zero field resistivity such as $2.31 (\mu\Omega cm)$ for the 1.4 at% Fe and $2.11 (\mu\Omega cm)$ for the 4.5 at% Ni sample. These ρ_0 values are in good agreement with the results given by previous measurements (e.g. Tari et al 1971 for PdNi alloys).

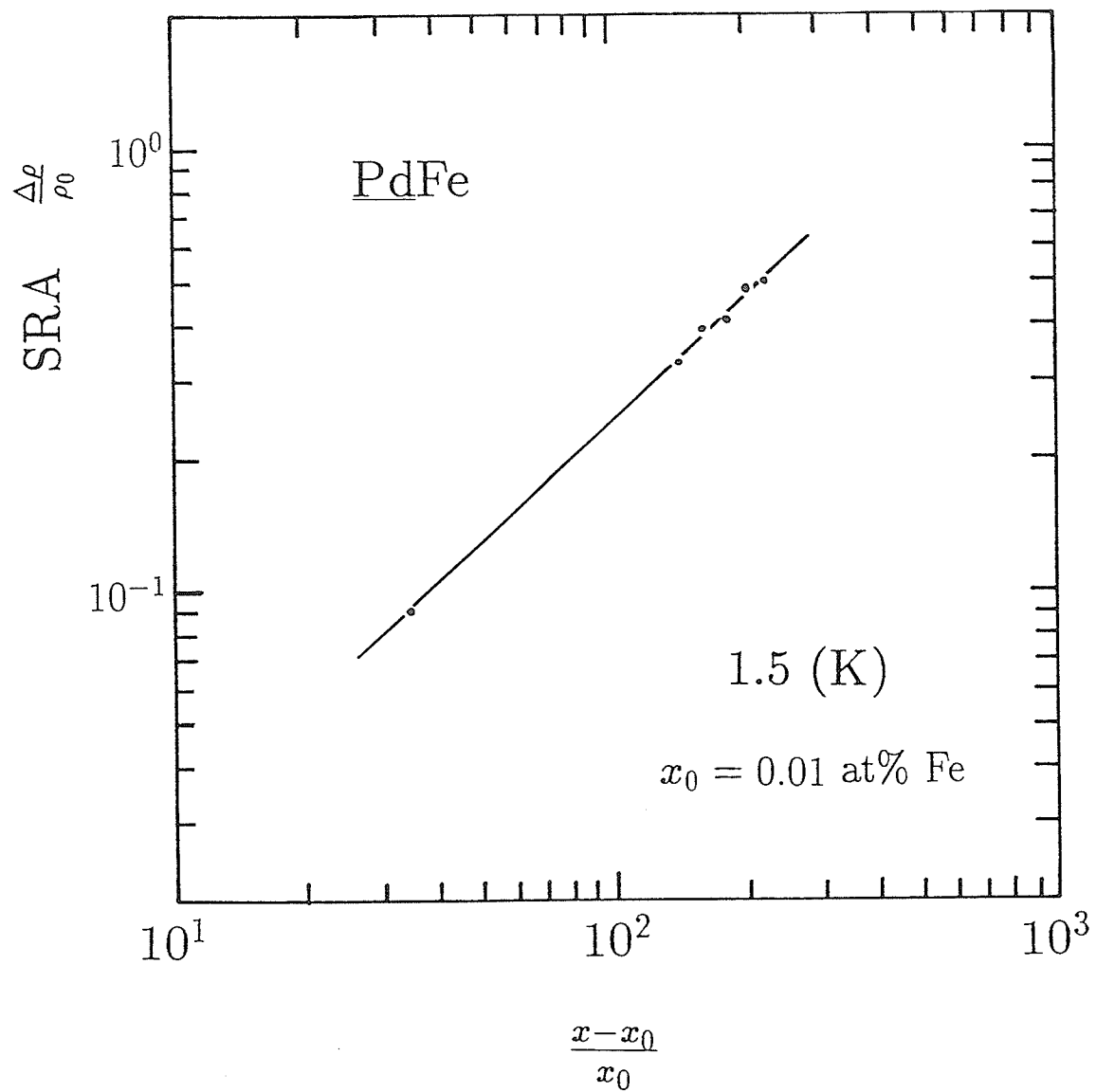


Figure 4.51: SRA versus reduced Fe concentration on a double log plot at 1.5 K.

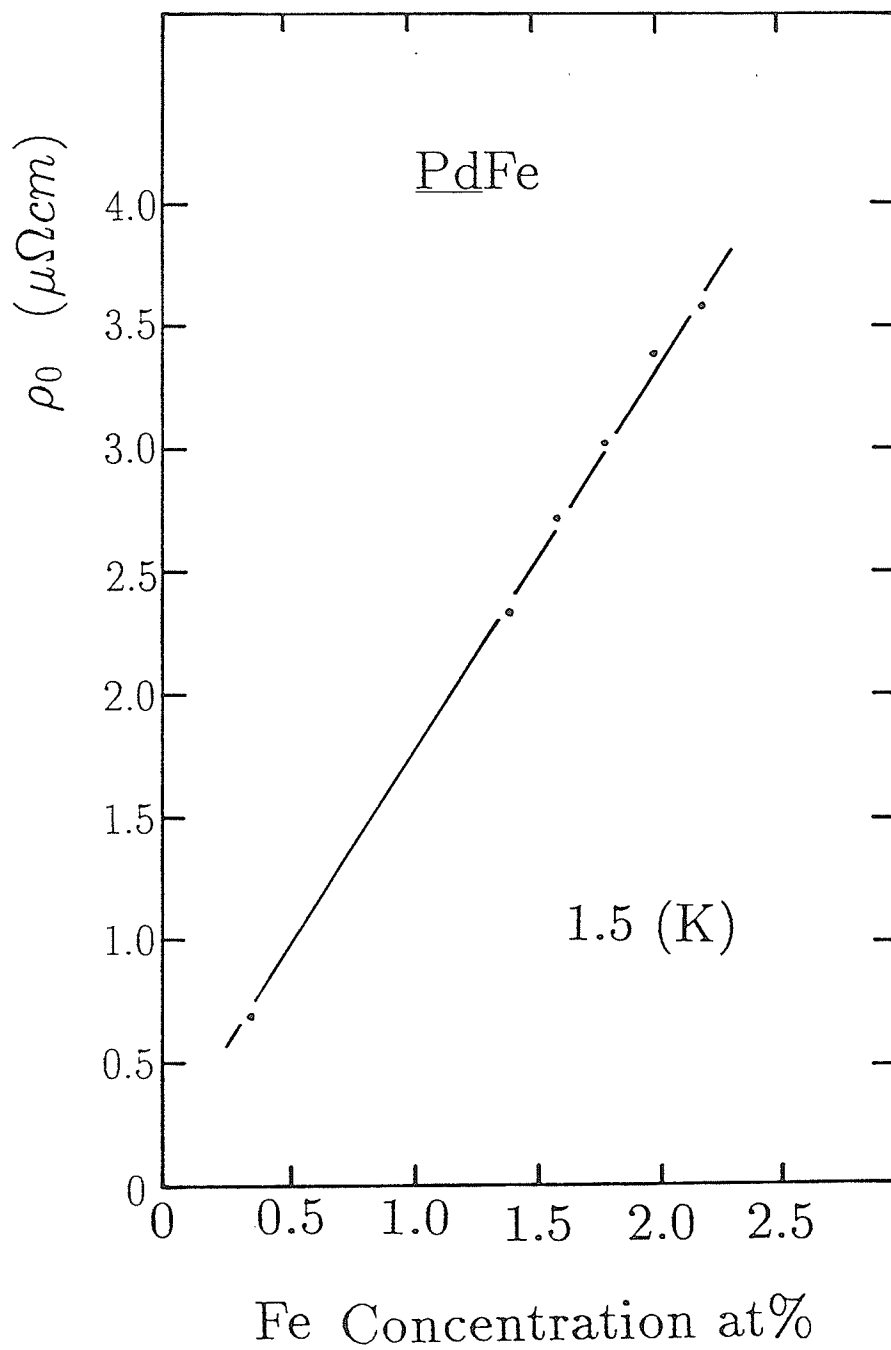


Figure 4.52: Zero field resistivity versus Fe concentration at 1.5 K.

Table 4.7: Summary of parameters taken from the *ac* magnetoresistance data for the PdFe alloys at 1.5 and 4.2 K

Fe (at%)	$T = 1.5$ (K) Anisotropy ($\mu\Omega cm$)	1.5 (K) SRA (%)	1.5 (K) ρ_0 ($\mu\Omega cm$)	$T = 4.2$ (K) Anisotropy ($\mu\Omega cm$)	4.2 (K) SRA (%)
2.2	0.0176(8)	0.49(8)	3.552(4)	0.0172(0)	0.48(3)
2.0	0.0157(8)	0.46(9)	3.366(5)	0.0156(8)	0.46(5)
1.8	0.0121(2)	0.40(5)	2.991(8)	0.0114(9)	0.38(4)
1.6	0.0106(1)	0.39(3)	2.696(2)	0.0103(7)	0.38(4)
1.4	0.0068(5)	0.29(6)	2.317(0)	0.0065(3)	0.28(1)
0.35	0.0006(0)	0.09(1)	0.672(1)	≤ 0.0001	≤ 0.01

4.7 SRA Results for the Dilute (PdFe)Mn System

The results reported below have been selected from measurements carried out on five dilute (Pd + x at% Fe) + 5 at% Mn alloys containing between 0.35 and 2.2 at% Fe.

Figure 4.53 reproduces data from a 2.2 at% Fe sample (this alloy has a Curie temperature of 47.9 K, which has been lowered from 80.6 K by the addition of 5 at% Mn) at 1.5 K in the form of plots of resistivity ρ against applied field H_a with fields up to 10 kOe . These data typify the results obtained from all the (PdFe)Mn alloys studied. This figure indicates that adding 5.0 at% Mn to the PdFe host alloy changes the magnetoresistive properties substantially (compare with Fig. 4.46).

As shown in this figure, the zero field resistivity ($\rho_0 = 12.40 \mu\Omega cm$) which is some four times larger than that exhibited by the host alloy Pd_{97.8}Fe_{2.2}. This figure also demonstrates a marked component in both the longitudinal $\rho_{||}$ and the transverse magnetoresistivities ρ_{\perp} in higher fields, and they remain unsaturated up to fields of 10 kOe ($d\rho_{||}/dH_a \approx d\rho_{\perp}/dH_a = -98.4 n\Omega cm/kOe$, the absolute value of the slope is much larger than that of PdNi and PdFe alloys with comparable impurity concentration), thus complicating quantitative analysis. Similar behaviour has been seen for the (PdNi)Mn system (Kunkel et al 1987). This figure, however, does demonstrate a difference between $\rho_{||}$ and ρ_{\perp} , thus confirming the presence of a resistive anisotropy in this sample with a sign (higher field data) which agrees

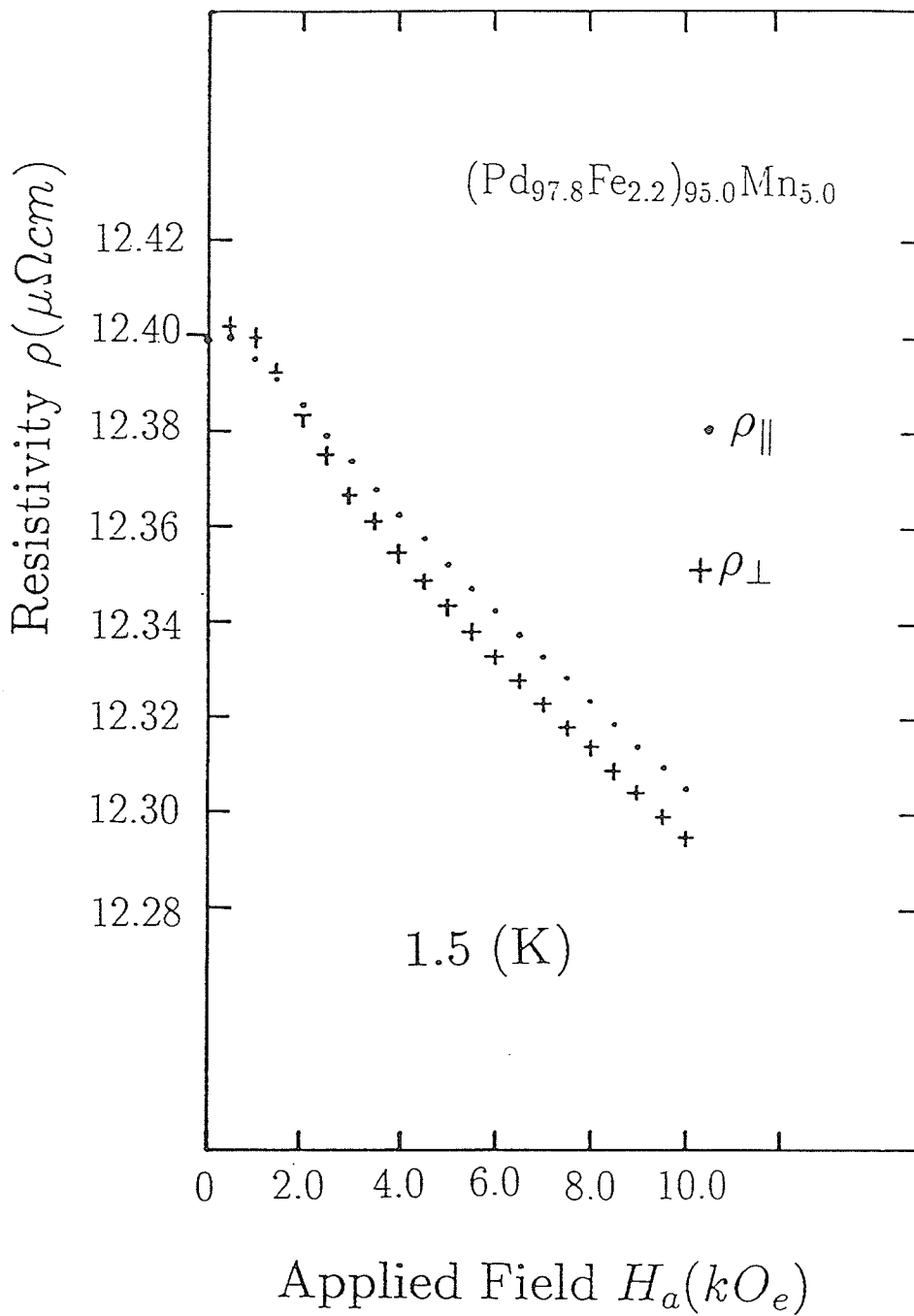


Figure 4.53: Resistivity versus applied field for the (Pd_{97.8}Fe_{2.2})₉₅Mn_{5.0} sample at 1.5 K.

with that exhibited in the host alloys as discussed in Section 4.6. The data also show a change in the sign of the anisotropy at lower fields as $\rho_{\parallel} < \rho_{\perp}$. However, recall that in order to extract numerically reliable estimates for the anisotropy the resistivities ρ_{\parallel} and ρ_{\perp} should be plotted against magnetic induction B , rather than applied field H_a . Because we have no direct knowledge of the magnetization for the system, as a first approximation in treating these data, it was decided to use, or extrapolate where necessary, the magnetization values from the literature (e.g. from Sato et al 1985). In Figure 4.54, the longitudinal ρ_{\parallel} and the transverse resistivities ρ_{\perp} are plotted against the magnetic induction B (upper part of the figure) at 1.5 K for the (Pd + 2.2 at% Fe) + 5 at% Mn alloy. As shown in these figures (Figures 4.53 and 4.54), there is virtually no difference between $\rho_{\perp}(H_a)$ and $\rho_{\perp}(B)$ for this sample. There are, however, significant differences between $\rho_{\parallel}(H_a)$ and $\rho_{\parallel}(B)$. The conventional higher field extrapolated anisotropy, as shown in Figure 4.54, is 0.030(5) ($\mu\Omega cm$), and the associated the SRA is 0.24(6)%, which represents only about 50% of the value (0.49(8)%) measured in the PdFe host alloy.

The alternative higher field extrapolation procedure, from the plot of resistivity difference ($\rho_{\parallel} - \rho_{\perp}$) at a given induction against the induction, is illustrated in the lower part of Figure 4.54. It is apparent that the simple linear form reproduces the data well, and the SRA value is found to be 0.24(2)%, which agrees well with that obtained using the first technique.

The longitudinal ρ_{\parallel} and the transverse resistivity ρ_{\perp} at 1.5 K for 2.0, 1.8 and 1.6 at% Fe (Pd + x at% Fe) + 5 at% Mn alloys display the same

basic trend as the 2.2 at% (PdFe)Mn alloy, namely the presence of a resistive anisotropy ($\Delta\rho \neq 0$), which is positive (as $\rho_{\parallel} > \rho_{\perp}$), and a marked negative component in both the longitudinal and the transverse magnetoresistivities (confirmed by the data listed in Table 4.8). These data also demonstrate the occurrence of a decreasing of zero field resistivity (ρ_0) and a smaller difference between ρ_{\parallel} and ρ_{\perp} as the Fe concentration is lowered all confirmed by the data listed in Table 4.8.

In Figure 4.55, the longitudinal resistivity ρ_{\parallel} and the transverse resistivity ρ_{\perp} of the (Pd + 0.35 at% Fe) + 5 at% Mn alloy (the most Fe dilute sample among the five (PdFe)Mn alloys studied) are plotted against the magnetic induction B at 1.5 K. These data are similar to those for the other (PdFe)Mn alloys as they show a substantial negative magnetoresistance and no sign of saturation. As shown in this figure, the SRA in this sample is very small. This is not unexpected as we have seen a similar Fe concentration dependence of the SRA in the host PdFe alloy system as presented in Section 4.6.

The magnetoresistance data for the five (PdFe)Mn samples studied at 4.2 K are also listed in Table 4.8. These data are very similar to those at 1.5 K, the sign of the anisotropy is positive and shows a substantial negative magnetoresistance.

It should be pointed out there is no obvious change in the magnetoresistive properties on passing through the re-entrant spin glass temperature (as discussed in Section 4.4; (Pd + 0.35 at% Fe) + 5 at% Mn is a re-entrant

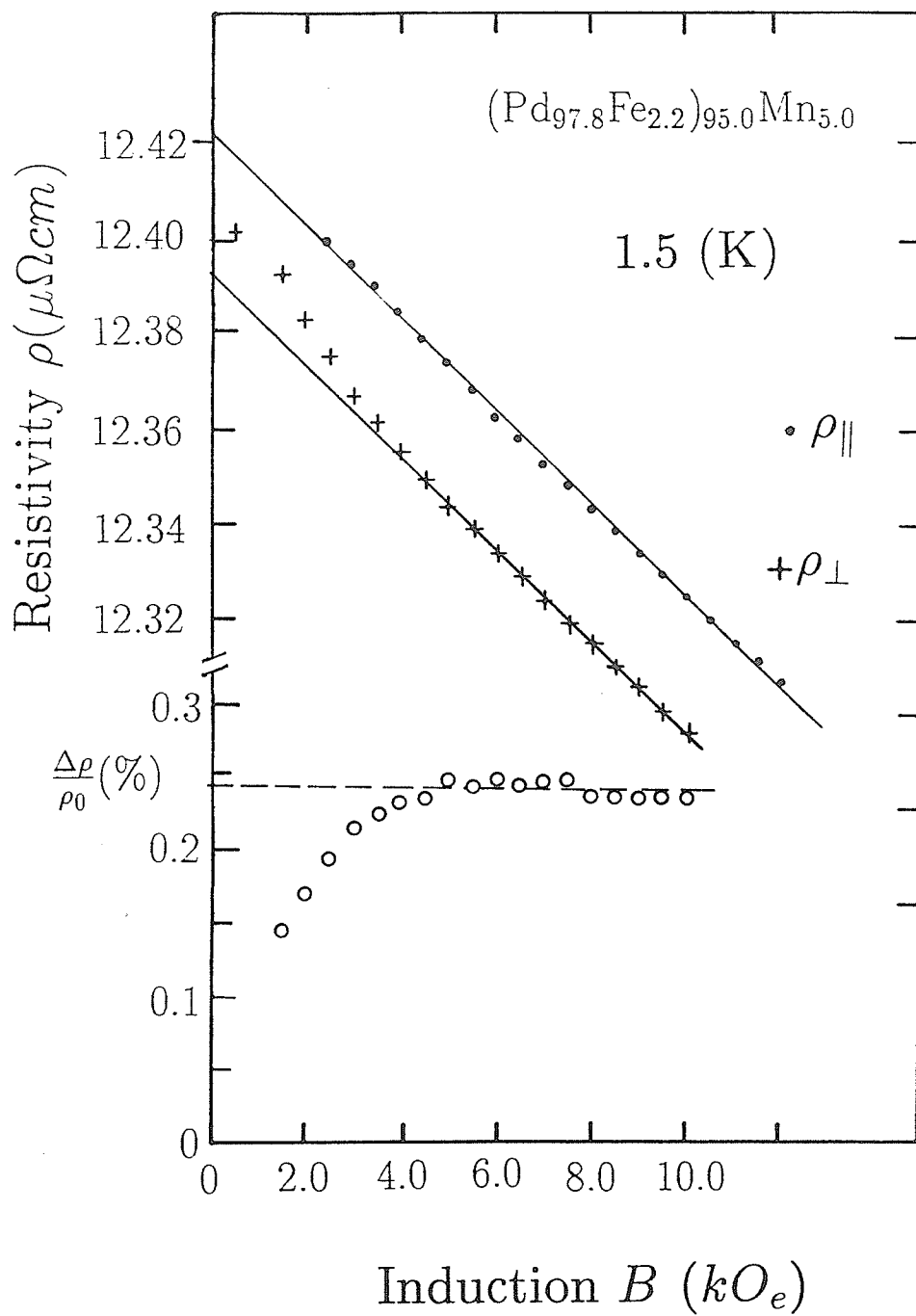


Figure 4.54: Resistivity as well as SRA versus magnetic induction for the (Pd + 2.2 at% Fe) + 5 at% Mn sample at 1.5 K.

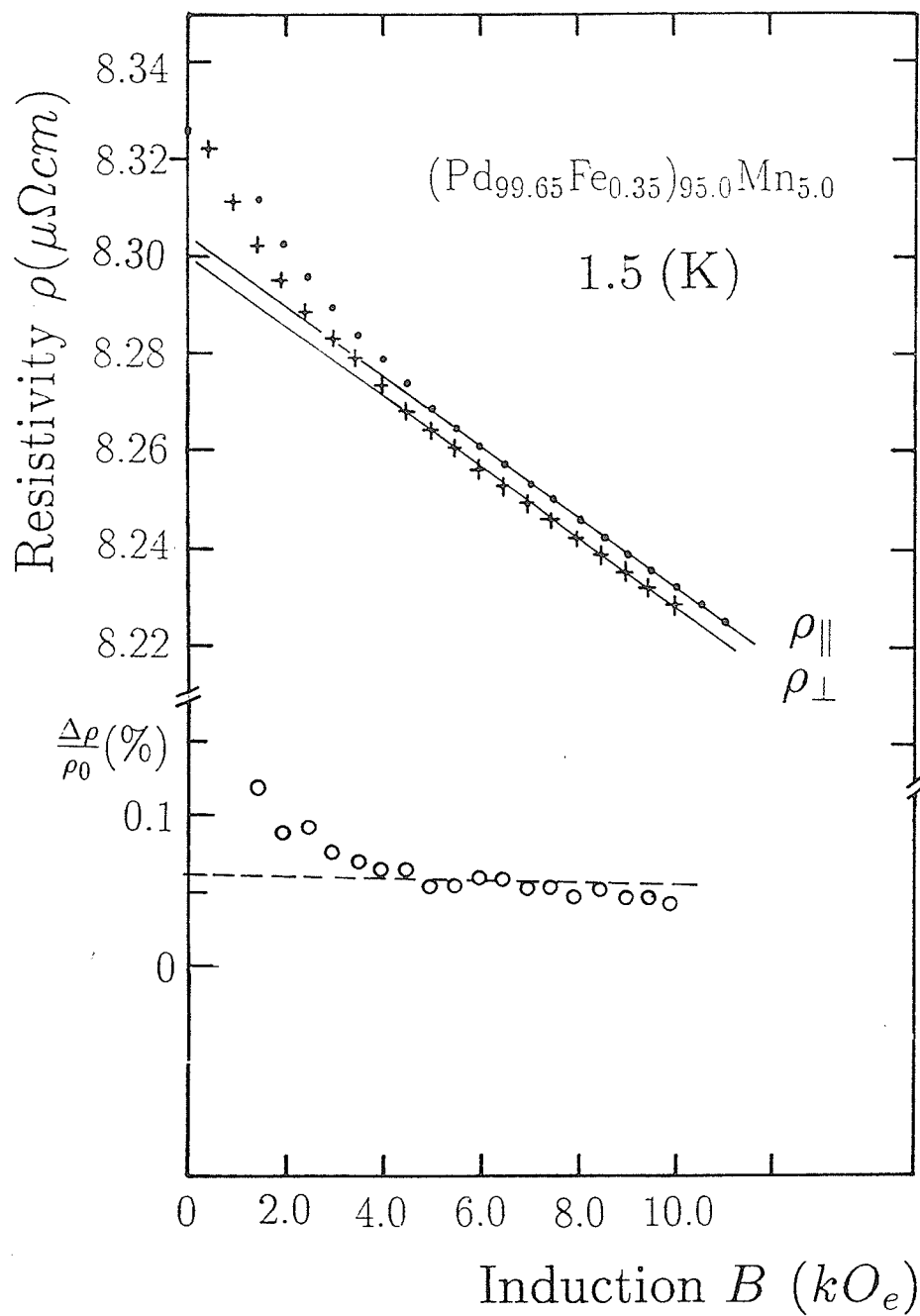


Figure 4.55: Resistivity and SRA versus magnetic induction for the $(\text{Pd}_{99.65}\text{Fe}_{0.35})_{95.0}\text{Mn}_{5.0}$ alloy at 1.5 K

Table 4.8: Summary of parameters taken from the *ac* magnetoresistance data for the (PdFe)Mn alloys at 1.5 and 4.2 K

Fe at%	$T = 1.5$ (K) Anisotropy ($\mu\Omega cm$)	1.5 (K) SRA (%)	1.5 (K) ρ_0 ($\mu\Omega cm$)	1.5 (K) $d\rho/dH$ ($n\Omega cm/kOe$)	$T = 4.2$ (K) Anisotropy ($\mu\Omega cm$)	4.2 (K) SRA (%)
2.2	0.030(5)	0.24(6)	12.399(0)	-98.4	0.029(9)	0.24(1)
2.0	0.027(8)	0.23(4)	11.889(7)	-95.6	0.027(9)	0.23(4)
1.8	0.023(5)	0.20(4)	11.486(9)	-93.7	0.024(0)	0.20(9)
1.6	0.019(0)	0.17(1)	11.117(9)	-88.3	0.017(5)	0.15(7)
0.35	0.005(0)	0.06(0)	8.32(5)	-71.7	0.004(0)	0.04(8)

system with a T_f of 4.07 K).

The possibility of a power-law relationship, as discussed in Section 4.5 (see Equation 4.7), between the SRA and the reduced concentration has also been examined for the dilute (PdFe)Mn alloys studied. The power-law relationship does reproduce the SRA estimates at 1.5 K for the samples studied with parameters

$$x_0 = 0.2 \pm 0.1 \text{ at\% Fe, and } \eta = 0.9 \pm 0.1.$$

A substantial negative magnetoresistance, with no sign of saturation

below 10 kOe , is one of the remarkable feature of the dilute (PdFe)Mn alloys studied. This prompted us to study the resistive properties of these alloys at even higher fields. The longitudinal resistivity $\rho_{||}$ at 1.5 and 4.2 K of the (PdFe)Mn samples (2.2, 2.0, 1.8, and 1.6 at% Fe) were measured to 85 kOe . As the data are similar at both temperatures, only those at 1.5 K are shown in Figure 4.56. These data show a substantial negative magnetoresistance which does not saturate in the highest applied field used. It further indicates that the system does not behave as a uniform ferromagnet, and confirms that the spins in this low temperature state are not fully aligned, in agreement with conclusions drawn, for example, from nuclear orientation studies (Kettschau et al 1983).

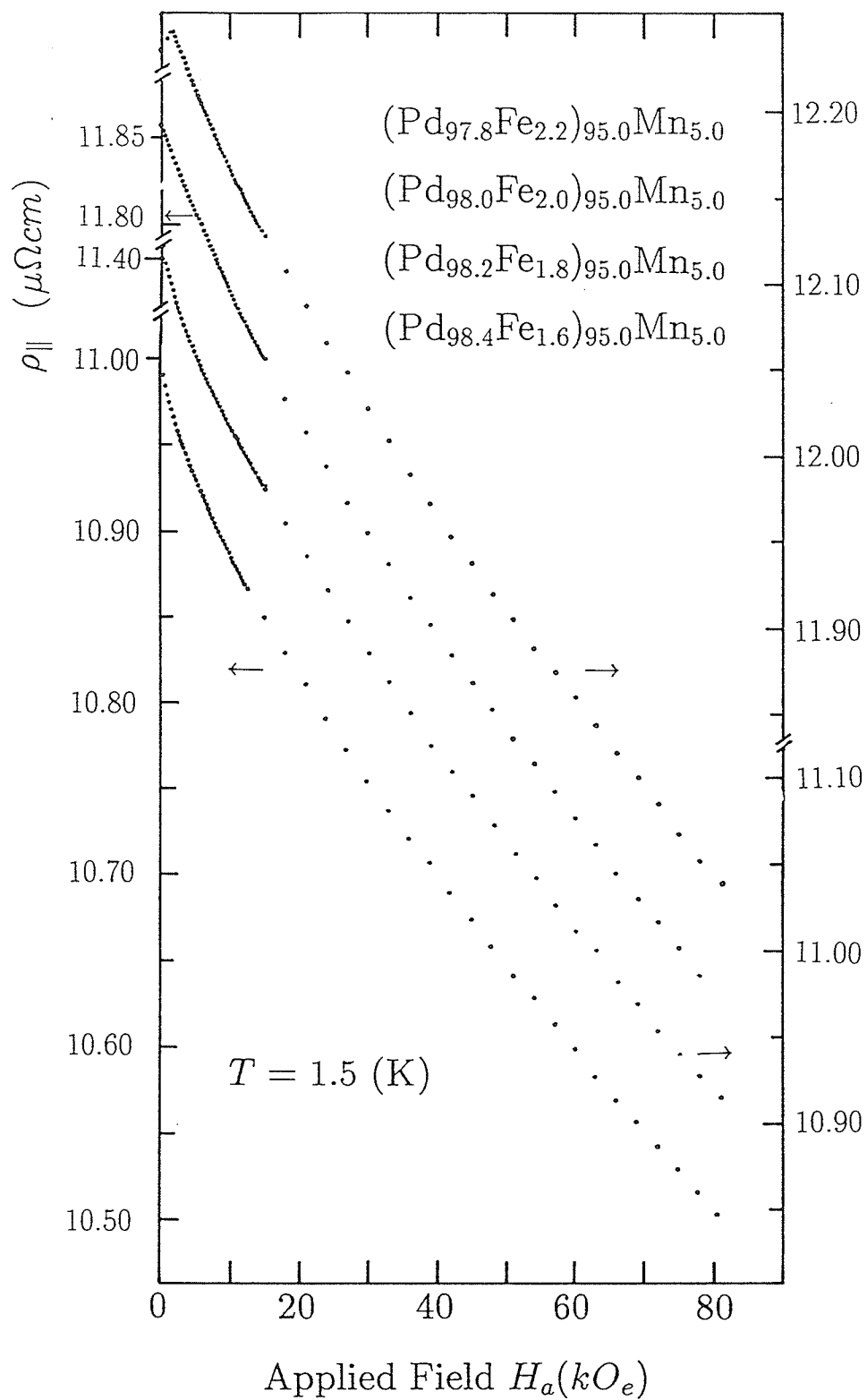


Figure 4.56: Longitudinal resistivity versus applied field for the $(\text{Pd}_{1-x}\text{Fe}_x)_{95}\text{Mn}_{5.0}$ samples. at 1.5 K.

4.8 The Effects of Hydrogen

The effects of hydrogen on the geometric and magnetic properties of a typical PdNi specimen, Pd_{95.0}Ni_{5.0}, have been measured and these are summarized in Figures 4.57 to 4.59. The hydrogen charging was done electrochemically at room temperature as described in Chapter 3, while the hydrogen discharging was achieved electrochemically and/or by annealing the sample at high temperature. The amount of hydrogen was controlled in a semiquantitative way by setting a constant electrolysis current and recording the charging time.

Hydrogen has dramatic effects on the dilute PdNi system as the induced elongation is sufficiently large to be studied by a Picker travelling micrometer. The expansion variation ($\Delta L/L_0$) as a function of charging time (T in minutes), and therefore the amount of hydrogen in the Pd + 5.0 at% Ni sample, is examined in Figure 4.57. Starting from a virgin sample (before hydrogen treatment), the expansion ($\Delta L/L_0$) increases approximately linearly with increasing charging time initially, and then rather abruptly reaches the saturation state. Hydrogen produced a maximum increase of 1.8% in the length of the PdNi sample, achieved in a charging time of about 40 minutes with current densities on the order of 100 (mA/cm^2). These data can be used to estimate the hydrogen-to-metal ratio if this ratio is taken to be about 0.7 in the plateau region (Mydosh 1974).

Hydrogen not only produces changes in the sample's geometrical structure, but it also modifies strongly the magnetic properties. Figure 4.58 reproduces some of the experimental data in the form of true zero field suscep-

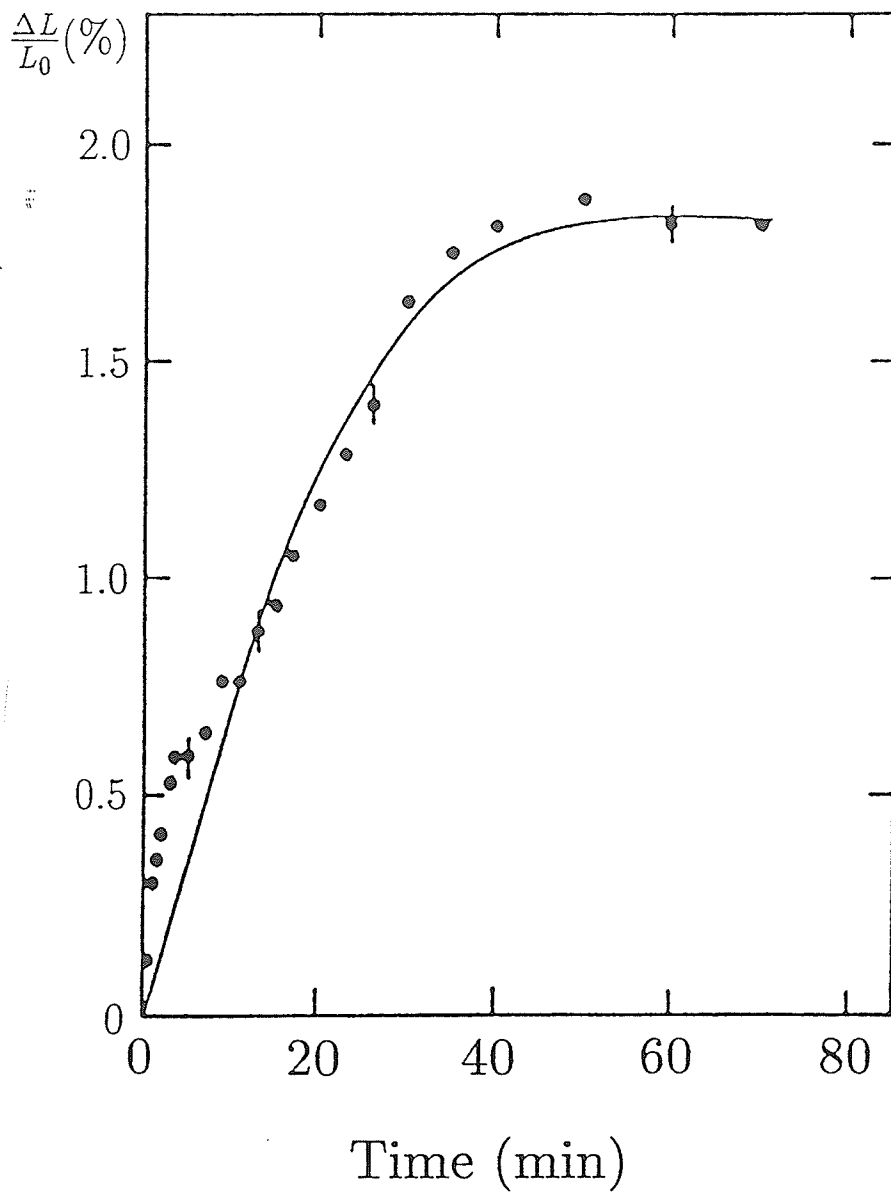


Figure 4.57: The expansion variation $\Delta L/L_0$ of a $\text{Pd}_{95.0}\text{Ni}_{5.0}$ sample versus charging time.

tibility χ_t versus temperature T for the $\text{Pd}_{95.0}\text{Ni}_{5.0}$ sample with the different hydrogen treatments. The sample were first fully loaded with hydrogen (curve (a)), and then discharged progressively. Two methods were used to discharge hydrogen from this alloy; the first was by annealing and the second by reverse electrolysis (electrochemical discharge). For the former, the specimen was sealed in a quartz glass tube at 10^{-6} torr pressure prior to annealing, and then annealed at 800 K for three hours; the resulting effects are shown by curve (b). The second method resulted in curves (c) and (d) following discharging time for two and four minutes, respectively. In this figure the curves (e) to (g) represent data from charging the same specimen for an additional three, six and nine minutes. It is apparent from the figure that the susceptibility is charging time dependent which is in turn related to the amount of hydrogen in the sample; the hydrogen content increases from top to bottom (curves (d) to (a)).

Careful examination of the present data enable the following comments to be made about the effects of hydrogen on the magnetic properties of this specimen.

(1) By adding hydrogen to the alloy, the magnetic susceptibility of the present sample can be almost completely suppressed. This can be clearly seen in curve (a) (selected from the measurements between temperature $T = 1.8 - 300$ K), in which the magnitude of the susceptibility and its temperature derivative is very small ($\chi \leq 10^{-5} \text{ emu/Oeg}$) after fully loading with hydrogen.

(2) Annealing the specimen produced similar results to the electrochem-

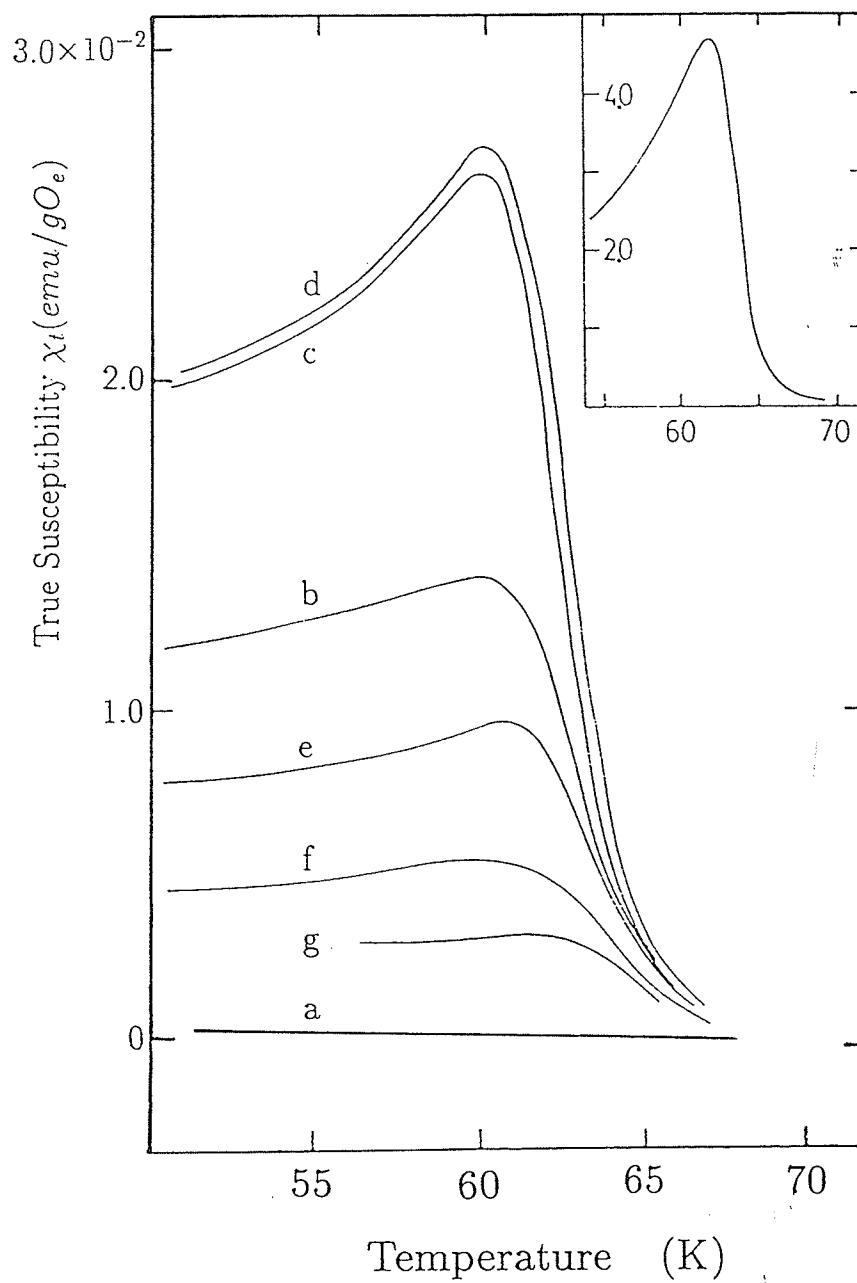


Figure 4.58: True zero field susceptibility χ_t versus temperature T for the hydrogen-free and hydrogenated PdNi alloy.

ical method, in the sense of discharging hydrogen. The experimental data indicate that the zero field susceptibility increases with decreasing amounts of hydrogen, as shown in curves (a) to (d); however the temperature at which the peak susceptibility occurs remains essentially unchanged (at 61 ± 1 K). This indicates that the Curie temperature of the specimen does not change substantially with loading hydrogen (presumably the Hopkinson peak temperature provides a qualitative indication of the behaviour of the ordering temperature). This further indicates that there is no significant change in the magnetic interactions as the Curie temperature reflects such interaction.

(3) Compared to the virgin sample, the height of the zero field susceptibility is reduced (representing only about 60% of the original value or less in the case of (b) to (d)); the width of the zero field susceptibility peak is broader and the background susceptibility is larger. These observations might be related to an increase in the coercive field (H_c) (because of the defects introduced by hydrogen; and H_c is a structurally sensitive parameter). This latter explanation is directly confirmed by the observation of a large increase in the coercive field from 18 Oe for the virgin sample, to 56 Oe (at 4.2 K) after just 5 minutes charging, as shown in Figure 4.59 (in which the susceptibility at 4.2 K is shown as a function of static biasing field). The coercive field H_c is essentially half the separation (in field) between the maximum slopes of the hysteresis loop. This conclusion also receives support from the observation of the change in length after hydrogen absorption as shown in figure 4.57. The length of the sample increases with increasing amounts

of hydrogen, which then changes the coercive field and susceptibility of the sample.

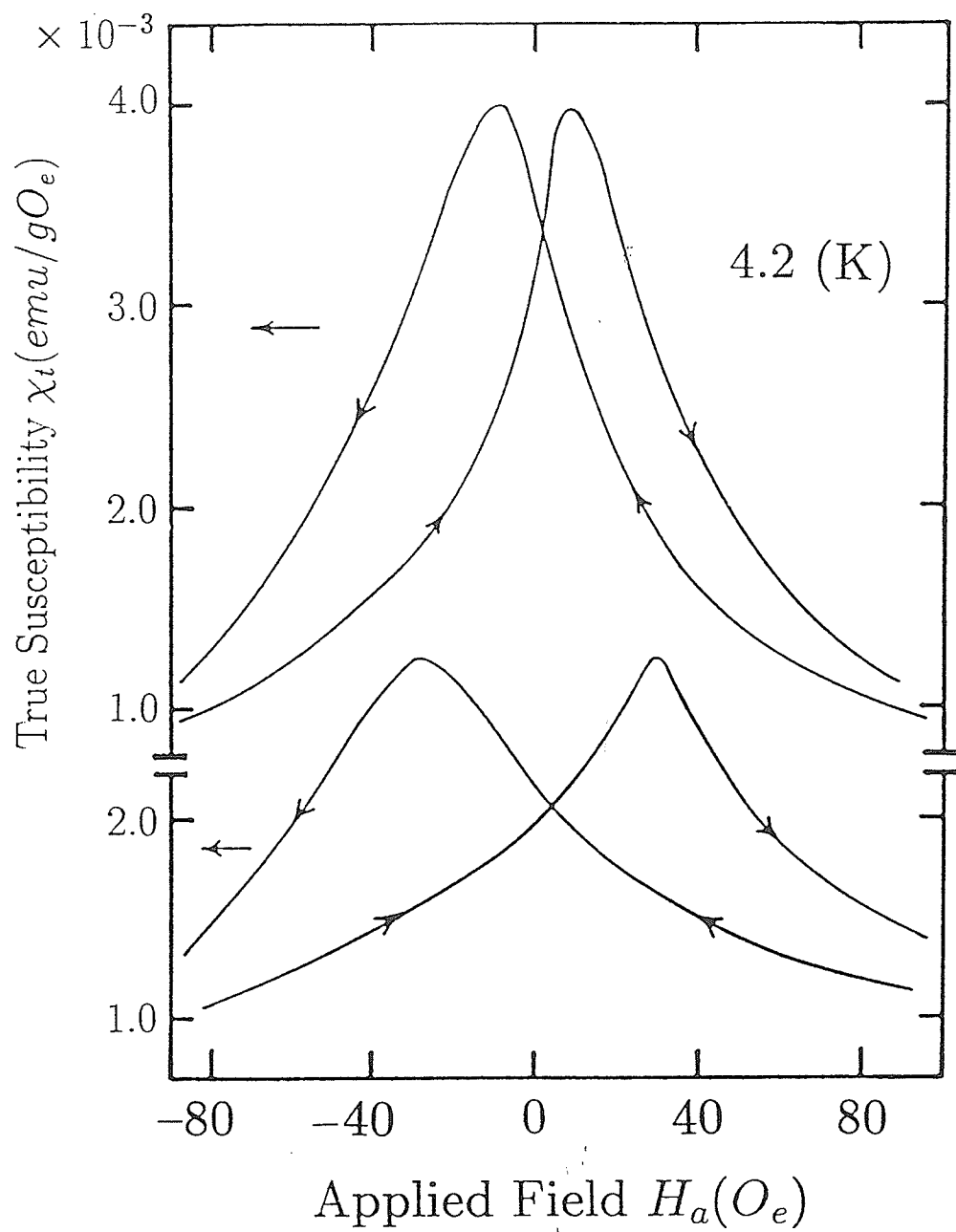


Figure 4.59: The true *ac* susceptibility χ_t as a function of field at 4.2 K for the hydrogen-free and hydrogenated PdNi alloy.

4.9 Summary and Conclusions

We have presented the first extensive study of the *ac* susceptibility and *ac* magnetoresistance of a number of dilute PdNi, PdFe, and (PdFe)Mn alloys with Ni or Fe concentration close the critical composition; we have also presented the effects of hydrogen absorption on the magnetic properties of a typical PdNi sample.

The temperature and field dependent susceptibility of all three Pd based dilute systems studied have a number of features in common. Specifically, they all display an emerging critical peak in the vicinity of T_c in small static biasing fields; this peak decreases in amplitude and shifts upwards in temperature as the static biasing field increases, in agreement with the predictions of the static scaling law.

Reliable estimates of the critical exponents and the Curie temperature of a $\text{Pd}_{98.6}\text{Fe}_{1.4}$ sample have been made by analysing the behaviour of such peaks, and yields

$$\gamma = 1.36 \pm 0.05; \delta = 4.0 \pm 0.1; \beta = 0.49 \text{ and } T_c = 55.6 \pm 0.1 \text{ K.}$$

These exponent values are close to those found in elemental ferromagnets like pure Ni, and shows that the susceptibility of the alloy can be well described by the scaling law, the critical exponents (γ , β and δ) obeying the Widom equality $\gamma = \beta(\delta - 1)$. The field dependent susceptibility data, normalized to its peak value, and measured in a number of fixed non-zero fields h as a function of temperature, fit precisely on a universal curve as also predicted by the scaling law.

Low temperature susceptibility measurements in various collinear fields have been carried out on PdFe alloys containing between 0.35 and 2.4 at% Fe. The data show that all the seven samples studied are soft ferromagnets as the critical peaks can be observed in external fields of only a few *Oe*. A quantitative analysis of the peak susceptibility shows that for most of the PdFe samples studied the δ values (between 2.4 and 3.1) are less than that found for elemental ferromagnets, but are comparable with the values obtained in some other Pd based dilute alloys, such as the PdMn alloys of intermediate concentration; the zero field susceptibility data show the effective γ^* values in PdFe exhibit a strong temperature dependence. These data also indicate that the regular contribution to the susceptibility (with the presence of spin-orbit coupling) plays some role, and probably precludes reliable estimates for the critical exponents.

The impurity concentration dependence of the Curie temperature exhibits a linear dependence on the Fe concentration between 1.4 and 2.4 at%, with the ratio $\frac{dT_c}{dx} \approx 32\text{K/at}\%$ Fe; the 0.35 at% Fe sample has a $T_c = 7.50$ K.

The *ac* susceptibility measurements of five (PdFe)Mn alloys containing between 0.35 and 2.2 at% Fe with an additional 5 at% Mn have shown these alloys are magnetically harder. Applied fields in excess of about 20 *Oe* are required before the emerging critical peaks can be resolved, which is about an order of magnitude larger than that required to produce similar effects in the PdFe alloys with comparable amounts of Fe. The impurity concentration dependence of the Curie temperature displays a simple linear relationship,

with $\frac{dT_c}{dx} \approx 16$ K/at%Fe for the alloys with Fe concentration between 1.6 and 2.2 at%. This latter ratio is only about half of the measured ratio for the PdFe alloys (≈ 32 K/at%Fe).

The $(\text{Pd}_{99.65}\text{Fe}_{0.35})_{95}\text{Mn}_5$ sample is particularly interesting because it is a re-entrant system. The *ac* susceptibility data show that this latter alloy has a ferromagnetic Curie temperature $T_c = 9.30$ K and a spin glass temperature $T_f = 4.07$ K; the ferromagnetic transition is characterised by critical exponent values $\delta = 4.1 \pm 0.1$, $\gamma = 1.64 \pm 0.07$, and $\beta = 0.53(5) \pm 0.08$. The non-linear magnetic response of the re-entrant system $(\text{Pd}_{99.65}\text{Fe}_{0.35})_{95}\text{Mn}_5$ has also been studied in the vicinity of both transitions. For the upper transition, the coefficient of the H^2 term predicted by the scaling theory is confirmed. For the lower transition, an anomaly in the non-linear response has been clearly shown for the first time. It is suggested that this is a strong indication of a second transition and may be an intrinsic feature of a true re-entrant ferromagnetic-spin glass transition.

Detailed measurements of the field and temperature dependent *ac* susceptibility of a number of PdNi alloys containing between 2 and 5 at% Ni have been presented. In the ferromagnetic samples attempts were made to analyse these data for Curie temperature and critical exponent values. The *ac* susceptibility data indicate the Curie temperature T_c of the alloys can be determined by an approximate method based on a simple single power law relationship. The Curie temperature estimated by this method ranged from 1.95 ± 0.1 K for the 2.4 at% Ni sample to 62.7 ± 1 K for 5.0 at% alloy. The

Curie temperature exhibits a nearly linear dependence on Ni concentration between 3.0 and 5.0 at% with a ratio $\frac{dT_c}{dx} \approx 25$ K/at% Ni. Below 3.0 at% the Curie temperature drops much more slowly as the Ni composition decreases. The data also indicate that spin orbit induced anisotropy associated with a Ni orbital moment precludes reliable estimations for any critical exponents (γ , β or δ), though such anisotropy is necessary to make the observation of a spontaneous resistive anisotropy (SRA) possible. Nevertheless the ac susceptibility data are consistent with the suggestion that a spin-glass ground state would appear at low temperatures for Ni concentrations at or below about 2 at% if complications arising from the single ion Kondo compensation of a low spin state were absent. These data are also shown to be consistent with assigning a low spin value ($S = 1/2$) to the Ni site.

The magnetoresistance data on PdNi alloys show for the first time that the onset of ferromagnetic order can be investigated via a non-zero spontaneous resistive anisotropy (SRA) without extrapolation, and the low field SRA data confirm the critical Ni composition x_0 necessary to establish a ferromagnetic ground state at low temperature by direct observation. The appearance of a minimum in $\rho_{||}(H_a)$ has been exploited to obtain quantitatively reliable measurements for SRA directly at a unique field (H_a^{min}). The SRA value using this method is defined by the ratio

$$\frac{\Delta\rho(H_a^{min})}{\rho_0} = \frac{\rho_{||}(H_a^{min}) - \rho_{\perp}(H_a^{min})}{\rho_0} \quad (4.8)$$

The results show that in those cases where the comparison is possible,

estimates of the SRA based on $\rho_{\parallel}(H_a^{min})$ agree very well with those obtained using established extrapolation techniques. For those lower Ni concentration specimens where an extrapolation procedure is not reliable or not possible, the new method still can be used to estimate the SRA at low field.

We have also demonstrated for the first time a power law relationship between the SRA and the reduced composition close to x_0 of the form

$$\frac{\Delta\rho}{\rho_0} \propto \left(\frac{x - x_0}{x_0}\right)^\eta \quad (4.9)$$

The corresponding value of x_0 and the critical exponent η in this relationship are 2.25 at% Ni and 2.25 respectively. Prompted by the scaling approach, we have attempted to calculate the scattering per Ni site by normalizing the resistivity to ρ_0 as well as Curie temperature for ferromagnetic samples (or the measuring temperature for paramagnetic alloys). Plotting the scaled slopes $(1/\rho_0)(d\rho_{\perp}/dH_a)(1/T_c)$ at 1.5 K versus the Ni concentration has again confirmed the estimate for x_0 given above.

Measurements of the magnetoresistance in PdFe alloys show that an H_a^2 field dependence reproduces the data best at high field. These data demonstrate a difference between ρ_{\parallel} and ρ_{\perp} , thus confirming the presence of a positive resistive anisotropy in these alloys, and provides clear evidence of a considerable exchange field in the samples; the SRA values however represent only about 15 percent of the values observed in PdNi alloys with comparable Curie temperatures. The possibility of a power-law relationship, as observed in PdNi alloys, between SRA and the reduced concentration has

also been examined, and shows that a power-law relationship does again reproduce very well the SRA estimates at 1.5 K for all the PdFe samples studied with parameters: $x_0 = 0.010 \pm 0.005$ at% Fe, and $\eta = 0.9 \pm 0.1$. This result confirmed the critical Fe concentration x_0 necessary to establish a ferromagnetic ground state by magnetoresistance anisotropy measurements.

Measurements of the magnetoresistance in (PdFe)Mn alloys indicate that adding 5.0 at% Mn to the PdFe host alloy changes the magnetoresistive properties of the system substantially. It is demonstrated that a marked component exists both longitudinal ρ_{\parallel} and the transverse magnetoresistivities ρ_{\perp} in higher fields, and this remains unsaturated up to fields of 85 kOe, thus complicating quantitative analysis. These data, however, demonstrate a difference between ρ_{\parallel} and ρ_{\perp} , thus confirming again the presence of a resistive anisotropy in these samples, with a sign which agrees with that exhibited in the host alloys (PdFe). The SRA values represent only about 50% of that measured in PdFe alloys with comparable Fe concentration. The possibility of a power-law relationship, as observed in dilute PdNi and PdFe alloys, between SRA and the reduced concentration has also been examined, and shows that a power-law relationship does again reproduce the SRA estimates at 1.5 K for the (PdFe)Mn samples studied with parameters: $x_0 = 0.2 \pm 0.1$ at% Fe, and $\eta = 0.9 \pm 0.1$. This result demonstrates for the first time a critical Fe concentration x_0 necessary to establish a ferromagnetic ground state by magnetoresistance anisotropy measurements for the (PdFe)Mn system.

We also show that hydrogen has dramatic effects on both the specimen

dimensions and the magnetic properties of the dilute PdNi system. The susceptibility is very sensitive to the amount of hydrogen, and it can be completely destroyed by fully loading with hydrogen. The results also show that the magnetic susceptibility responds to hydrogen loading in a reversible way, while the coercive field H_c responds irreversibly (unless annealing is used as a method of discharging hydrogen). An exhaustive study of the effects of hydrogen on the magnetic, electrical and structural properties of Pd based alloys would be a very interesting project, and we hope the present measurements will stimulate further study in this area.

Appendix

A. *ac* Susceptibility Data

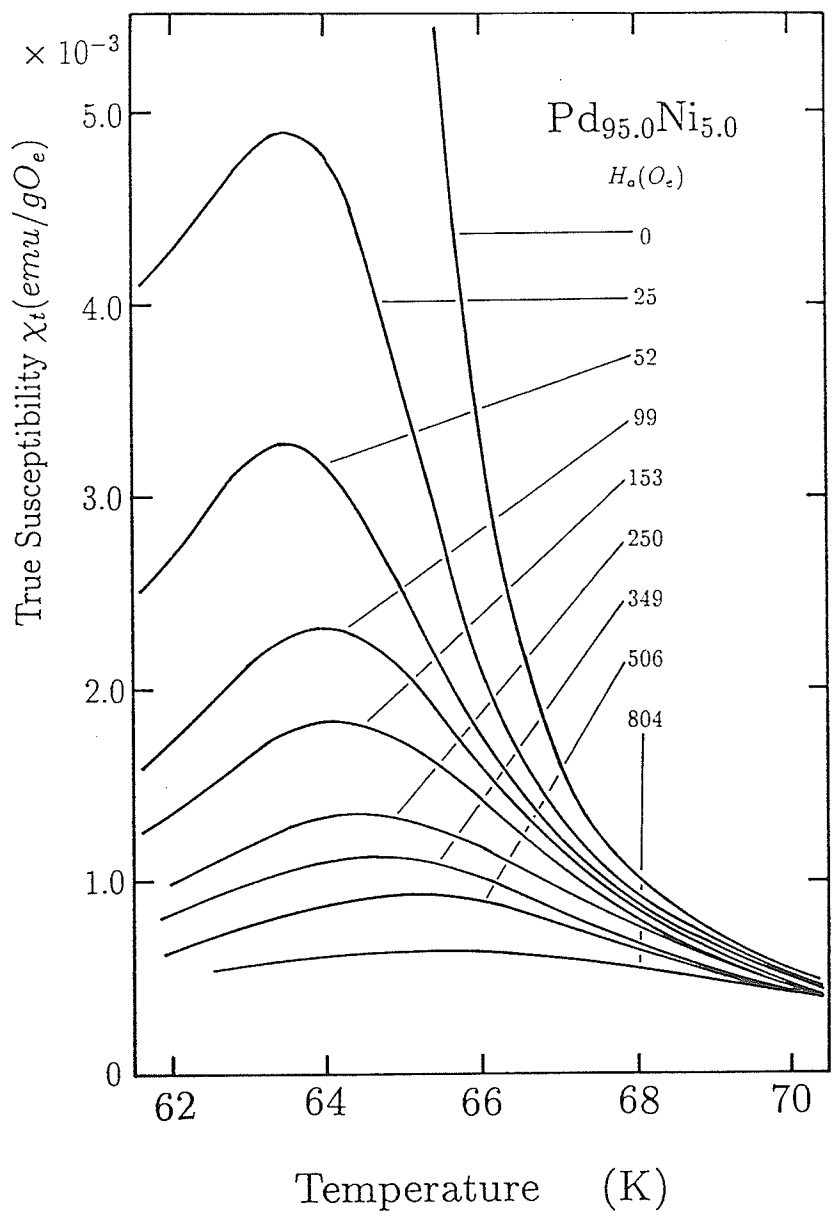


Figure A1: The selected *ac* susceptibility data as a function of temperature for the Pd_{95.0}Ni_{5.0} alloy in various fields.

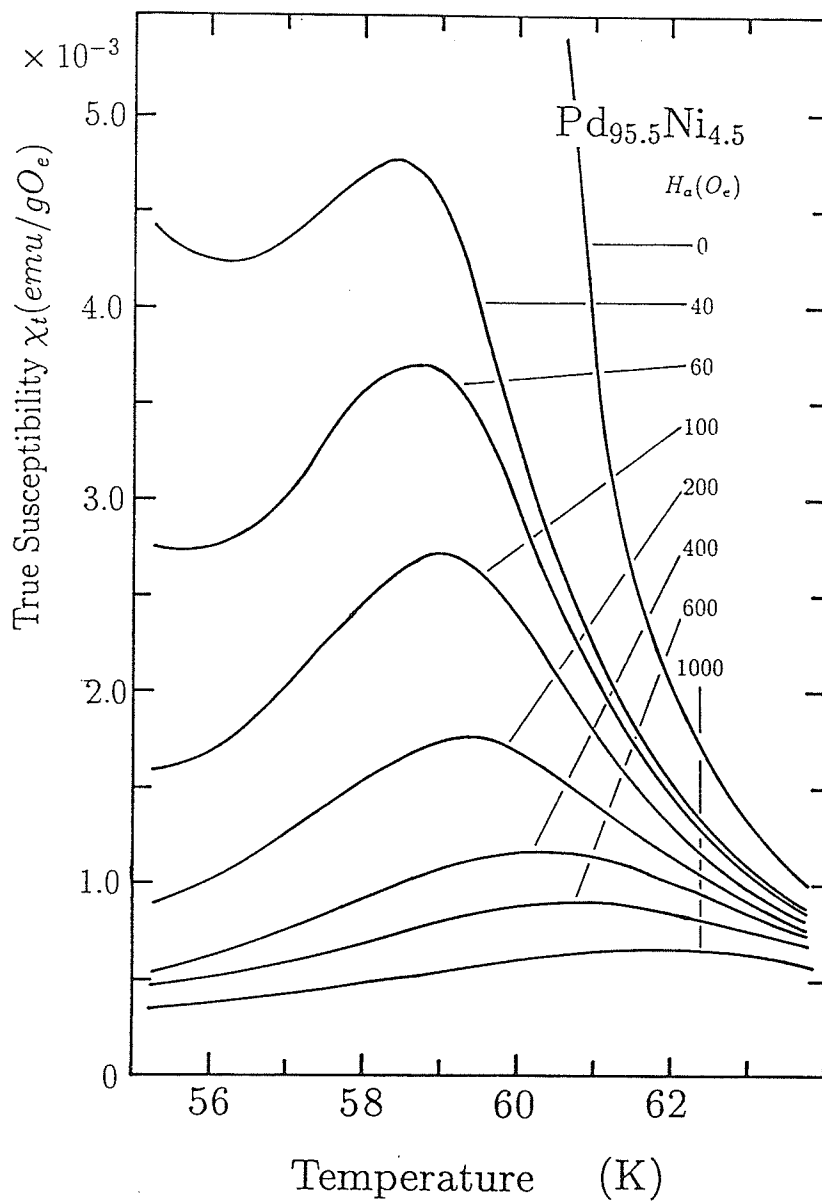


Figure A2: The selected *ac* susceptibility data as a function of temperature for the $\text{Pd}_{95.5}\text{Ni}_{4.5}$ alloy in various fields.

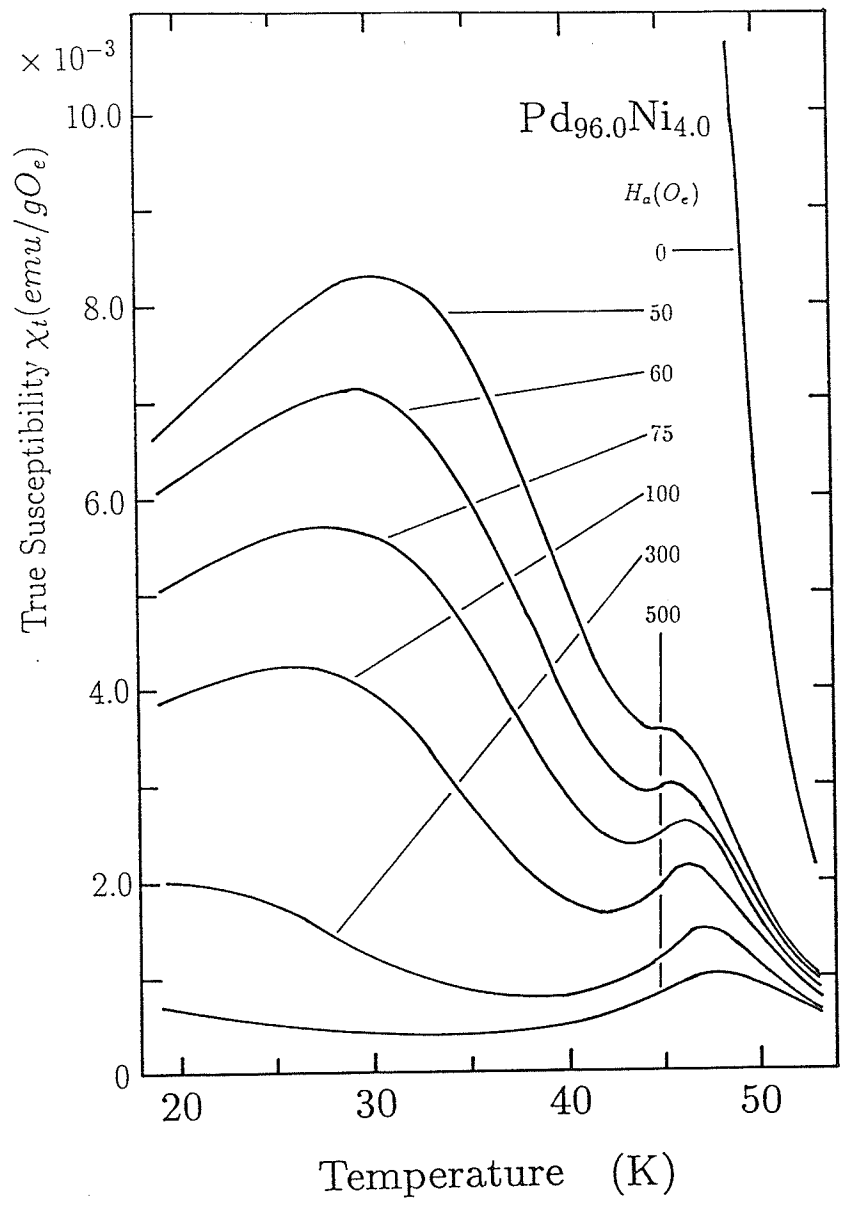


Figure A3: The selected *ac* susceptibility data as a function of temperature for the Pd_{96.0}Ni_{4.0} alloy in various fields.

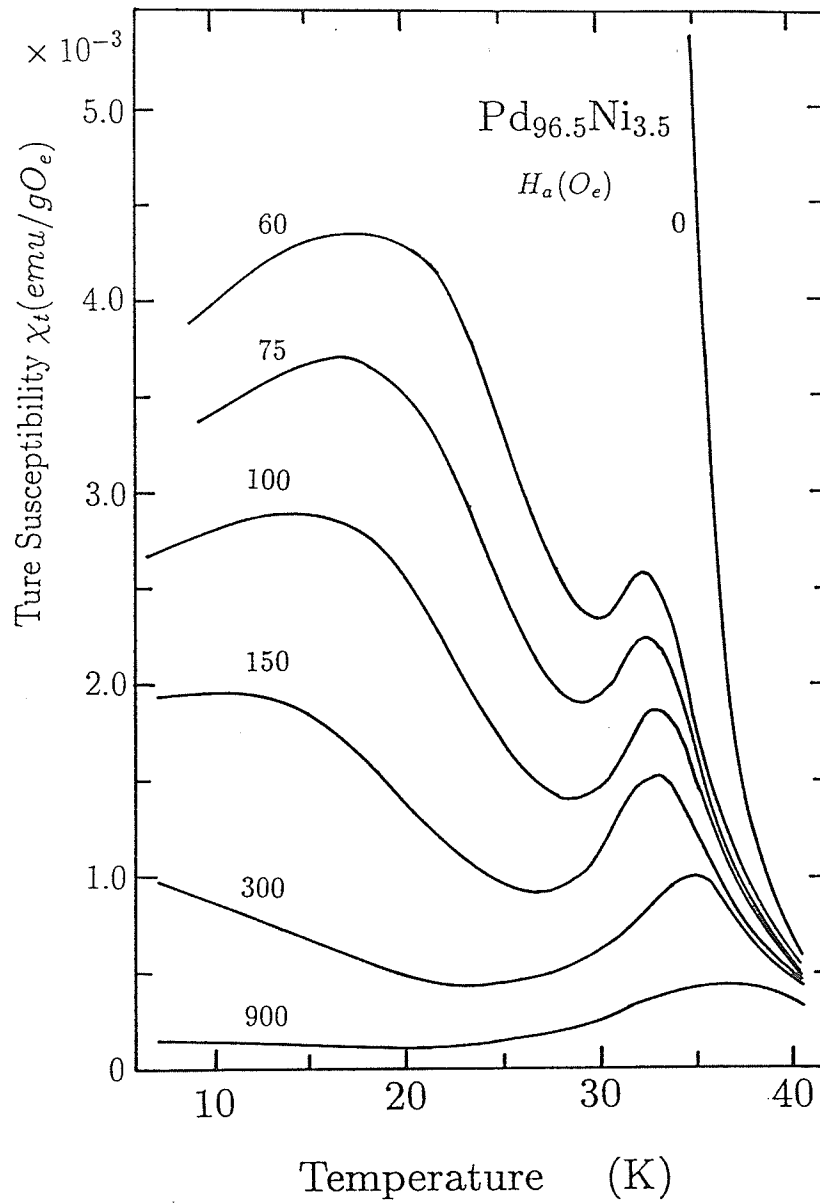


Figure A 4: The selected *ac* susceptibility data as a function of temperature for the $\text{Pd}_{96.5}\text{Ni}_{3.5}$ alloy in various fields.

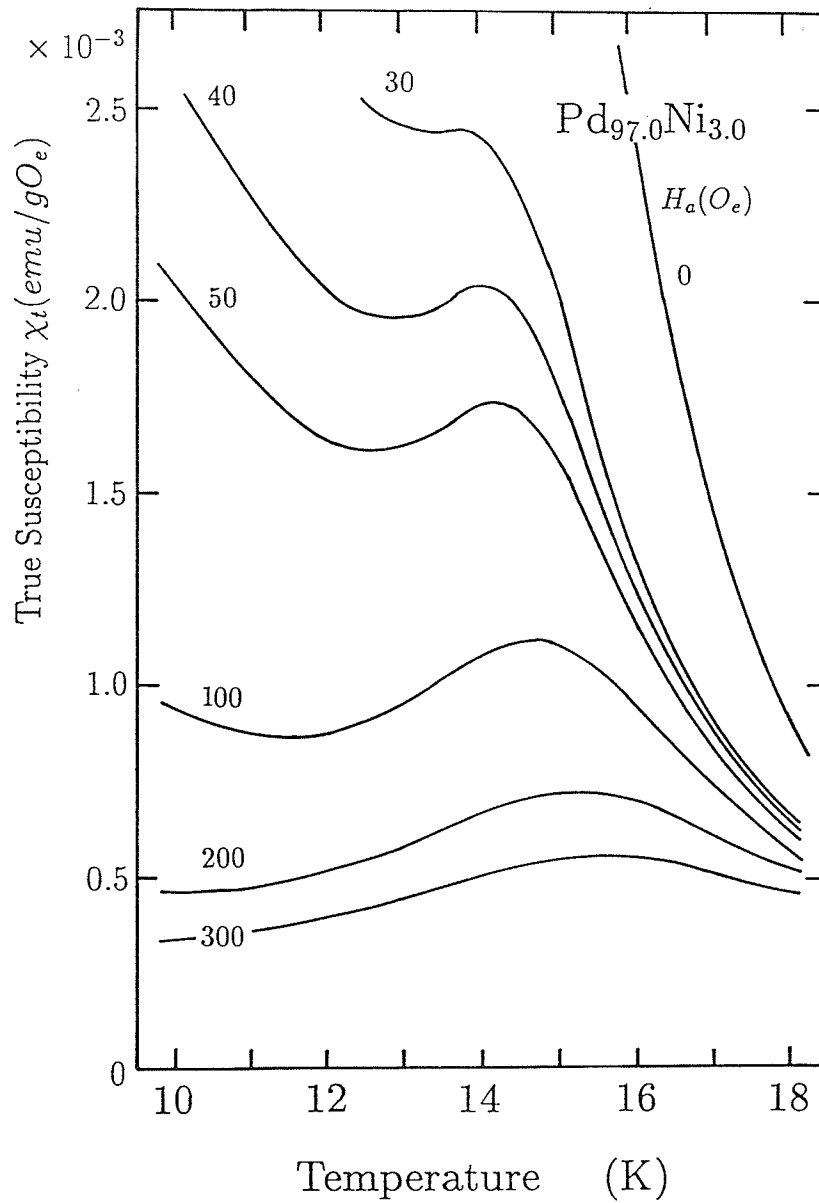


Figure A5: The selected *ac* susceptibility data as a function of temperature for the $\text{Pd}_{97.0}\text{Ni}_{3.0}$ alloy in various fields.

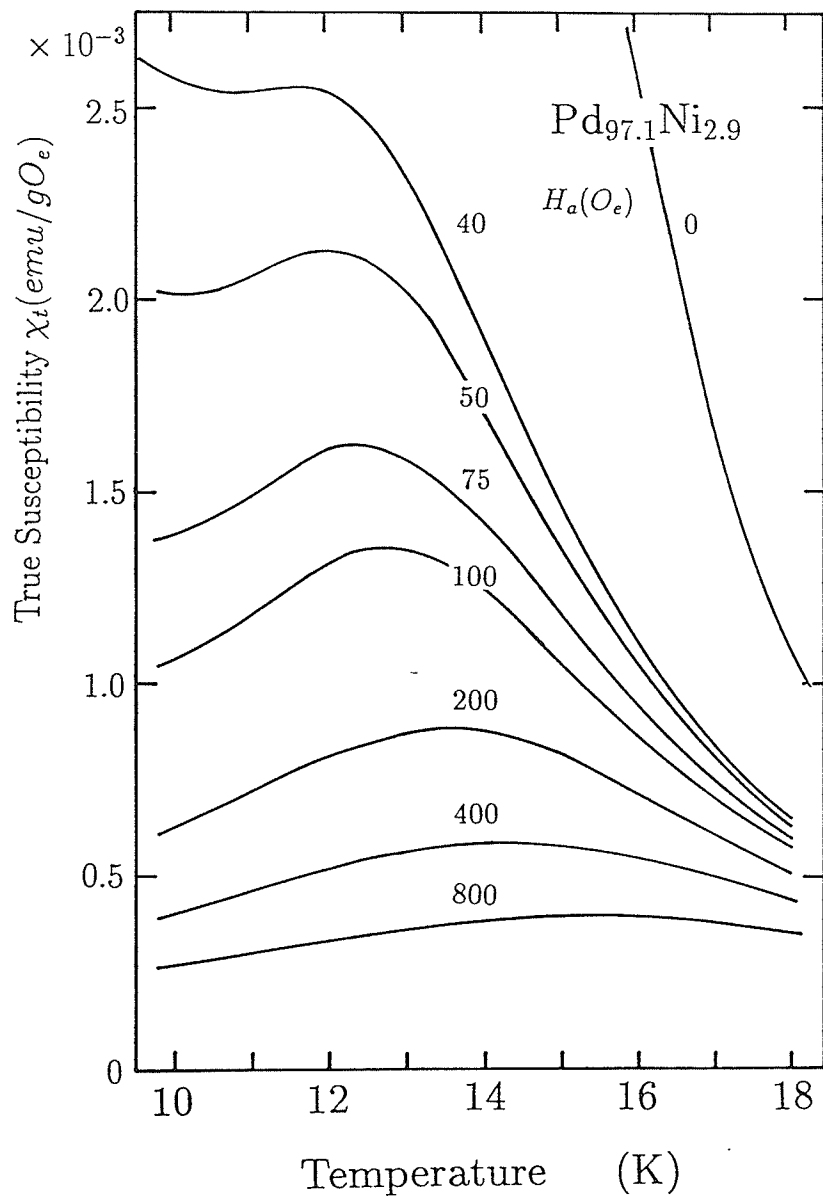


Figure A6: The selected *ac* susceptibility data as a function of temperature for the $\text{Pd}_{97.1}\text{Ni}_{2.9}$ alloy in various fields.

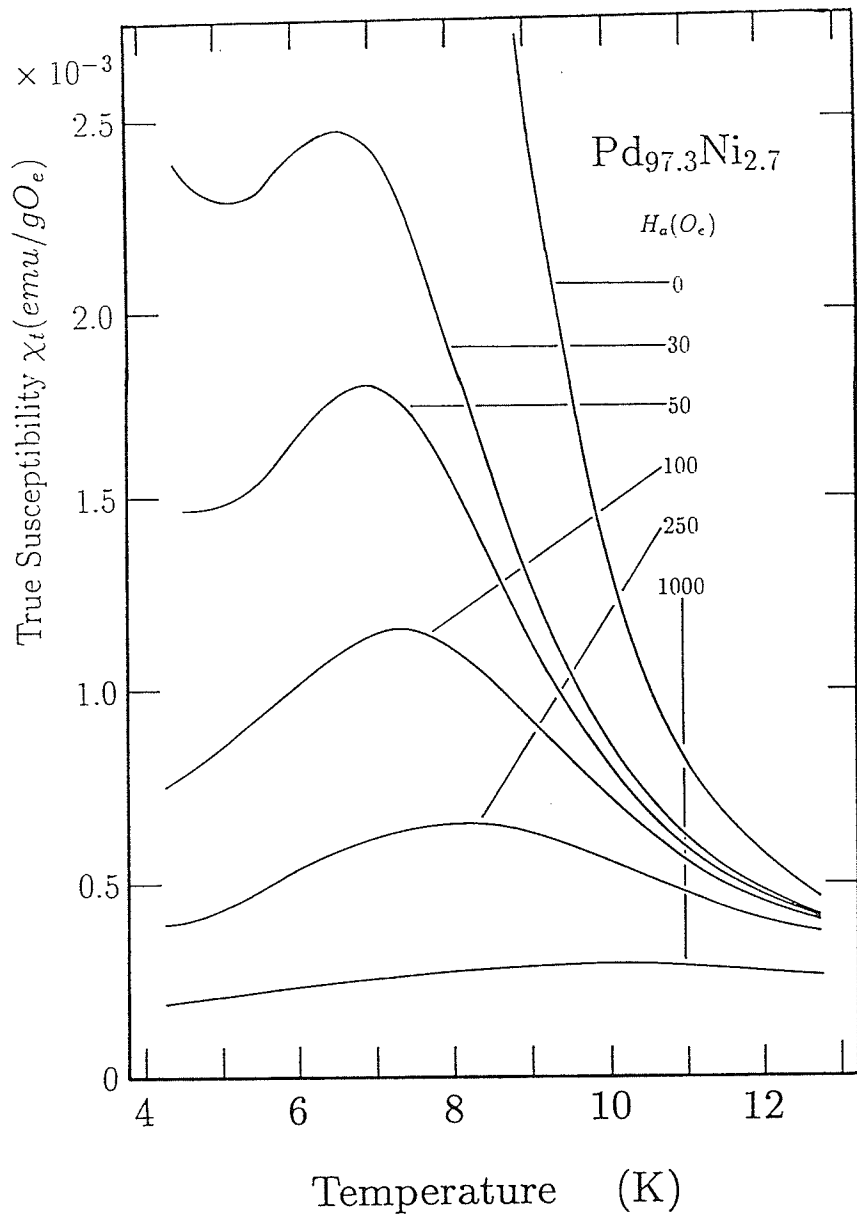


Figure A7: The selected *ac* susceptibility data as a function of temperature for the $\text{Pd}_{97.3}\text{Ni}_{2.7}$ alloy in various fields.

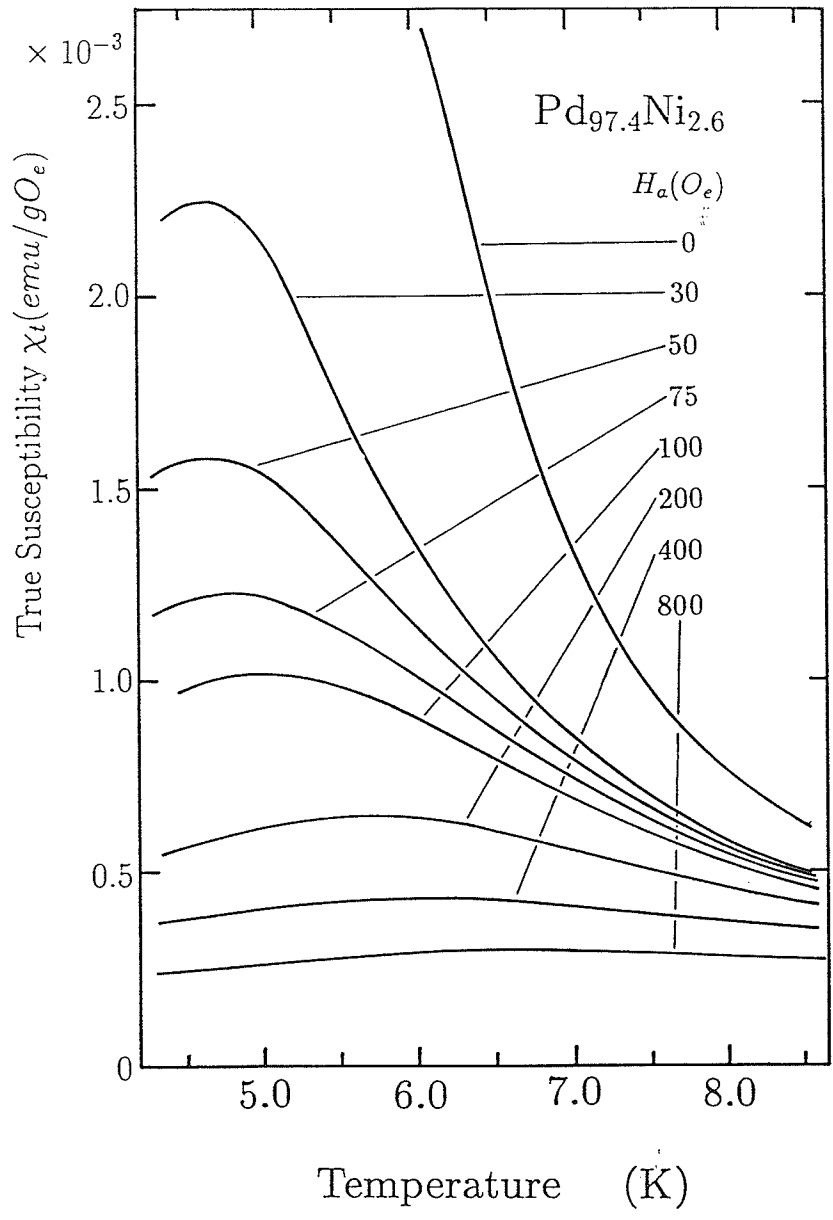


Figure A 8: The selected *ac* susceptibility data as a function of temperature for the Pd_{97.4}Ni_{2.6} alloy in various fields.

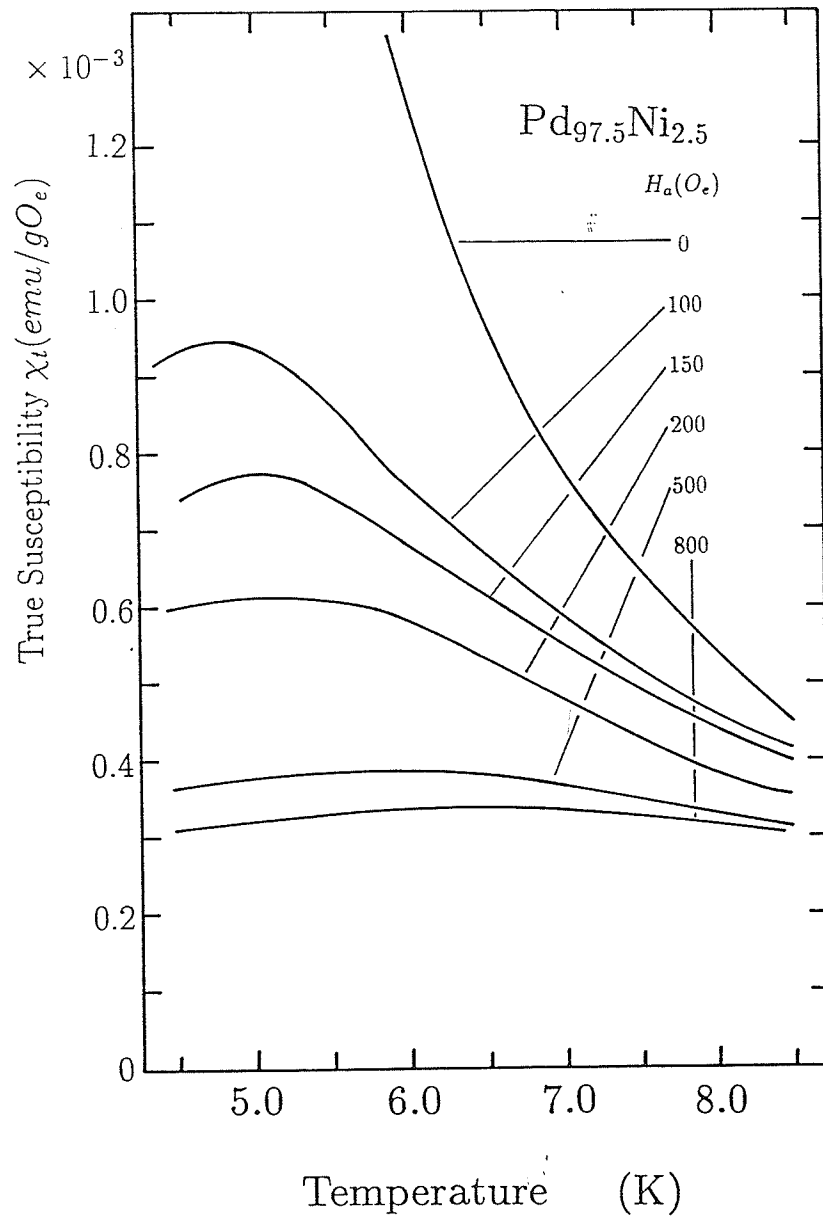


Figure A9: The selected *ac* susceptibility data as a function of temperature for the Pd_{97.5}Ni_{2.5} alloy in various fields.

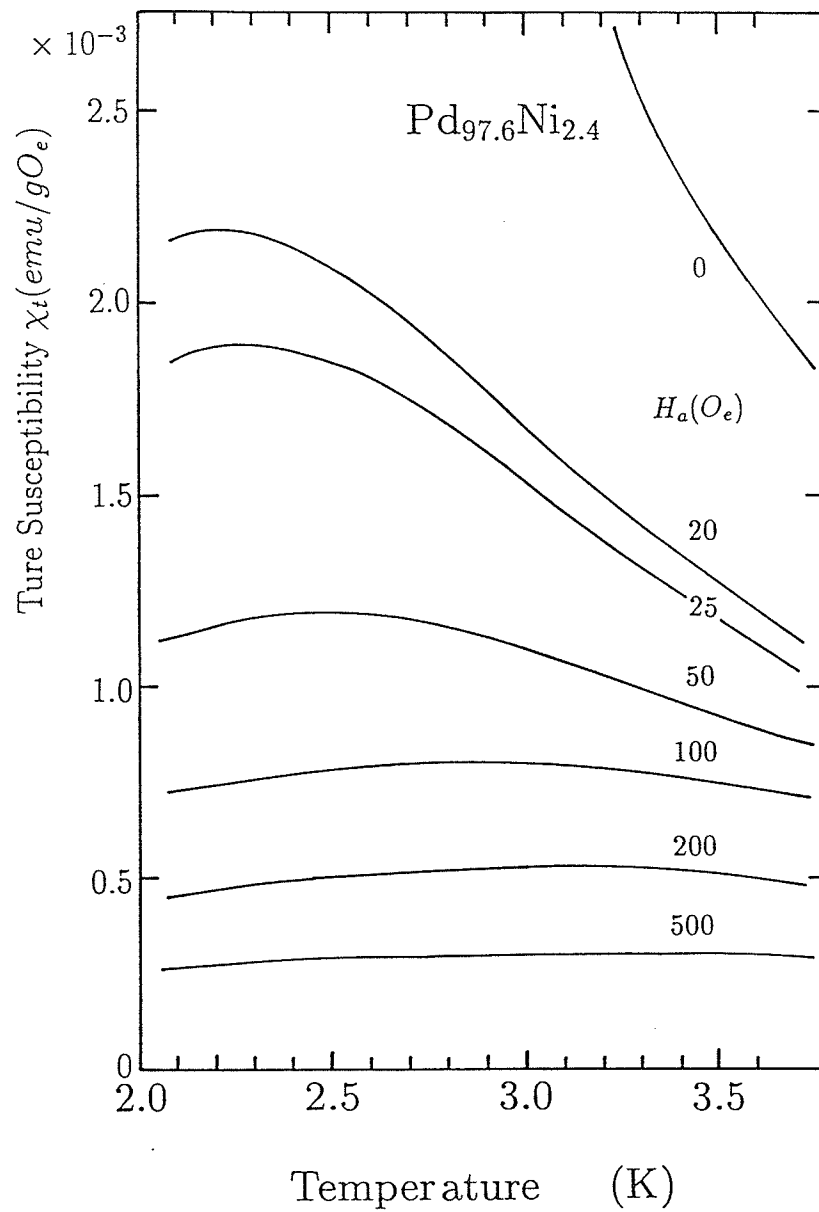


Figure A10: The selected *ac* susceptibility data as a function of temperature for the $\text{Pd}_{97.6}\text{Ni}_{2.4}$ alloy in various fields.

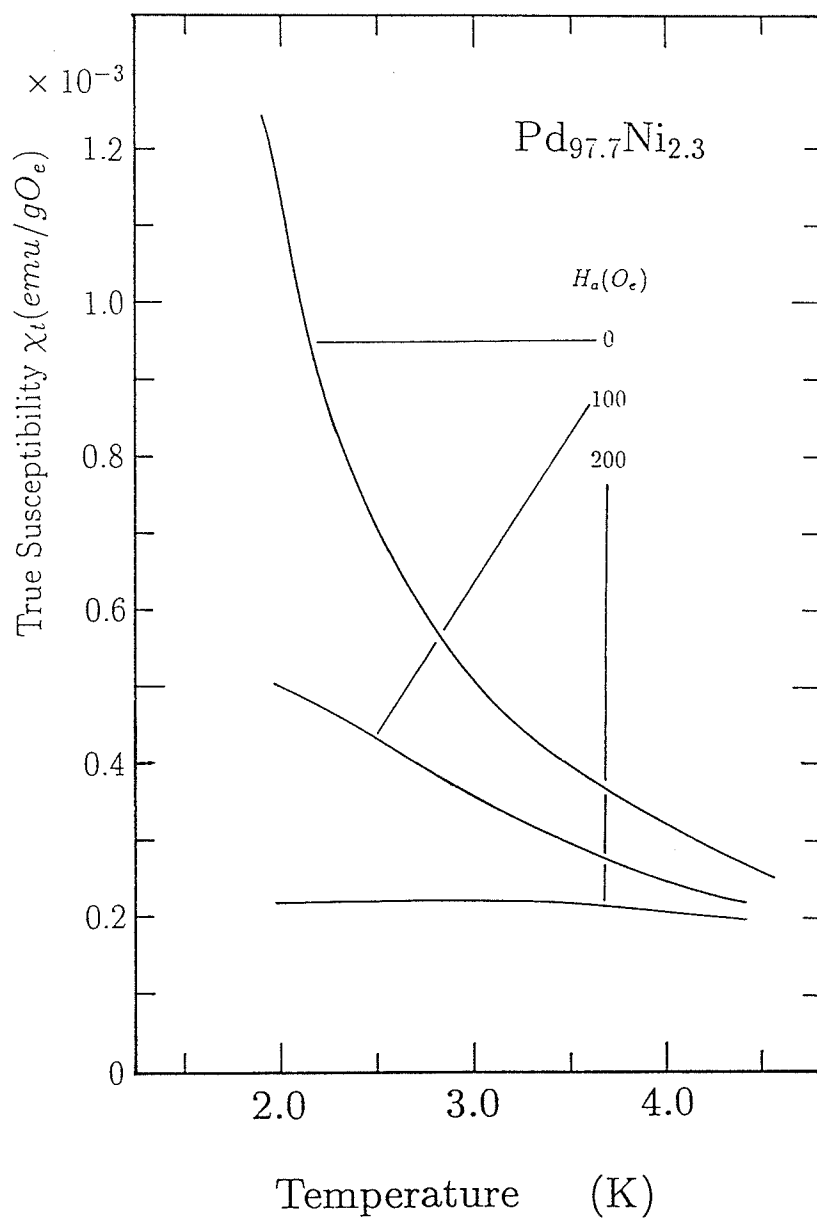


Figure A 11: The selected *ac* susceptibility data as a function of temperature for the $\text{Pd}_{97.7}\text{Ni}_{2.3}$ alloy in various fields.

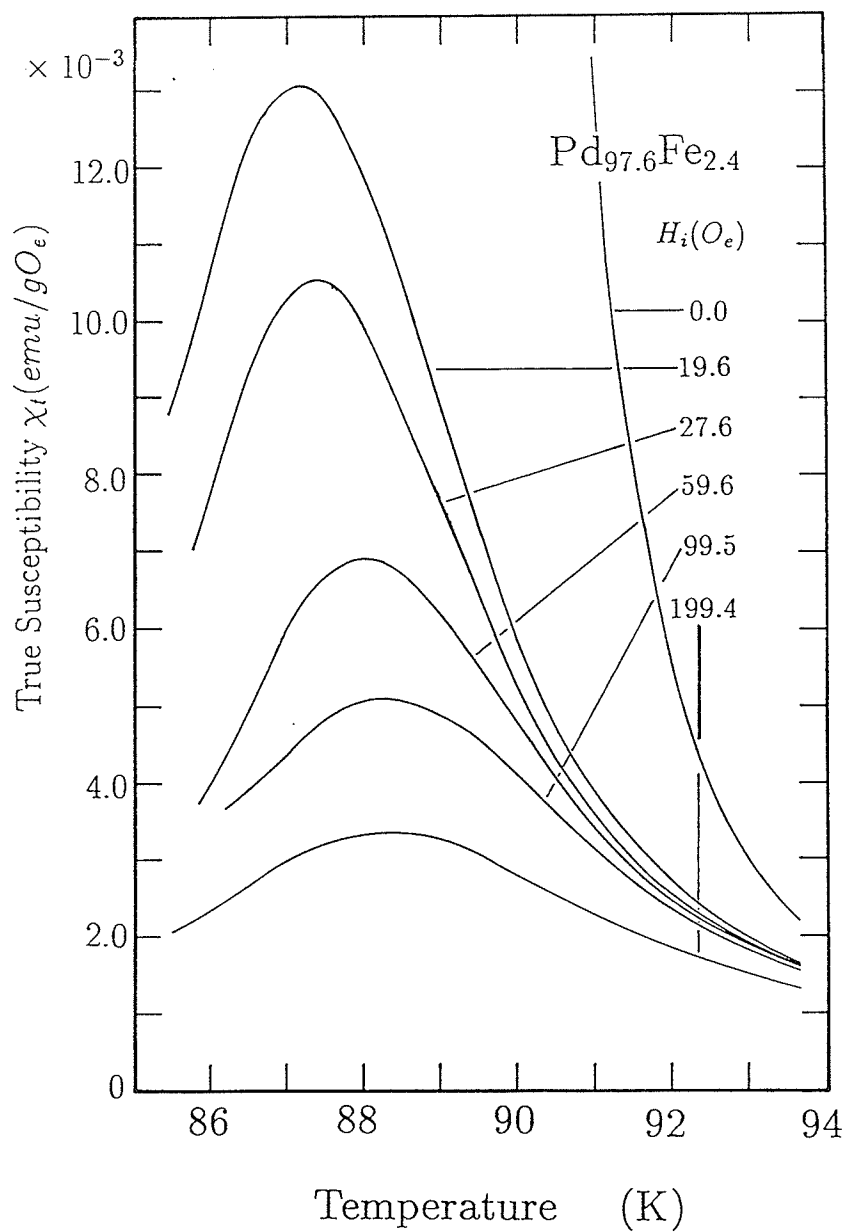


Figure A12: The selected *ac* susceptibility data as a function of temperature for the Pd_{97.6}Fe_{2.4} alloy in various fields.

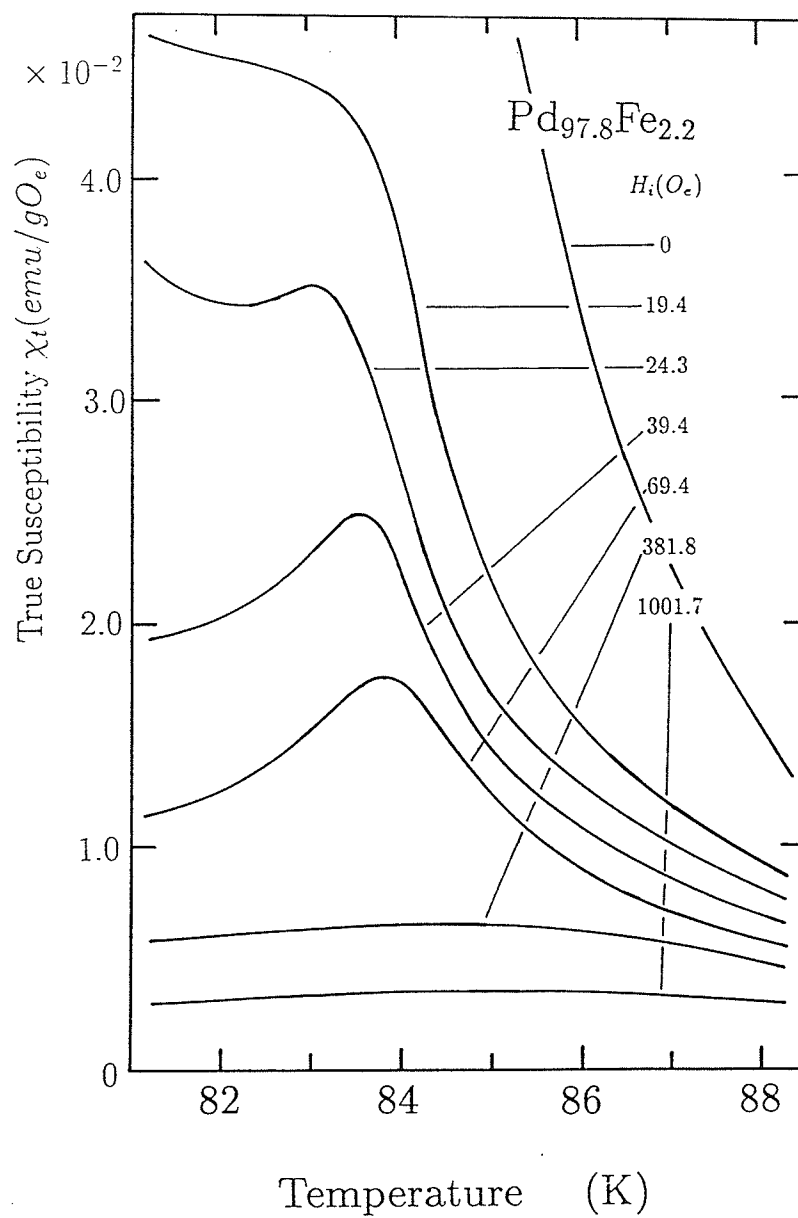


Figure A13: The selected *ac* susceptibility data as a function of temperature for the $\text{Pd}_{97.8}\text{Fe}_{2.2}$ alloy in various fields.

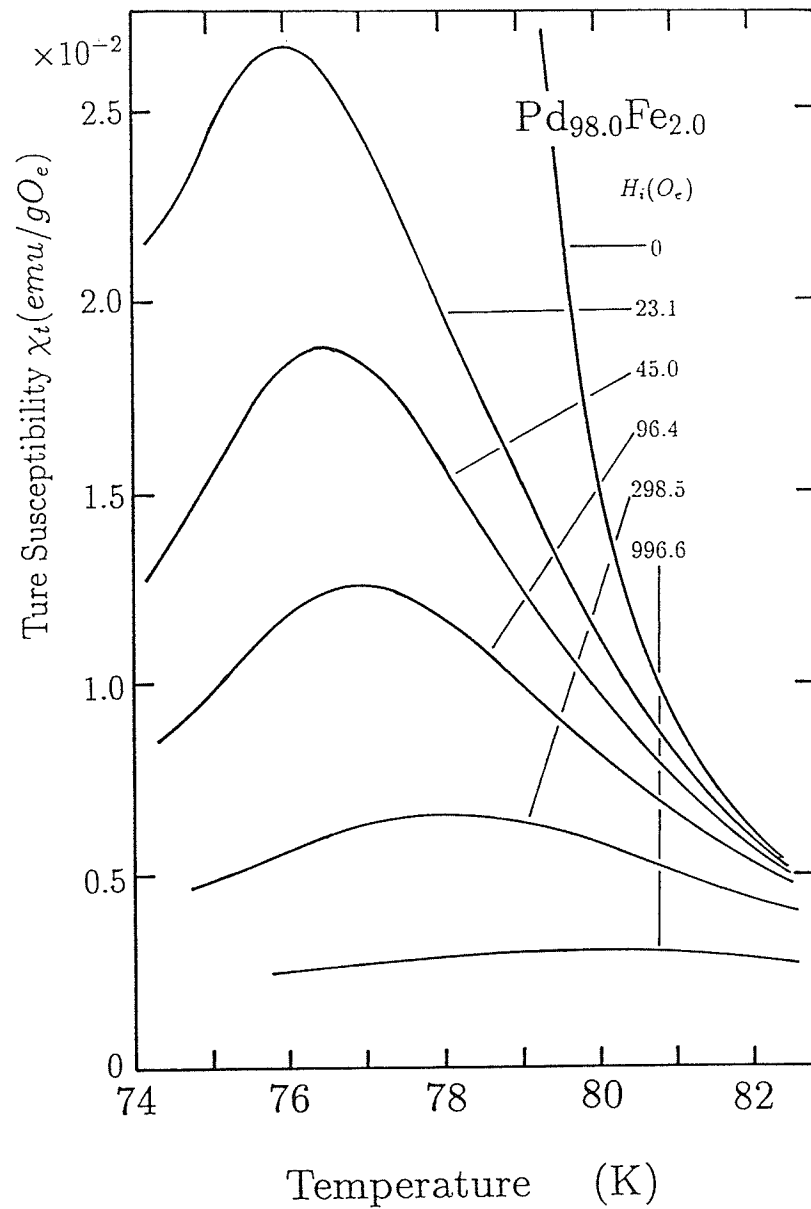


Figure A14: The selected *ac* susceptibility data as a function of temperature for the $\text{Pd}_{98.0}\text{Fe}_{2.0}$ alloy in various fields.

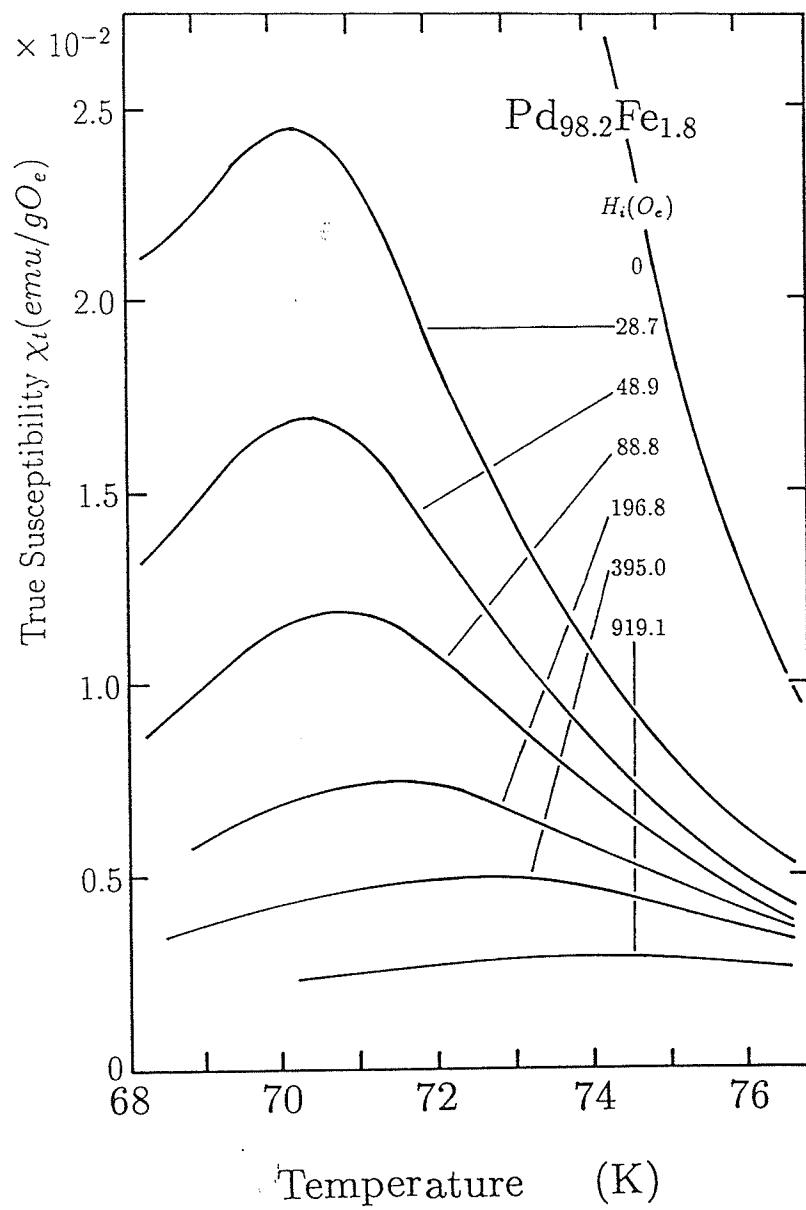


Figure A15: The selected *ac* susceptibility data as a function of temperature for the Pd_{98.2}Fe_{1.8} alloy in various fields.

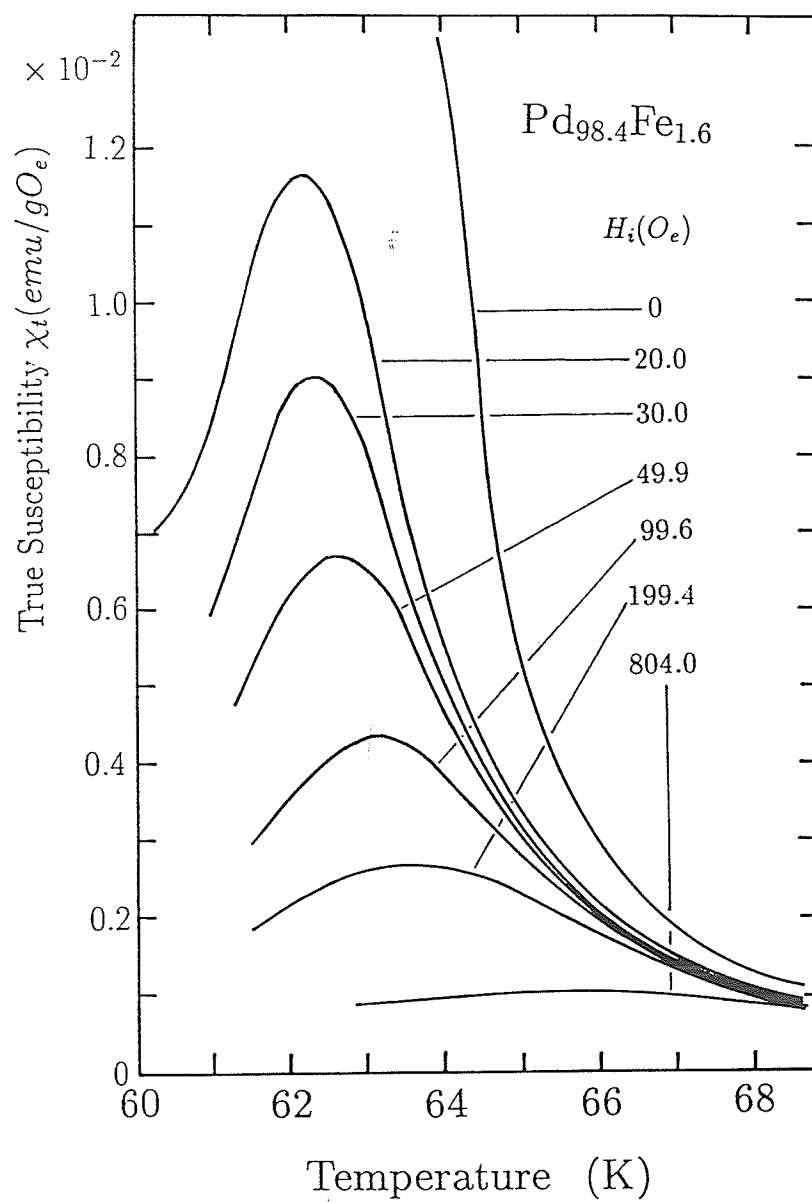


Figure A16: The selected *ac* susceptibility data as a function of temperature for the Pd_{98.4}Fe_{1.6} alloy in various fields.

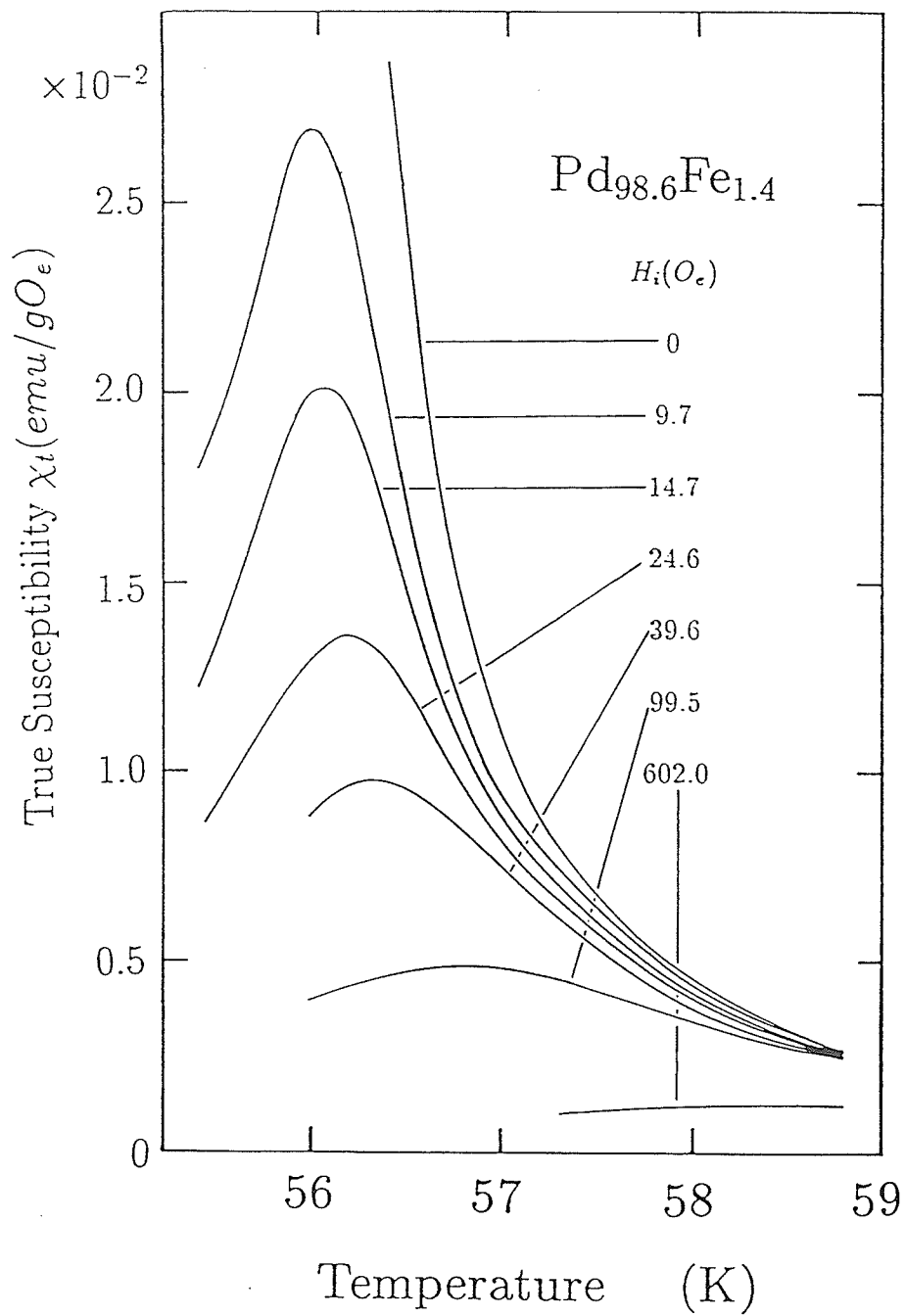


Figure A17: The selected *ac* susceptibility data as a function of temperature for the $\text{Pd}_{98.6}\text{Fe}_{1.4}$ alloy in various fields.

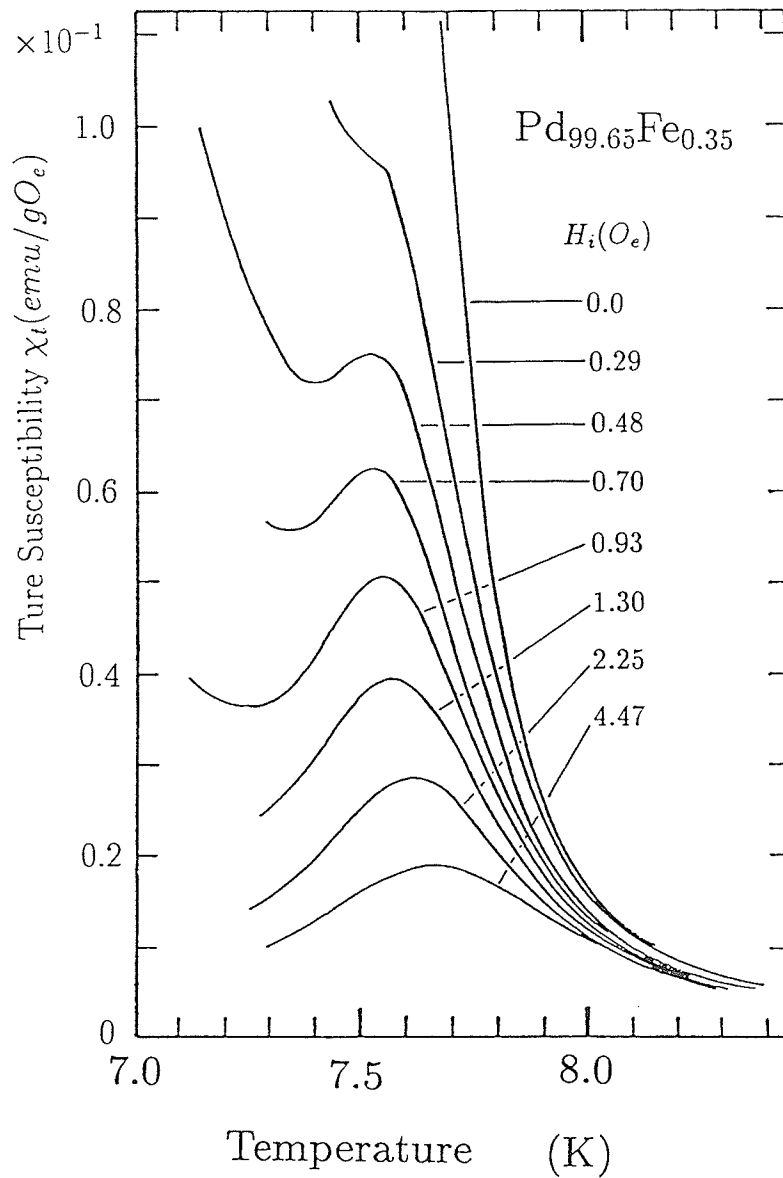


Figure A18: The selected *ac* susceptibility data as a function of temperature for the $\text{Pd}_{99.65}\text{Fe}_{0.35}$ alloy in various fields.

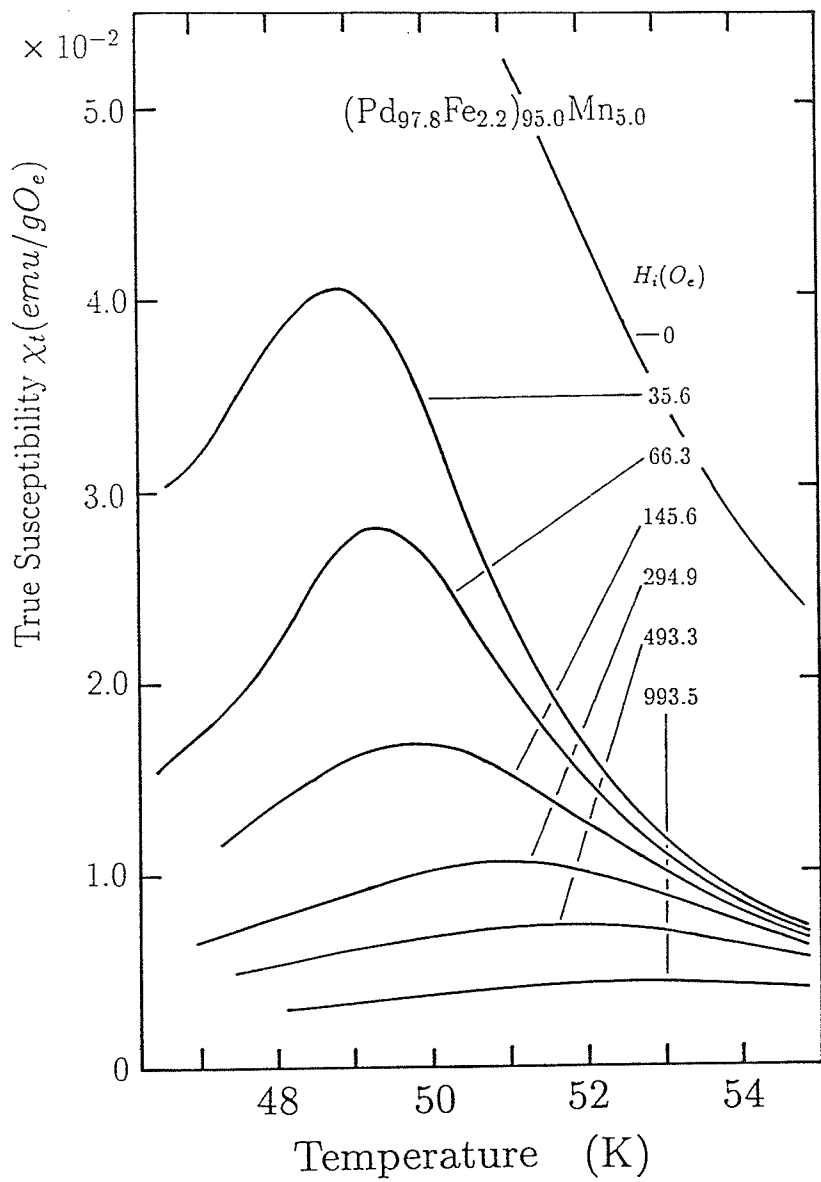


Figure A19: The selected *ac* susceptibility data as a function of temperature for a (PdFe)Mn alloy with 2.2 at% Fe in various fields.

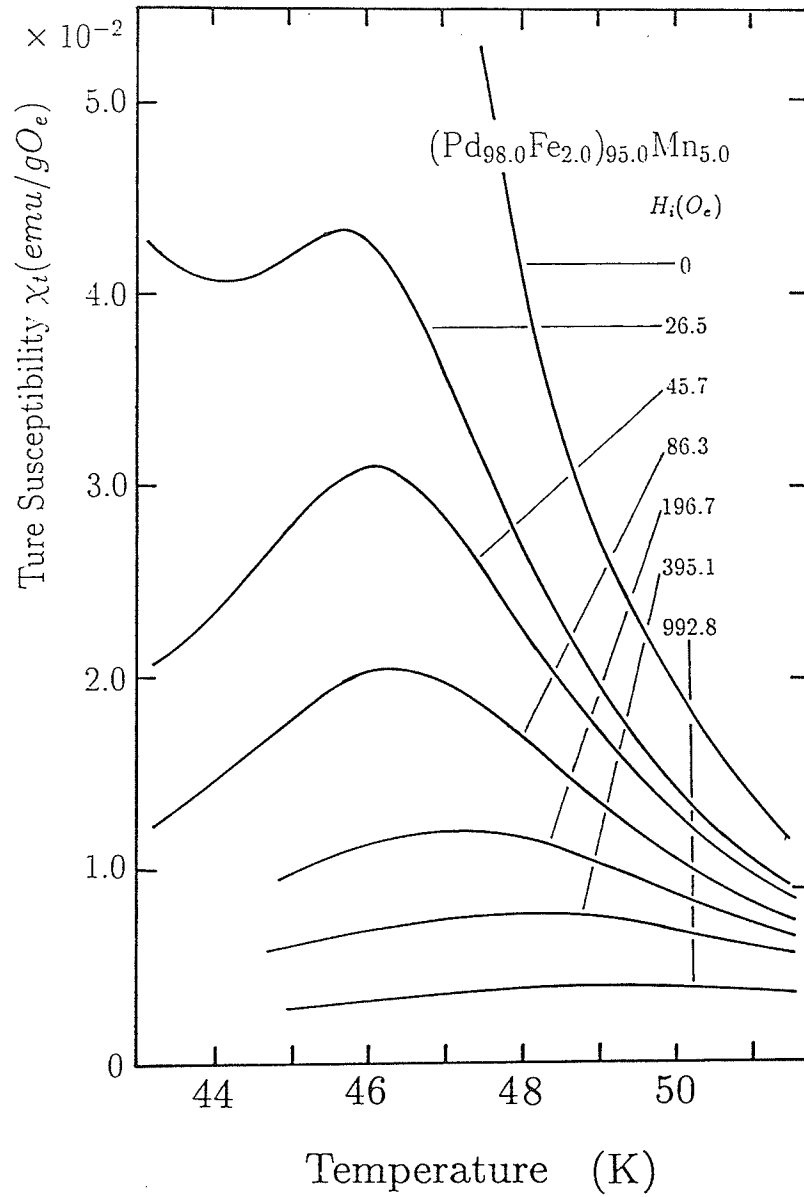


Figure A20: The selected *ac* susceptibility data as a function of temperature for a (PdFe)Mn alloy with 2.0 at% Fe in various fields.

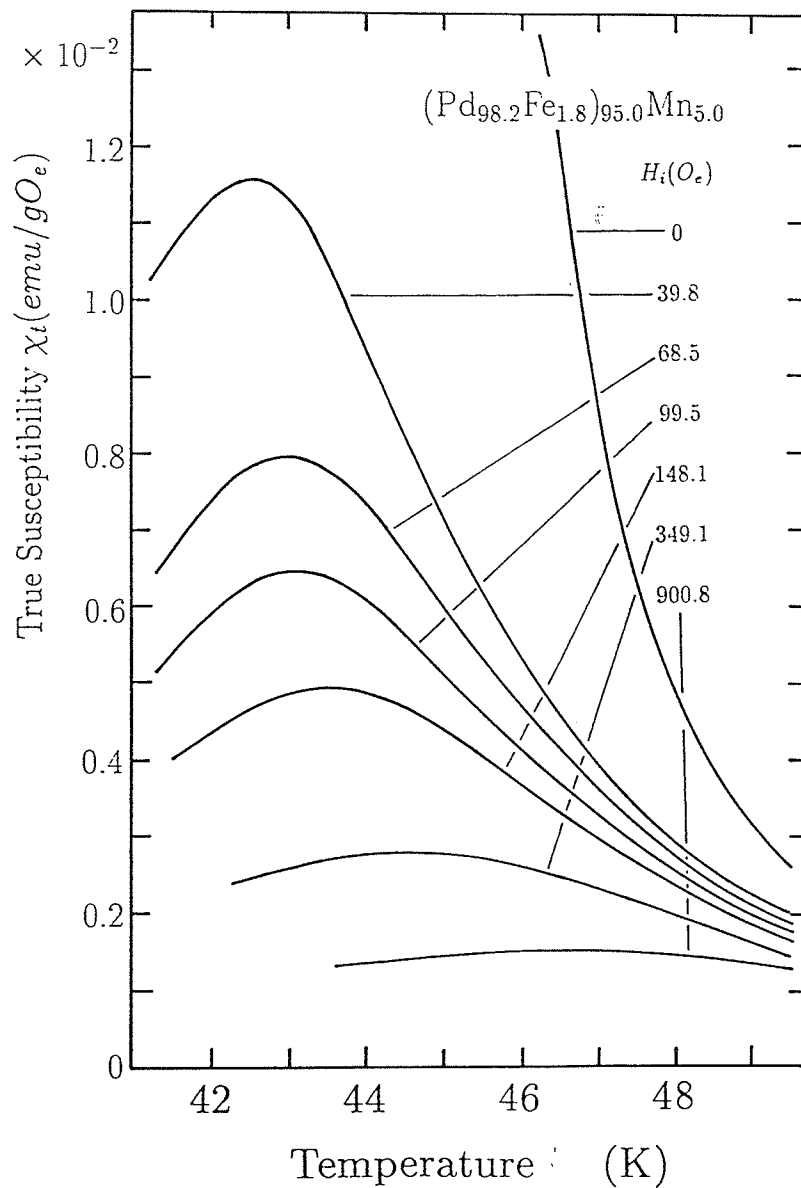


Figure A21: The selected *ac* susceptibility data as a function of temperature for a (PdFe)Mn alloy with 1.8 at% Fe in various fields.

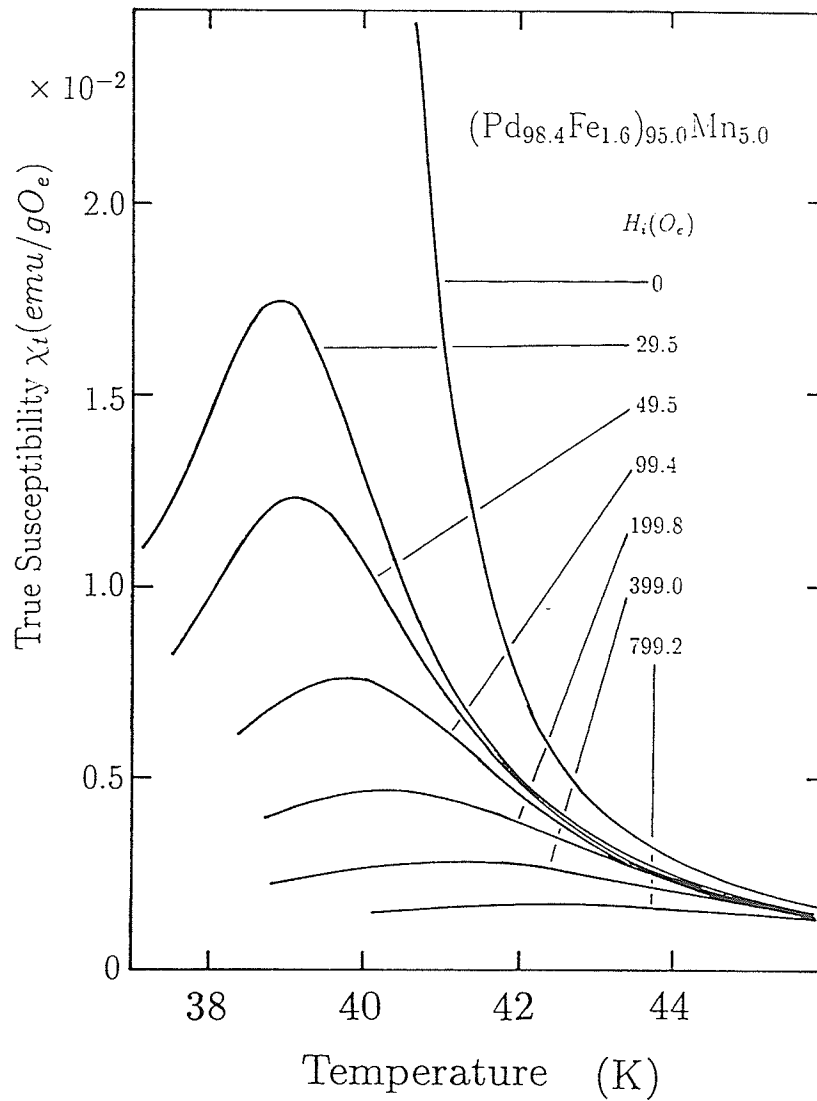


Figure A22: The selected *ac* susceptibility data as a function of temperature for a (PdFe)Mn alloy with 1.6 at% Fe in various fields.

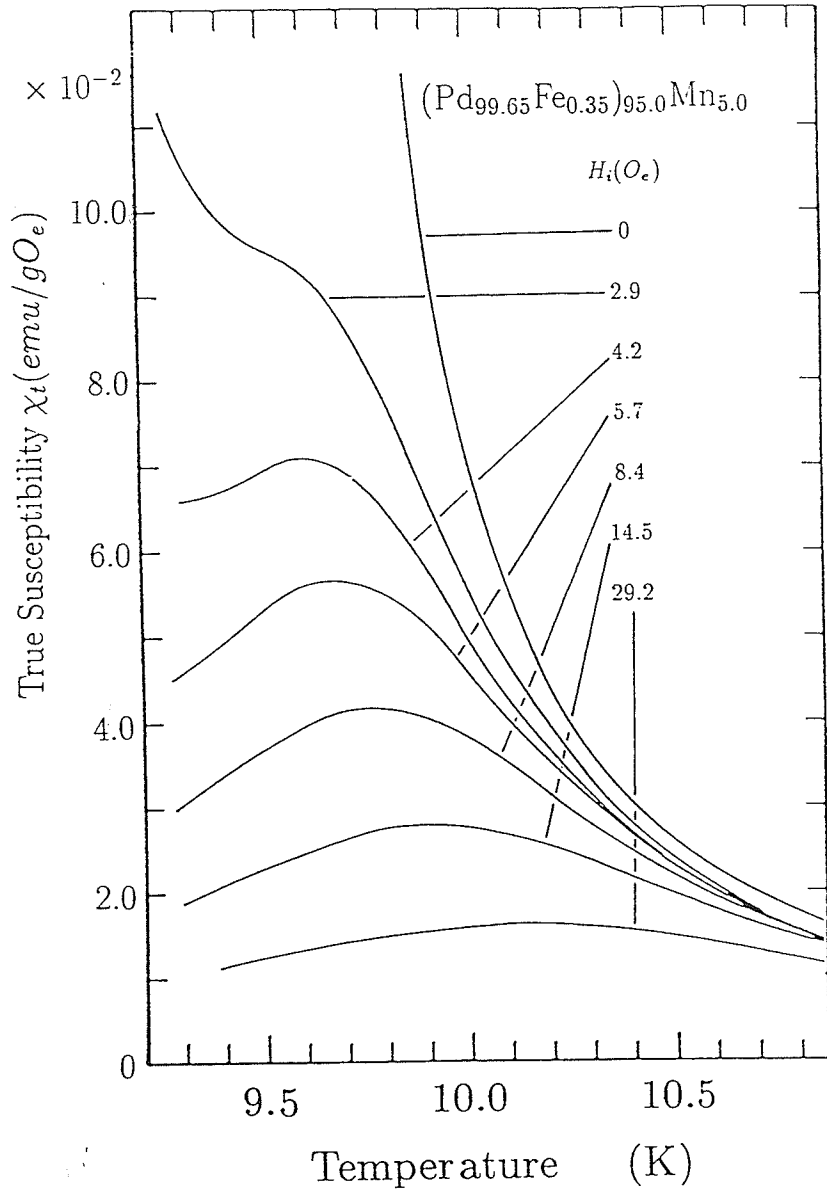


Figure A23: The selected *ac* susceptibility data as a function of temperature for a (PdFe)Mn alloy with 0.35 at% Fe in various fields.

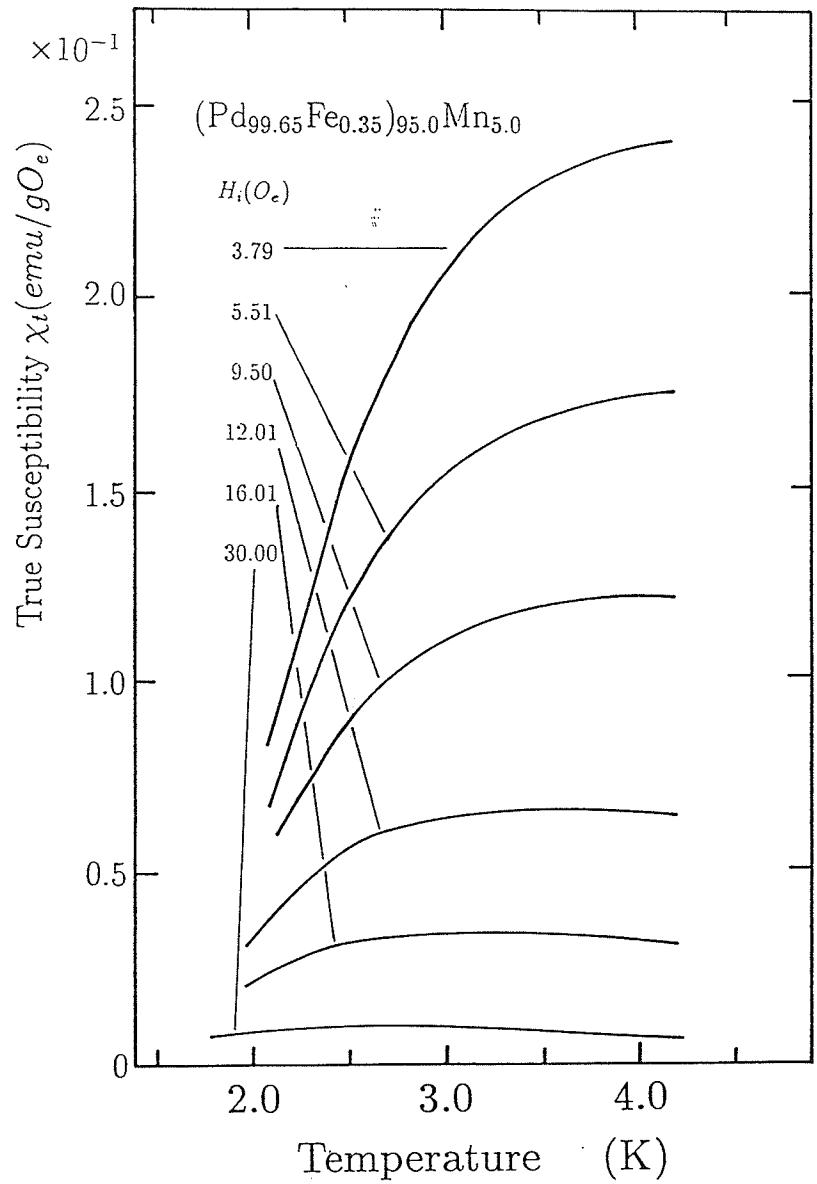


Figure A24: The selected *ac* susceptibility data as a function of temperature for a (PdFe)Mn alloy with 0.35 at% Fe in various fields.

B. *ac* Magnetoresistance Data

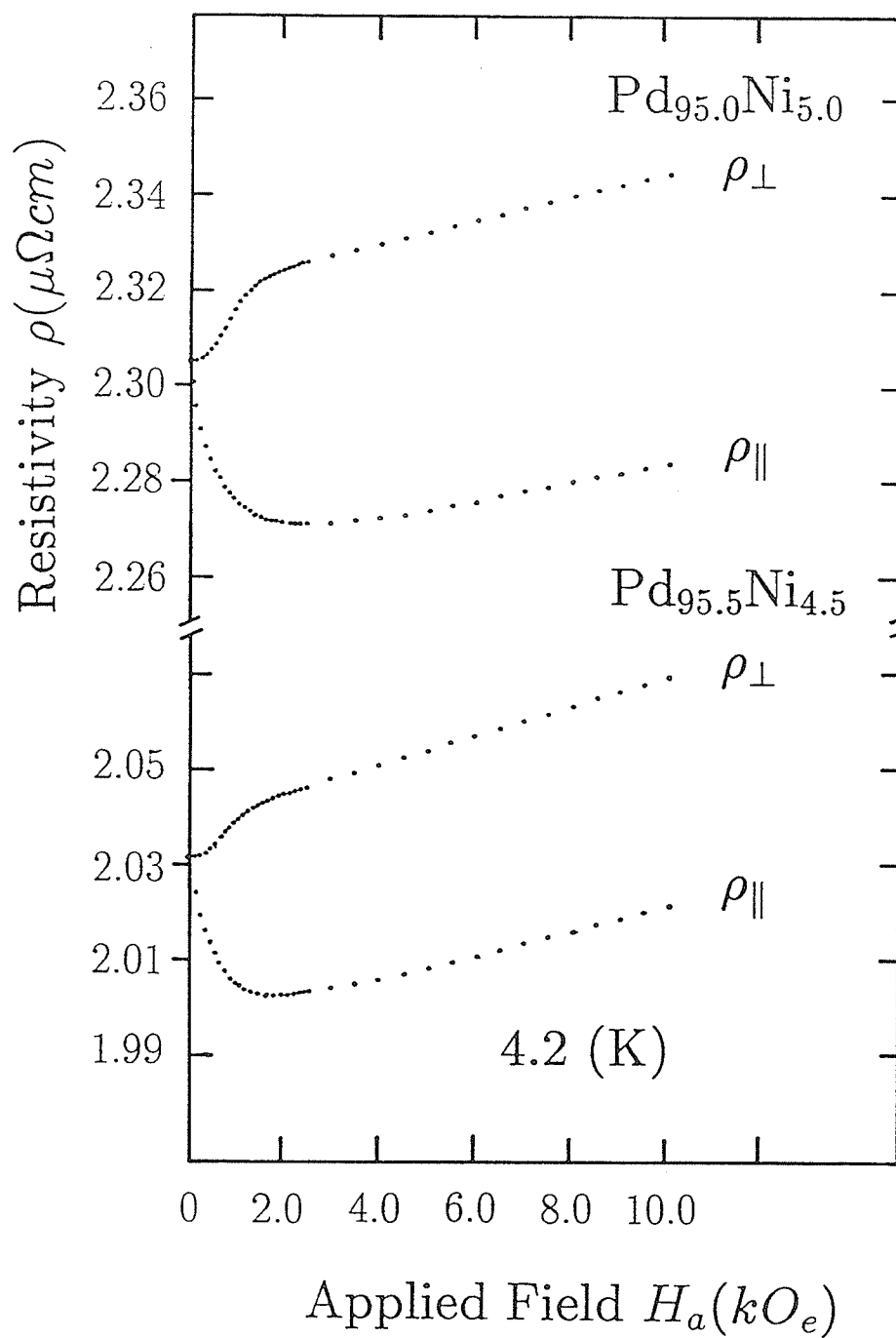


Figure B1: Resistivity versus applied field for the Pd_{95.0}Ni_{5.0} and Pd_{95.5}Ni_{4.5} alloys at 4.2 K.

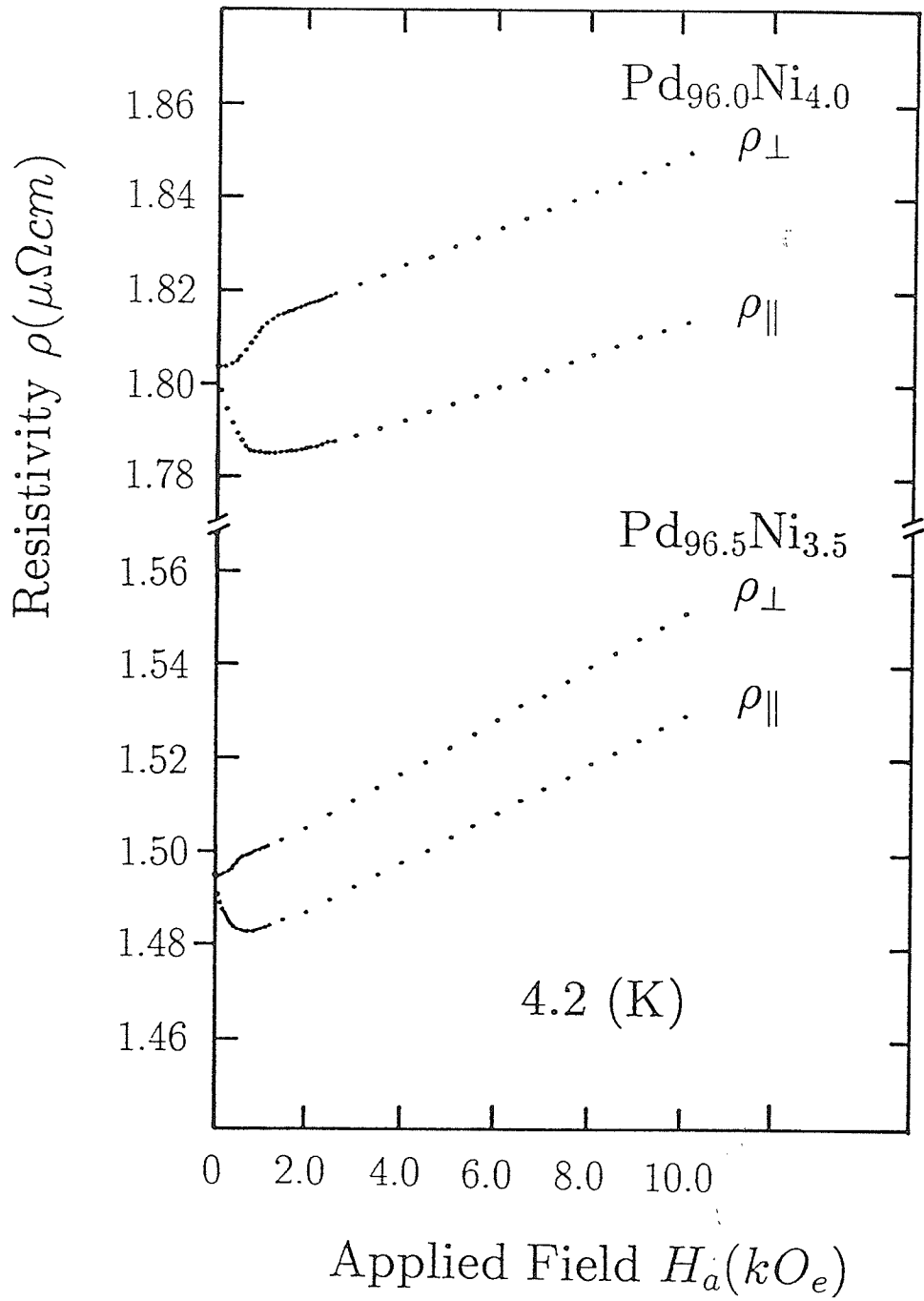


Figure B2 : Resistivity versus applied field for the $Pd_{96.0}Ni_{4.0}$ and $Pd_{96.5}Ni_{3.5}$ alloys at 4.2 K.

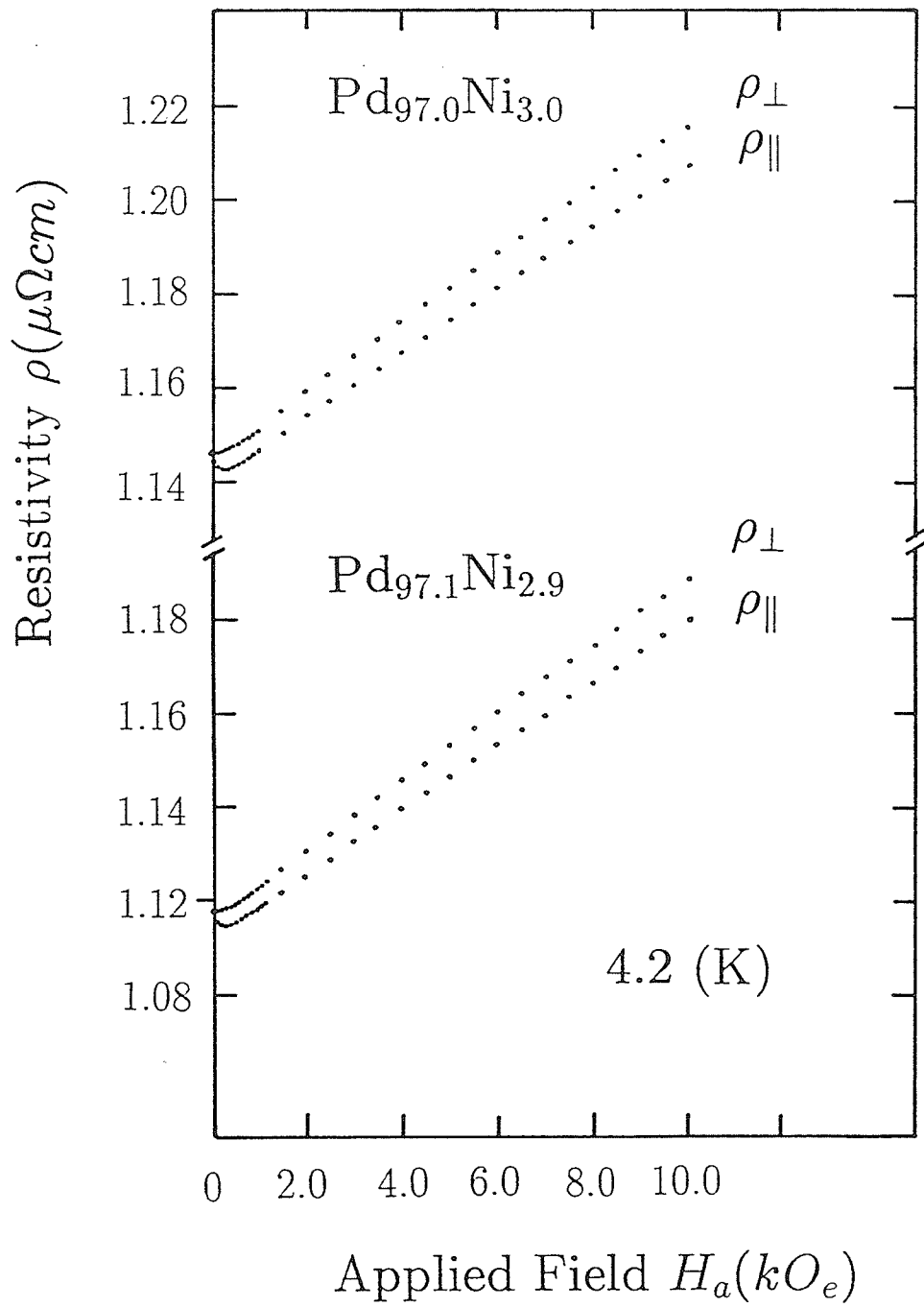


Figure B3: Resistivity versus applied field for the $Pd_{97.0}Ni_{3.0}$ and $Pd_{97.1}Ni_{2.9}$ alloys at 4.2 K.

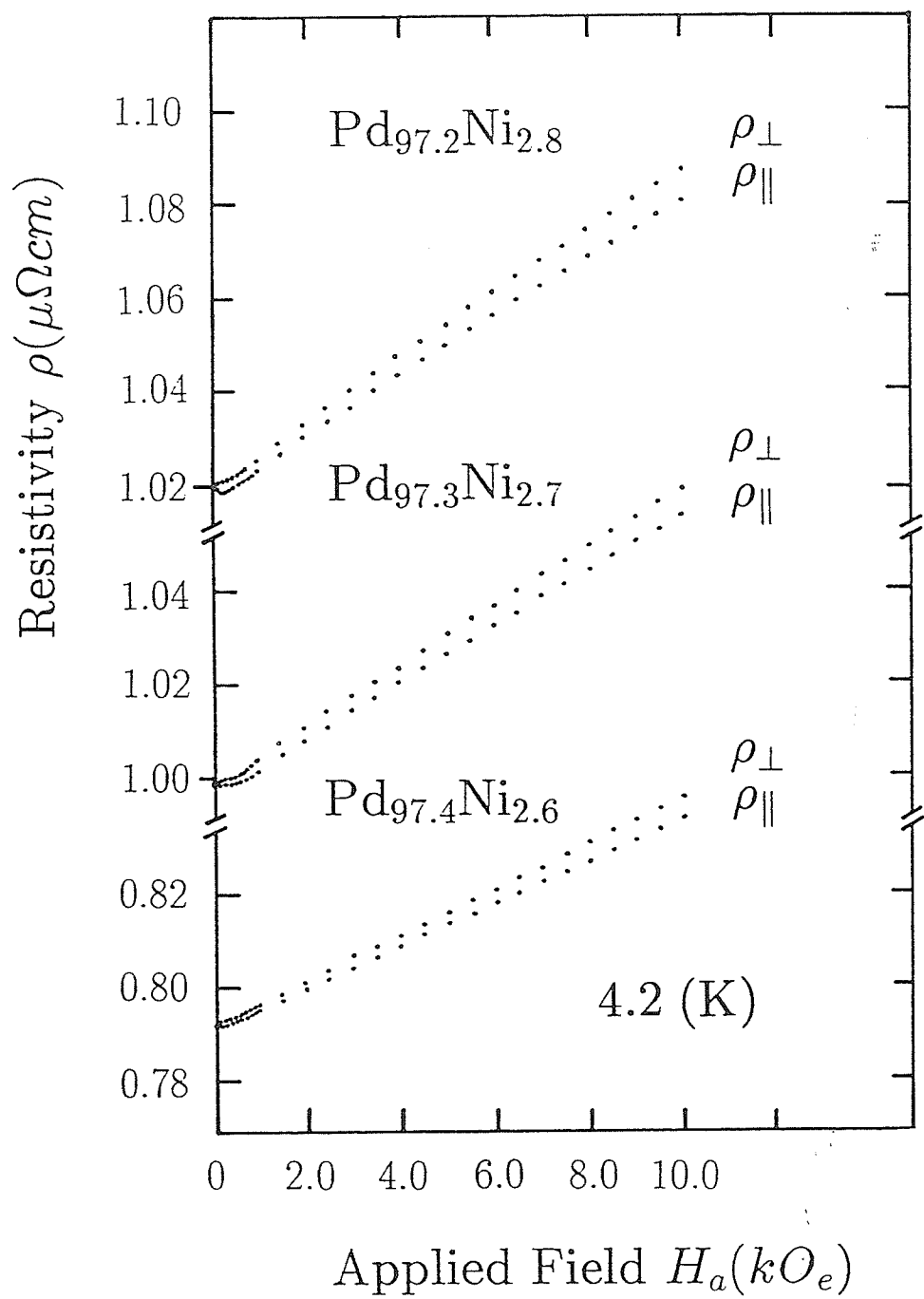


Figure B4: Resistivity versus applied field for the Pd_{97.2}Ni_{2.8}, Pd_{97.3}Ni_{2.7}, and Pd_{97.4}Ni_{2.6} alloys at 4.2 K.

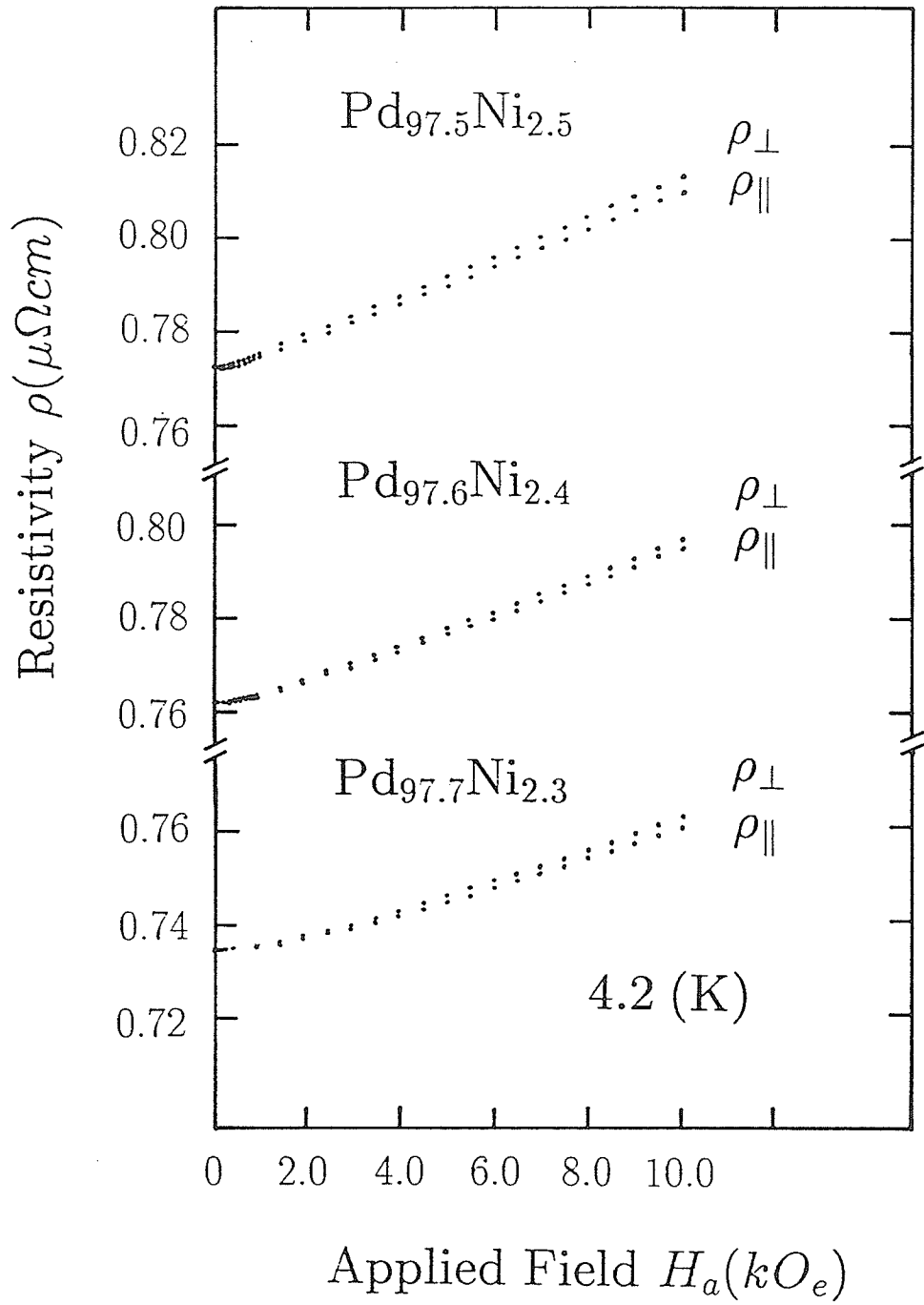


Figure B5: Resistivity versus applied field for the Pd_{97.5}Ni_{2.5}, Pd_{97.6}Ni_{2.4}, and Pd_{97.7}Ni_{2.3} alloys at 4.2 K.

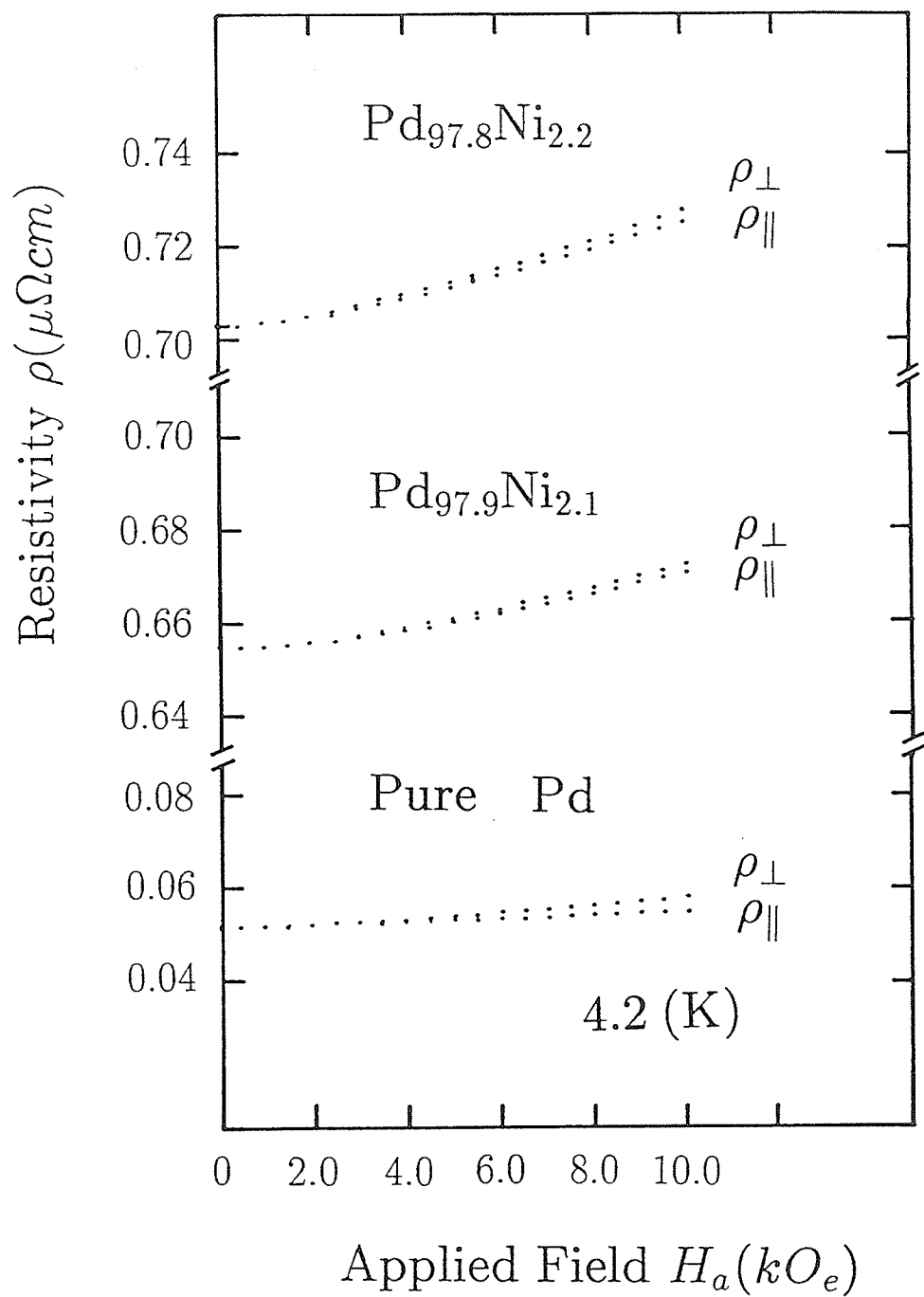


Figure B6: Resistivity versus applied field for the Pd_{97.8}Ni_{2.2}, Pd_{97.9}Ni_{2.1} alloys, and pure Pd metal at 4.2 K.

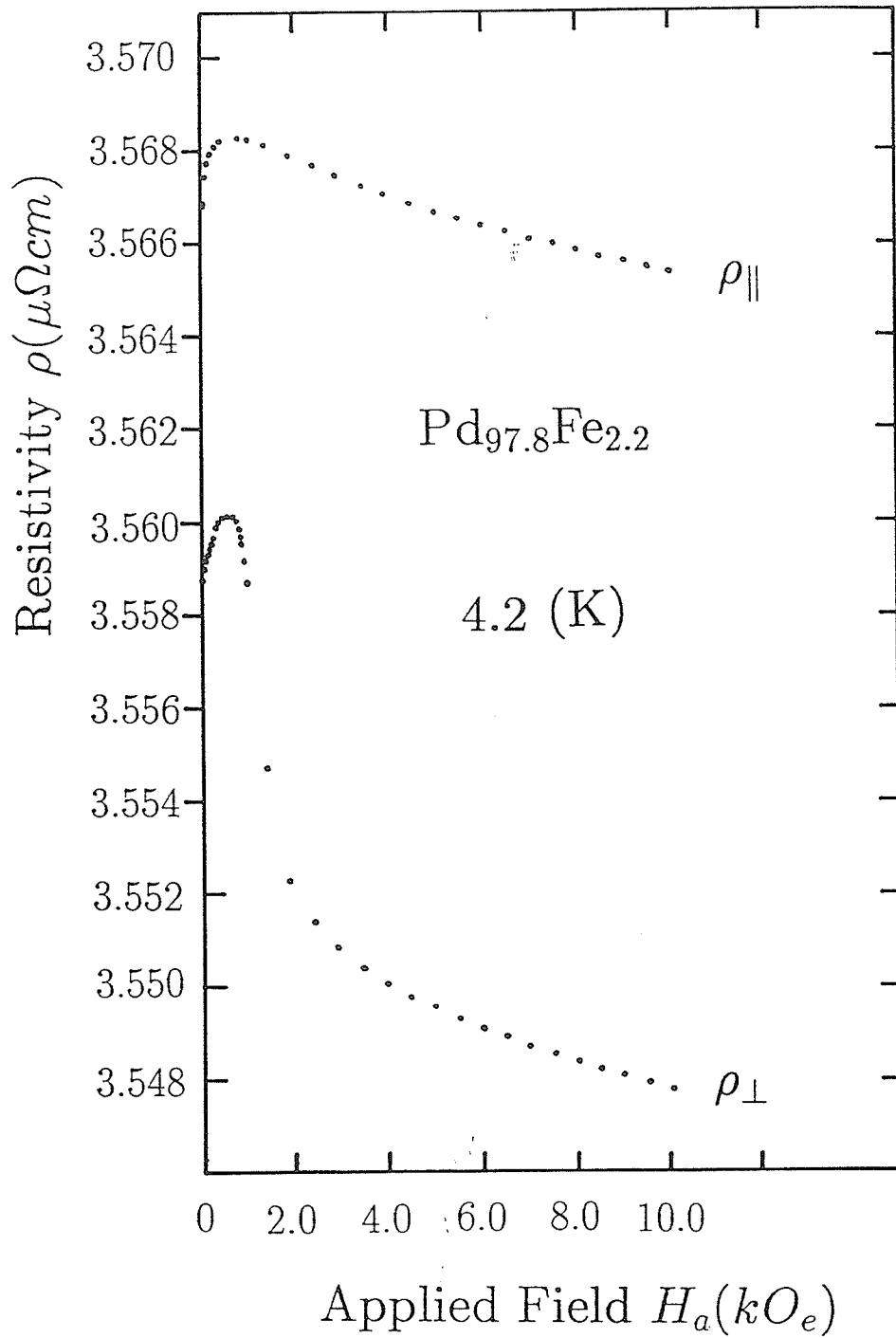


Figure B7: Resistivity versus applied field for the Pd_{97.8}Fe_{2.2} alloy at 4.2 K.

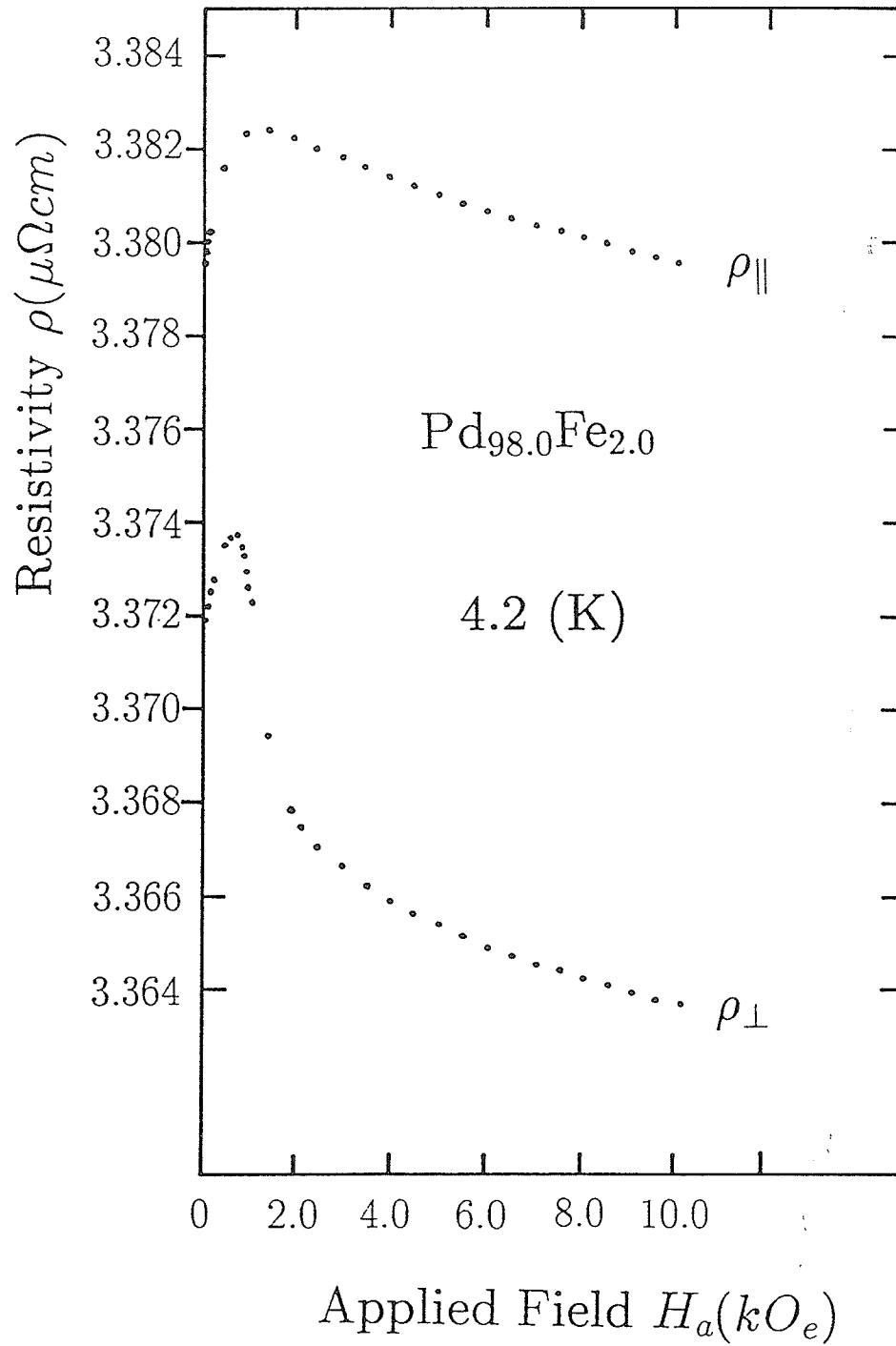


Figure B8: Resistivity versus applied field for the $\text{Pd}_{98.0}\text{Fe}_{2.0}$ alloy at 4.2 K.

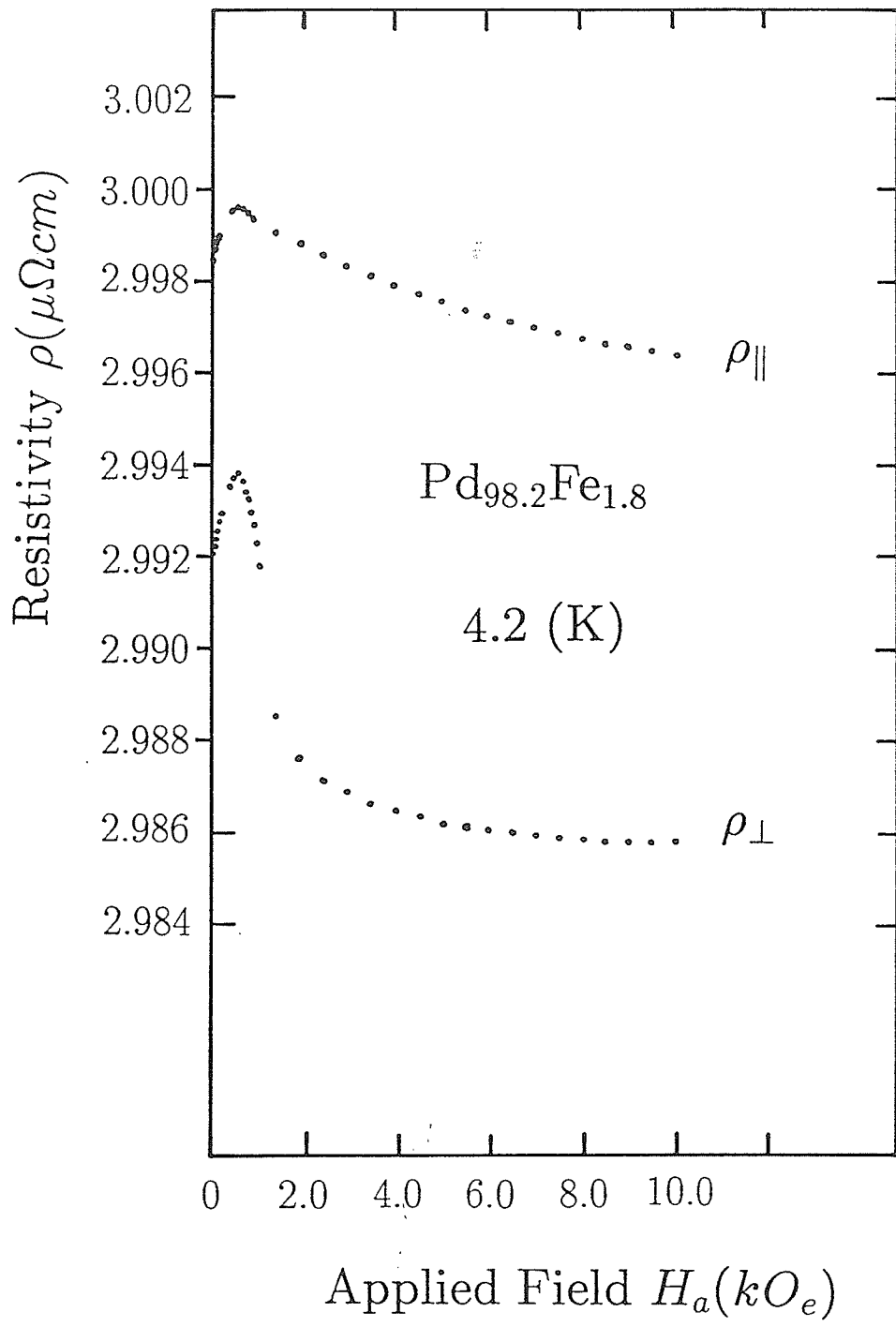


Figure B9: Resistivity versus applied field for the $\text{Pd}_{98.2}\text{Fe}_{1.8}$ alloy at 4.2 K.

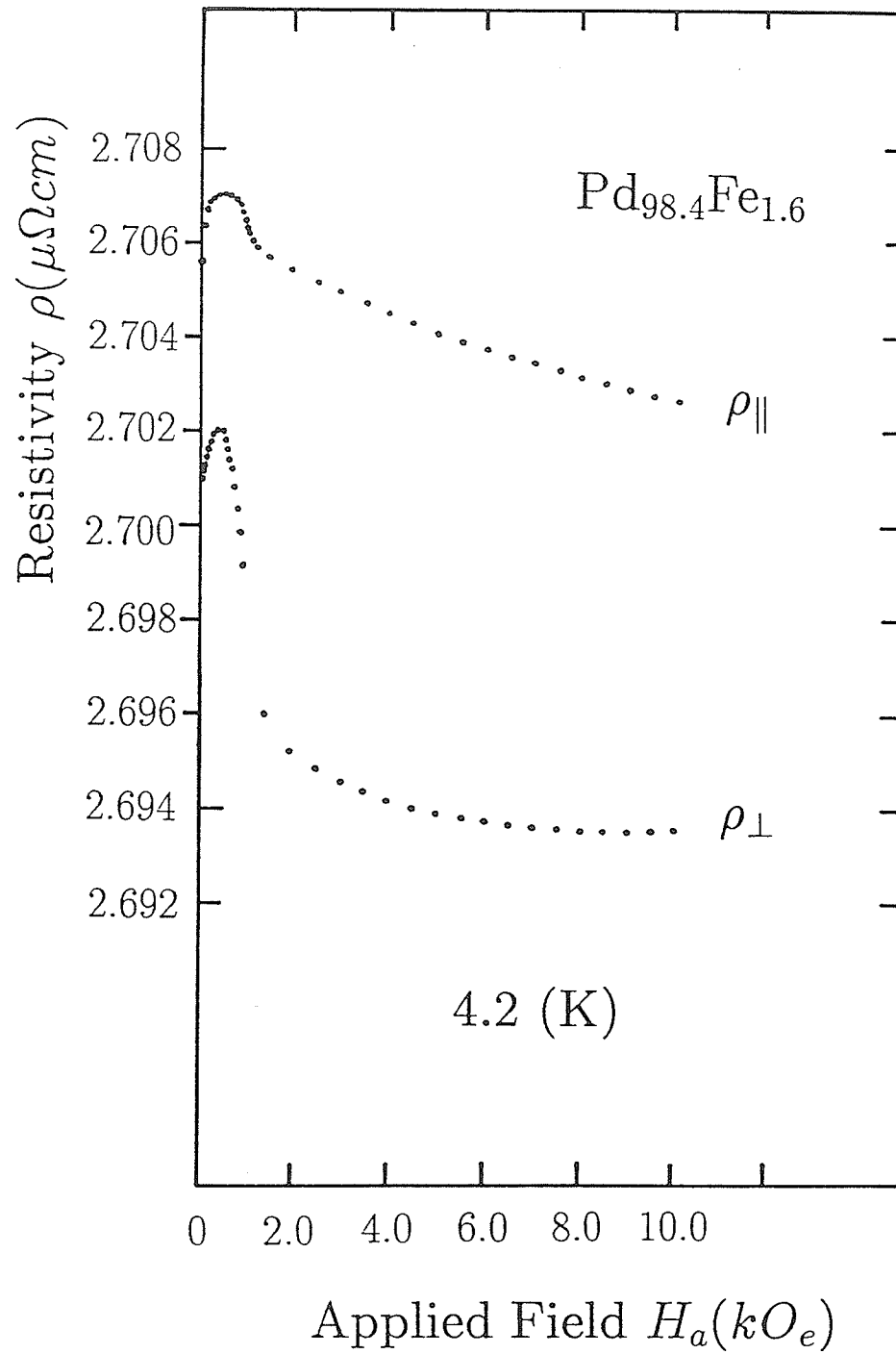


Figure B10: Resistivity versus applied field for the Pd_{98.4}Fe_{1.6} alloy at 4.2 K.

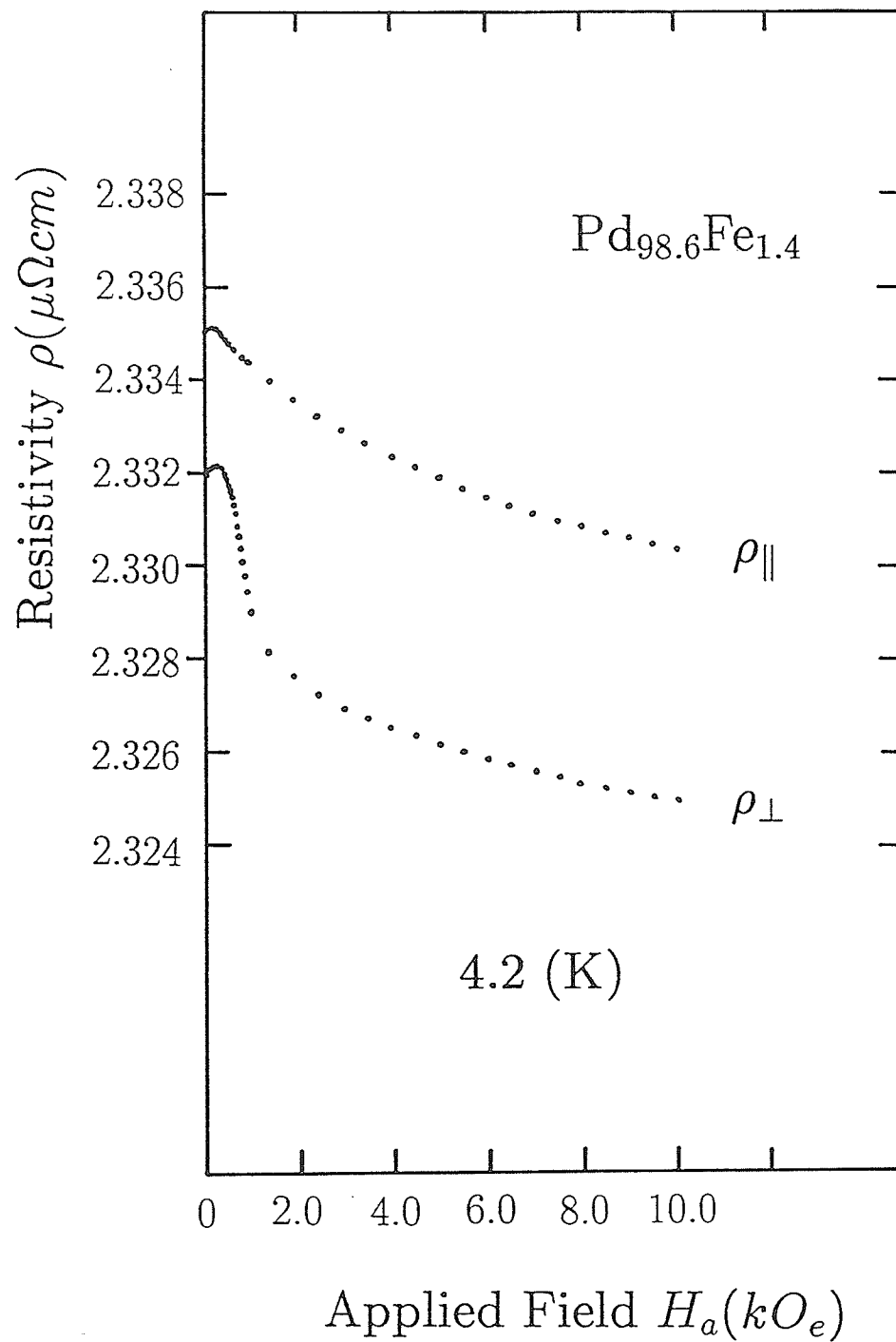


Figure B11: Resistivity versus applied field for the $\text{Pd}_{98.6}\text{Fe}_{1.4}$ alloy at 4.2 K.

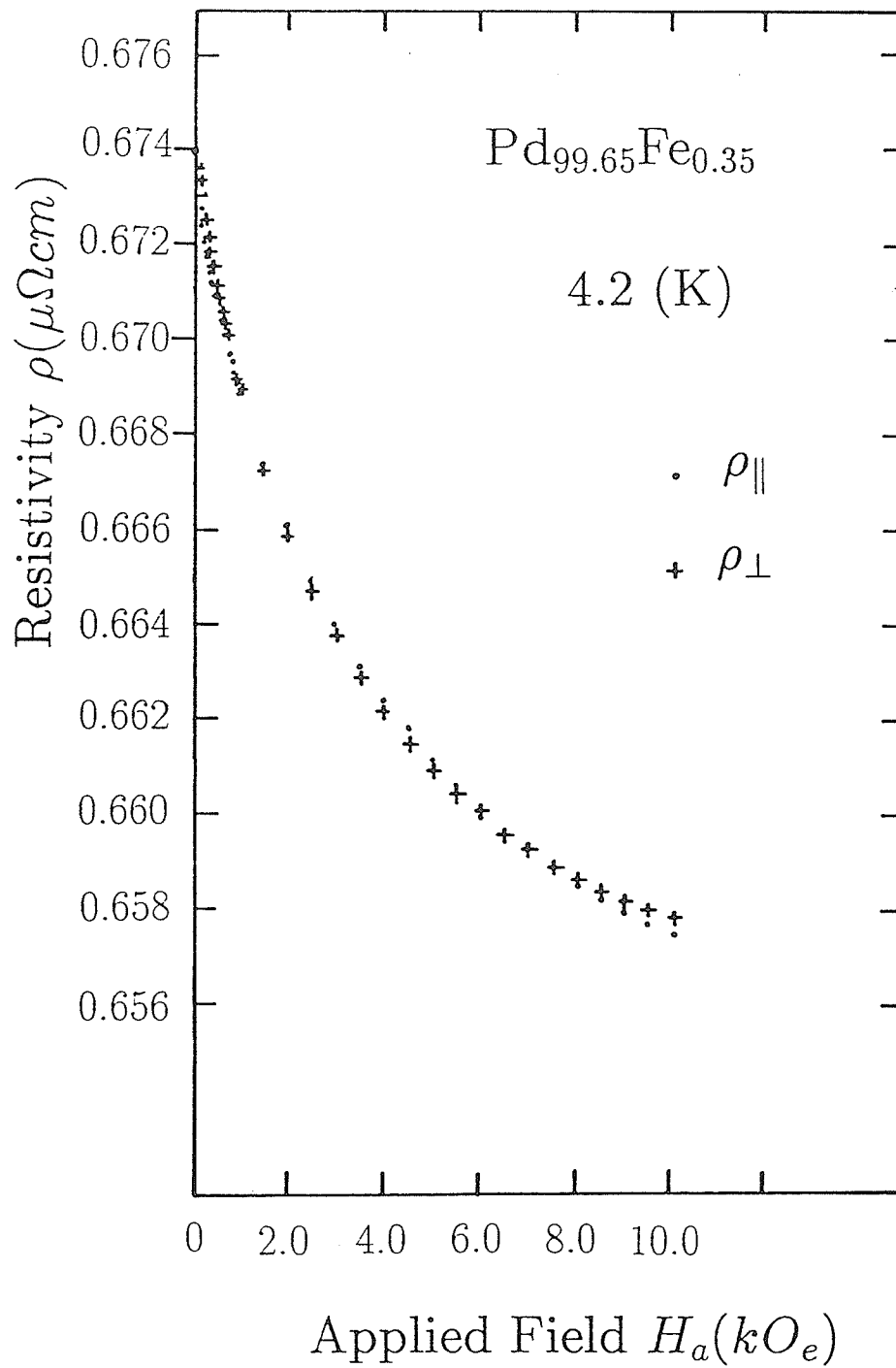


Figure B12: Resistivity versus applied field for the Pd_{99.65}Fe_{0.35} alloy at 4.2 K.

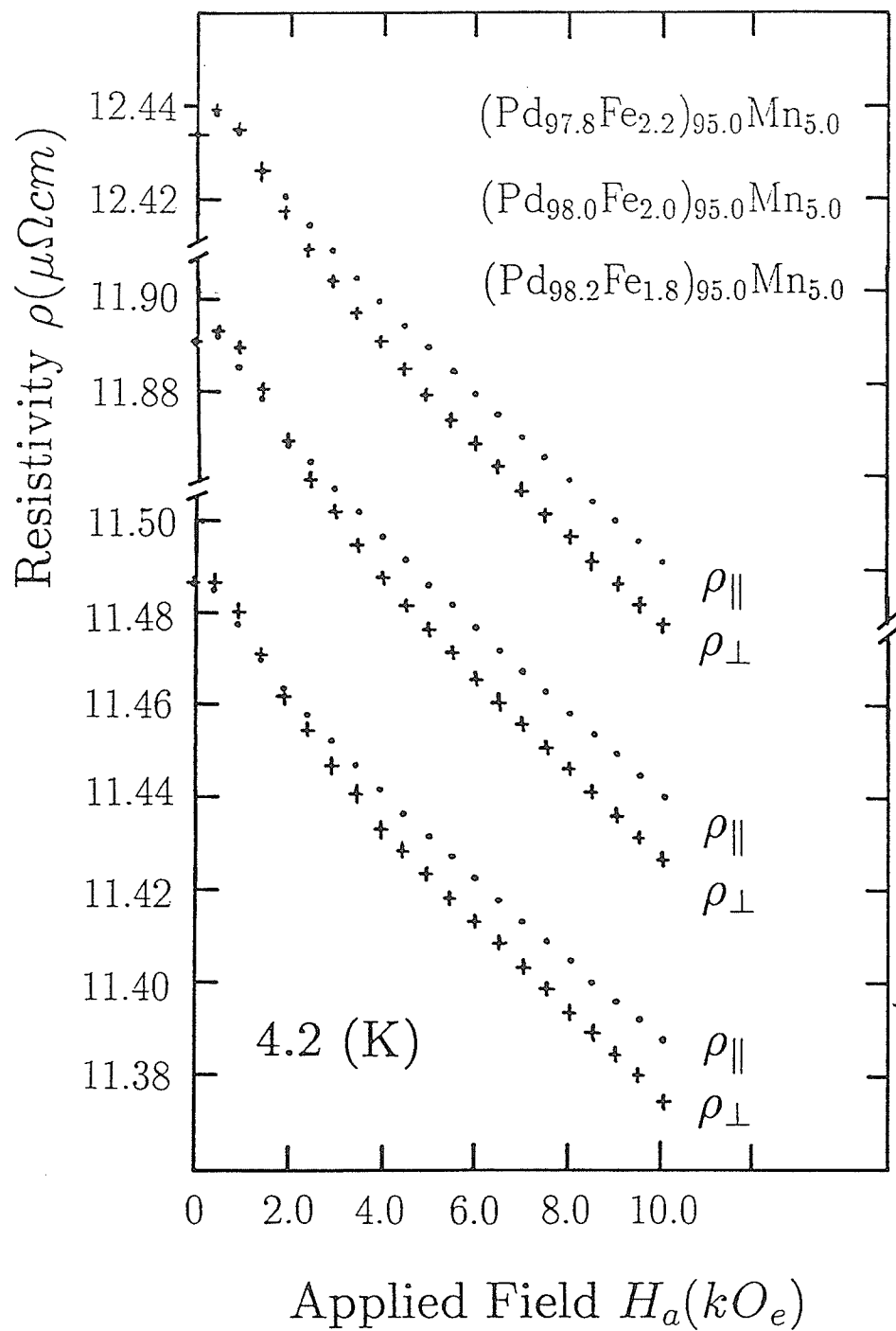


Figure B13: Resistivity versus applied field for the (PdFe)Mn alloys with 2.2, 2.0, and 1.8 at%Fe at 4.2 K.

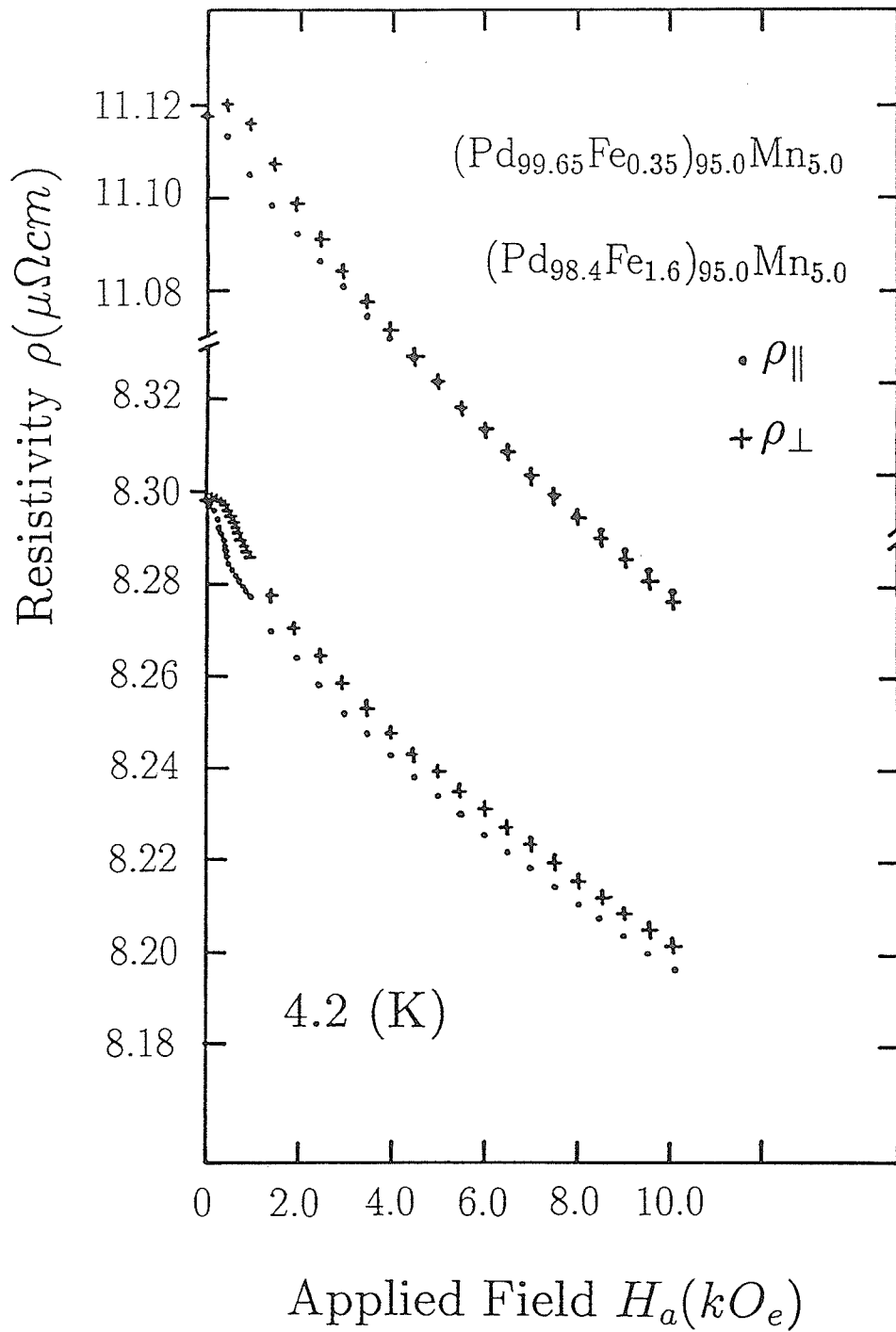


Figure B14: Resistivity versus applied field for the (PdFe)Mn alloys with 1.6 and 0.35 at%Fe at 4.2 K.

References

- Aldred A T, Ramford B D and Stringfellow M W
1970 *Phys. Rev. Lett.* 24 897
- Berger L 1978 *J. Appl. Phys.* 49 2156
- Binder K and Young A P 1986 *Rev. Mod. Phys.* 58 801
- Birss R R 1964 Symmetry and Magnetism *North Holland*, Amsterdam
- Bloch F 1930 *Z. Phys.* 52 208
- Boerstael B M 1970 *Thesis* University of Leiden
- Bozorth R M, Wolff P A, Davis D D, Compton V B, and Wernick J H
1961 *Phys. Rev.* 122 1157
- Campbell I A and Fert A 1982 Ferromagnetic Materials Vol.2
North Holland, Amsterdam
- Campbell I A, Fert A and Jaoul O
1970 *J. Phys. C: Solid State Phys.* 3 S95
- Chang K J and Lee K C 1980 *J. Phys. C* 13 2165
- Cheung T D, Kouvel J S and Garland J W 1981 *Phys. Rev. B* 23 1245
- Chouteau G and Tournier R 1972 *J. de Phys.* 32 C1-1002
- Chouteau G, Tournier R and Mollard P 1974 *J. Physique* 35 C4 185
- Chikazumi S 1964 Physics of Magnetism *Plenum*, New York
- Collins M F 1989 Magnetic Critical Scattering
Oxford University Press, Oxford
- Cooper M J 1968 *Phys. Rev.* 168 183
- Crangle J and Scott W R 1965 *J. Appl. Phys.* 36 921
- Domb C and Hunter D L 1965 *Proc. Phys. Soc.* 86 1147

- Doniach S and Engelsberg S 1966 *Phys. Rev. Lett.* 17 750
- Dorleijin J W F 1976 *Philips Res. Rep.* 31 287
- Dorleijin J W F and Miedema A R 1976 *AIP Conf. Proc.* 34 50
- Fahnle M 1987 *J. Magn. Magn. Mat.* 65 1
- Fahnle M, Braun P, Reisser R, Seeger M and Kronmuller H
1988 *J. Physique* C8 1201
- Farrell T and Greig D 1968 *J. Phys. C* 1 sur 2 1359
- Fawcett E, Bucher E, Brinkman W F and Maita J P
1968 *Phys. Rev. Lett.* 21 1183
- Fert A 1969 *J. Phys. C* 2 1784
- Fert A and Campbell I A 1968 *Phys. Rev. Lett.* 21 1190
1976 *J. Phys. F* 6 849
- Friederich A and Fert A 1974 *Phys. Rev. Lett.* 33 1214
- Gaunt P, Ho S C, Williams G and Cochrane R W
1981 *Phys. Rev. B* 23 251
- Grassie A D C, Swallow G A, Williams G and Loram J W
1971 *Phys. Rev. B* 3 4154
- Griffiths R B 1965 *Phys. Rev. Lett.* 14 623
- Hall N G, Roshko R M and Williams G
1984 *J. Phys. F: Met. Phys.* 14 711
- Hamzic A, Senoussi S, Campbell I A and Fert A
1978 *J. Phys. F: Met. Phys.* 8 1947
1980 *J. Phys. F: Met. Phys.* 10 L165

- Ho S C 1982 *Thesis* University of Manitoba
- Ho S C, Maartense I and Williams G
- 1981a *J. Phys. F: Met. Phys.* 11 699
- 1981b *J. Phys. F: Met. Phys.* 11 1107
- Hsu Y, Schmidt J E, Gupta M, Jen S and Berger L
- 1983 *J. Appl. Phys.* 54 (4) 1887
- Hurd C M 1974 *Adv. Phys.* 23 315
- Ising E 1925 *Z. Phys.* 31 253
- Kadanoff L P 1966 *Physics* 2 263
- Kaiser A B and Doniach S 1970 *Int. J. Mag.* 1 11
- Kettschau A, Boysen J, Brewer W D, and Campbell I A
- 1983 *J. Magn. Magn. Mater.* 37 L1
- Kasuya T 1956 *Progr. Theoret. Phys.* 16 58
- Kaul S 1985 *J. Mag. Mag. Mat.* 53 5
- Kim D J 1966 *Phys. Rev.* 149 434
- Kleiman R N and Williams G 1982 *J. Phys. F: Met. Phys.* 12 169
- Kohler M 1938 *Ann. Phys* (5) 32 211
- Kondo J 1962 *Prog. Theor. Phys. Kyoto* 27 772
- Kornik K, Kunkel H and Roshko R M 1988 *J. Appl. Phys.*
- 1988 *J. Appl. Phys.* 64 (10) 5619
- Kouvel J S and Fisher M E 1964 *Phys. Rev. A* 136 1626
- Kouvel J S and Comly J S
- 1971 Critical Phenomena in Alloys, magnets and Superconductors

- Kunkel H P and Williams G
1988a *J. Phys. F: Met. Phys.* 18 1271;
1988b *J. Mag. Mag. Mat.* 75 98
- Kunkel H P, Wang Z and Williams G
1987 *J. Phys. F: Met. Phys.* 17 L157
- Kunkel H P, Kucukturhan K, Wang Z and Williams G
1988a *J. Phys. F: Met. Phys.* 18 89
- Kunkel H P, Roshko R M and Williams G 1988b *Phys. Rev. B* 37 5880
- Kunkel H P, Wang Z and Williams G
1989 *J. Phys.: Condens. Mat.* 1 3381
- Kunkel H P, Wang Z and Williams G
1990 *J. Phys.: Condens. Mat.* 2 4173
- Landau L D and Lifshitz E M 1969 Statistical Physics
2nd edn. Pergamon Press, Oxford
- Lederer P and Mills D L 1968 *Phys. Rev.* 165 837
- LeGuillou L C and Zinn-Justin J 1980 *Phys. Rev. B* 21 3976
- Lipton D and Jabobs R L 1971 *J. Phys.* F1 469
- Loewen C, Saran M and Williams G
1986 *J. Pys. F: Met. Phys.* 12 43
- Loram J W and Mirza K A 1985 *J. Pys. F: Met. Phys.* 15 2213
- Loram J W, Mirza K A and Chen Z 1986 *J. Pys. F: Met. Phys.* 16 233
- Long P D and Turner R E 1970 *J. Phys. C: Metal Phys.* 2 S127
- Low G G and Holden T M 1966 *Proc. Phys. Soc.* 89 119

- Maartense I 1970 *Rev. Sci. Instrum.* 41 657
- Maartense I and Williams G 1976 *J. Phys. F* 6 L121
- Malozemoff A P 1986 *Phys. Rev. B* 34 1853
- McDougald M and Manuel A J 1968 *J. Appl. Phys.* 39 961;
1970 *J. Phys. C* 39 147
- McLennan J C and Smith H Grayson 1926 *Proc. Roy. Soc.*
A 112 110
- Morrish A H 1965 The Physical Principles of Magnetism
Wiley, New York
- Moriya T 1967 Proc. Int. 'Enrico Fermi' School of Physics New York
- Mott N F 1936 *Proc. R. Soc. A* 153 699; 1964 *Adv. Phys.* 13 325
- Muir W B and Strom-Olsen J O 1976 *J. Phys. E: Sci. Instrum* 9 163
- Muller F A, Gersdorf R, and Roeland L W 1970 *Phys. Letters* 31A 424
- Murani A P, Tari A and Coles B R 1974 *J. Phys. F: Met. Phys.* 4 1769
- Mydosh J 1974 *Phys. Rev. Lett.* 33 1562
- Nieuwenhuys G J 1974 *Thesis* University of Leiden;
1975 *Adv. Phys.* 24 515
- Nuffield E W 1966 X-Ray Diffraction Methods, Wiley, New York
- Ododo J C 1985 *J. Phys. F* 4 941
- Onsager L 1944 *Phys. Rev.* 65 117
- Osborn J A 1945 *Phys. Rev.* 67 351-7
- Parra R E and Medina R 1980 *Phys. Rev. B* 22 5460-70
- Pearson W B 1958 A Handbook of Lattice and Structures of Metals

and Alloys Pergamon Press, New York

Peters R P, Buchal Ch, Kubota M, Mueller R M and Pobell F

1984 *Phys. Rev. Lett.* 53 1108

Roshko R M and Williams G 1984 *J. phys. F: Met. Phys.* 14 703

Sain D and Kouvel J S 1978 *Phys. Rev. B* 17 2257

Sarachik M P and Shaltiel D 1967 *J. Appl. Phys.* 38 1155

Saran M 1986 *Thesis* University of Manitoba

Saran M and Williams G 1987 *J. Phys. F: Met. Phys.* 17 731

Crangle J et al 1985 *J. Phys. Soc. Japan.* 50(5) 1989

Schinkel C J and Van Amstel W D 1973 *Phys. Lett.* 7 467

Seeger M and Kronmuller H 1989 *J. Mag. Mag. Mat.* 78 393

Senoussi S, Campbell I A and Fert A

1977 *Solid State Commun.* 21 269

Sherrington D and Kirkpartrick S 1975 *Phys. Rev. Lett.* 35 1792

Skalski S, Kawatra M P, Mydosh J A and Budnick J I

1970 *Phys. Rev. B* 2 3613

Smit J 1951 *Physica* 17 612

Smit J J, Nieuwenhuys G J and de Longh L J

1979 *Solid State Commun.* 30 243

Southern B W 1976 *J. Phys. C: Solid State Phys.* 9 4011

Stanley H E 1971 Introduction to Phase Transitions and Critical

Phenomena Oxford, Clarendon

Star W M, Foner S and McNiff Jr E J 1975 *Phys. Rev. B* 12 2690-709

- Stauffer D 1979 *Phys. Rep.* 54 1
- Stoner E C 1933 *Phil. Mag.* 15 1080; 1938 *Proc. Roy. Soc.*
A165 372; 1948 *Repts. Prog. Phys.* 11 43
- Takahashi T and Shimizu M 1965 *J. Phys. Soc. Japan* 20 26
- Tari A and Coles B R 1971 *J. Phys. F: Met. Phys.* 1 L69
- Thomson W 1851 *Proc. Roy. Soc. (London)* 8 546
- Thomson J O and Thompson J R 1979 *J. Appl. Phys.* 50 7364
- Verbeek B H, Nieuwenhuys G J, Stocker H, and Mydosh J A
Phys. Rev. Lett. 40 586
- Webb R A, Crabtree G W, and Vuillemin J J
1979 *Phys. Rev. Lett.* 43 796
- Widom B 1965 *J. Chem. Phys.* 43 3892
- Williams G 1970 *J. Phys. Chem. Solids* 31 529;
1976 *Solid State Commun.* 19 821
- Williams G and Loram J W 1969 *J. Phys. Chem. Solids* 30 1827
- Williams G, Swallow G A and Loram J W 1973 *Phys. Rev. B* 7 257
- Wohlfarth E P 1976 Magnetism Selected Topics
- Yeung I, Roshko R M and Williams G 1986 *Phys. Rev. B* 34 3456
- Ziman J M 1960 Electrons and Phonons Oxford Univ. Press, Oxford
- Zweers H A 1976 *Thesis* University of Leiden